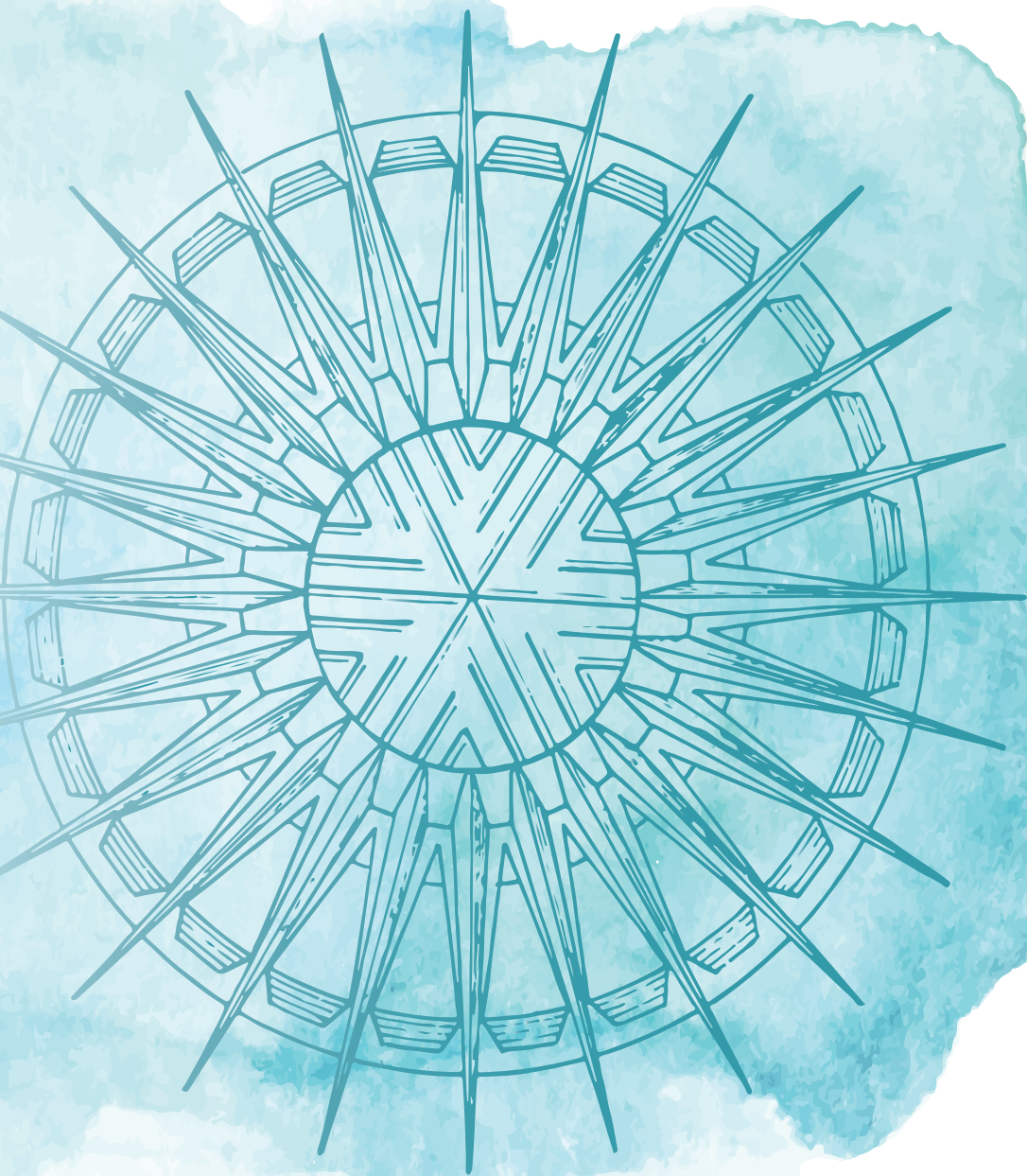# Including active excretion in physiologically based kinetic models for new approach methodologies

Annelies Noorlander

Propositions

1. Including active excretion in physiologically based kinetic (PBK) models still requires in vivo data.
(this thesis)

2. Transfected cell models provide the best in vitro models for defining kinetic parameters for active transport in PBK models.
(this thesis)

3. Patients' pharmacogenetic profiles need to be available more rapidly to their pharmacists to optimize drug therapy.

4. Modelling water and soil interaction without including evaluation of the predicted outcomes against real time spatial data leads to a digital paper reality and mandatory measures to non-existing problems.

5. Self-development is essential in order to obtain a PhD degree.

6. Good parenting is inextricably linked to mental and emotional stability.

Propositions belonging to the thesis, entitled

"Including active excretion in physiologically based kinetic models for new approach methodologies"

Annelies Noorlander

Wageningen, 2 November 2022

Including active excretion in physiologically based kinetic models for new approach methodologies

Annelies Noorlander

Thesis committee

Promotors
Prof. Dr I.M.C.M. Rietjens
Professor of Toxicology
Wageningen University & Research

Prof. Dr B. van Ravenzwaay
Professor of Reproduction and Developmental Toxicology
Wageningen University & Research
Former Senior Vice President of Experimental Toxicology and Ecology BASF, SE
Ludwigshafen, Germany

Other members
Prof. Dr J. Keijer, Wageningen University & Research
Prof. Dr P. Jennings, VU University Amsterdam
Prof. Dr J.J. Garcia Marin, University of Salamanca, Spain
Dr R. Landsiedel, BASF SE, Ludwigshafen, Germany

This research was conducted under the auspices of the Graduate School VLAG (Advanced studies in Food Technology, Agrobiotechnology, Nutrition and Health Sciences)

Including active excretion in physiologically based kinetic models for new approach methodologies

Annelies Noorlander

Thesis
submitted in fulfilment of the requirements for the degree of doctor
at Wageningen University
by the authority of the Rector Magnificus,
Prof. Dr A.P.J. Mol,
in the presence of the
Thesis Committee appointed by the Academic Board
to be defended in public
on Wednesday 2 November 2022
at 1:30 p.m. in the Omnia Auditorium.

Content

Chapter I

General introduction

Chapter I

1.1   Background on new approach methodologies (NAMs)

The development of science-based non-animal testing strategies of chemicals is important in current human safety testing. In the last decades this research has been boosted by the report from the US National Research Council (NRC) of the National Academies of Science entitled; Toxicity testing in the Twenty-first Century: A vision and a Strategy (Krewski et al. 2010). Also, in the Netherlands the organization ZonMW (ZorgOnderzoek Nederland Medische Wetenschappen) has stimulated the development of alternatives to animal testing for over 20 years with their program 'More knowledge with less animals' (Dutch: Meer Kennis met Minder Dieren (MKMD) focussing on the 3R fundamental principles of Replacement, Reduction and Refinement as first described by Russell and Burch in 1959. From 2018 to 2020, MKMD focussed on supporting the acceleration programme 'Transition to Animal-free Innovation' whereafter in 2020 the Ministry of Agriculture, Nature and Food Quality (ANFQ) requested a prolongation of this programme ((TPI) 2020). As a result, MKMD extended their programme and wrote a four year plan (2021-2024) on the development and application of new and existing animal-free innovations with a budget of the ministry of ANFQ of 6.8 million euros where the ambitious aim is to make the Netherlands the forerunner in the international transition to animal-free innovation (ZonMw 2020).

Many efforts in this area focus on the development and use of especially *in vitro* testing strategies using cells in culture that provide concentration-response curves for selected cellular endpoints. However, concentration-response curves from *in vitro* models alone are insufficient for human risk and safety assessment because risk assessment requires *in vivo* dose-response curves from which points of departure (PODs) (commonly expressed in mg/kg body weight per day) like a Benchmark dose lower confidence limit for 10% effect above background (BMDL$_{10}$) or a no observed adverse effect level (NOAEL) can be derived for defining health based guidance values (HBGVs) like Derived No-Effect Levels (DNELs), occupational exposure limits (OELs), Acceptable Daily Intakes (ADIs) or Tolerable Daily Intakes (TDIs) (Greim 2018). The concentration-response curves for effects on cells in culture can at best be used for identification of possible hazards but do not provide PODs when in risk assessment safe levels of human exposure need to be defined. As a result, the use of these alternative testing approaches in risk assessment requires a method to translate the *in vitro* data to *in vivo* dose-response data that can replace the data from animal bioassays. Given that the rat is not the ideal model for human it would be an improvement when human relevant *in vitro* assays as well as their dose-response curves could be used for quantitative human risk assessment.

To bridge the gap between the *in vitro* and *in vivo* situation so-called reverse-dosimetry by physiologically based kinetic (PBK) modelling is of use. Figure 1 illustrates how the use of PBK modelling-facilitated reverse dosimetry can translate the *in vitro* based testing results into *in vivo* dose-response curves that are required for risk assessment. When the

in vitro and PBK model used relate to humans this concept can even provide dose-response curves for toxicity in humans (Louisse et al. 2017). Examples of first proofs-of-principle that *in vivo* dose-response curves and PODs for human risk assessment can be defined based on a combined *in vitro*-PBK modelling approach can be found in previous work (Abdullah et al. 2016; Louisse et al. 2015; Louisse et al. 2010; Ning et al. 2019a; Shi et al. 2020; Strikwold et al. 2013). The predicted endpoints of toxicity in these proofs-of-principle examples included developmental toxicity, kidney toxicity, hepatotoxicity and cardiotoxicity. The use of non-animal based approaches such as *in vitro* toxicity testing together with PBK-modelling for the hazard and risk assessment of chemicals is an example of new approach methodologies (NAMs).
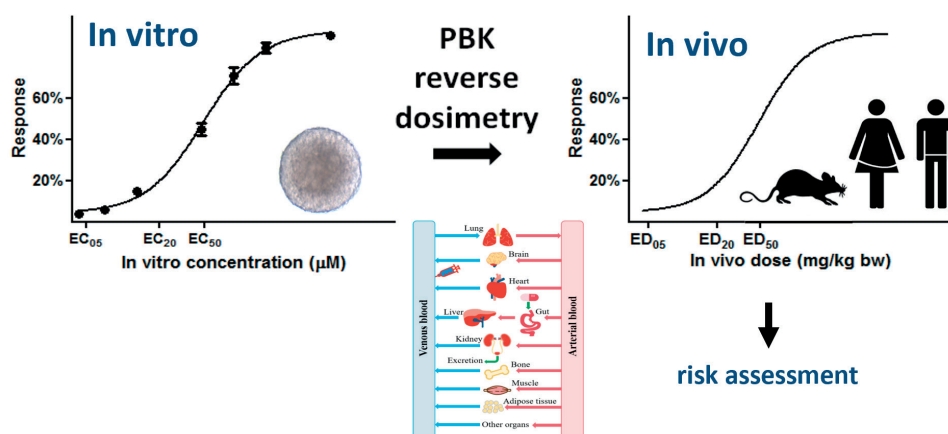
Figure I.
The use of physiologically based kinetic (PBK) modelling to translate *in vitro* concentration response curves to *in vivo* dose response curves as an alternative way for risk assessment.

The rate at which *in vitro* toxicity data are currently generated is high. For example, the EPA ToxCast project completed the evaluation of over 2,000 chemicals from a broad range of sources, including industrial and consumer products, food additives, and potentially "green" chemicals that could be safer alternatives to existing chemicals (Richard et al. 2016). These chemicals were tested in over 700 different high-throughput *in vitro* screening assays covering a range of endpoints and signalling pathways. To use these data for risk assessment purposes, the *in vitro* concentration-response data should be translated to *in vivo* dose-response data via PBK modelling-facilitated reverse dosimetry. In the process of chemical development, this PBK modelling-facilitated reverse dosimetry approach is useful to select chemicals for which low toxicity is expected in the *in vivo* situation (for example to select chemicals for which toxic effects will be observed at ≥1000 mg/kg bw, which is unlikely to be reached in most real-life exposure situations). PBK models should be able, ideally with a minimum amount of

effort to generate the required parameter values, to predict whether effect concentrations obtained in an *in vitro* assay translate to *in vivo* relevant doses, that is: whether the *in vivo* doses required to reach the effect concentrations in plasma or a target tissue are above 1000 mg/kg bw, the maximum dose level required in regulatory safety testing, indicating it is unlikely to be relevant in real life.

Given that the development of a PBK model for each individual compound can be resource and time consuming, it is obvious that in order to be able to judge the impact of the *in vitro* toxicity data for the *in vivo* situation, efforts have to be directed at the development of efficient and generic PBK models for large groups of compounds. Such generic PBK models need to be relevant and efficient to cope with many chemicals. However, the generic models developed so far may not be applicable (i.e. generate results that do not correlate with the actual *in vivo* situation) for compounds with specific characteristics. This may hold especially for compounds where active transport is involved in their excretion via the bile or the kidney. So far, excretion processes are generally ignored and not included in the generic PBK models mainly because for many compounds their clearance is not dominated by their rate of active excretion and because adequate *in vitro* models to characterize and quantify the relevant kinetic parameters for active excretion are missing.

Aim of the present thesis
The aim of the present thesis is to incorporate excretion via active transport through either urine or bile in generic physiologically based kinetic (PBK) models based on *in vitro* data. To meet this aim, *in vitro* models for both renal and biliary excretion are needed to obtain kinetic data on the active transport of different model compounds. Subsequently, the data are implemented in the PBK model to predict blood concentration time curves and compare the predictions made to existing *in vivo* kinetic data. These results are then compared to predictions made without taking active excretion into account. When the model is evaluated a follow-up step is made by using it for quantitative *in vitro in vivo* extrapolation (QIVIVE) purposes and prediction of the toxicity of the model compounds by deriving a POD for their risk assessment.

I.2   Physiologically based kinetic modelling

A physiologically based kinetic (PBK) model is a tool, which assumes that a set of mathematical equations can describe the absorption, distribution, metabolism and excretion (ADME) characteristics of a compound within an organism (Louisse et al. 2017). In a PBK model, organs and tissues are defined in separate or combined compartments, which represent key organs in the ADME or toxicity of the compound

of interest e.g. the liver for metabolism, or the lungs as a route of exposure or the heart as a target organ for adverse effects. Any tissue or organ not directly contributing to ADME or being relevant for the toxicity of a compound can be included in either a slowly or richly perfused tissue compartment. A PBK model consists of differential equations describing the change in the amount of the compound of interest or its relevant metabolite(s) over time in the various compartments (Rietjens et al. 2011). To define these differential equations three types of parameters are required, which are a) physiological and anatomical parameters (e.g., weight of tissues and organs, cardiac output and blood flow to the tissues), b) physicochemical parameters (e.g., the blood/ tissue partition coefficients) and c) kinetic parameters (e.g. the kinetic constants for metabolism or active excretion). The physiological and anatomical parameters can be found in literature (Brown et al. 1997a; Hall et al. 2012) and the physicochemical parameters can be calculated based on quantitative property-property relationship (QPPR) approaches (Berezhkovskiy 2004; DeJongh et al. 1997; Poulin and Theil 2000; Rodgers and Rowland 2006). The kinetic parameters can be obtained from experimental *in vitro* work or taken from the literature. With a PBK model physiologically relevant concentrations of a compound in any target organ of interest can be modelled for a certain dose, time point and route of administration. Upon validation of the model against available *in vivo* data from literature, the PBK model can be used to convert *in vitro* concentrations to relevant *in vivo* exposure levels, by so-called reverse dosimetry. In this reverse dosimetry approach, unbound *in vitro* concentrations of the concentration-response curve are set equal to unbound plasma or tissue concentrations of the respective compound in the PBK model, following which the PBK model can calculate the corresponding *in vivo* dose level for any given route of administration. Subsequent benchmark dose (BMD) modelling can be applied on the predicted *in vivo* dose-response data, enabling the determination of a POD for risk assessment, like a $BMDL_{10}$.

I.3   Excretion

The body has a number of routes for the excretion of compounds present in the systemic circulation or tissues, including excretion via the kidneys into urine, via the stool, via the liver into bile, via the lungs in exhaled air, or through sweat, saliva, tears, and via mothers' milk (Lu 2019). In this thesis, the focus lies on the two most important routes; excretion via the liver (bile) and the kidney (urine). In particular, the excretion that involves active (drug) transporters is taken into account.

I.3.I   Active transporters

Virtually all cell membranes contain active transporters that can have an important role in the kinetics of a compound. In humans approximately 400 transporter-like

genes are expressed and are categorized into two major superfamilies: the ATP-binding cassette (ABC) transporters and the solute carrier (SLC) transporters where the ABC transporters are in minority (48 members) compared to the SLC transporters (over 300 members) (Keogh 2012). The superfamilies can be categorized further, based on similarity of function and/or gene sequence of the transporters. The broad substrate specificities of the ABC transporters and SLC transporters include, metal ions, bile salts, sugars, hormones, amino and nucleic acids, small peptides and nucleosides, and xenobiotics (Keogh 2012). All the ABC and many of the SLC transporters behave as active transporters. ABC transporters are multimembrane-spanning proteins, which drive the transport of solutes against an electrochemical gradient, using energy from ATP hydrolysis (Morrissey et al. 2013; Wilkens 2015). This mode of active transport is generally referred to as primary active transport since no additional biochemical step other than ATP hydrolysis is needed (Sherrmann 2008). SLC transporters are integrated into the membrane and function to move solutes into or out of cells either by facilitated transport along the electrochemical gradient or by cotransport against an electrochemical gradient where they use the concentration gradient of another solute (Colas et al. 2016; Morrissey et al. 2013). This mode of active transport is referred to as secondary active transport (Sherrmann 2008).

I.3.2   Biliary excretion

The route of biliary excretion is relevant for chemicals, drugs, metabolites and endogenous compounds such as bile acids and metabolites of hormones. Via the portal venous blood or hepatic portal blood the compounds reach the sinusoidal side of the hepatocytes. Upon entering the hepatocytes, compounds can be metabolised, bind non-specifically, efflux actively or passively back into the hepatic portal blood or towards the hepatic venous blood or be transported over the canalicular membrane and excreted into the bile (Yang et al. 2009). Uptake into the hepatocyte can either be through passive diffusion or via active transport. When the uptake is active, it is facilitated by one or more of the several organic anion transporting polypeptides (OATPs) (OATP1B1/3; *SLCO1B1* and *1B3,* OATP2B1*; SLCO2B1*), organic anion transporters (OATs) (OAT2; *SLC22A7*) and organic cation transporters (OCTs) (OCT1; *SLC22A1*) (Patel et al. 2016). Secretion into the bile is always facilitated by active transporters with especially P-glycoprotein (Pgp, or multidrug resistance transporter (MDR-1); *ABCB1*), multidrug resistance associated protein 2 (MRP2; *ABCC2*), breast cancer resistance protein (BCRP; *ABCG2*) or the bile salt export pump (BSEP; *ABCB11*) being involved in the active biliary excretion of xenobiotics (Jetter and Kullak-Ublick 2020). Subsequently, the xenobiotics are excreted with the bile into the intestine where they will either be excreted with faeces or can be reabsorbed, undergoing enterohepatic circulation. Common properties of compounds and metabolites that are excreted via the bile are that they have a high polarity and ionisable groups causing them to have low membrane permeability and have a molecular

weight above a cut off of 475 Da (in humans) (400 Da for rats) (Rollins and Klaassen 1979; Yang et al. 2009). Note: throughout the entire introduction a distinction between human and rat transporters is made by referring to human transporters with all capital letters and to rat with small letters where only the first letter is in capital.
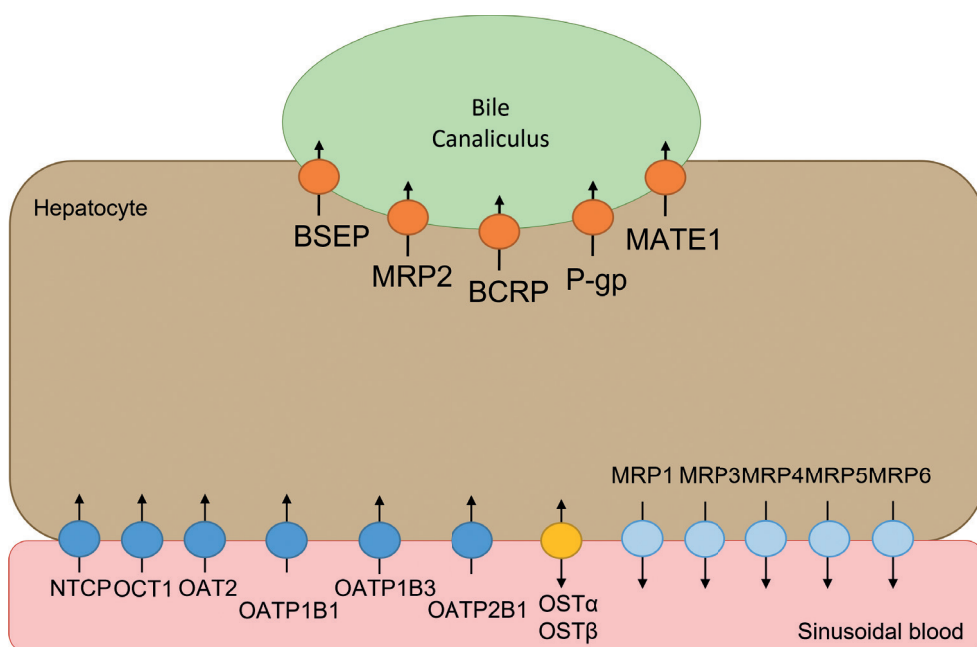
Figure 2.
Overview of the drug transporters present in the hepatocyte with uptake transporters from blood to cell in blue, bidirectional transporters in yellow, efflux transporters from cell back to blood in light blue and efflux transporters from cell to the bile canaliculus in orange.

PBK models incorporating biliary excretion to date

In pharma, research in physiologically based pharmacokinetic (PBPK) models and their application is ahead of similar research in toxicology especially with respect to incorporating biliary excretion. This is due to the fact that certain drug classes are known to make extensive use of the transport proteins present in the hepatocytes such as statins and angiotensin II receptor antagonists (Hirano et al. 2004; Yamashiro et al. 2006) and that for these compounds many clinical studies have been performed that are now useful for PBPK model evaluation. For instance, a study by Watanabe et al. (2009) developed a rat and human PBK model for pravastatin incorporating *in vitro* transporter kinetics for OATP1B1and MRP2 obtained using hepatocytes and canalicular membrane vesicles together with metabolism data from liver S9 incubations. The PBK model consisted of a comprehensive liver compartment containing five units of extracellular and subcellular compartments to fit the hepatic disposition to the dispersion model. In the

same year, Poirier et al. (2009) reported on a human (and rat) PBK model for valsartan incorporating *in vitro* transporter kinetics for OATP1B1/1B3 obtained using fresh and cryopreserved hepatocytes from rat and human and a cell line with overexpression of the mentioned transporters. Jones et al. (2012) reported on incorporating human *in vitro* transport data of seven OATP substrates (pravastatin, cerivastatin, bosentan, fluvastatin, rosuvastatin, valsartan and repaglinide) using sandwich-cultured hepatocytes to define the kinetic parameters for the PBK modelling. Furthermore, a study by Jamei et al. (2014) focussed on the IVIVE of liver *in vitro* transporter data using rosuvastatin as the model compound and further predicted the drug-drug interactions with cyclosporine in human. In 2015, Chapy et al. (2015) reported on incorporating *in vitro* transporter data from both hepatocytes and cell systems overexpressing OATP transporters for the compound irbesartan and developed a human PBK model.

Each of the mentioned studies provided different methods of translating the *in vitro* obtained kinetic transport parameters into *in vivo* transport. As later in this chapter a whole section is dedicated to scaling methods, the ones used in the mentioned studies are only briefly summarized here. Hepatocytes obtained transporter kinetic data were scaled to whole liver using a so-called physiological scaling factor of 1.2×10^8 cells/g liver (Watanabe et al. 2009) or with multiple factors such as the mg protein/million hepatocytes and the million hepatocytes/g liver (Poirier et al. 2009). So-called relative activity factors (RAF) or relative expression factors (REF) were obtained (Chapy et al. 2015; Jamei et al. 2014; Jones et al. 2012) and empirical scaling factors were used (Jones et al. 2012). A scaling factor for hepatocytes reported by Jamei et al. (2014) was based on the multiplication of the million hepatocytes/g liver, liver weight, the REF, and conversion factors such as time and volume to go from *in vitro* clearance to *in vivo* clearance.

I.3.3 Renal excretion

The kidneys are very important excretory organs for the removal of drugs, metabolites and endogenous waste products. The smallest unit of the kidney is the nephron of which humans contain around 1 million per kidney (Bertram et al. 2011). The nephron consists of Bowman's capsule which contains the glomerulus where filtration takes place. The filtrate subsequently passes through the different segments of the nephron (proximal convoluted tubule, loop of Henle and distal convoluted tubule), and ends at the collecting ducts where the filtrate is led to the bladder to store the formed urine before it is excreted (Lote 2012). Renal excretion is determined by three different processes: (1) glomerular filtration, (2) active tubular secretion, (3) active and passive reabsorption (Yin and Wang 2016). In brief, chemical/drug compounds and endogenous waste products are transported via the renal arteries to the kidneys, where the unbound low molecular mass molecules are passively filtered by the glomerulus into

pro-urine, subsequently following the route described earlier. The molecules that are bound to plasma proteins or are too large to pass the porous glomeruli remain in the arterioles, which after the glomerulus wrap around the rest of the nephrons and then are referred to as peritubular capillaries. Via the peritubular capillaries the chemicals reach the first segment of the nephron where the renal proximal tubular epithelial cells (RPTEC) are located. Using the active transporters in the basolateral membrane of the RPTEC and the active transporters in the apical membrane, the chemicals can cross this cellular barrier and reach the tubular lumen to eventually be excreted. The main secretory transporter present in the RPTEC for cationic compounds is the organic cation transporter 2 (OCT2; *SLC22A2*) on the basolateral membrane and the multidrug and toxin extrusion proteins MATE1 (*SLC47A1*) and MATE2K (*SLC47A2*) on the apical membrane. The weak acidic compounds are transported over the RPTECs using OAT1 (*SLC22A6*) and OAT3 (*SLC22A8*) at the basolateral membrane and MRP2 and MRP4 (*ABCC4*) at the apical membrane. Furthermore, efflux transporters such as P-gp and BCRP are present as well.
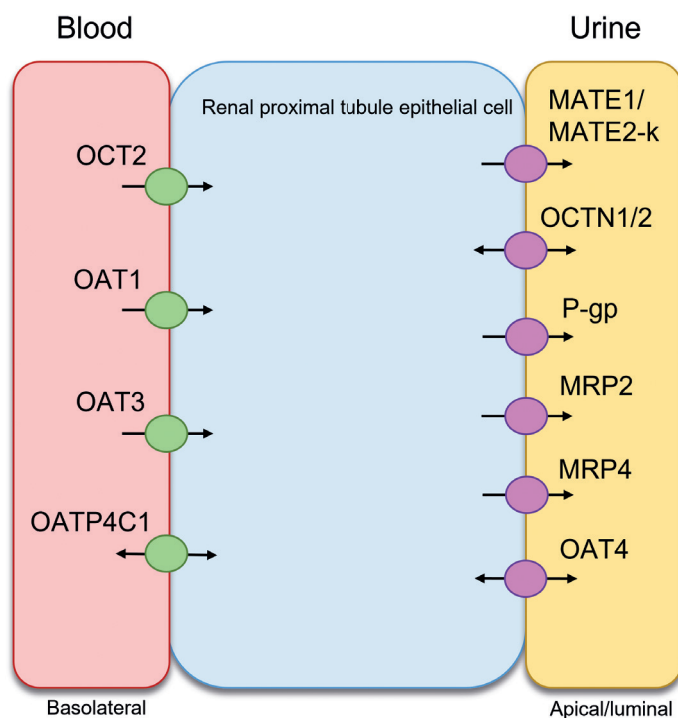
Figure 3.
Overview of the drug transporters present in the renal proximal tubule epithelial cells with uptake transporters from blood to cell in green, efflux transporters from cell to renal lumen in pink and bidirectional transporters with double arrowheads.

OCT2 transporter

Organic cation transporter 2 (OCT2) is the most abundant cation transporter present in RPTEC and plays an important role in clearance of chemicals and drugs from the body. OCT2 translocates usually small and hydrophilic cations from the blood circulation into the renal tubule cells. Its transport is electrogenic and Na$^+$-independent, and is facilitated by the inside-negative membrane potential existing in the RPTEC (Yin and Wang 2016). For example, weak bases with a nitrogen moiety bear a net positive charge at physiological pH. This results in an electro-statical interaction with the binding sites of OCT2 (Koepsell 2013; Sherrmann 2008). In the present thesis, the focus lies on OCT2 for several reasons. 1) OCT2 is expressed predominantly in the kidney rather than other tissues (in rats exclusively in the S3 segment of the proximal tubule) (Dresser et al. 2001). 2) OCT2 is the most abundant OCT in the RPTEC basolateral membrane, it is polyspecific meaning that it transports multiple structurally different substrates and thus is a relevant transporter to investigate renal excretion of compounds (Koepsell 2013). 3) Transport of organic cations via OCT2 takes place in one direction (from blood to RPTEC), there is no reabsorption back into the blood, which can be the case with some organic anion transporters (Wright 2019).

I.4   Kidney models known to date

Over the years, attempts to describe and include renal clearance into mechanistic (kidney) models have been made. The first attempt on describing such a model was done by Russel et al. (1987). They incorporated glomerular filtration and a compartment representing the renal proximal tubular cells for salicyluric acid (a metabolite of salicylic acid) excretion in dogs and included nonlinear protein binding. The kinetic parameters were calculated from the plasma concentration time curves and renal excretion rate-time curves obtained in the dogs and the data points were interpolated. Other examples are: inclusion of saturable reabsorption of the water-soluble vitamin riboflavin where linearization of the *in vivo* experimental data resulted in determination of an overall Vmax and Km (since in this study it was not yet unravelled that there are different transporters) (Jusko and Levy 1970), inclusion of reabsorption of four drugs, sulfanilamide, sulfamethizole, theophylline, and ethanol by using nonlinear least squares regression analysis with the Gauss-Newton method on the *in vivo* data (Komiya 1986) and inclusion of reabsorption via monocarboxylate transporter 1 (MCT1) of a drug of abuse, γ-hydroxybutyrate (GHB), based on fitting of the kinetic parameters to the *in vivo* data (Wang et al. 2008). Until this point in time (circa 2008), no attempts have been made to include reabsorption or excretion based on *in vitro* input. Also the prediction of human renal clearance using PBK-models was usually based on allometric approaches, which were proven to perform poorly (Fagerholm 2007; Paine et al. 2011). A study in

2010 by Felmlee et al. (2010) reported on the prediction of the urinary excretion of GHB also focussing on active renal absorption via MCT by estimating the Km by a first-order conditional estimation method with a so-called ADVAN9 differential equation solver. This resulted in an estimated Km of 0.46 mg/mL, which was in line with earlier findings from *in vitro* uptake studies in MCT1expressing MDA-MB231 cells reporting a Km amounting to 0.48 mg/mL (Wang et al. 2006). At present, not even a handful of studies have tried to incorporate *in vitro* experimental data from active excretion and/or reabsorption for PBK-model predictions. The study by Worley and Fisher (2015) reported on a rat PBK-model containing *in vitro* kinetic data for the organic anion transporter (Oat) 1 and 3 and the organic anion transporting polypeptide (Oatp) 1a1 for active transport to predict perfluorooctanoic acid urinary excretion. The previously reported Vmax values of the *in vitro* obtained kinetic data for perfluorooctanoic acid from human embryonic kidney (HEK-293) cells or Chinese hamster ovary (CHO) cells overexpressing the aforementioned transporters were translated to *in vivo* Vmax parameters using relevant scaling factors (which will be presented in some more detail in a later section) (Nakagawa et al. 2008; Weaver et al. 2010). Another study by Huang and Isoherranen (2018) reported on incorporating *in vitro* permeability data of 46 compounds consisting of mainly Caco-2 data and a few Madin-Darby Canine Kidney (MDCK) II data into a PBK-model to predict renal clearance based on filtration and pH-dependent passive reabsorption. These studies demonstrated the feasibility of the model to include active excretion of para-aminohippuric acid (PAH) and cimetidine by inclusion of *in vitro* kinetic data for transporters: NTP1, MRP2/4, OAT1/3 OCT2 and MATE1/2K. The assumption was that the transporter expression level per mg of *in vitro* system was equal to the transporter expression level per mg of human kidney and that a person has 300 grams of kidney. Although the predicted renal clearance data were for 87% of the drugs withing two-fold from the observed data, the PBK-model existed of 35 compartments making it not a very generic model.

I.4.1 Kidney cell lines

To obtain kinetic parameters for renal excretion in an *in vitro* model, a cell line needs to be chosen with functional active transporters. This is not as straight forward as it would seem, because most available kidney cell lines – including for example cells from the human kidney (HK-2) cell line, the normal rat kidney (NRK-52E) cell line, the MDCK-II cell line and the porcine kidney (LLC-PK1) cell line – (like cell lines of other tissues) only reflect the RPTEC *in vivo* to a certain extent meaning that certain transporters are not present or the expression (in animal cell lines) shows substantial variation compared to human (Jenkinson et al. 2012; Lechner et al. 2021; Sanchez-Romero et al. 2020). Additionally, the use of primary RPTEC cells in culture results in a rapid loss of expression of transporters and other energy consuming proteins (Lechner 2014) and show large donor-to-donor variation (Bajaj et al. 2018) making

them inconvenient for transport studies. To overcome this drawback of using these cell lines to study active renal excretion, two approaches can be followed. The first approach includes use of transfected cell lines with overexpression of the transporter of interest (in parallel with a mock transfected cell line for comparison). The gene for the transporter of interest can be cloned into a common cell type e.g., HEK-293 or CHO cells (usually uptake transporters) or into membrane vesicles (usually efflux transporters). Generally, membrane vesicles are prepared from *Spodoptira frugiperda* (Sf9) insect cells and can be transfected with genes encoding efflux transporters. Preparation of membrane vesicles from Sf9 cells results in a percentage that are in an inside-out configuration. This allows the transporters to shuttle substrates from the buffer and trap them inside the vesicles (van Staden et al. 2012). Transport studies with these systems (HEK-293 or CHO cells and membrane vesicles with transfected transporter of interest) result in kinetic parameter values for the respective transporter without confounding contributions of other cellular transporters given that these are absent in the original cell lines. However, such transfected cell models are almost never representative for the tissue of interest (NB: insect cell membranes). The second approach is to go for a physiologically relevant cell line. The availability of such cell lines is, however, limited. There is the immortalized RPTEC/TERT1 cell line where the expression of most relevant transporters was reported to be stable, except for the OAT1 and OAT3 which were hardly expressed, and detected only when the cells were cultured in 3D (Secker et al. 2018; Secker et al. 2019). The same holds true for the conditionally immortalized proximal tubule epithelial cell line (ciPTEC) (Wilmer et al. 2010). To overcome this, the ciPTEC cells were completed by transfection of the OAT1 and OAT3 (Nieskens et al. 2016). In the present thesis we have selected a human kidney cell line (SA7K-clone) developed by the group of Li et al. (2017c). The SA7K cell line was generated via zinc finger nuclease-mediated knockout of a cell cycle protein to bypass cellular senescence. This pseudo-immortalized cell line had extended cell doubling capacity and was characterized in terms of kidney-specific functional properties, such as response to a limited number of known human nephrotoxicants, as well as with respect to uptake and efflux transporter activities. Also, here on mRNA level OAT1 and OAT3 were not detectable, although contrasting results were shown when uptake of the OAT1 substrate p-aminohippuric acid (PAH) was inhibited in the presence of probenecid, raising an issue that remains to be elucidated. For this thesis, however, the presence or absence of the OAT transporters was not of concern as the OCT2 transporter was the target transporter.

I.5   Scaling *in vitro* to in vivo

For clinical pharmacokinetic predictions from animal data to human, allometric scaling is often used and appeared useful for drugs that are eliminated passively (glomerular filtration). However, allometry does not seem to be a reliable scaling method when it comes to compounds that are predominantly cleared via a transporter-mediated process due to species differences in transporter function and expression (Chu et al. 2013a; Mathialagan et al. 2017). Therefore, to extrapolate kinetic data of membrane transporters from the *in vitro* to the *in vivo* situation appropriate scaling factors should be defined (Choi et al. 2019). Kinetic data of membrane transporters are for a large part obtained via cell systems or membrane vesicles overexpressing the transporter of interest (Chan et al. 2019; Hirano et al. 2004). When including these data in a PBK model the Michaelis-Menten kinetic constant, Km, of the transporter for the compound of interest is assumed to be the same *in vitro* and *in vivo*. However, the Vmax *in vitro* (expressed in pmol/min/mg protein) has to be translated to a Vmax *in vivo* (expressed in μmol/hr). Factors to take into account for appropriate scaling and *in vitro* to *in vivo* extrapolation are: differences in the amount of protein per gram tissue, differences in the (negative) membrane potential *in vitro in vivo*, differences in transporter expression, and transporter abundance and species differences. Two main approaches often chosen for extrapolation from cells or vesicles overexpressing a desired transporter to the *in vivo* situation are 1) determining the relative activity factor (RAF) or 2) determining the relative expression factor (REF). With the RAF approach a probe substrate for the transporter of interest is needed. The activity of the transporter for the probe substrate is divided by the activity for the compound of interest. For the REF approach, the abundance of the transporter is quantified *in vivo* and *in vitro* providing the basis to define the REF value as the quotient between these two abundancies. Both approaches have been used successfully for extrapolation purposes for both liver transporters and kidney transporters with no significant difference between the REF or the RAF method (Izumi et al. 2018; Kumar et al. 2020; Kunze et al. 2014; Mathialagan et al. 2017). Using an *in vitro* model resembling the physiology of the organ of interest, it means that direct targeting of one transporter faces more challenges, because more transporters may be present and involved. In this case acquiring transport data requires transport studies in the absence and presence of an inhibitor of the transporter of interest.

I.6   Model compounds

To provide proofs-of-principle regarding the stated aim of the thesis, several model compounds were chosen (Figure 4). For studies including both excretion routes, the main required characteristic for the model chemicals chosen is that the compound

should be preferably cleared via transport and not via metabolic conversion and that the transport process chosen was rate-limiting in the elimination. For biliary excretion it was important to choose a substrate with a main excretion route via hepatic transporters to the bile and a negligible clearance through the kidneys. Thereby it is best and easiest to model following intravenous administration of the compound, as biliary excretion takes place directly after exposure and bioavailability following oral administration does not need to be taken into account. For renal excretion the characteristics were that the chemicals were substrates for the OCT2 transporter facilitating a unilateral excretion pathway, which eliminates the need for including reabsorption of the chemical, and that the biliary excretion route was negligible. This resulted in selection of estradiol-17β glucuronide (figure 4) for studies on biliary excretion and of mepiquat chloride, paraquat dichloride and tetrodotoxin (figure 4) for studies on renal clearance.
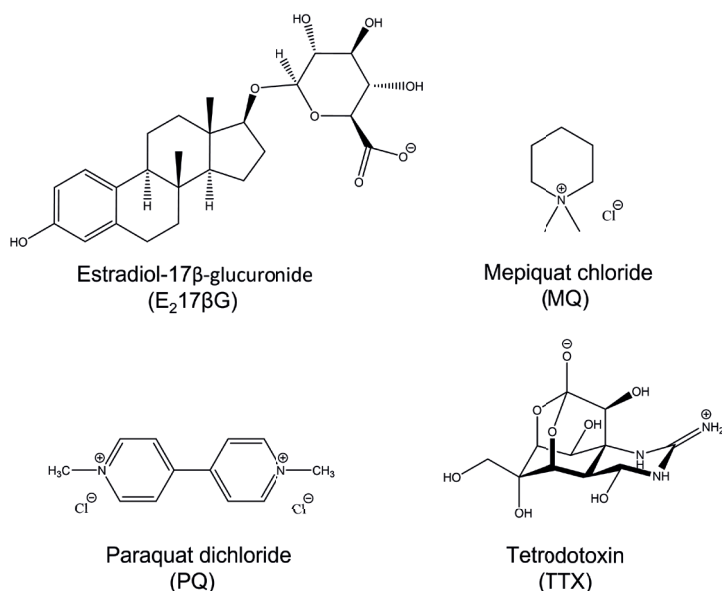
Figure 4.
Molecular structures of the model compounds used in this thesis, where estradiol-7β-glucuronide is a model compound for biliary excretion and mepiquat chloride, paraquat dichloride and tetrodotoxin are model compounds for renal excretion

Estradiol-17β-glucuronide (biliary excretion)
Estradiol-17β-glucuronide (E$_2$17βG) is an anionic endogenous oestrogen glucuronide conjugate well known for its high affinity for active transport in the liver. Elimination of E$_2$17βG proceeds by uptake from the blood (sinusoidal side) via the organic anion transporting polypeptides (OATP1B1/1B3) into the hepatocytes and subsequent

excretion into the bile canaliculi via the multidrug resistance associated protein 2 (MRP2). The OATP uptake of $E_217\beta G$ into the hepatocytes is the rate-limiting step for its elimination via bile (Varma et al. 2012).

Mepiquat chloride (renal excretion)

Mepiquat (MQ) chloride (N,N-dimethyl-piperidinium chloride) is a plant growth regulator pesticide that is used exclusively on cotton crops (Tung 2020). Use of MQ will increase cotton yield through inhibition of gibberellic acid synthesis. MQ is a water soluble cationic quaternary ammonium compound, which is not metabolised and excreted predominantly in its parent form via the urine (Agency 1997). Animal studies showed fast urinary excretion of MQ pointing at an active secretory component in addition to glomerular filtration (BASF, oral communication/ unpublished results). MQ therefore makes a good substrate for the most abundantly expressed active transporter in the kidney, the organic cation transporter 2 (OCT2). The role of active transport for MQ kinetics has not been studied thus far and will be further elucidated aided by PBK modelling.

Paraquat dichloride (renal excretion)

Paraquat (PQ) dichloride (N,N′-dimethyl-4,4′-bipyridinium dichloride) is a herbicide belonging to the bipyridylium quaternary ammonium herbicide family. The herbicidal properties of PQ were first discovered in 1955 at the Jealotts' Hill international Research Centre, Bracknell, UK and PQ came on the market 1962 via Plant Protection Division Ltd of Imperial Chemical Industries (ICI; now Syngenta) (Dinis-Oliveira et al. 2008). Exposure to too high levels of PQ is accompanied by serious toxicity, especially in the lungs where PQ will undergo a redox-reaction in the presence of oxygen leading to production of reactive oxygen species and ultimately leading to lung fibrosis and respiratory failure (Allen 2019). Other organs affected by PQ intoxication are the kidneys and the liver (Dinis-Oliveira et al. 2008). Due to its toxicity PQ has been banned in 2007 for use in the European Union ((EU) 2007). PQ is rapidly absorbed from the small intestine although the fraction absorbed is low (5%) (Houze et al. 1990). Furthermore, PQ is hardly metabolized and its predominant route of excretion is in unmodified form via the kidneys into urine. While glomerular filtration plays a pivotal role in its elimination, PQ clearance exceeds the glomerular filtration rate, indicating an active secretion component which was reported to mainly involve OCT2 and the multidrug and toxic compound extrusion (MATE) transport protein (Chan et al. 1998; Chen et al. 2009; Chen et al. 2007).

Tetrodotoxin (renal excretion)

Tetrodotoxin (TTX) is a naturally occurring neurotoxin that can be found in various marine gastropods and some fish species (Bane et al. 2014; Control and Prevention 1996). TTX is a potent voltage gated sodium channel blocker (Sui et al. 2002) preventing depolarization and propagation of action potentials in nerve cells, resulting in the loss of sensation (Bane et al. 2014). The acute exposure to TTX leads to a wide range of acute adverse effects including skeletal muscle fasciculations, apathy, lethargy, ataxia, paralysis and even death (Bane et al. 2014). Upon oral exposure, TTX absorption is rapid but incomplete (around 7%), there is hardly metabolism of TTX in the liver and with its highly hydrophilic characteristic TTX is predominantly excreted via the urine (Hong et al. 2017; Hong et al. 2018). Due to the charges on the molecule it is foreseen that excretion of TTX, next to glomerular filtration, will proceed via active transporters in the renal proximal tubule epithelial cells, most likely the OCT2 transporter with a lesser contribution of OCTN1/2, MATE and OATs (Matsumoto et al. 2017). Using PBK modelling the active transport of TTX will be further unravelled.

1.7   Outline of the thesis

Chapter 1 gives an introduction on the topic of new approach methodologies, incorporation of active excretion via bile and urine into physiologically based kinetic models and formulates the aim of the thesis: to incorporate excretion via active transport through either urine or bile in physiologically based kinetic (PBK) models based on *in vitro* data.

Chapter 2 shows a first proof of principle on how to incorporate active biliary excretion into a PBK model using estradiol-17β-glucuronide (E$_2$17βG) as the model compound. The PBK model kinetic parameters for transport of E$_2$17βG via the organic anion transporting polypeptides (Oatps) in rat were obtained from literature studies with rat hepatocytes and the scaling factor required to convert the *in vitro* kinetic data to the *in vivo* situation were determined by fitting the predictions made to available *in vivo* kinetic data.

Chapter 3 establishes a first proof of principle on how to incorporate active renal excretion of the model compound mepiquat (MQ) via the organic cation transporter 2 (OCT2) in a PBK model using *in vitro* data obtained from the human renal proximal tubule epithelium cell line (SA7K). Data from this cell line were obtained via characterisation of the time- and concentration-dependent uptake of MQ in the absence and presence of the OCT2 inhibitor doxepin. The obtained Vmax and apparent Km were implemented in a PBK model and blood concentrations in time were predicted. A

scaling factor was determined and included to link the PBK model predictions to the *in vivo* data.

Chapter 4 aims to incorporate OCT2 transport of the model compound paraquat (PQ) using SA7K cells in to a PBK model and subsequently apply reverse based dosimetry to determine PODs of PQ. *In vitro* concentration-response curves obtained by exposing rat alveolar type II cells (RLE-6tn) to increasing concentration of PQ to measure cytotoxicity were translated to *in vivo* dose response curves for the toxicity of PQ, which were compared to literature data on *in vivo* PQ toxicity.

Chapter 5 provides a proof of principle for predicting acute neurotoxicity of the model compound tetrodotoxin (TTX) in rodents using *in vitro* toxicity data and PBK modelling. Renal excretion via both glomerular filtration and active excretion were included in the model for TTX. Gathered *in vitro* concentration-response curves for TTX toxicity by the rat MEA assay and mouse neuro-2a cells were translated to *in vivo* dose-response curves using the PBK models. PODs were established for both rat and human and compared to *in vivo* toxicity data.

Chapter 6 encompasses the general discussion on points that laid beyond the scope of the individual chapters. The chapter gives more insights in the use of *in vitro* models for incorporating transporter kinetics in PBK models and the pros and cons of using the SA7K cell line as a model to quantify transport kinetics *in vitro*. Furthermore, an in-depth discussion is provided on the use of generic PBK-models, the choice of model compounds, scaling factors for QIVIVE, how this work will contribute to the 3Rs, the importance of taking active excretion into account for a number of chemicals, future work and next steps.
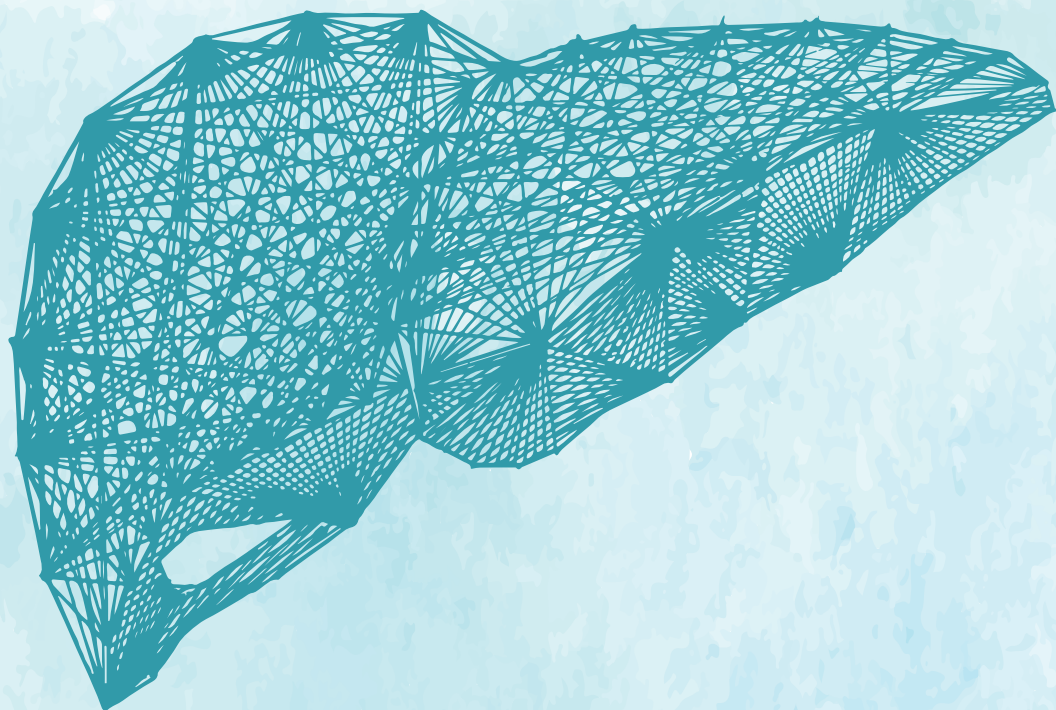
Chapter 2

Novel testing strategy for prediction of rat biliary excretion of intravenously administered estradiol-17β glucuronide

Annelies Noorlander, Eric Fabian, Bennard van Ravenzwaay, Ivonne M.C.M. Rietjens

Abstract

The aim of the present study was to develop a generic rat physiologically based kinetic (PBK) model that includes a novel testing strategy where active biliary excretion is incorporated using estradiol-17β glucuronide (E$_2$17βG) as the model substance. A major challenge was the definition of the scaling factor for the *in vitro* to *in vivo* conversion of the PBK-model parameter Vmax. *In vitro* values for the Vmax and Km for transport of E$_2$17βG were found in literature in four different studies based on experiments with primary rat hepatocytes. The required scaling factor was defined based on fitting the PBK-model based predicted values to reported experimental data on E$_2$17βG blood levels and cumulative biliary E$_2$17βG excretion. This resulted in a scaling factor of 129 mg protein/g liver. With this scaling factor the PBK-model predicted the *in vivo* data for blood and cumulative biliary E$_2$17βG levels with on average less than 1.8-fold deviation. The study provides a proof of principle on how biliary excretion can be included in a generic PBK-model using primary hepatocytes to define the kinetic parameters that describe the biliary excretion.

Keywords: Physiologically based kinetic modelling · Biliary excretion · Primary rat hepatocytes · Scaling factor

List of abbreviations: ADME (absorption, distribution, metabolism, excretion), **E$_2$17βG** (estradiol-17β glucuronide), **Oatp**, (Organic anion transporting polypeptide), **PBK** (Physiologically based kinetic), **QIVIVE** (quantitative *in vitro – in vivo* extrapolation), **RAF** (relative activity factor), **TE** (transporter efficiency)

2.1 Introduction

The kinetic profile of a substance is of importance when considering human safety assessment and drug development. Prediction of these kinetic profiles based on absorption, distribution, metabolism and excretion (ADME) using physiologically based kinetic (PBK) modelling has been shown of value not only to predict blood levels of drugs following defined dose levels in forward dosimetry, but also in so-called reverse dosimetry for quantitative *in vitro – in vivo* extrapolation (QIVIVE) (Louisse et al. 2017; Rietjens et al. 2011). QIVIVE aims to contribute to the 3Rs of Russel and Burch (reduction, replacement and refinement) of animal experiments (Flecknell 2002; Louisse et al. 2015; Zhang et al. 2018a). Up to now, proofs of principle for human safety assessment using PBK-model facilitated QIVIVE have been mainly provided for chemicals that do not depend on active excretion via either kidneys or liver (Fabian et al. 2019; Louisse et al. 2010; Moxon et al. 2020; Ning et al. 2019b; Punt et al. 2019; Strikwold et al. 2017b).

In drug development, there already have been studies on QIVIVE using PBK-modelling focussing on especially excretion of certain drugs via active transport from the liver to the bile (Chapy et al. 2015; Jamei et al. 2014; Jones et al. 2012). In addition, both endogenous and exogenous glucuronide conjugates have also been shown to be actively excreted via this route (Cronholm et al. 1971; Ge et al. 2016; Hjelle and Klaassen 1984). The common properties of the compounds for which this active transport from liver into bile was shown important are that they have a low membrane permeability, a molecular weight cut off of 475 Da (400 Da for rats), remain mostly unchanged and therefore are excreted via active uptake and efflux in and from the liver cells into bile (Yang et al. 2009).

Given these structural characteristics it can be foreseen that biliary excretion may not only be relevant for drugs but also for other chemicals, including new chemicals (Choi et al. 2019). For these substances, active excretion should be included in the PBK-models to obtain an adequate description of their kinetics and subsequent prediction of *in vivo* effective dose levels. However, due to the lack of well-established and validated *in vitro* assays to quantify kinetics for active excretion there is a lack of PBK-models including active biliary and/or renal excretion. When not including active excretion in QIVIVE, the prediction of the time-dependent blood concentration can deviate from the *in vivo* situation resulting in incorrect determination of points of departure for human safety assessment when based on PBK-model facilitated reverse dosimetry (Louisse et al. 2017).

To be of value for novel non-animal based testing strategies, parameters required for the

PBK-models should preferably be defined using *in silico* and *in vitro* approaches. When using *in vitro* models for biliary excretion, important challenges relate to the type of *in vitro* model to be used and the subsequent translation of the *in vitro* data to the *in vivo* situation using adequate scaling factors (Choi et al. 2019). When using for example a cell model with overexpression of a transporter of interest, proper scaling depends on the expression level of the transporter in the cell model compared to its expression level in the organ *in vivo*. To solve this matter a relative expression factor (REF) can be used (Chan et al. 2019; Jamei et al. 2014). Moreover, because the activity of the transporter in the transfected cell can differ from its *in vivo* activity often a relative activity factor (RAF) is used as well (Izumi et al. 2018; Poirier et al. 2009). Other factors may further complicate this *in vitro* to *in vivo* scaling, such as the fact that the cell of origin used to generate the transfected cell model (e.g. human embryonic kidney cells, Chinese hamster ovaries, *Xenopus Laevis* oocytes, (Cattori et al. 2001; Eckhardt et al. 1999; van de Steeg et al. 2013)) may not fully represent the cell type of the designated organ making the *in vitro* to *in vivo* translation more complex. This implies that hepatocytes may provide an alternative model to define the kinetic parameters for biliary excretion (Cantrill 2017; Chu et al. 2013b; Yabe et al. 2011). Therefore, the aim of the present study was to develop a generic rat PBK-model incorporating a novel testing strategy of including active biliary excretion, focussing on hepatocytes as the *in vitro* cell model *and* the scaling factor to be used to obtain adequate *in vitro* to *in vivo* translation. This was done using estradiol-17β glucuronide ($E_2$17βG) (Fig. 1) as the model substance (molecular weight 448.5 g/mole). $E_2$17βG is an anionic endogenous estrogen glucuronide conjugate well known for its high affinity for active transport in the liver where it is taken up from the blood (sinusoidal side) via the (rat) organic anion transporting polypeptides (Oatps) into the hepatocytes, to be subsequently excreted into the bile (Kanai et al. 1996). This uptake of $E_2$17βG into the hepatocytes via the Oatps is the rate-limiting step for its elimination (Varma et al. 2012).
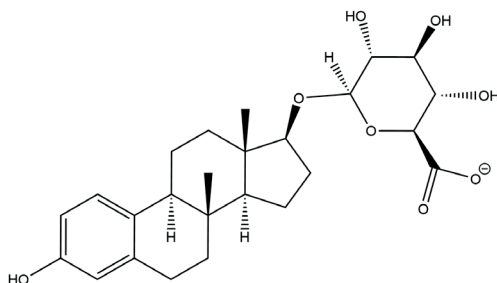
Figure I.
Chemical structure of estradiol-17β glucuronide

2.2 Materials and methods

Physiologically based kinetic (PBK) modelling

A conceptual PBK-model was developed for $E_2 17\beta G$ in rat (Fig 2). The model contained separate compartments for blood, fat and liver. All other organ tissues were divided in either a rapidly perfused tissue compartment (brain, heart, lungs, kidneys) or a slowly perfused tissue compartment (bone, skin, muscle). The gastro-intestinal tract was not included as a separate compartment since administration of $E_2 17\beta G$ was intravenously. Physiological and anatomical parameters such as tissue blood flow and tissue weight were obtained from Brown et al. (1997a). Tissue:blood partition coefficients were determined by a mathematical method described by DeJongh et al. (1997) based on the log Kow of $E_2 17\beta G$ (2.05 ALOGPS). Table 1 presents a detailed overview of the parameters.
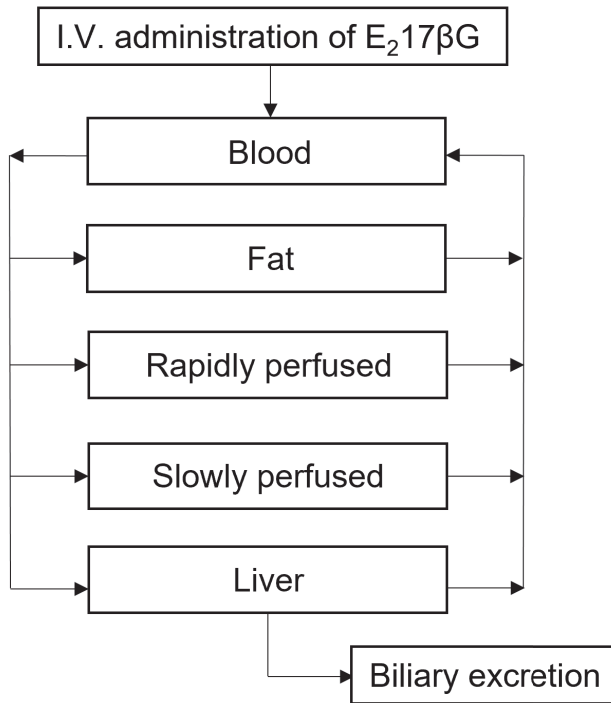
Figure 2.
Schematic overview of the PBK-model for $E_2 17\beta G$ including biliary excretion

The transport of $E_2 17\beta G$ from liver to bile was described by Michaelis-Menten kinetics using the following formula:

$$AL = QL \times (CB - CVL) - \left(Vmax_{E217bG} \times \frac{CVL}{(Km_{E217bG} + CVL)} \right)$$

(1)

where AL is the change in the amount of $E_217\beta G$ in the liver over time (μmol/hr), QL the blood flow to the liver (L/hr), CB the concentration of $E_217\beta G$ in arterial blood (μmol/L), CVL the venous concentration of $E_217\beta G$ in the liver (μmol/L), $Vmax_{E217bG}$ and Km_{E217bG} the maximum rate (μmol/hr) and Michaelis-Menten constant (μmol/L) for the transport of $E_217\beta G$. The model equations were encoded and solved using Berkeley Madonna 8.3.18 (UC Berkeley, CA, USA).

Although it is known that $E_217\beta G$ undergoes enterohepatic circulation, this was not taken into account in the model because for all the *in vivo* data included in this study the bile duct of the rats was cannulated, therefore, enterohepatic circulation could not take place.

Table 1.
Physiological and physico-chemical parameters used in the model code

Physiological and physico-chemical parameters	Rat
Body weight (kg)	0.250
Tissue volume fraction of the body weigh [a]	
Fat tissue	0.07
Liver tissue	0.034
Fraction of the blood	0.074
Rapidly perfused tissue	0.098
Slowly perfused tissue	0.724
Cardiac output (L/hr)	$15*BW^{\wedge 0.74}$
Blood flow fraction [a]	
Fat	0.07
Liver	0.174
Rapidly perfused tissues	0.234
Slowly perfused tissues	0.522
Tissue:blood partition coefficients [b]	
Fat:blood	19.87
Liver:blood	1.33
Rapidly perfused tissue:blood	1.33
Slowly perfused tissue:blood	0.60

[a] Brown et al. (1997a), [b] DeJongh et al. (1997)

In vitro kinetic data

The *in vitro* kinetic data for transport of $E_2$17βG into hepatocytes were obtained from the literature. Four studies, (Brock and Vore 1984; Brouwer et al. 1987; Ishizuka et al. 1998; Kouzuki et al. 1999) reported Vmax (pmol/min/mg protein) and Km (μM) values for the transport of $E_2$17βG into hepatocytes. Briefly, all studies used freshly isolated primary hepatocytes from Sprague-Dawley rats and radio-labelled $E_2$17βG. Three studies used a hepatocyte suspension system where concentration dependent uptake of [³H]-$E_2$17βG under linear conditions with respect to time was determined. At the end of each incubation, a fraction of hepatocyte suspension was removed from the incubations. This fraction was added to a tube containing silicon oil and 3 M KOH. The tube was centrifuged and cut at the silicone oil layer. The hepatocyte pellet was placed in a scintillation vial and radioactivity was measured. The other study cultured the freshly isolated hepatocytes on collagen-coated dishes. After washing the dishes three times with either a Krebs-Henseleit buffer or choline buffer, the uptake was initiated by adding [³H]-$E_2$17βG. The uptake was stopped and cells were washed three times using ice-cold Krebs-Henseleit buffer for both procedures. The cells were solubilised in 1 N NaOH, distilled water was added and [³H]-$E_2$17βG was measured with liquid scintillation. Protein content in all studies was determined using either the method of Lowry (Lowry et al. 1951) or the method of Bradford (Bradford 1976) with bovine serum albumin as a standard. The Vmax and Km values were determined by plotting the rate of uptake (pmol/min/mg protein) of [³H]-$E_2$17βG by the hepatocytes against the [³H]-$E_2$17βG concentration (μM) fitting the curve using the Michaelis-Menten equation.

Scaling factor

In the present study the scaling factor was determined by fitting the PBK-model based predicted values for blood concentrations and the cumulative biliary excretion of $E_2$17βG to the data reported for these endpoints in rat experiments found in literature. Table 2 presents an overview of available *in vivo* studies. They included *in vivo* rat kinetic data for the time-dependent plasma concentration of $E_2$17βG upon an intravenous dose level of 81 ng/kg bw (Gotoh et al. 2002; Morikawa et al. 2000) and 23 ng/kg bw (Slikker et al. 1983) and the time dependent cumulative biliary excretion of $E_2$17βG upon an intravenous dose level 81 ng/kg bw (Gotoh et al. 2002; Morikawa et al. 2000) and 48 ng/kg bw (Takikawa et al. 1996). Three of these studies used male Sprague-Dawley rats, one study used female Sprague-Dawley rats (Slikker et al. 1983). All studies quantified [³H]-$E_2$17βG by liquid scintillation counting. Since the PBK-model predicts whole blood concentrations and the *in vivo* data present time-dependent plasma concentrations, the plasma concentrations were converted to whole blood concentrations using the following formula:

$$C_{blood} = C_{plasma} \times (1 - Hct) \tag{2}$$

where C_{blood} is the concentration of E$_2$17βG in whole blood (μmol/L), C_{plasma} the concentration of E$_2$17βG in plasma (μmol/L) and Hct the rat haematocrit, which was set at 40%, the average of the range published (Probst et al. 2006). (See figure S1 in supplementary material A for original plasma concentration data).

Table 2.
Overview of *in vivo* studies reporting time-dependent blood concentration and cumulative biliary excretion upon intravenously administered E$_2$17βG in rats.

	Dose (ng/kg bw)	Time of sample collection (hr)	Reference
Time-dependent plasma concentration	81	0 - 1	Morikawa et al. (2000)
	81	0 - 1	Gotoh et al. (2002)
	23	0 - 1.5	Slikker et al. (1983)
Cumulative biliary excretion	81	0 - 2	Morikawa et al. (2000)
	81	0 - 2	Gotoh et al. (2002)
	48	0 – 1.5	Takikawa et al. (1996)

Comparison of the time-dependent plasma concentration reported by Morikawa et al. (2000) and Gotoh et al. (2002) using a similar dose of 81 ng/kg bw, indicated the data point at t = 1 hr reported by Gotoh et al. (2002) to be an outlier (figure S1 supplementary material A), and this data point was aligned with that from Morikawa et al. (2000) before further use of the Gotoh et al. (2002) data. In addition, because the time-dependent plasma concentrations reported by Slikker et al. (1983) at a dose of 23 ng/kg bw completely overlapped with both *in vivo* data sets at a dose of 81 ng/kg bw (figure S2 supplementary material A), these data were corrected to bring them in line with the rest of the data by correcting the blood concentrations by a factor of 0.284 (23 /81).

Combining the four *in vitro* kinetic data sets for the Vmax and Km of E$_2$17βG transport in rat hepatocytes with the six *in vivo* data sets on plasma E$_2$17βG and on cumulative biliary excretion of E$_2$17βG provided 24 fitted scaling factors, which were combined to generate a mean value for further PBK-model based predictions. All predicted curves and reported *in vivo* data were graphically illustrated using GraphPad Prism 5 (GraphPad Software Inc., San Diego, CA, USA)

To define the scaling factor as described above *in vitro* Vmax values expressed in pmol/min/mg protein have to be converted to an *in vivo* Vmax value expressed in μmol/hr/whole liver. This was done using the following formula :

$$\textit{In vivo } \text{Vmax} = \left(\frac{\textit{In vitro } \text{Vmax}}{1,000,000}\right) \times 60 \times \text{SF} \times \text{Volume of Liver} \times 1000 \tag{3}$$

where the factor 1,000,000 is used to convert pmol to μmol, 60 to convert minutes to hours, SF is the scaling factor expressed in mg protein/g liver, multiplied by the volume of the liver expressed in kilograms (Table 1), which is multiplied by 1000 to convert kilograms to grams.

The full model code is presented in Supplementary material B

Sensitivity analysis

To assess the influence of the scaling factor on the model predictions and to assess the model parameters that can influence the model output most, a sensitivity analysis was performed for both the predicted concentration of $E_2 17\beta G$ in blood and its predicted cumulative biliary excretion. To carry out the sensitivity analysis, a dose level of one of the available rat studies was used, 81 ng/kg bw. The analysis was performed using the values for Km and Vmax obtained from the rat hepatocyte study with the lowest transporter efficiency (TE) (calculated as V_{max}/K_m) (Brouwer et al. 1987) and the highest transporter efficiency (Kouzuki et al. 1999). Based on the method reported by Evans and Andersen (2000) the sensitivity coefficients (SCs) for the model parameters were calculated as follows:

$$\text{SC} = (\text{C}' - \text{C})/(\text{P}' - \text{P}) \times \text{P/C} \tag{4}$$

where C indicates the initial value of the model output, C' indicates the modified value of the model output resulting from an increase in the parameter value. P indicates the initial parameter value and P' indicates the modified parameter value after a 5% increase of its value, keeping all other parameters at their original value.

2.3   Results

In vitro kinetic data

Data from the four studies reporting values for the kinetic parameters Vmax and Km for $E_2 17\beta G$ transport by hepatocytes are listed in Table 3. For both the Km and Vmax the maximum fold difference between the values from the different data sets was not higher than 11. The resulting transporter efficiencies (TE) vary less than 3.1-fold.

Table 3.
In vitro kinetic parameter values for active hepatic transport of [3H]-E217βG obtained from literature

Rat hepatocyte system	Km (μM)	Vmax (pmol/min/mg protein)	Transporter efficiency (TE) (Vmax/Km)	Reference
1	4.54±2.5	149±9.5	32.8	Brouwer et al. (1987)
2	6.5±1.6	470±120	72.3	Ishizuka et al. (1998)
3	12.9±1.3	1300±100	100.7	Kouzuki et al. (1999)
4	45.5±11.8	1620±210	35.6	Brock and Vore (1984)

Predicted versus observed time dependent blood levels of E$_2$17βG

Using the Vmax and Km values presented in Table 3, PBK-model based predictions for E$_2$17βG levels in blood were calculated optimising the scaling factor to obtain the best fit between predicted and actually reported experimental data for the three available *in vivo* data sets (Table 2). To this end an iterative process varying the scaling factor within the range of 5 – 500 mg protein/g liver was performed to find the best fit. For each *in vivo* data set four optimisations were carried out, one for each of the data sets for Vmax and Km derived from rat hepatocytes (Table 3). Since the four fitted predictions thus obtained for each of the three experimentally observed time-dependent blood concentration of intravenously administered E$_2$17βG in rats were similar, only the predictions for one out of the four data sets are displayed in figure 3 (all twelve predictions can be found in supplementary material A fig. S3). The scaling factors in mg protein/g liver for conversion of *in vitro* hepatocyte protein levels to *in vivo* liver protein levels optimised to obtain the predicted curves are presented in Table 4.

The data thus obtained reveal that with all kinetic hepatocyte data adequate fits can be obtained with scaling factors that differ only to a limited extent for the four kinetic hepatocyte data sets. The scaling factors for the fits of the 3 different *in vivo* data sets for blood levels of E$_2$17βG varied here amounting to at most a 6-fold difference when comparing results *within* a hepatocyte data set.
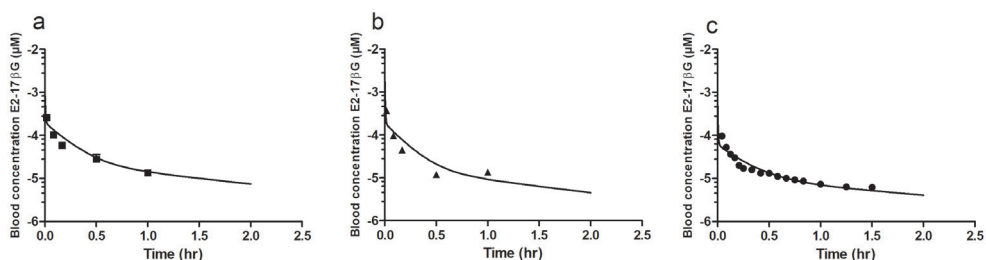
Figure 3.

Predicted and observed blood concentrations (corrected from reported plasma concentrations) of $E_2 17\beta G$ in rats upon intravenous administration. Symbols represent rat *in vivo* data obtained at a dose of (a) 81 ng/kg bw (squares) (Morikawa et al. 2000), (b) 81 ng/kg bw (triangles) (Gotoh et al. 2002) and (c) 23 ng/kg bw (dots) (Slikker et al. 1983). Data represent the mean (and the SD where available). Predictions (lines) are based on the Vmax and Km values for hepatocyte transport of $E_2 17\beta G$ from rat hepatocyte system 1 obtained from literature and presented in Table 3. The predictions for all four Vmax and Km data sets are presented in supplementary material A figure S3. The details of the *in vivo* data sets are presented in Table 2

Predicted versus observed time dependent cumulative biliary excretion of $E_2 17\beta G$

Next to the time-dependent blood concentration, the cumulative biliary excretion was predicted using the same approach (Fig. 4). Since also for these three data sets on the time-dependent biliary excretion the predictions obtained using the four Vmax and Km data sets were similar, only the predictions for one out of the four data sets are displayed in figure 4. All twelve predictions can be found in supplementary material A fig. S4. The values for the scaling factor in mg protein/g liver for conversion of *in vitro* hepatocyte protein levels to *in vivo* liver protein levels optimised to obtain the predicted curves are presented in Table 4.

The data obtained reveal that also for prediction of the cumulative biliary excretion all kinetic hepatocyte data can provide adequate fits with scaling factors that differ only to a limited extent for the four kinetic hepatocyte data sets. The scaling factors for the fits of the 3 different *in vivo* data sets for blood $E_2 17\beta G$ varied somewhat more compared with the scaling factors obtained from the time-dependent blood concentration amounting from a 6-fold to a 9-fold difference when comparing results *within* a hepatocyte data set. Taking all 24 scaling factors together resulted in an average scaling factor of 129 ± 24 mg protein/g liver (mean ± SEM).
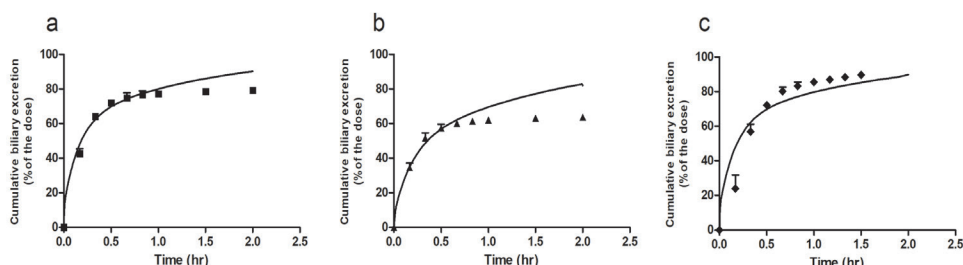
Figure 4.

Predicted and observed cumulative biliary excretion of $E_217\beta G$ in rats upon intravenous administration expressed as percentage of the dose (%). Symbols represent rat *in vivo* data obtained at a dose of (a) 81 ng/kg bw (squares) (Morikawa et al. 2000), (b) 81 ng/kg bw (triangles) (Gotoh et al. 2002) and (c) 48 ng/kg bw (diamonds) (Takikawa et al. 1996). Data represent the mean and the SD where available. Predictions (lines) are based on the Vmax and Km values for hepatocyte transport of $E_217\beta G$ from rat hepatocyte system 1 obtained from literature and presented in Table 3. The predictions for all four Vmax and Km data sets are presented in supplementary material A figure S4. The details of the *in vivo* data sets are presented in Table 2

Table 4.

Fitted values for the scaling factor and the resulting average scaling factor (mg protein/g liver)

Rat hepatocyte system	Morikawa et al. (2000)	Gotoh et al. (2002)	Slikker et al. (1983)	Morikawa et al. (2000)	Gotoh et al. (2002)	Takikawa et al. (1996)
	Blood concentration			Cumulative biliary excretion		
	Scaling factor (mg protein /g liver)			Scaling factor (mg protein/g liver)		
1[a]	80	200	35	200	65	400
2[b]	40	90	15	150	30	200
3[c]	30	65	11	120	22	200
4[d]	80	180	30	300	60	400
Average scaling factor ± SEM (mg protein/g liver)	**129 ± 24**					

Scaling factors were obtained by fitting the *in vivo* reported data on blood and cumulative biliary excretion levels with the PBK-model predictions based on the *in vitro* kinetic input.

[a] 1: Km = 4.54 μM, Vmax = 149 pmol/min/mg protein (Brouwer et al. 1987)
[b] 2: Km = 6.5 μM, Vmax = 470 pmol/min/mg protein (Ishizuka et al. 1998)
[c] 3: Km = 12.9 μM, Vmax = 1300 pmol.min/mg/protein (Kouzuki et al. 1999)
[d] 4: Km = 45.5 μM, Vmax = 1620 pmol/min/mg protein (Brock and Vore 1984)

Evaluation of the scaling factor

To further evaluate the scaling factor, the *in vivo* kinetic data on time-dependent $E_217\beta G$ blood concentration and cumulative biliary excretion were predicted using this average value and compared to the experimental data in figure 5 and 6. The results obtained

reveal that with this average scaling factor all experimental data for blood $E_2 17\beta G$ levels were on average predicted with a less than 1.8-fold deviation, while for the data for the cumulative biliary excretion of $E_2 17\beta G$ the averaged deviation was less than 1.4-fold. The largest deviations were observed for the *in vivo* data on blood $E_2 17\beta G$ levels of Slikker et al. (1983) where the model somewhat overpredicted the clearance of $E_2 17\beta G$ from the blood (Fig. 5c, f, i, l) ranging from a 4 to 12- fold difference and for the *in vivo* data on cumulative biliary excretion reported by Gotoh et al. (2002) that were too, somewhat overpredicted with a maximum of 6-fold deviation (Fig. 6b, e, h, k).
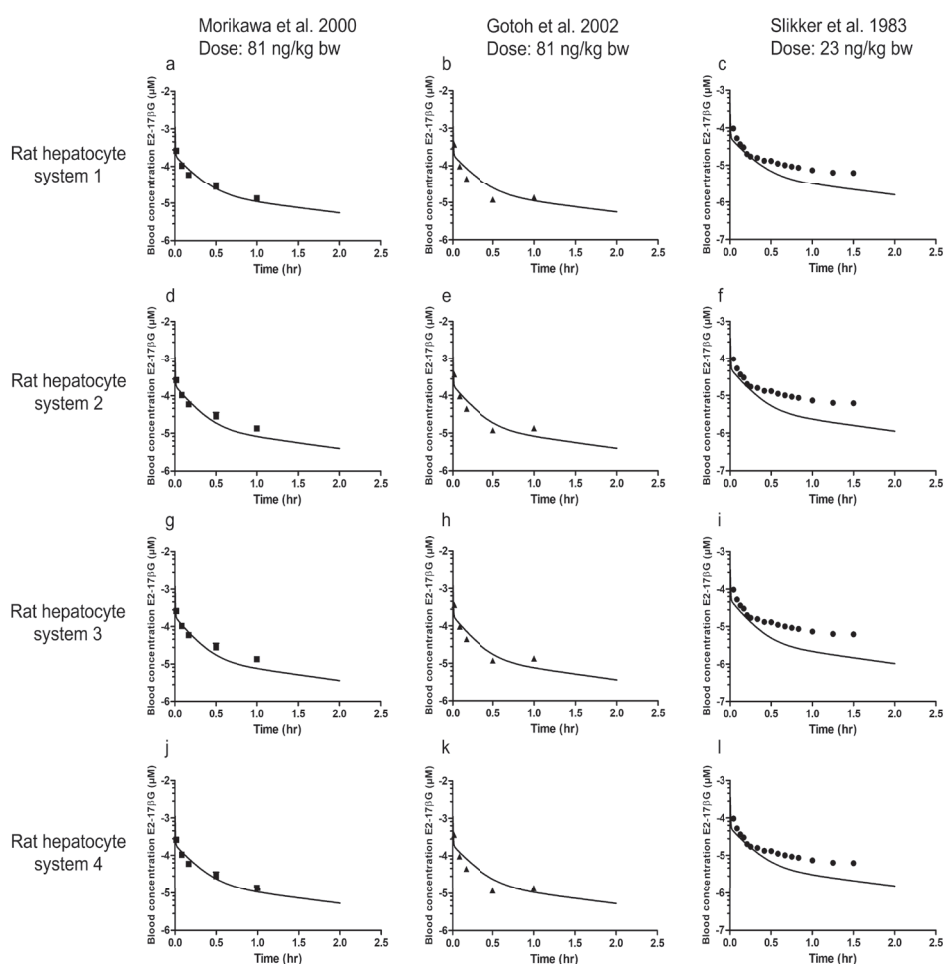
Figure 5.
Predictions of the blood concentration in time of $E_2 17\beta G$ in rats upon intravenous administration using the average value for the scaling factor (129 mg protein/g liver) compared with the observed blood concentrations. Symbols represent rat *in vivo* kinetic data obtained at a dose of (a, d, g, j) 81 ng/kg bw (squares) (Morikawa et al. 2000), (b, e, h, k) 81 ng/kg bw (triangles) (Gotoh et al. 2002) and (c, f, i, l) 23 ng/kg bw (dots) (Slikker et al. 1983). Data represent the mean (and the SD where available). Predictions

(lines) are based on the Vmax and Km values for hepatocyte transport of E$_2$17βG obtained from literature and presented in Table 3
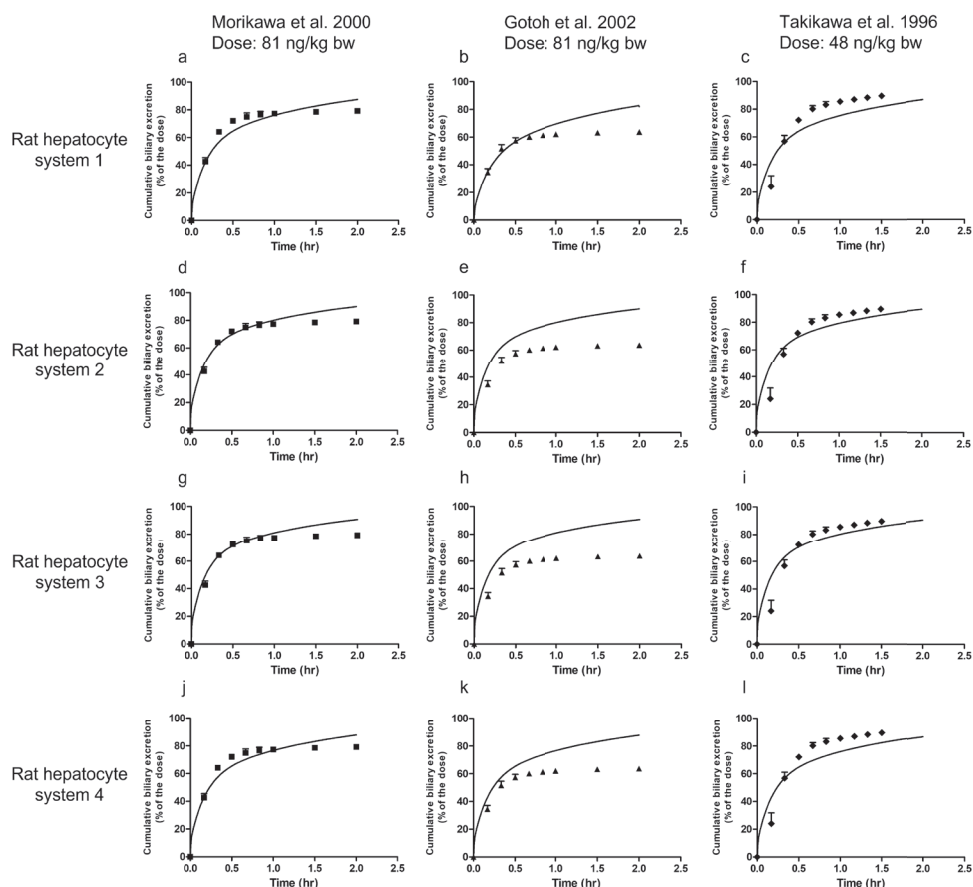
Figure 6.
Predictions of the cumulative biliary excretion in time of E$_2$17βG in rats upon intravenous administration expressed as percentage of the dose (%) using the average value for the scaling factor (129 mg protein/g liver) compared with the observed cumulative biliary excretion. Symbols represent rat *in vivo* kinetic data obtained at a dose of (a, d, g, j) 81 ng/kg bw (squares) (Morikawa et al. 2000), (b, e, h, k) 81 ng/kg bw (triangles) (Gotoh et al. 2002) and (c, f, i, l) 48 ng/kg bw (diamonds) (Takikawa et al. 1996). Data represent the mean (and the SD where available). Predictions (lines) are based on the Vmax and Km values for hepatocyte transport of E$_2$17βG obtained from literature and presented in Table 3

Sensitivity analysis

To further evaluate the influence of the scaling factor on the model predictions and also elucidate which PBK-model parameters influence the predictions most a sensitivity analysis was performed. The predicted blood concentration and cumulative biliary excretion levels of E$_2$17βG at a time point of 0.5 hr were used as the basis for this

analysis. Only parameters with a normalized sensitivity coefficient > 0.1 are presented. The results reveal that for prediction of both the blood $E_2 17\beta G$ concentration (Fig. 7a) and the cumulative biliary excretion (Fig. 7b) the blood flow to liver (QLc) is most influential parameters while for prediction of the cumulative biliary excretion also the blood flow to the liver (QLc) is influential. At different transporter efficiencies (TE) for the hepatocyte transport the normalized sensitivity coefficients are somewhat different, but the parameters that have the largest influence remain the same. The influence of the scaling factor on both model outcomes shows not to be substantial with a sensitivity coefficient at the highest and lowest CE of 0.2 and -0.4 for the blood concentration and 0.04 and 0.13 for the cumulative biliary excretion.
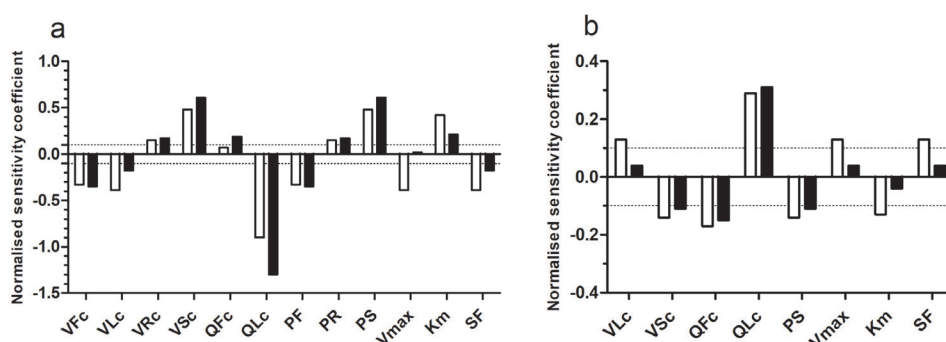
Figure 7.
Sensitivity coefficients of the PBK-model parameters for prediction of (a) the E217βG blood concentration and (b) the cumulative active biliary excretion of E217βG at an intravenous dose of 81 ng/kw bw, t = 0.5 hr with the Vmax and Km that result in the lowest transporter efficiency (TE) (black bars) (Brouwer et al. 1987) and the Vmax and Km that result in the highest TE (grey bars) (Kouzuki et al. 1999) (see Table 3). VFc = volume fat tissue, VLc = volume liver tissue, VRc = volume of rapidly perfused tissues, VSc = volume of slowly perfused tissue, QFc = blood flow to fat, QLc = blood flow to liver, QRc = blood flow to rapidly perfused tissue, QSc = blood flow to slowly perfused tissue, PF = partition coefficient of fat, PR = partition coefficient of rapidly perfused tissue, PS = partition coefficient of slowly perfused tissue, Vmax = maximum rate of E217βG transport in hepatocytes, Km = Michaelis-Menten constant of E217βG transport in hepatocytes, SF = scaling factor

2.4 Discussion

The aim of the present study was to provide a proof of principle for including biliary excretion into a generic rat PBK-model with a major focus on determining the *in vitro* to *in vivo* scaling factor to be used when defining the kinetics of biliary transport using primary rat hepatocytes. A scaling factor is required to convert a kinetic value obtained in the *in vitro* cellular model, to a value that reflects the same biological function for the

relevant whole organ. In this study, the scaling factor was needed to translate the *in vitro* Vmax value for $E_2 17\beta G$ transport in hepatocytes expressed in pmol/min/mg protein to an *in vivo* rate for $E_2 17\beta G$ transport by the liver expressed in μmol/hr. The scaling factor expressed in mg protein/g liver enabled use of the *in vitro* hepatocyte Vmax value in the PBK model to enable prediction of *in vivo* blood and cumulative biliary excretion levels of intravenously administered $E_2 17\beta G$. We used $E2 17\beta G$ as a model substance because the substance is excreted as such, with its active excretion into bile via the activity of the Oatp transporters in the sinusoidal membrane of hepatocytes being the rate limiting step for its elimination (Varma et al. 2012). Using the obtained value for the scaling factor, 129 mg protein/g liver, resulted in PBK-model based predictions of the blood and cumulative biliary excretion levels of $E_2 17\beta G$ that were on average within a 1.8-fold deviation from reported *in vivo* data, thus showing the value of the use of primary hepatocytes as an *in vitro* system to determine kinetic parameters for describing biliary excretion.

It is of importance to note that main deviations between predicted and observed *in vivo* data could be related to especially differences between reported experimental data at the same dose level. Even though the *in vivo* time-dependent blood concentration and the corresponding cumulative biliary excretion reported by Gotoh et al. (2002) and Morikawa et al. (2000) were obtained from the same laboratory, the outcomes were different resulting in different values for the individual scaling factors obtained when fitting the data. This difference between the experimental data sets might be explained by the two year time-lap between the two studies and the fact that animal experiments are depending on an array of guideline protocols and conditions that might have been slightly changed over the two years influencing the (expected) outcome (Council 2011). This deviation in reported *in vivo* data becomes even more apparent when looking at the *in vivo* data from Slikker et al. (1983) where at one third of the dose level the data for $E_2 17\beta G$ blood levels were overlapping with the data of the two studies using a 3 fold higher dose level. This discrepancy could be related to the sex of the rats used (female not male) in the Slikker et al. (1983) study. However, Gotoh et al. (2002) reported *in vivo* data on blood levels of $E_2 17\beta G$ in female Sprague-Dawley rats, and showed that these levels were comparable to the levels found in the male Sprague-Dawley rats. Other factors that could play a role in the differences in *in vivo* data are the vehicle used for the IV administration, which was distilled water: polyethylene glycol: ethanol (10:4:1 v/v) in the studies reported by Gotoh et al. (2002) and Morikawa et al. (2000) but saline: propylene glycol: ethanol (10:4:1 v/v) in the study of Slikker et al. (1983). Use of a different vehicle may influence the bioavailability, which may have been higher in the Slikker et al. (1983) study. Furthermore, the type and rate of IV administration, which for one study was an IV infusion (Takikawa et al. 1996) while for the other three studies a bolus IV administration was utilized.

In the present study the apparent deviation shown in the data reported by Slikker et al. (1983) was corrected for before using the data to define the scaling factor. Without this correction scaling factors obtained for the Slikker et al. (1983) data set appeared to amount to a maximum 10 mg protein/g liver, representing values that are not substantially different from the ones reported in Table 4. This observation corroborates the results of the sensitivity analysis that revealed that the scaling factor was not an influential parameter for the PBK-model based predictions.

Until now, not much has been published about the scaling factor expressed in mg protein/g liver to convert *in vitro* hepatocyte protein levels to *in vivo* liver data in rats. A study by Sohlenius-Sternbeck (2006) reported a protein concentration in rat liver homogenate of 112 mg/g liver, but did not define how that value relates to primary hepatocytes, the model system of the present study. However, to further support the scaling factor now obtained the following theoretical approach could be applied to approximate the scaling factor by the use of a hepatocellularity number. There are a few studies that determined and reported this number ranging from 117 to $135 \cdot 10^6$ cells (hepatocytes)/ g liver (Bayliss et al. 1999; Houston 1994a; Sohlenius-Sternbeck 2006). Sohlenius-Sternbeck (2006) also reported on the protein concentration in a hepatocyte suspension (0.985 mg/10^6 cells). Together with the weight of the liver (Table 1) these numbers would result in a scaling factor ranging from of 115 – 132 mg protein/ g liver. Our modelled and averaged scaling factor based on 24 fitted predictions using *in vitro* input data from rat hepatocytes on active uptake of $E_2$17βG and *in vivo* kinetic data is fully in line with this theoretical estimate.

The predictions made using of the defined scaling factor revealed 1) that the value 129 mg protein/g liver is suitable to translate the *in vitro* Vmax from hepatocytes to an *in vivo* Vmax in liver obtaining predictions that are in line with the *in vivo* kinetic data for blood and cumulative biliary excretion levels of $E_2$17βG and also 2) that hepatocytes provide an adequate *in vitro* model to obtain kinetic parameters Vmax and Km for active uptake of an Oatp substrate, $E_2$17βG in our study. Given the uncertainty in scaling factors that would be required when using transfected cell models, use of hepatocytes to describe biliary excretion may be preferred over the use of *in vitro* systems with an overexpression of individual transporters. This is also because $E_2$17βG has affinity for more than one Oatp which will all be taken into account when using hepatocytes known to contain multiple Oatps (e.g. 1a1, 1a5, 361 1b2, 2b1) thus better mimicking the overall transport in the organ of interest (Hagenbuch and Meier 2003; Richert et al. 2006). Taking all together it is concluded that freshly isolated hepatocytes provide an adequate *in vitro* system to investigate uptake via active transport resulting in kinetic parameters that are able to include biliary excretion into PBK-models (Harris et al. 2004; Sahi et al. 2010). Use of this model also eliminates the need for the use of REFs

and RAFs to scale expression and activity of transporters from *in vitro* systems to a full organ, diminishing uncertainties.

With this study we demonstrated a proof of principle by introducing a novel testing strategy for including biliary excretion into a generic PBK-model at the same time defining the scaling factor for the vitro system (primary rat hepatocytes) used to obtain adequate *in vitro* to *in vivo* translation. We confirmed based on the predictions using the averaged scaling factor that primary rat hepatocytes can be the gold standard for studies on biliary transport in addition to their use as the golden standard for many *in vitro* (human) hepatic endpoints (e.g. hepatic metabolism, hepatoxicity, induction/inhibition of cytochrome P450s) (Guguen-Guillouzo and Guillouzo 2010; Zeilinger et al. 2016). However, known downfalls of the use of primary hepatocytes are the inter individual differences and their non-high through put character. To what extent such bottlenecks would affect their use as a model for biliary transport remains to be elucidated. This also holds for their use to mimic biliary transport of other substrates for Oatps and substrates for other hepatic transporters (Oat2 and Oct1) involved in biliary excretion. To this end similar studies with other substrates for Oatps such as statins and ACE inhibitors (Izumi et al. 2018; Watanabe et al. 2010) or for other hepatic transporters such as antineoplastic drugs, antivirals. antidiuretics and some alkaloids (Burckhardt 2012; Lozano et al. 2013; Marada et al. 2015) may be of use. Nevertheless, the proof of principle described in the present paper provides a first important step towards including biliary excretion in PBK-models for reverse dosimetry based QIVIVE and alternative testing strategies.

Acknowledgements

Compliance with ethical standards
Conflict of interest The authors declare that they have no conflict of interest

Supplementary material A
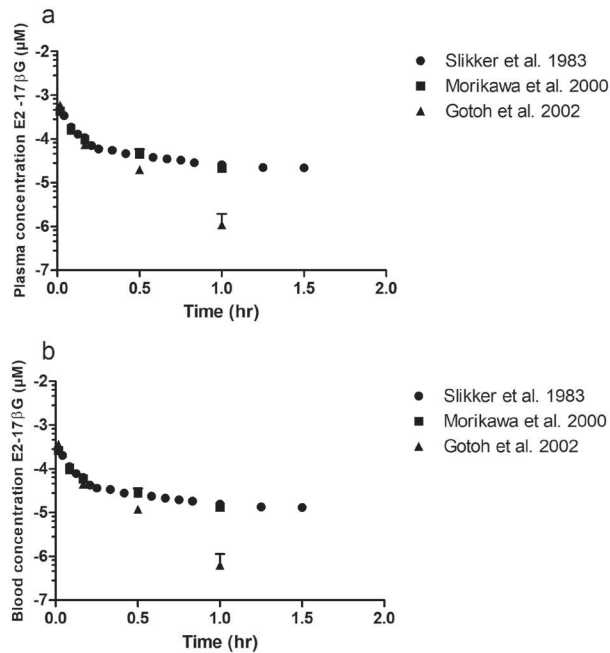
Figure S1.
Original plasma concentration data (a) of E$_2$17βG obtained from three different *in vivo* data sets at dose levels of 23 ng/kg bw (Slikker et al. 1983) (circles) and 81 ng/kg bw (Gotoh et al. 2002; Morikawa et al. 2000) (triangles and squares, respectively). Calculated whole blood concentration data (b) with the formula $C_{blood} = C_{plasma} \times (1\text{-Hct})$ using 40% as the haematocrit in rat.
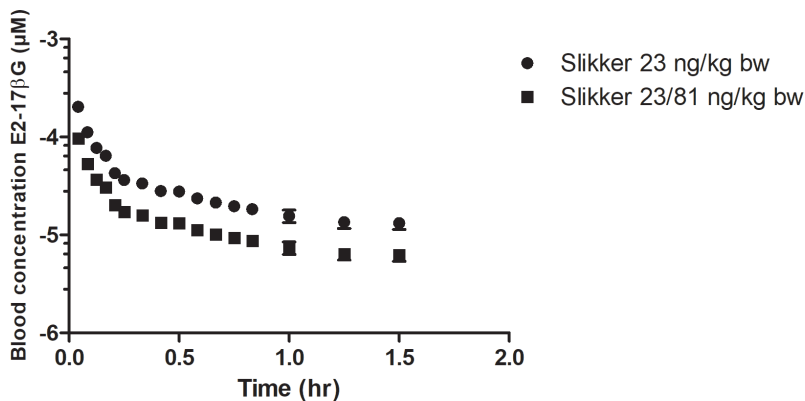
Figure S2.
The *in vivo* data of Slikker et al. (1983) where the plasma to blood converted data (circles) have been modified 23/81 (squares).
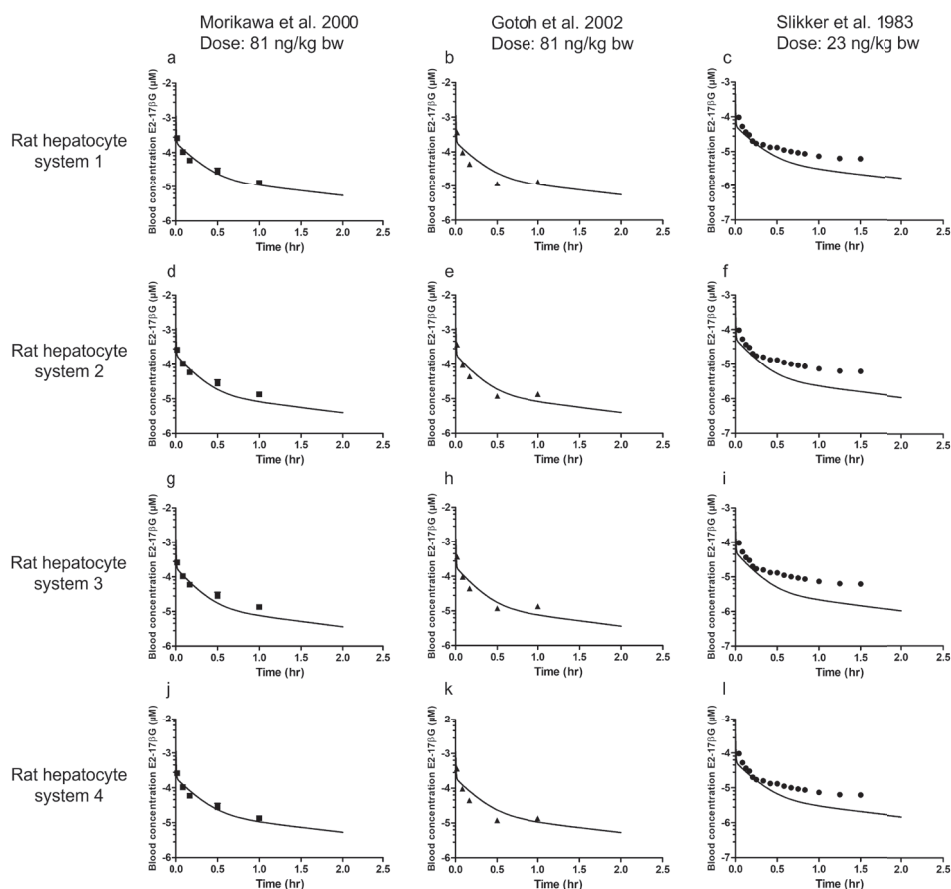
Figure S3.
Fitted predictions and observed blood concentrations (corrected from reported plasma concentrations) of $E_2 17\beta G$ in rats upon intravenous administration. Symbols represent rat *in vivo* data obtained at a dose of (a, d, g, j) 81 ng/kg bw (squares) (Morikawa et al. 2000), (b, e, h, k) 81 ng/kg bw (triangles) (Gotoh et al. 2002) and (c, f, i, l) 23 ng/kg bw (dots) (Slikker et al. 1983). Data represent the mean and the SD where available. Predictions (lines) are based on the Vmax and Km values for hepatocyte transport of $E_2 17\beta G$ obtained from literature and presented in table 3
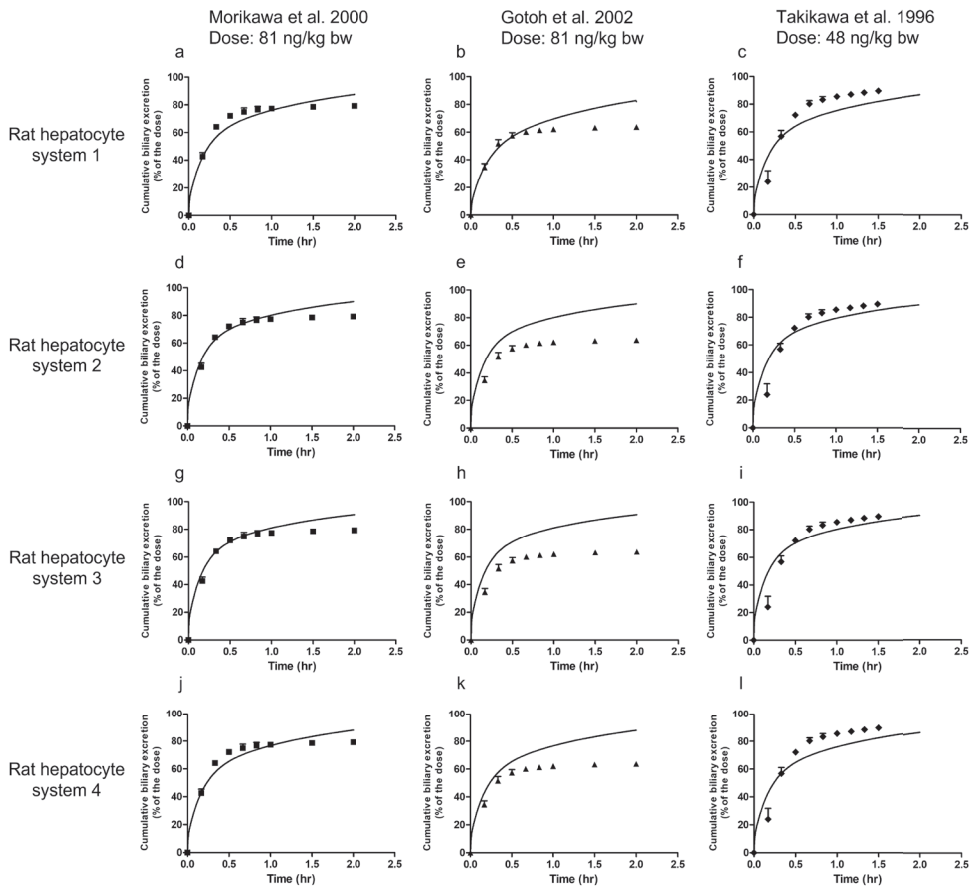
Figure S4.
Fitted predictions and observed cumulative biliary excretion of E$_2$17βG in rats upon intravenous administration. Symbols represent rat *in vivo* data obtained at a dose of (a, d, g, j) 81 ng/kg bw (squares) (Morikawa et al. 2000), (b, e, h, k) 81 ng/kg bw (triangles) (Gotoh et al. 2002) and (c, f, i, l) 48 ng/kg bw (diamonds) (Takikawa et al. 1996). Data represent the mean and the SD where available. Predictions (lines) are based on the Vmax and Km values for hepatocyte transport of E$_2$17βG obtained from literature and presented in table 3

Supplementary material B

; Date: January 2019
; Purpose: PBK Model of estradiol-17B-glucuronide (E217G), built with *in vitro* (from literature) and *in silico* derived parameter values
; Species: Rat
; Compiled by: Annelies Noorlander
; Organisation: Wageningen University

```
;==================================================================
;Physiological parameters
;==================================================================
; tissue volumes
```

BW = 0.250 (Kohane et al.)	; body weight rat (variable, dependent on study)	
VFc = 0.07	; fraction of fat tissue	reference: Brown et al. Table 21 (1997)
VLc = 0.034	; fraction of liver tissue	reference: Brown et al. Table 21 (1997)
VBc = 0.074	; fraction of blood	reference: Brown et al. Table 21 (1997)
VRc = 0.098	; fraction of richly perfused tissue	reference: Brown et al. Table 21 (1997)
VSc = 0.724	; fraction of slowly perfused tissue	reference: Brown et al. Table 21 (1997)

```
VF = VFc*BW          {L or Kg} ; volume of fat tissue (calculated)
VL = VLc*BW          {L or Kg} ; volume of liver tissue (calculated)
VB = VBc*BW          {L or Kg} ; volume of blood (calculated)
VR = VRc*BW          {L or Kg} ; volume of  richly perfused tissue (calculated)
VS = VSc*BW          {L or Kg} ; volume of  slowly perfused tissue (calculated)
```

```
;------------------------------------------------------------------------------------------------
;blood flow rates
```

QC = 15*(BW)^0.74	{L/hr} ; cardiac output	reference: Brown et al. p.453 (1997)
QFc = 0.07	; fraction of blood flow to fat	reference: Brown et al. Table 25 (1997)
QLc = 0.174	; fraction of blood flow to liver	reference: Brown et al. Table 25 (1997)
QRc = 0.234	; fraction of blood flow to richly perfused tissue	reference: Brown et al. Table 25 (1997)
QSc = 0.522	; fraction of blood flow to slowly perfused tissue	reference: Brown et al. Table 25 (1997).

```
QF = QFc*QC          {L/hr}    ; blood flow to fat tissue (calculated)
QL = QLc*QC          {L/hr}    ; blood flow to liver tissue (calculated)
QS = QSc*QC          {L/hr}    ; blood flow to  slowly perfused tissue (calculated)
QR = QRc*QC          {L/hr}    ; blood flow to richly perfused tissue (calculated)
```

```
;==================================================================
;Physicochemical parameters
;==================================================================

;partition coefficients --> logP E217G from ALOGPS: 2.05

PF = 19.87452      ; fat/blood partition coefficient                    calculated   using   QPPR   of:
                                                                         (DeJongh, 1997)
PL = 1.332858      ; liver/blood partition coefficient                  calculated   using   QPPR   of:
                                                                         (DeJongh, 1997)
PR = 1.332858      ; richly perfused tissue/blood partition coefficient calculated   using   QPPR   of:
                                                                         (DeJongh, 1997)
PS = 0.600644      ; richly perfused tissue/blood partition coefficient calculated   using   QPPR   of:
                                                                         (DeJongh, 1997)



;==================================================================
;Kinetic parameters
;==================================================================

;Transport from needle to blood
kn  =  1000000      ; injection {/hr}


;----------------------------------------------------------------------------------------------------------
;Biliary excretion from liver

;based on uptake and elimination of E217G via active transporters in rat hepatocytes (Oatps)
VmaxE217Gc= 149 {pmol/min/mg}                      ; data derived from Brouwer et al. 1987
SF = 129 {mg/g liver}                              ;Averaged scaling factor
VMaxE217G = (VMaxE217Gc/1000000)*SF*60*VL*1000   {umol/hr}


;E217G uptake and elimination, affinity constants for uptake transporters in rat hepatocytes (Oatps)
(umol/L)
KmE217G = 4.54                                     ; data derived from Brouwer et al. 1987


;==================================================================
;Run settings
;==================================================================

;Molecular weight E217G
MW = 448.512


;----------------------------------------------------------------------------------------------------------

;IV dose
IVDOSEmg = 0.000081 {mg/kg bw}                          ; IVDOSEmg = given IV dose in
                                                         mg/kg bw

IVDOSEumol2 = IVDOSEmg*1E-3/MW*1E6  {umol/kg bw}        ; IVDOSEumol2 = given IV dose
                                                         recalculated to umol/kg bw

IVDOSEumol=IVDOSEumol2*BW;                              ; IVDOSEumol = umol given IV
```

```
;time
Starttime = 0          ; in hr
Stoptime = 24          ; in hr



;===================================================================
;Model calculations
;===================================================================

; Model E217G

;needle compartment
;ANe  = amount in needle, umol
;ANe' = Change in amount of E217G in time in the needle,  umol/hr

ANe'  = -kn*ANe
Init ANe = IVDOSEumol
;--------------------------------------------------------------------------------------------------------------
;liver compartment

;AL = Amount E217G in liver tissue, umol
;AL' = Change in amount of E217G in time,  umol/hr

AL' =  QL*(CB - CVL) - AME217G'
          Init AL = 0
          CL = AL/VL
          CVL = CL/PL


;AME217G = amount E217G excreted from the liver by biliary excretion over time (umol/L)
     AME217G' = VmaxE217G*CVL/(KmE217G + CVL)
     init AME217G = 0


;--------------------------------------------------------------------------------------------------------------
;fat compartment

;AF = Amount E217G in fat tissue (umol)
;AF' = Change in amount of E217G in time,  umol/hr
     AF' = QF*(CB-CVF)
     Init AF = 0
     CF = AF/VF
     CVF = CF/PF
```

```
;-------------------------------------------------------------------------------------------------------------
;tissue compartment richly perfused tissue

;AR = Amount E217G in richly perfused tissue (umol)
;AR' = Change in amount of E217G in time,  umol/hr
     AR' = QR*(CB-CVR)
     Init AR = 0
     CR = AR/VR
     CVR = CR/PR


;-------------------------------------------------------------------------------------------------------------
;tissue compartment slowly perfused tissue

;AS = Amount E217G in slowly perfused tissue (umol)
;AS' = Change in amount of E217G in time,  umol/hr
     AS' = QS*(CB-CVS)
     Init AS = 0
     CS = AS/VS
     CVS = CS/PS


;-------------------------------------------------------------------------------------------------------------
; blood compartment

;AB = Amount E217G in blood (umol)
;AB' = Change in amount of E217G in time,  umol/hr
     AB' = (kn*ANe + QF*CVF +  QL*CVL  + QS*CVS + QR*CVR - QC*CB)
     Init AB = 0
     CB = AB/VB



;====================================================================
;Mass balance calculations
;====================================================================

Total = IVDOSEumol
Calculated = ANe + AL + AME217G + AF + AS + AR  + AB

ERROR=((Total-Calculated)/Total+1E-30)*100
MASSBBAL=Total-Calculated + 1
```
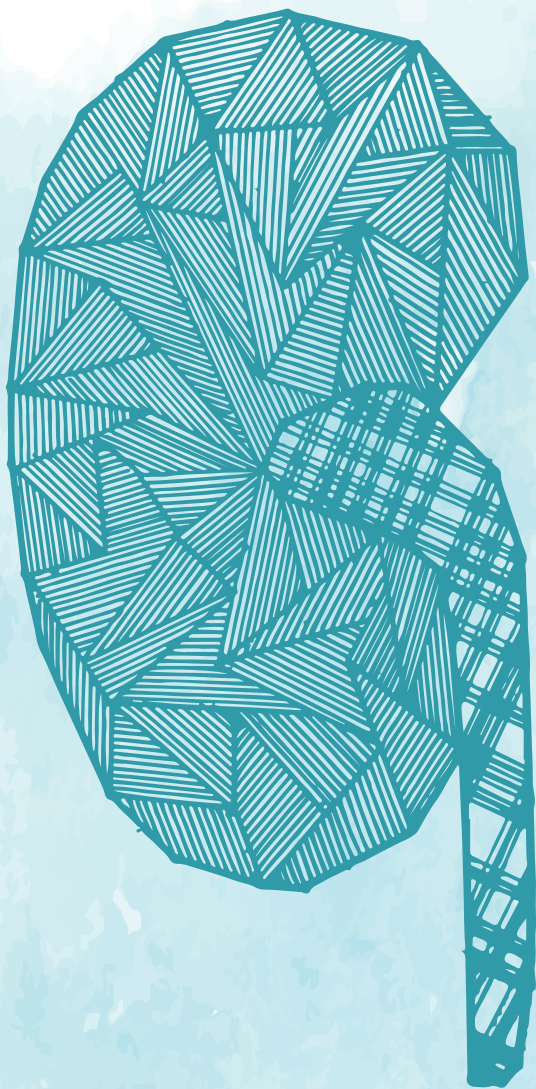
Chapter 3

Incorporating renal excretion via the OCT2 transporter in physiologically based kinetic modelling to predict *in vivo* kinetics of mepiquat in rat

Annelies Noorlander, Sebastiaan Wesseling, Ivonne M.C.M. Rietjens and Bennard van Ravenzwaay

Abstract

The present study aimed at incorporating active renal excretion via the organic cation transporter 2 (OCT2) into a generic rat physiologically based kinetic (PBK) model using an *in vitro* human renal proximal tubular epithelial cell line (SA7K) and mepiquat chloride (MQ) as the model compound. The Vmax (10.5 pmol/min/mg protein) and Km (20.6 μM) of OCT2 transport of MQ were determined by concentration-dependent uptake in SA7K cells using doxepin as inhibitor. PBK model predictions incorporating these values in the PBK model were 6.7-8.4-fold different from the reported *in vivo* data on the blood concentration of MQ in rat. Applying an overall scaling factor that also corrects for potential differences in OCT2 activity in the SA7K cells and *in vivo* kidney cortex and species differences resulted in adequate predictions for *in vivo* kinetics of MQ in rat (2.3-3.2-fold). The results indicate that using SA7K cells to define PBK parameters for active renal OCT2 mediated excretion with adequate scaling enables incorporation of renal excretion via the OCT2 transporter in PBK modelling to predict *in vivo* kinetics of mepiquat in rat. This study demonstrates a proof-of-principle on how to include active renal excretion into generic PBK models.

Abbreviations: **ADME** (absorption, distribution, metabolism, excretion), **BSA** (bovine serum albumin), **GFR** (glomerular filtration rate), **LC-MS/MS** (Liquid chromatography mass spectrometry), **MATE** (multidrug and toxin extrusion transporter), **MQ** (Mepiquat), **MRM** (multiple reaction monitoring), **OCT2** (Organic cation transporter 2), **PBK** (Physiologically based kinetic), **QIVIVE** (quantitative *in vitro – in vivo* extrapolation), **RPTEC** (renal proximal tubule epithelial cell), **SA7K** (human RPTEC cell line), **TE** (transporter efficiency)

3.1   Introduction

Physiologically based kinetic (PBK) modelling-facilitated reverse dosimetry is a useful tool for quantitative *in vitro-in vivo* extrapolation (QIVIVE) to predict *in vivo* toxicity (Louisse et al. 2017; Zhang et al. 2018a). Jointly with the results of *in vitro* methods, QIVIVE provides an alternative strategy for risk assessment for human safety without the use of animal experiments, thus contributing to the 3Rs (replacement, reduction and refinement of animal experiments) in the field of toxicology (Bessems et al. 2015).

Until now, proofs-of-principle for QIVIVE based on PBK modelling facilitated reverse dosimetry have been provided for a number of adverse outcomes including liver toxicity (Ning et al. 2019b), kidney toxicity (Abdullah et al. 2016), developmental toxicity (Louisse et al. 2015; Strikwold et al. 2017b) and cardiotoxicity (Shi et al. 2020). These examples, however, did not relate to model compounds for which plasma and tissue concentrations depend on kinetics for excretion.

A few reasons for this lack of including excretion in the PBK models can be identified and relate to: 1) the assumption that for most compounds excretion is not a rate limiting step since molecular weights up to 2000 g/mol can easily pass the filter of the glomeruli (Fagerholm 2007), 2) the fact that following metabolism to more water soluble and often less toxic metabolites, the role of excretion in determining the physiological concentrations of the relevant parent compound is often negligible (Fabian et al. 2019), and 3) the fact that there is a lack of adequate *in vitro* models for renal excretion due to its complexity (Bessems et al. 2015).

Renal excretion is the result of three main processes, 1) passive glomerular filtration; 2) active tubular secretion and 3) passive and active tubular reabsorption (Zeidel et al. 2014). This implies that developing *in vitro* models to predict renal excretion, should enable adequate description of all three processes which may be a challenge especially when active transport is involved. A study by Felmlee et al. (2013) has compared four mechanistic pharmacokinetic models for active secretion and reabsorption and concluded that especially the Vmax of active transporters in renal proximal tubules plays a pivotal role in the prediction of renal excretion.

The most abundant active drug transporter present in the renal proximal tubules of both human and rat is the organic cation transporter 2 (OCT2) located basolaterally (Motohashi and Inui 2013). OCT2 secretes, together with the H^+/organic cation antiporter multidrug and toxin extrusion (MATE) transporter, cations to the renal lumen. Since OCT2 is Na^+-independent and electrogenic, its transport is driven by the inside-negative membrane potential that exists within the proximal tubule cells (Yin

and Wang 2016). Consequently, the route of renal excretion of cations via the OCT2/ MATE complex should be considered when including renal excretion in a PBK model.

The aim of the present study was to develop a proof-of-principle to include active renal excretion in a rat PBK model using renal proximal tubule epithelial cells (RPTEC) to obtain kinetic parameters for OCT2 transport. To this end we used the SA7K cell line described by Li et al. (2017c), which is an RPTEC cell line generated from human primary kidney proximal tubule epithelial cells by executing a zinc-finger nuclease-mediated knockout of a cell cycle protein making the cell line so-called pseudo-immortalized. The group of Li et al. (2017c) was able to generate this cell line with preserved expression and activity of relevant transporters when cells are in culture, of which OCT2 was one. As a model compound we selected mepiquat chloride (MQ; molecular structure of mepiquat cation is shown in Table 1), a positively charged, non-metabolised compound that is excreted predominantly via the kidneys (Agency 1997). Implementing the kinetic parameters of MQ transport via OCT2 into a rat PBK model together with the appropriate scaling factors should provide an improved prediction of the blood concentration–time curve compared to predictions made by a model that does not take active renal excretion into account.

3.2   Materials and methods

Chemicals
Doxepin hydrochloride was purchased from Carbosynth (Berkshire, UK). (±)Verapamil hydrochloride, bovine serum albumin (BSA) and formic acid were purchased from Sigma-Aldrich (Zwijndrecht, the Netherlands). BASF SE kindly provided mepiquat chloride (MQ). Dimethyl sulfoxide (DMSO) used for dissolving doxepin and verapamil was purchased from Merck (Darmstadt, Germany). Acetonitrile was purchased from Biosolve (Valkenswaard, the Netherlands). Ultrapure water from a system of Arium Pro VF Sartonius (Rotterdam, the Netherlands) was used to dissolve MQ.

Cell culture
SA7K cells (Sigma-Aldrich, Zwijndrecht, the Netherlands), a human renal proximal tubule epithelial cell (RPTEC) line containing functional active transporters (Li et al. 2017c) were cultured in MEMα (Sigma-Aldrich, Zwijndrecht, the Netherlands) supplemented with RPTEC Complete Supplement (Sigma-Aldrich, Zwijndrecht, the Netherlands), 2.5 mM L-glutamine (Gibco), 30 µg/mL gentamicin and 0.015 µg/mL amphotericin B at 37°C with 5% (v/v) CO_2 and 95% (v/v) humidity. For uptake studies cells were seeded in 6-well plates at a density of 1.5×10^6 cells/well and grown for 2 days prior to use with a medium change after one day. Cells used in this study were between 6 – 22 cell passages.

OCT2 uptake of MQ

To confirm OCT2 dependent uptake of MQ, SA7K cells were pre-incubated in pre-warmed (37°C) uptake buffer (136 NaCl, 5.3 mM KCl, 1.1 mM KH_2PO_4, 0.8 mM $MgSO_4$ x 7 H_2O, 1.8 mM $CaCl_2$ x 2 H_2O, 11 mM D-glucose, 10 mM HEPES, pH 7.4) within the presence or absence of the OCT2 inhibitors doxepin and verapamil (Hacker et al. 2015; Li et al. 2017c) (final concentration 10 µM and 100 µM, respectively, added from 200 times concentrated stock solutions in DMSO as starting concentrations based on uptake/inhibition studies using the SA7K cell line by Li et al. (2017c)) for 10 minutes at 37°C. After 10 minutes, substrate MQ (final concentration 1 µM and 10 µM added from 200 times concentrated stock solutions in ultrapure water) was added and the cells were incubated for 30 and 60 minutes. After incubation medium was removed and cells were washed twice with ice-cold PBS containing 0.2% (w/v) BSA (to avoid unspecific binding) and once with ice-cold PBS alone. Cells were lysed with ultrapure water in a freeze-thaw cycle. Protein was measured using the Pierce BCA protein assay kit (Thermo Fischer Scientific Bleiswijk, the Netherlands). MQ present in the cell lysate was quantified using LC-MS.

Time optimisation for OCT2 uptake

SA7K cells were pre-incubated in pre-warmed (37°C) uptake buffer within the presence or absence of the OCT2 inhibitor doxepin (final concentration 100 µM added from a 200 times concentrated stock solution in DMSO) for 10 minutes at 37°C. After 10 minutes, substrate MQ (final concentration 10 µM added from a 200 times concentrated stock solution in ultrapure water) was added and the cells were incubated for 2, 5, 10, 30 and 60 minutes. MQ present in the cell lysate was quantified using LC-MS.

Quantification of OCT2 mediated transport of MQ

Under time-optimised conditions, uptake experiments were continued following the same approach as described above in the absence and presence of the OCT2 inhibitor doxepin at 100 µM final concentration to quantify the OCT2 mediated transport of MQ. After 10 minutes incubation in the presence or absence of doxepin, substrate MQ (final concentrations 10, 25, 50, 100, 200, 300, 400 and 500 µM added from 200 times concentrated stock solutions in ultrapure water) was added to the cells. MQ present in the cell lysate was quantified using LC-MS. OCT2 mediated uptake of MQ was derived from the difference in transport in the absence and presence of the OCT2 inhibitor.
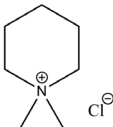
Liquid chromatography mass spectrometry (LC–MS/MS) analysis

MQ (Table 1) was analysed on an LC-MS/MS system (Shimadzu, Kyoto, Japan), which contained a Nexera XR LC-20AD SR UPLC system coupled to a triple quadrupole mass spectrometer LCMS-8045. A Luna Omega polar C18 column (Phenomenex) (100 x 2.1 mm, 1.6 µm particle size) was used for separation. The mobile phase consisted of water

(A) and acetonitrile (B) both containing 0.1 % (v/v) formic acid (gradient: 0.00 - 6.00 min 25-100% B, 6.00 - 6.50 min 100% B, 6.50 - 7.00 min 100-25% B, 7.00 - 10.50 min 25% B) and was delivered at a flow rate of 0.3 mL/min. The injection volume was 5 µL and the column oven was set at 40°C. Under these conditions the retention time of MQ was 0.83 min. The parameters used in multiple reaction monitoring (MRM) were as follows: positive-ion mode, electrospray ionisation source, nebulizer gas flowrate: 2.0 L/ min, heating gas flow rate: 10.0 L/min, interface temperature: 300°C, DL temperature: 250°C, heating block temperature: 400°C, drying gas flow rate: 10.0 L/min, dwell time: 10 ms, and fragments and ESI-S parameters are presented in Table 1.

Table 1.
Molecular structure of mepiquat cation from mepiquat chloride (MQ), fragments and ESI-MS parameters used in this study

Chemical	Molecular structure	MRM transition	Q1 pre Bias (V)	CE (V)	Q3 Pre bias (V)
MQ		$114.1 \rightarrow 98.10$	-21.0	-28.0	-19.0
		$114.1 \rightarrow 70.10$	-20.0	-36.0	-26.0
		$114.1 \rightarrow 58.10$	-18.0	-26.0	-23.0
		$114.1 \rightarrow 42.10$	-19.0	-47.0	-15.0

Physiologically based kinetic (PBK) modelling

A physiologically based kinetic model for MQ in rat was developed. The model consists of separate compartments for GI-tract, liver, fat, blood and kidney (Figure 1). All other organ tissues were placed under rapidly perfused tissue (brain, lungs, heart) or slowly perfused tissue (bone, skin, muscle). The physiological and anatomical parameters including tissue weight and tissue blood flow were obtained from the literature (Brown et al. 1997a). Tissue:blood partition coefficients were calculated by a quantitative property-property relationship method described in literature (Rodgers and Rowland 2006) and obtained via the QIVIVE toolbox developed by Punt et al. (2020). Toolbox input of MQ: LogP = -3.55 (safety data sheet BASF), molecular weight = 149.7 g/mol, pKa = not applicable, ticked box for the presence of quaternary N atom(s). Since MQ is hardly metabolised in the body, no equations and kinetic parameters for clearance were included in the model. For describing active renal excretion of MQ via OCT2, the kinetic parameters of OCT2 mediated membrane translocation of MQ need to be included in the model. Each compartment of the model contains its own set of mathematical equations. The equation to describe the amount of MQ excreted via the kidney included a term for glomerular filtration (Felmlee et al. 2013) and a term to describe active renal excretion, and was as follows:

$$AKe = \left(GFR \times (CVK \cdot Fub)\right) + \left(\frac{Vmax_{OCT2} \times CVK}{(Km_{OCT2} + CVK)}\right) \tag{1}$$

where AKe is the amount of MQ excreted via the kidney in time (μmol/hr), GFR is the glomerular filtration rate of rat (L/hr), CVK the venous concentration of MQ in the kidneys (μmol/L), $Vmax_{OCT2}$ and Km_{OCT2} the maximum rate (μmol/hr) and Michaelis-Menten constant (μmol/L) for the active transport of MQ by OCT2, and Fub the fraction unbound of MQ in blood, which was 1 (Neef and Meijer 1984).

The glomerular filtration rate in the model was included as a formula depending on the body weight of rat and the glomerular filtration rate in rat, which was reported to be 5.2 mL/min/kg bw (Walton et al. 2004). The formula included was the following:

$$GFR = 0.0052 * BW * 60 \tag{2}$$

where GFR is the glomerular filtration rate (L/hr), BW the body weight (kg) and 60 to convert minutes to hours.

Besides renal excretion, a fraction of 10 % of an oral dose given is known to be excreted via the faeces, indicted in the model as Fef set at 0.1. Berkeley Madonna software (UC, Berkeley, CA, USA version 8.3.18) was used to solve the equations.
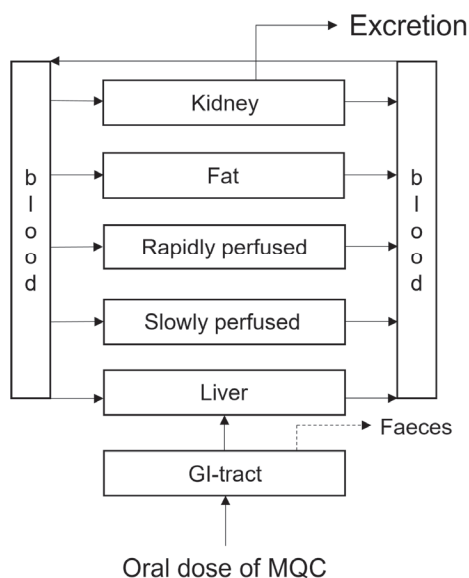
Figure 1.
Schematic overview of the conceptual PBK model for MQ including renal excretion.

Plasma to whole blood

In the PBK model the blood compartment relates to whole blood. However six out of the eight rat *in vivo* kinetic data sets (provided by BASF) for model evaluation on time-dependent MQ concentrations were obtained in plasma (the other two data sets were obtained in whole blood). Therefore, the MQ plasma concentrations were converted to whole blood concentrations assuming that the concentration in plasma is equal to the concentration in the erythrocytes using the following formula:

$$C_{blood} = C_{plasma} \times (1 - Hct) \tag{3}$$

where C_{blood} is the concentration of MQ in whole blood (µmol/L), C_{plasma} the concentration of MQ in plasma (µmol/L) and Hct the rat haematocrit, which was set at 40%, the average of the range published (Probst et al. 2006). (See Fig. A.1 and A.2 in supplementary material for original plasma-concentration time data).

Scaling factor

To convert the *in vitro* obtained Vmax value for OCT2 uptake of MQ in SA7K cells expressed in pmol/min/mg protein into an *in vivo* Vmax expressed in µmol/hr/kidneys a scaling factor is needed. The scaling factor used in this study consisted of three parts. Part one of the scaling factor was applied to convert the activity expressed per mg protein present in the cells *in vitro* expressed in pmol/min/mg cellular protein to the activity expressed in a unit that represents the activity in the two whole kidneys expressed in pmol/min/g kidneys. Therefore, we need to know how the amount of protein in the cells *in vitro* relates to the amount of protein present in the kidneys. A study performed by Kumar et al. (2018) has experimentally quantified how much protein (mg) is present in 1 mg of kidney resulting in 0.3 mg protein/mg kidney, which equals to 300 mg protein/g kidney (units appropriate for our conversion). Using this conversion factor the activity expressed per mg protein in the cells *in vitro* was converted to the activity expressed per g kidney *in vivo*. Part two of the scaling factor was required because OCT2 might be only expressed in the cortex part of the kidneys and not in the whole kidneys. This assumption is based on the assumptions also made by Kumar et al. (2018) indicating that OCT2 is located in the RPTEC cells, which in their turn are located in the kidney cortex. This means that conversion of the *in vitro* OCT2 activity in the cells to an *in vivo* activity in the kidneys cannot be done based on the total kidney weight, but needs to take into account that only the cortex, that is 70% of the total kidney weight will contain OCT2. Thus, to convert the activity in the two whole kidneys expressed in pmol/min/g kidneys, obtained by applying the first part of the scaling factor, to a Vmax expressed for the kidneys as a whole in pmol/min/whole kidneys requires multiplication by 0.7 times the weight of the kidney in grams. Finally, part three is required for the scaling that accounts for conversion of the expression and activity of OCT2 in SA7K

cells compared to its expression and activity in the renal tubule cells in the kidney cortex. This third part includes i) the differences in the level of OCT2 expression, ii) potential differences in membrane potential between the relevant cells *in vitro* and *in vivo* and also, iii) given that the SA7K cell line is a human derived cell line and the PBK model relates to rat, interspecies differences between human and rat. The actual size of this third part of the overall scaling factor was quantified by fitting the PBK model based predictions to available *in vivo* data, altering the *in vitro* obtained Vmax in Berkeley Madonna to obtain the best fit. The overall scaling factor was obtained by multiplying the three factors (see results). The conversion of the Vmax for OCT2 mediated transport obtained *in vitro* to the Vmax for OCT2 mediated transport *in vivo* could thus be done using the following formula :

$$In\ vivo\ \text{Vmax} = \left(\frac{In\ vitro\ \text{Vmax}}{1{,}000{,}000}\right) \times 60 \times \text{SF} \times (\text{Volume of kidneys}) \times 1000 \tag{4}$$

where the factor 1,000,000 is used to convert pmol to µmol, 60 to convert minutes to hours, 1000 to convert kg kidney weight to g kidney weight and SF is the scaling factor encompassing the three parts mentioned above expressed in mg protein/g kidney.

The full model code is presented in Appendix B of the supplementary material.

Evaluation of the PBK model and sensitivity analysis

The developed PBK model for MQ was evaluated by comparing the predicted blood concentration time curve with available experimental data on the blood concentration time curve of MQ in rat (data from BASF). To visualise the effect of including the urinary excretion in the model the predicted blood concentration time curve was compared with the predicted blood concentration time curve obtained without including this active excretion. In addition, a sensitivity analysis was performed to assess model parameters that influence the model output maximum blood concentration (C_{max}) most. The sensitivity analysis was performed at dose levels used in the available rat studies including a low dose (1.2 mg/kg bw) and a high dose (12 mg/kg bw). Normalised sensitivity coefficients (SCs) were calculated for the model parameters based on the method reported in the literature (Evans and Andersen 2000) as follows:

$$SC = (C' - C)/(P' - P) \times (P/C) \tag{5}$$

were C is the initial value of the model output, C' is the modified value of the model output resulting from an increase in the parameter value. P is the initial parameter value and P' is the modified parameter value after a 5% increase in its value.

Data analysis

The apparent Km and Vmax for OCT2 uptake of MQ were determined by non-linear regression analysis in GraphPad Prism version 5.04 using the formula:

$$V = \frac{Vmax \times [S]}{Km_{app} + [S]} \tag{6}$$

where V is the transport rate in pmol/min/mg protein, Vmax the maximum transport rate of MQ in pmol/min/mg protein, S the substrate concentration in μmol/L, Km_{app} the apparent Michaelis-constant in μmol/L.

Given that the kinetics were derived from curves obtained in the presence of the OCT2 inhibitor doxepin, the Km_{app} can be described as follows:

$$Km_{app} = Km \left(1 + \frac{[I]}{Ki}\right) \tag{7}$$

Rewritten:

$$Km = \frac{Km_{app}}{\left(1 + \frac{[I]}{Ki}\right)} \tag{8}$$

where Km is the Michaelis-Menten constant of MQ in μmol/L, I is the concentration of the inhibitor doxepin in μmol/L and Ki the inhibitor constant of doxepin for OCT2 in μmol/L.

As the inhibitory constant of doxepin for OCT2 was not available in the literature an alternative approach was used to obtain the Ki based on the half maximum inhibitory concentration (IC50) of doxepin for OCT2 (in the presence of substrate1-methyl-4-phenylpyridinium (MPP$^+$)). The following formulas apply (Burlingham and Widlanski 2003):

$$IC50 = Ki \left(1 + \frac{[S]}{Km}\right) \tag{9}$$

Rewritten:

$$Ki = \frac{IC50}{\left(1 + \frac{[S]}{Km}\right)} \tag{10}$$

where IC50 is the half maximum inhibitory concentration of doxepin in μmol/L, Km the Michaelis-Menten constant of MPP$^+$ for OCT2 transport in μmol/L and [S] the concentration of MPP$^+$ in μmol/L.

Using data from Zolk et al. (2009) with: IC50 for doxepin = 13 μmol/L, Km of MPP$^+$ = 19.5 μmol/L and concentration MPP$^+$ S = 10 μmol/L, resulted in a Ki of doxepin for OCT2 of 8.6 μmol/L applying formula (10). The value for Ki was used to determine the Km of MQ for OCT2 applying formula (8).

3.3   Results

OCT2 mediated uptake of MQ

To ensure that MQ is indeed an OCT2 substrate, the uptake of MQ was measured in the presence and absence of the OCT2 inhibitors doxepin and verapamil. Fig. 2 shows that the uptake of MQ at 1 μM (Fig. 2a) and 10 μM (Fig. 2b) by SA7K cells is inhibited in the presence of doxepin by 34 – 49% and verapamil by 59 – 73%. This confirms that MQ uses an organic cationic transport system, OCT2, to be taken up from the medium into the SA7K cells, which represents the first step in its active elimination via the kidneys.
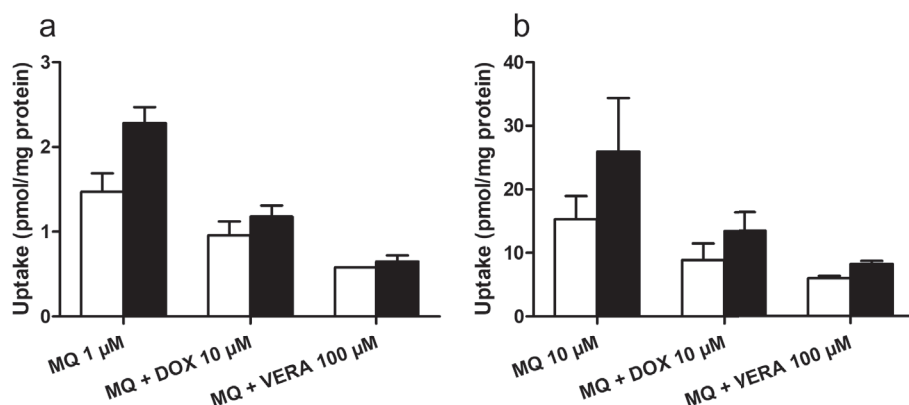
Figure 2.
Uptake and inhibition of MQ uptake in SA7K cells at 1 μM (a) and 10 μM (b) via OCT2 at 30 minutes (white bars) and 60 minutes (black bars). Inhibitors used were 10 μM doxepin and 100 μM verapamil. Each bar represents the mean ± SEM of two biological replicates, each with three technical replicates.

Optimization of uptake time

To effectively determine kinetic parameter values for Vmax and Km, MQ uptake via OCT2 needed to occur under linear conditions with respect to time. Time-dependent uptake of MQ was studied in the absence and presence of the inhibitor doxepin at 100 μM. Although verapamil showed a slightly stronger inhibition on the OCT2 uptake of MQ, inhibition with doxepin was more consistent throughout the whole study. Given the Ki for doxepin mediated OCT2 inhibition of 8.6 μmol/L (see materials and methods)

a concentration of 100 μM was used to effectively block OCT2 mediated transport. The total uptake and the uptake remaining in the presence of the inhibitor are displayed in Fig. 3a. To obtain the net OCT2 mediated active uptake, the uptake remaining in the presence of the inhibitor was subtracted from the total uptake, demonstrating linearity of the OCT2 mediated uptake up until 30 minutes (Fig. 3b). Therefore, we chose to work with 30 minutes as incubation time for the concentration-dependent uptake.
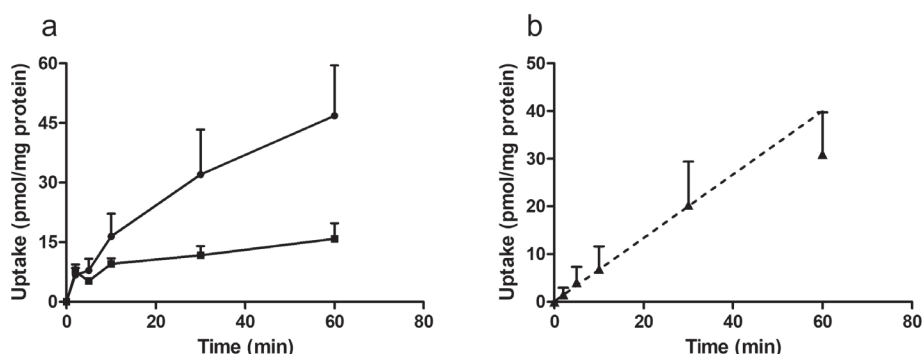
Figure 3.
Time-dependent OCT2 uptake (2, 5, 10, 30 and 60 minutes) of MQ (10 μM) into SA7K cells. (a) The uptake remaining in the presence of doxepin (100 μM) (squares) was subtracted from the total uptake (circles) to obtain (b) the net OCT2 mediated uptake of MQ. Each data point represents the mean ± SEM of three biological replicates, each with three technical replicates.

Kinetic constants for OCT2 mediated uptake of MQ

Under optimised conditions, concentration-dependent OCT2 uptake studies of MQ were performed. Fig. 4a shows the total uptake and the remaining uptake in the presence of doxepin of MQ. (A detailed overview of the uptake until 100 μM is found in Supplementary Fig. A.3). Fig. 4b presents the concentration dependent OCT2 mediated transport and reveals that the net OCT2-mediated uptake is following Michaelis-Menten kinetics. Parameter values were obtained following equation (6) with V_{max} = 10.5±3.5 pmol/min/mg protein and Km_{app} = 260±193 μM. Using equations (7) to (10), the calculated Km of MQ for OCT2 transport was 20.6 μM.
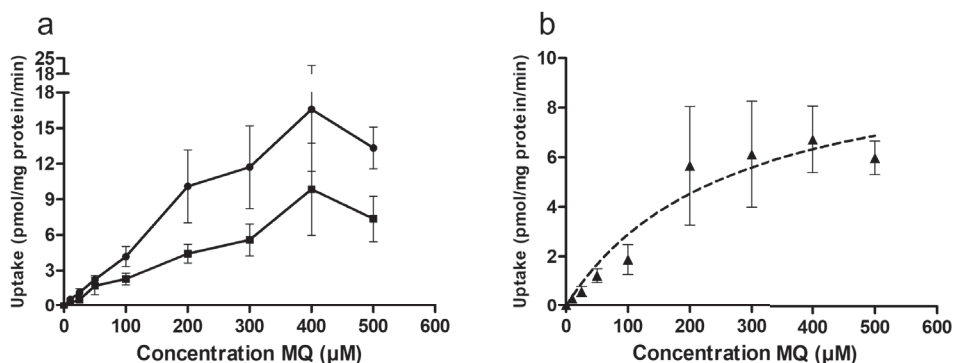
Figure 4.
Concentration-dependent OCT2 uptake of MQ into SA7K cells. (a) The uptake remaining in the presence of doxepin (100 μM) (squares) was subtracted from the total uptake (circles) to obtain (b) the net uptake of MQ (triangles), which follows Michaelis-Menten kinetics with a Vmax of 10.5 pmol/min/mg protein and a Km_{app} in the presence of inhibitor amounting to 260 μM resulting in a Km of MQ for OCT2 transport of 20.6 μM. Each data point represents the mean ± SEM of four biological replicates, each with three technical replicates.

PBK model predictions of blood concentrations

With the input of the *in vitro* obtained kinetic parameter values, PBK model predictions were made. For the *in vivo* data set of 12 mg/kg bw there is no maximal blood concentration (C_{max}) for comparison, so it was decided to predict and compare the concentration detected at t = 1 hour ($C_{t=1}$). Fig. 5a and b show that with the partial scaling factor (for protein and the cortex fraction of the kidney of 0.7) the PBK model is overpredicting with the predicted C_{max} being 6.7-fold higher than what was reported (Fig. 5a) (Table 2). When in absence of a C_{max} using $C_{t=1}$, the difference is somewhat bigger amounting to 8.4-fold (Fig 5b). This indicates that scaling of the *in vitro* kinetic data from the SA7K cells with a protein factor and correction for the cortex fraction of the liver alone does not suffice to predict the excretion-dependent blood concentration in time of MQ, indicating that additional scaling is needed. To investigate what parameters would influence the predictions to the highest extent and could be used for this additional scaling first a sensitivity analysis was performed. This sensitivity analysis should also reveal whether further scaling of Vmax would likely influence the predictions.
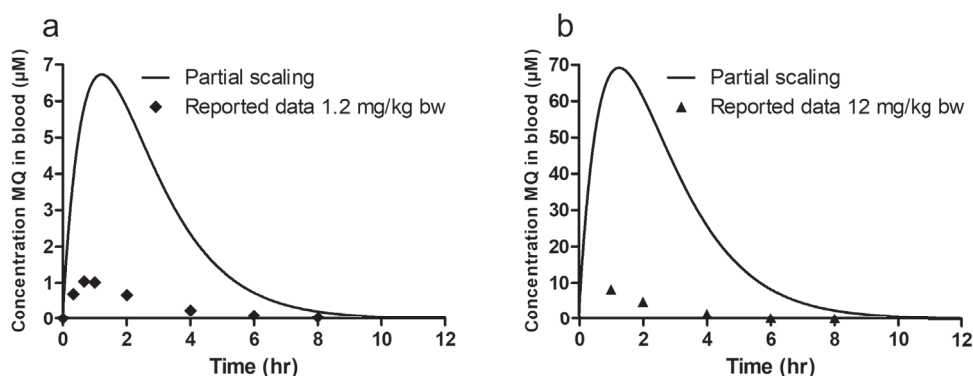
Figure 5.
Predicted and observed blood concentrations (corrected from reported plasma concentrations) of MQ in rats upon oral administration using scaling of the *in vitro* Vmax obtained in SA7K cells for only a protein factor and correction for the cortex fraction of the kidney. The symbols represent the *in vivo* data obtained at a dose of (a) 1.2 mg/kg bw (diamonds) and (b) 12 mg/kg bw (triangles). The lines represent the predictions based on partial scaling of the Vmax (SF; 300*0.7 mg protein/g kidney). Each data point represents the mean ± SEM of four replicates of rat studies, each study containing five animals.

Sensitivity analysis

Figure 6 presents the results of the sensitivity analysis. Model parameters with an absolute value for the normalised sensitivity coefficient of ≥ 0.1 were considered. This reveals that the absorption rate constant ka and also the kinetic constants Vmax and Km for the OCT2 mediated transport are influential parameters. This indicates that further scaling of Vmax can be expected to have an effect on the accuracy of the predictions. Therefore it was investigated what extra scaling factor would be required to optimise the predictions, since that scaling factor would be of use in future studies using the SA7K cells as an *in vitro* model to define PBK model parameters for taking active OCT2 mediated excretion into account.

3

Table 2.
Predicted maximum blood concentration (C_{max} and $C_{t=1}$ [a]), and time of maximum blood concentration (T_{max}) with the fold difference (predicted/observed) of PBK model predictions of orally administered MQ in rats.

		Partial scaling		Full scaling		Fitted ka		Passive elimination	
1.2 mg/kg bw	Observed	Predicted	Fold difference	Predicted	Fold difference	Predicted	Fold difference	Predicted	Fold difference
C_{max} (**μmol/hr**)	1.0	6.7	**6.7**	2.3	**2.3**	1.0	**1.0**	7.0	**7.0**
T_{max} (**hr**)	0.67	1.10	**0.75**	0.46	**0.69**	0.67	**1.00**	1.27	**1.90**
12 mg/kg bw	Observed	Predicted	Fold difference	Predicted	Fold difference	Predicted	Fold difference	Predicted	Fold difference
$C_{t=1}$ [a] (**μmol/hr**)	8.2	69.1	**8.4**	26.6	**3.2**	11.2	**1.4**	70.2	**8.5**

[a] $C_{t=1}$ is the concentration MQ at t = 1 hour. In the data set at dose 12 mg/kg bw no actual C_{max} is presented.
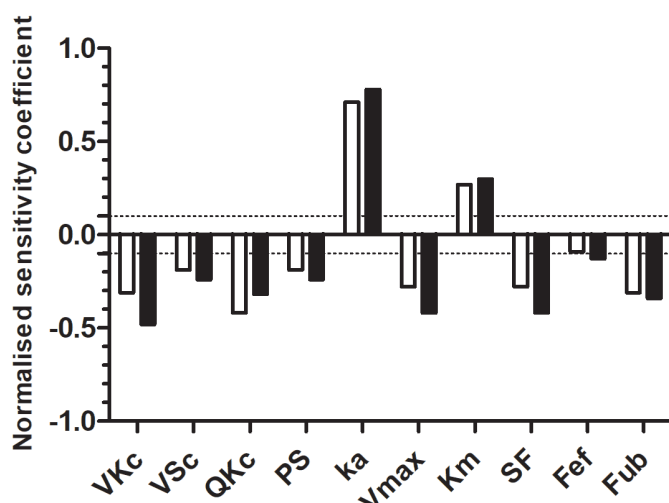
Figure 6.
Normalized sensitivity coefficients of PBK model parameters for the predicted C_{max} of MQ in blood after an oral administration of 1.2 mg/kg bw (white bars) and 12 mg/kg bw (black bars). Only model parameters with normalized sensitivity coefficients with an absolute value higher than 0.1 are shown. VKc = volume of the kidneys, VSc = volume of the slowly perfused tissues, QKc = fraction of blood flow to the kidneys, PS = partition coefficient of slowly perfused tissue, ka = absorption rate constant, Vmax = maximum rate of MQ transport via OCT2, Km = Michaelis-Menten constant of MQ transport via OCT2, SF = scaling factor, Fef = Fraction excreted to faeces, Fub = fraction unbound.

PBK model predictions of the blood concentrations with further scaling of Vmax and ka

Given the deviation between observed and predicted plasma levels it was considered that additional scaling of the Vmax obtained in the SA7K cells when converting it to the Vmax *in vivo* was required to account for i) the level of expression of OCT2 in the SA7K cells as compared to renal tubule cells *in vivo*, ii) the effect of differences in the negative membrane potential driving the activity of OCT2 (Kumar et al. 2018) in the SA7K cells and the *in vivo* situation and iii) species dependent differences in these factors given that the SA7K are human derived cells and *in vivo* data relate to rat. Given the absence of actual data on these factors the additional scaling factor was determined by defining the Vmax required to obtain the optimal fit for the PBK model predictions, in terms of C_{max}, the time at which C_{max} is obtained (T_{max}) and the profile for the time-dependent decrease in plasma concentrations after the C_{max} has been reached. This was achieved by applying an extra scaling factor of 100 resulting in a Vmax amounting to 1050 pmol/min/mg protein. Multiplying this additional scaling factor with the factor for protein content (300 mg protein/g kidney) and the factor 0.7 for cortex content of the kidney results in an overall scaling factor of 21,000 mg protein/g kidney. In this scaling factor the virtual

amount of protein exceeds the kidney weight because the substantially lower expression level of OCT2 in the SA7K cells as compared to kidney tissue requires a virtually large amount of SA7K protein to equal the amount OCT2/g kidney.

Using this overall scaling factor of 21,000 mg protein/g kidney in the PBK model, new predictions were made. Fig.7a and b show that the model predictions improve compared to the reported *in vivo* kinetic data on the blood concentration of MQ resulting in a 2.3 and a 3.2-fold difference for the C_{max} and $C_{t=1}$, respectively (Table 2). This confirms the influence and importance of Vmax on the model outcome as already shown in the previous section. Furthermore, a full match between the PBK model predictions and the reported data could be obtained by also fitting the other influential parameter ka, the absorption rate constant for uptake of MQ from the gastrointestinal tract into the liver. Fitting the ka (default ka = 1 hr^{-1}, reflecting efficient uptake (Punt et al. 2008)), thereby reducing the rate of intestinal uptake, appears essential in approaching the shape of the reported *in vivo* kinetic concentration response-curve best. Using the optimised scaling factor and a ka of 0.36 hr^{-1} the predicted C_{max} was predicted 1 on 1 with the *in vivo* C_{max} and $C_{t=1}$ was 1.4-fold different from the *in vivo* $C_{t=1}$, respectively, while in this case the T_{max} of MQ in blood fits one to one (Table 2).
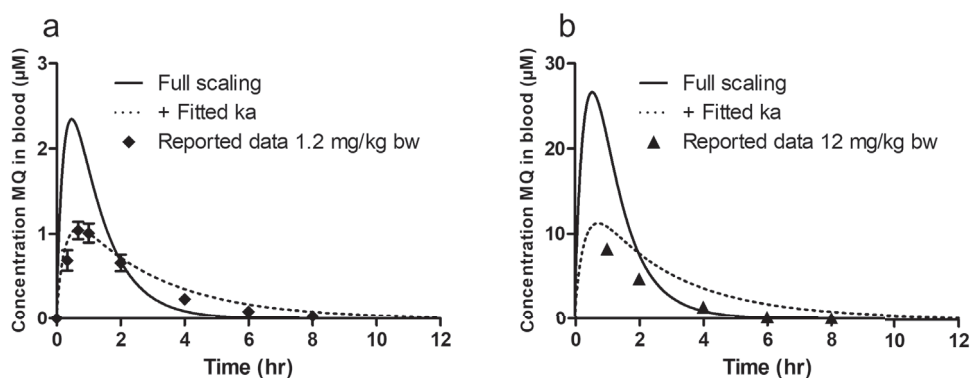
Figure 7.
Predicted and observed blood concentrations (corrected from reported plasma concentrations) of MQ in rats upon oral administration. The symbols represent the *in vivo* data obtained at a dose of (a) 1.2 mg/kg bw (diamonds) and (b) 12 mg/kg bw (triangles). The lines represent the different predictions based on full scaling of the Vmax (SF; 21,000 mg protein/g kidney) (black lines) and the full scaling plus an added fit of the absorption constant (ka) (0.36 hr^{-1}) (dotted lines). Each data point represents the mean ± SEM of four replicates of rat studies, each study containing five animals.

Finally, to further evaluate the importance of active transport in systemic clearance of MQ, Fig. 8 compares the contribution of glomerular filtration and active excretion via OCT2 to the total amount of MQ excreted after 24 hours as predicted by the newly

defined PBK model at different dose levels. It reveals that when a partial scaling factor for Vmax is applied the contribution of active transport via OCT2 is minimal (1 – 10 %). This explains directly why the C_{max} and $C_{t=1}$ were overpredicted by the PBK model and illustrates the need for further scaling of Vmax. Furthermore, the results presented in Fig. 8 also reveal that in the final PBK model, including the full scaling factor for Vmax in combination with the fitted ka, the contribution of OCT2 to the total clearance of MQ is 85% at a dose of 1.2- and 12 mg/kg bw corroborating that MQ clearance is predominantly dependent on OCT2 transport rather than glomerular filtration. Additionally, the model shows that at higher dose, 120 mg/kg bw, the active transport system may become saturated, resulting in a decrease in the relative contribution of OCT2 transport to the total clearance to 64%.
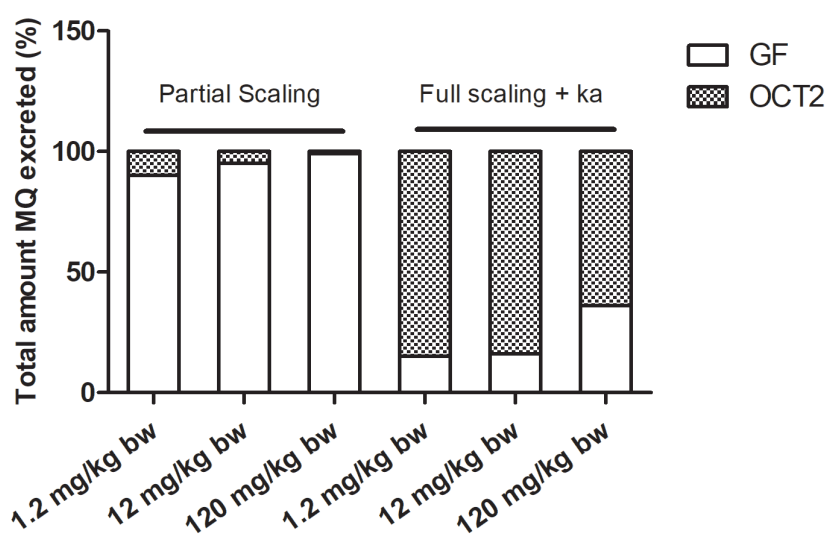
Figure 8.
Contribution (%) of glomerular filtration (GF) and OCT2 mediated excretion to the total amount of MQ excreted after 24 hours as predicted by the PBK model when using different scaling factors. Included are partial scaling of the Vmax (SF; 300* 0.7 mg protein/g kidney) and full scaling of the Vmax (SF; 21,000 mg protein/g kidney) combined with a fitted ka. The total amount excreted was predicted for the following doses: 1.2 mg/kg bw, 12 mg/kg bw and 120 mg/kg bw.

3.4   Discussion

Our study aimed at incorporating renal active excretion into PBK modelling using the RPTEC cell line SA7K to determine the values of kinetic parameters Vmax and Km for OCT2 transport of the model compound MQ. The SA7K cell line is a renal tubular kidney cell line generated with preserved expression and activity of OCT2 (Li et al. 2017c). This is the uptake transporter of interest in our study since the model compound chosen, MQ, is a cation that is not cleared from the systemic circulation by metabolism but predominantly via active excretion via the kidneys (Agency 1997). MQ was also chosen as the model compound for the present study because for this compound *in vivo* kinetic data for PBK model evaluation were available. The SA7K cell line is a kidney cell line and its use eliminates the need for scaling for differences in tissue type (Chan et al. 2019; Chapy et al. 2015). Nevertheless, there is still a need to consider interspecies differences since the SA7K cells represent a human RTPEC cell line, while the PBK model developed in the present study refers to rat. However, given that no rat RPTEC cell line with preserved expression and activity of transporters upon cultivation is available the SA7K cell line was considered the best available *in vitro* model.

In this SA7K model system MQ was shown to be excreted via active transport involving the OCT2 transporter since its transport was inhibited by the OCT2 inhibitors doxepin and verapamil. The Michaelis-Menten kinetic parameter values for Vmax and Km of OCT2 transport of MQ as determined in our present study amounted to 10.5 pmol/min/mg protein and 20.6 µM respectively. Implementing these values into the PBK model together with the partial scaling factor (300 mg protein/g kidney) and correcting for the fact that only 70% of the kidney volume consists of cortex where the RPTEC are located (Kumar et al. 2018) resulted in a predicted C_{max} that was 6.7-fold higher than the reported C_{max} value and 8.4-fold higher than the $C_{t=1}$ from the study where a C_{max} was not observed. This resulted in the understanding that scaling for protein and cortex volume alone would not allow use of the SA7K cell model data for *in vivo* predictions. Further optimisation of the scaling factor by fitting the Vmax to the experimental data resulted in an overall optimised scaling factor of 21,000 mg protein/g kidney, and model predictions for C_{max} and $C_{t=1}$ that deviated from reported values only 2.3 and 3.2-fold, respectively. The importance of Vmax as an influential parameter in the PBK model was in line with a previous study reporting that in the compared reabsorption and secretion models Vmax is critically important in determining renal excretion (Felmlee et al. 2013). Furthermore, this previous study also reported that when using higher dose levels the contribution of glomerular filtration to the renal clearance was increased due to saturation of the active transport system as shown by our model as well. Moreover, the study indicated that to incorporate *in vitro* obtained Vmax data for active transport into PBK models additional scaling is required. Comparison of available *in vivo* data to

the predictions by our initial PBK model also indicated that additional scaling of Vmax was essential.

The reasons potentially underlying the required further optimisation of the scaling factor are many-fold. First of all the level of expression of OCT2 in the SA7K cells as compared to renal tubule cells *in vivo* may be lower (Chan et al. 2019; Jamei et al. 2014). In addition, also the difference in activity of the OCT2 transporter is important since gene expression is not equal to activity (Izumi et al. 2018; Poirier et al. 2009; Vogel and Marcotte 2012). Another factor potentially affecting the difference in OCT2 activity in the SA7K cells and *in vivo* renal tubule cells may be related to potential differences in the negative membrane potential driving the activity of OCT2. Kumar et al. (2018) for example showed that a twofold factor was applied to correct the plasma membrane potential of their *in vitro* systems OCT2-expressing HEK293 and MDCKII cells (35 mV) to human RPTEC cells (70 mV). The third factor is related to species differences since the SA7K cells are human derived cells and the *in vivo* data and the PBK model predictions relate to rat.

A species difference in OCT2 activity may arise from: i) the amino acid identity of organic cation transporters and their expression. The amino acid identity of human OCT2 compared with rat OCT2 is 90% (Hayer-Zillgen et al. 2002; Koepsell et al. 2003). However, where humans have only OCT2 abundantly expressed in the RPTEC, rats also have OCT1 and to a lesser extent OCT3 expressed in the RPTEC (Chu et al. 2013a; Slitt et al. 2002). Since there is a broad overlap of substrates for OCT1-3 there is a probability that MQ in rats has affinity for and will be transported also by OCT1 and OCT3 (Nies et al. 2011; Volk 2013); ii) the difference in the amount of expression of OCT2 in human RPTEC compared with rat RPTEC in the kidneys. A study by Basit et al. (2019) determined the kidney cortex transporters in different species using quantitative proteomics. According to their results the abundance of OCT2 in human kidney cortex is 164.2 pmol/gram kidney and in rat kidney cortex 253.5 pmol/gram kidney, pointing at a 1.5 fold higher expression level in rat than human. Thus, it can be foreseen that the interspecies differences may account for part of the extra 100-fold scaling factor.

Furthermore, depending on the compound of interest additional transporters may be involved in the active elimination. The membranes of the RPTEC (and many other cell types) contain non-selective cation channels, which transport cations such as Na^+, K^+ or Ca^{2+} but also small compounds such as glycine ethyl ester and choline, hence non-selective (Flockerzi 2008). MQ is also a small cationic organic compound and could potentially be transported by these non-selective cation channels (Koepsell et al. 2003), and this factor may also contribute to the extra scaling factor.

A further increase of the scaling factor did reduce the fold difference in predicting the C_{max} but at the same time resulted in deviation from the overall fit of the curve with T_{max} being underpredicted and the clearance at prolonged time points being somewhat overpredicted. Fitting of the other influential parameter ka, could result in accurate predictions of the whole dose response curve with C_{max} and $C_{t=1}$ predicted with a 1.0 and 1.4-fold difference, respectively. With respect to further optimisation of this ka value the report from the US EPA only qualitatively describes absorption to be rapid with a bioavailability of 85% at the highest dose tested (12 mg/kg bw) (Agency 1997). Our data reveal that with an absorption rate of 0.36 hr^{-1} the *in vivo* reported data are fitted best. Whether further support for such a value can be provided has to await further studies.

This study is one of the few studies attempting on reporting on usage of an *in vitro* system with expression of active transporters to incorporate active renal excretion into generic PBK modelling for a compound of which the plasma and tissue concentration are known to depend on the kinetics of excretion. In the past, several attempts were made to include active renal clearance into a PBK model. One of the first models was proposed by Russel et al. (1987) including overall active tubular secretion of salicyluric acid (a metabolite of salicylic acid) in a dog PBK model. A more recent study by Huang and Isoherranen (2018) reported on a mechanistic kidney model to predict renal clearance with inclusion of active excretion based on literature-available *in vitro* transporter data from transfected cell lines and *in vitro* permeability data from Caco-2 cells. Although the authors were able to predict the renal clearance within two-fold, their model contained 35 compartments, making it complex rather than generic.

To summarize, we have used an *in vitro* approach with a fairly novel RPTEC cell line SA7K to obtain values for kinetic parameters Vmax and Km for renal OCT2 mediated active excretion of a model compound, MQ, to define the parameters needed to incorporate active excretion into a rat PBK model that can predict how *in vivo* plasma concentrations rely on active renal excretion. The use of this cell line is a step forward in studying renal transport since most kidney cell lines lose their expression of transporters when in culture (NRK-52E, Caki-1, IHKE-1 and even primary kidney cells) (Lechner 2014). Although the designers of the SA7K cell line state that their cell line is suitable for transport studies, we note that even though the cell line is kidney derived, the results of the present study reveal that there are still a set of challenges to overcome when translating data obtained in this *in vitro* model to the *in vivo* situation. While we were able to determine parameter values of Vmax and Km suitable for PBK modelling, several additional factors had to be considered when translating the *in vitro* OCT2-mediated MQ uptake measured in the SA7K cell line to kinetic data for *in vivo* OCT2-mediated uptake. To find out if the overall scaling factor now obtained of 21,000 mg protein/g

kidney will allow use of the SA7K model also for prediction of *in vivo* renal excretion of other OCT2 substrates requires more QIVIVE studies on OCT2 substrates using this SA7K cell line. All in all this study demonstrates a proof-of-principle on how to include active renal excretion into generic PBK models.

Declaration of Competing Interest
The authors report no declaration of interest.

Acknowledgement

Supplementary material A
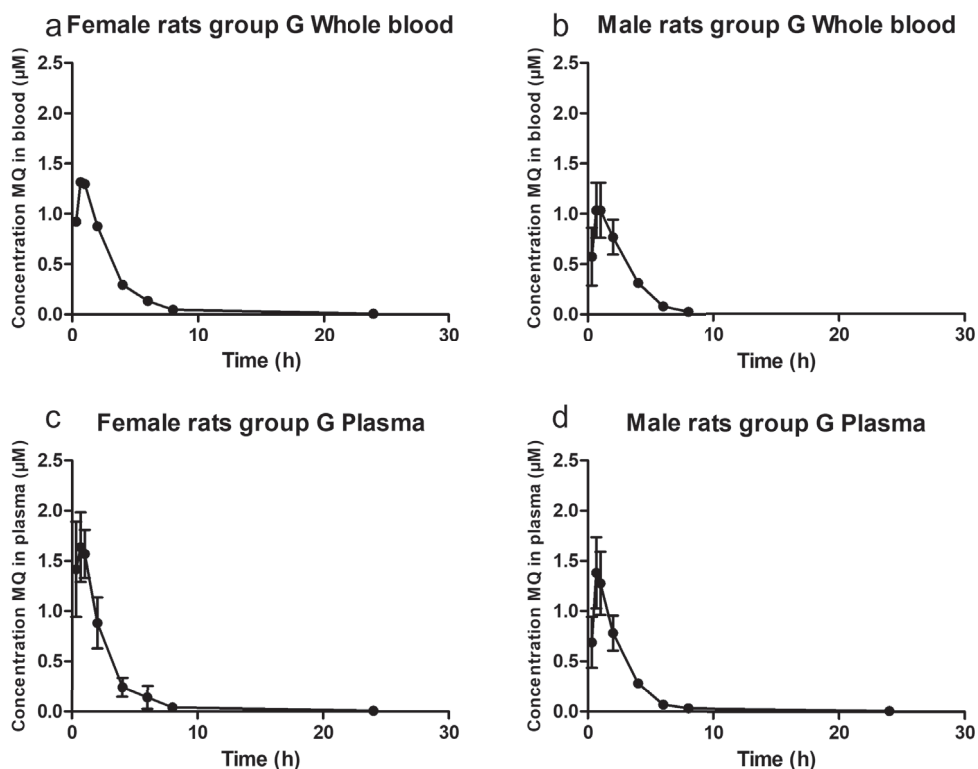
Fig. A.1.
Individual data sets of MQ at dose 1.2 mg/kg bw reported by BASF SE. A, B) Time-dependent concentration of MQ obtained in whole blood. C, D) Time-dependent concentration of MQ obtained in plasma. Each data point represents the mean ± SD of five animals.
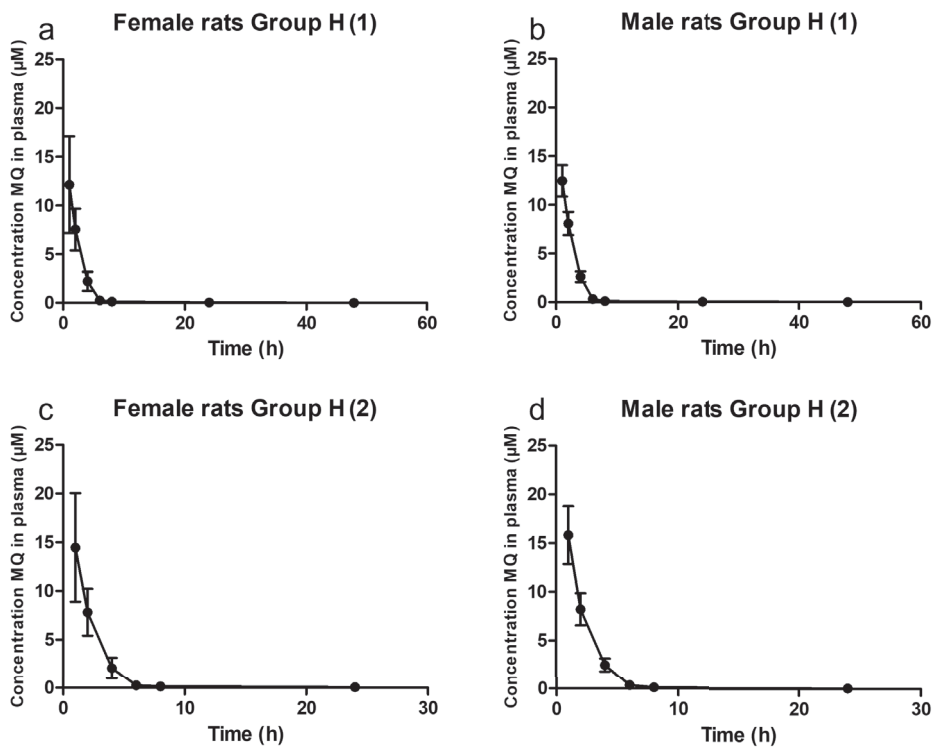
Figure A.2.
Individual data sets of MQ at dose 12 mg/kg bw reported by BASF SE. Time-dependent concentration of MQ obtained in plasma. Each data point represents the mean ± SD of five animals.
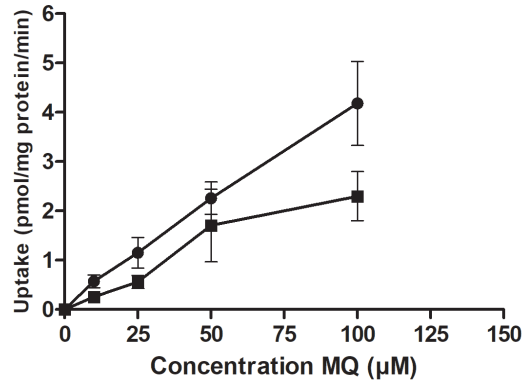
Figure A.3.
Uptake (circles) and inhibited uptake (squares) of MQ at concentrations 10 – 100 μM in the SA7K cells. Each data point represents the mean ± SEM of four biological replicates, each with three technical replicates.

Supplementary material B

Model code for PBK-model built in Berkeley Madonna
; Date: May 2019
; Purpose: PBK Model of mepiquat chloride (MQ), built with *in vitro* and *in silico* derived parameter values
; Species: Rat
; Compiled by: Annelies Noorlander
; Organisation: Wageningen University

;==
;Physiological parameters
;==
; tissue volumes
BW = 0.200 (Kohane et al.)   ; body weight rat (variable, dependent on study)
VFc = 0.07   ; fraction of fat tissue   reference: Brown et al. Table 21 (1997)

VLc = 0.034   ; fraction of liver tissue   reference: Brown et al. Table 21 (1997)

VKc = 0.007   ; fraction of kidney tissue   reference: Brown et al. Table 21 (1997)

VBc = 0.074   ; fraction of blood   reference: Brown et al. Table 21 (1997)

VRc = 0.091   ; fraction of richly perfused tissue   reference: Brown et al. Table 21 (1997)

VSc = 0.724   ; fraction of slowly perfused tissue   reference: Brown et al. Table 21 (1997)

VF = VFc*BW   {L or Kg} ; volume of fat tissue (calculated)
VL = VLc*BW   {L or Kg} ; volume of liver tissue (calculated)
VK = VKc*BW   {L or Kg} ; volume of kidney tissue (calculated)
VB = VBc*BW   {L or Kg} ; volume of blood (calculated)
VR = VRc*BW   {L or Kg} ; volume of richly perfused tissue (calculated)
VS = VSc*BW   {L or Kg} ; volume of slowly perfused tissue (calculated)

;--
;blood flow rates

QC = 15*BW^0.74 {L/hr}   ; cardiac output
                                     reference: Brown et al. p.453 (1997)
QFc = 0.07   ; fraction of blood flow to fat
                                     reference: Brown et al. Table 25 (1997)
QLc = 0.174   ; fraction of blood flow to liver
                                     reference: Brown et al. Table 25 (1997)
QKc = 0.141   ; fraction of blood flow to kidney
                                     reference: Brown et al. Table 25 (1997)
QRc = 0.093   ; fraction of blood flow to richly perfused tissue
                                     reference: Brown et al. Table 25 (1997)
QSc = 0.522   ; fraction of blood flow to slowly perfused tissue
                                     reference: Brown et al. Table 25 (1997).

```
QF = QFc*QC            {L/hr}            ; blood flow to fat tissue (calculated)
QL = QLc*QC            {L/hr}            ; blood flow to liver tissue (calculated)
QK = QKc*QC            {L/hr}            ; blood flow to kidney tissue (calculated)
QS = QSc*QC            {L/hr}            ; blood flow to  slowly perfused tissue (calculated)
QR = QRc*QC            {L/hr}            ; blood flow to richly perfused tissue (calculated)
```

```
;===================================================================
;Physicochemical parameters
;===================================================================
```

;partition coefficients --> logP MQ Safety data sheet BASF: -3.55

PF = 0.14   ; fat/blood partition coefficient   calculated using QPPR of: (Rodgers & Rowland, 2006)

PL = 0.66 ; liver/blood partition coefficient   calculated using QPPR of: (Rodgers & Rowland, 2006)

PK = 0.69; kidney/blood partition coefficient   calculated using QPPR of: (Rodgers & Rowland, 2006)

PR = 0.66; richly perfused tissue/blood partition coefficient   calculated using QPPR of: (Rodgers & Rowland, 2006)

PS = 0.42 ; richly perfused tissue/blood partition coefficient   calculated using QPPR of: (Rodgers & Rowland, 2006)

```
;===================================================================
;Kinetic parameters
;===================================================================
```

```
;Absorption from GI-tract to liver
ka  =  0.36                    ; absorption {/hr}
```

```
;--------------------------------------------------------------------------------------------------------------------
;Excretion from kidney
```

```
;Active uptake is described in first order kinetics where Vmax and Km become one constant number.
VmaxOCT2c = 10.5                              ;{pmol/min/mg}
```

```
VmaxOCT2 = (VmaxOCT2c/1000000)*60*SF*VK*1000      ;{umol/hr}
;300 mg prot./g kidney (Kumar et al. 2018)
;only 70% of whole kidney is cortex --> in cortex tubule cells thus OCT-2s are present (Kumar et al. 2018)
; 300 * 0.7 = 210 mg prot./g kidney
```

```
KmOCT2 = 20.6    ; {uM} transport constant of MQ via OCT2
SF = 210                ; mg/g protein
```

```
;=================================================================
;Run settings
;=================================================================


;Molecular weight MQ
MW = 149.7



;----------------------------------------------------------------------------------------------------------------


;Oral dose
ODOSEmg = 1.2 {mg/kg bw}                              ; ODOSEmg = given oral dose in mg/kg bw
ODOSEumol2 = ODOSEmg*1E-3/MW*1E6 {umol/kg bw}; ODOSEumol2  =  given  oral  dose
                                                 recalculated to umol/kg bw
ODOSEumol=ODOSEumol2*BW;                      ; ODOSEumol = umol given oral



;time
Starttime = 0              ; in hr
Stoptime = 24       ; in hr



;=================================================================
;Model calculations
;=================================================================

; Model MQC
;----------------------------------------------------------------------------------------------------------------

;stomach compartment
;Ast  = amount in stomach, umol

Ast' = -ka*Ast
Init ASt = ODOSEumol
;----------------------------------------------------------------------------------------------------------------
;liver compartment

;AL = Amount MQ in liver tissue, umol
;AL' = Amount of MQ in time (umol/hr)

AL' =  ka*Ast + QL*(CB - CVL) - AFae'
Init AL = 0
CL = AL/VL
CVL = CL/PL

;AFae = amount MQ in faeces 10 %
AFae' = Fef * (ka*ASt)
Fef = 0.10
Init AFae = 0
;----------------------------------------------------------------------------------------------------------------
;kidney compartment
```

;AK = Amount of MQ in kidney (umol)

;AK' = Amount of MQ in time (umol/hr)

AK' = QK*(CB-CVK)-GF'-AKe'
       Init AK = 0
       CK = AK/VK
       CVK = CK/PK

;GFR = glomerular filtration rate {L/hr}   ; Walton, et al 2004
;GFR rat = 5.2   ; mL/min/kg bw
       GFR = 0.0052*BW*60   ;L/hr

;GF = glomerular filtration of mepiquat (umol/hr)
       GF' = GFR*(CVK*Fub)
       Init GF = 0

;Fub = fraction unbound of MQ
       Fub = 1

;AKe = amount mepiqat actively excreted from the kidney (umol)
;AKe' = amount mepiqat actively excreted from the kidney in time (umol/hr)
AKe' = VmaxOCT2*(CVK*Fub)/(KmOCT2 + (CVK*Fub))
       Init AKe = 0

;---
;fat compartment

;AF = Amount MQ in fat tissue (umol)
     AF' = QF*(CB-CVF)
     Init AF = 0
     CF = AF/VF
     CVF = CF/PF

;---
;tissue compartment richly perfused tissue

;AR = Amount MQ in richly perfused tissue (umol)
     AR' = QR*(CB-CVR)
     Init AR = 0
     CR = AR/VR
     CVR = CR/PR

;---
;tissue compartment slowly perfused tissue

;AS = Amount MQ in slowly perfused tissue (umol)
     AS' = QS*(CB-CVS)
     Init AS = 0
     CS = AS/VS
     CVS = CS/PS

```
;---------------------------------------------------------------------------------------------------------
; blood compartment

;AB = Amount MQ in blood (umol)
    AB' = (QF*CVF + QL*CVL + QK*CVK + QS*CVS + QR*CVR - QC*CB)
    Init AB = 0
    CB = AB/VB



;====================================================================
;Mass balance calculations
;====================================================================

Total = ODOSEumol
Calculated = ASt + AL + AK + AKe + GF + AF + AS + AR + AB + AFae

ERROR=((Total-Calculated)/Total+1E-30)*100
MASSBBAL=Total-Calculated + 1
```

3
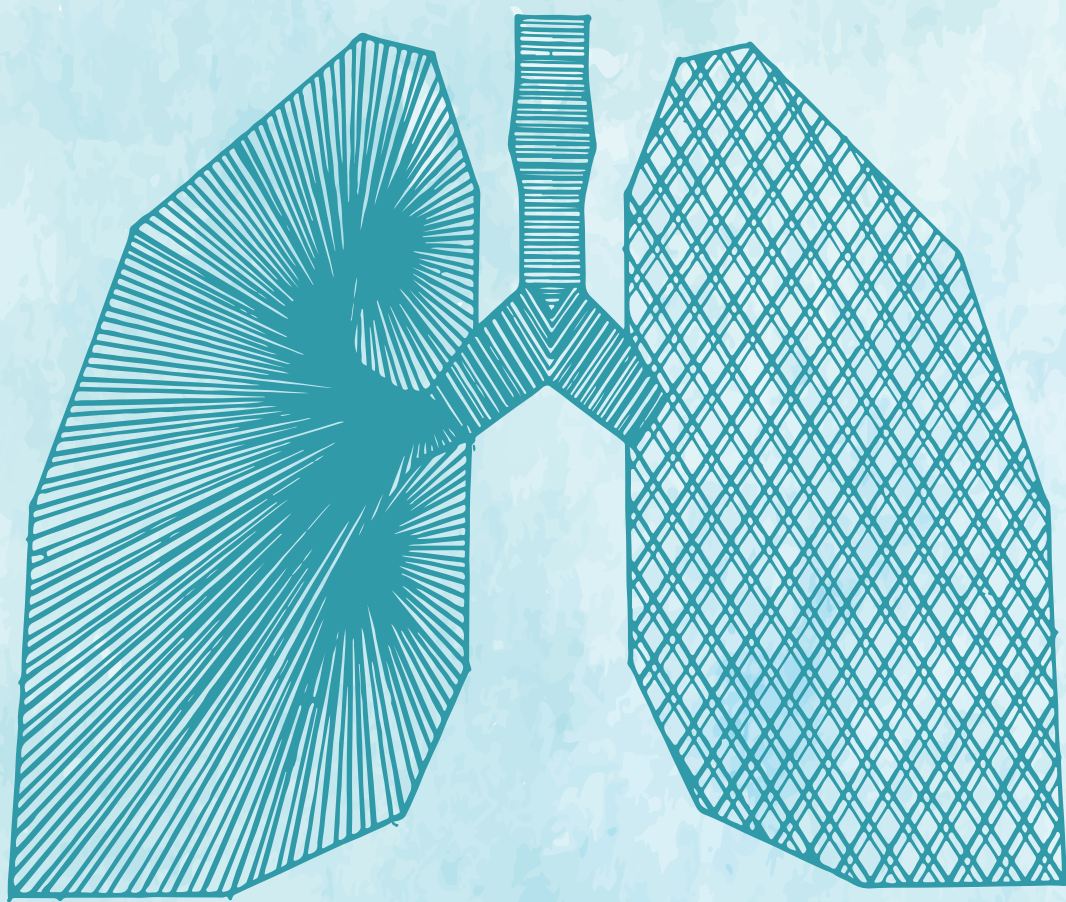
Chapter 4

Predicting acute paraquat toxicity using physiologically based kinetic modelling incorporating *in vitro* active renal excretion via the OCT2 transporter

Annelies Noorlander, Sebastiaan Wesseling, Ivonne M.C.M. Rietjens
and Bennard van Ravenzwaay

Abstract

The present study aimed at evaluating a new approach methodology (NAM) for predicting the acute toxicity of paraquat (PQ) based on the development of a physiologically based kinetic (PBK) model including *in vitro* kinetic input on the active excretion of PQ via the organic cation transporter 2 (OCT2). The PBK model was used to apply reverse dosimetry for quantitative *in vitro-in vivo* extrapolation (QIVIVE) to predict the acute *in vivo* toxicity of PQ. The kinetic parameters Vmax and Km for *in vitro* OCT2 transport of PQ were obtained from the literature. Appropriate scaling factors were applied to translate the *in vitro* Vmax to an *in vivo* Vmax. PQ is a pneumotoxicant, so the *in vitro* toxicity data used were from cytotoxicity studies performed in alveolar cell lines. Cytotoxicity data for rats were defined in the RLE-6TN and L2 cell lines and for humans, cytotoxicity data in the A549 cell line were taken from literature. With the developed PBK model the *in vitro* cytotoxicity concentration-response curves were translated to predicted *in vivo* toxicity dose-response curves from which the lower and upper bound benchmark dose (BMD) for 50% lethality ($BMDL_{50}$ and $BMDU_{50}$) were derived by applying BMD analysis and compared to the *in vivo* reported median lethal dose (LD_{50}) values for rat and human. The results obtained showed the approach to make a conservative prediction for the *in vivo* acute toxicity of PQ with the difference between the predictions and the different reported data for rat being at best 6.9-fold and those for human being comparable, thus providing a proof of principle showing how to include active renal excretion in PBK modelling and how to apply the model for QIVIVE translation to predict the acute *in vivo* toxicity, using PQ as the model compound.

Keywords: Acute toxicity, new approach methodologies, Physiologically based kinetic modelling, reverse dosimetry, paraquat, renal excretion, scaling factor

List of abbreviations: ADME (absorption, distribution, metabolism, excretion), **ARfD** (acute reference dose), **BMD** (Benchmark dose), **A549** (Human lung epithelial cell line), **$BMDL_{50}$** (lowest observed adverse effect level), **EFSA** (European Food Safety Authority), **FBS** (foetal bovine serum), **GF** (glomerular filtration), **HEK293** (human embryonic kidney cell line), **IM** (intramuscular), **IV** (intravenous), **LC-MS/MS** (Liquid chromatography mass spectrometry), **LD_{50}** (median lethal dose), **LOAEL** (lowest observed adverse effect level), **L2** (Rat lung epithelial cell line), **MATE** (multidrug and toxin extrusion transporter), **MRM** (multiple reaction monitoring), **MQ** (mepiquat), **NAM** (new approach methodology), **NOAEL** (no observed adverse effect level), **OCT2** (Organic cation transporter 2), **PBK** (Physiologically based kinetic), **PoD** (Point of departure), **PQ** (paraquat), **QIVIVE** (quantitative *in vitro – in vivo* extrapolation), **RAF** (relative activity factor), **REF** (relative expression factor), **RLE-6TN** (Rat lung epithelial cell line), **RPTEC** (renal proximal tubule epithelial cell), **TE** (transporter efficiency)

4.1   Introduction

For some compounds the absorption, distribution, metabolism and excretion (ADME) characteristics are substantially influenced by active transport in for example the intestine, kidneys, liver, placenta or the blood-brain-barrier. Incorporating this active transport into physiologically based kinetic (PBK) models based on *in vitro* data is still in a developing stage (Kasteel et al. 2021; Noorlander et al. 2021a; Noorlander et al. 2021b; Noorlander et al. 2022; Poirier et al. 2009; Strikwold et al. 2017b; Worley and Fisher 2015). The challenges related to incorporation of active transport are for example the type of *in vitro* models to be used to quantify the kinetics of the active transporters involved and the scaling factors needed to translate *in vitro* obtained data to the *in vivo* situation. Recent work by our group (Noorlander et al. 2021b) using the herbicide mepiquat (MQ) chloride as the model compound showed that an *in vitro* model using the renal proximal tubule epithelial cell (RPTEC) line SA7K with maintained expression of functionally active transporters (Li et al. 2017c) can be useful to quantify PBK model parameters for active transport via the organic cation transporter 2 (OCT2). The obtained *in vitro* Michaelis-Menten kinetic parameter values Vmax and Km for this OCT2 mediated transport in the SA7K cells were scaled to the *in vivo* situation and incorporated into a PBK model that was able to adequately predict the time-dependent blood concentrations of MQ only when taking this active OCT2 mediated transport into account (Noorlander et al. 2021b).

A subsequent step would be to extend this first proof of principle and evaluate the use of the SA7K cell model and the defined scaling factor to predict the *in vivo* kinetics of another OCT2 substrate. The first aim of the present study was to provide this further proof of principle using paraquat (PQ) dichloride (N,N′-dimethyl-4,4′-bipyridinium dichloride) (figure 1) as the model compound.

PQ is a herbicide belonging to the bipyridylium quaternary ammonium herbicide family. The ADME characteristics of PQ include a rapid but incomplete (5%) absorption from the small intestine followed by its distribution over the tissues and the systemic circulation (Dinis-Oliveira et al. 2008; Houze et al. 1990). PQ is hardly metabolised and systemically eliminated unchanged via the kidneys using active transport in addition to glomerular filtration (Chan et al. 1997; Dinis-Oliveira et al. 2008), making it a suitable model substrate for the aim of the present study.

4
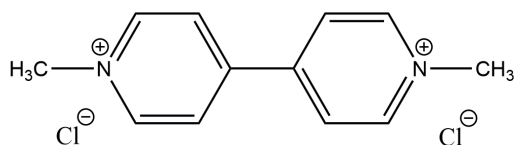
Figure 1.
Molecular structure of paraquat (PQ) dichloride.

Given the cationic nature of PQ the active transporters mainly involved in the renal excretion of PQ are the uptake transporter OCT2 and the multidrug and toxin compound extrusion (MATE) efflux transporter (Chen et al. 2007; George et al. 2017). Several studies reported the activity of OCT2 and MATE for PQ transport, but it remains to be evaluated to what extent OCT2 mediated secretion affects the total plasma clearance *in vivo* (Chan et al. 1998; Chen et al. 2009; Chen et al. 2007). This is also illustrated by the fact that previous PBK models for PQ ignored this active excretion component deliberately assuming that glomerular filtration of PQ would suffice for the model predictions (Campbell et al. 2021; Lohitnavy et al. 2017; Stevens et al. 2021).

The use of PQ as a weed killer has been banned in many countries due to its toxic properties where exposure mainly originates from accidental or intentional ingestion, or exposure via damaged skin (occupational) or inhalation (Watts 2011) and may lead to death. The US Environmental Protection Agency (EPA) reported in 2019 on an oral no observed adverse effect level (NOAEL) of 0.5 mg paraquat ion/kg bw/day based on the incidence of gross lung lesions, increased lung weight and severity of chronic pneumonitis in two co-critical subchronic and chronic dog oral toxicity studies (EPA 2019). With the uncertainty factors for inter- and intraspecies variability this NOAEL resulted in a health based guidance value (HBGV) of 0.005 mg paraquat ion/kg bw/day. Acute toxicity in rat and human has been reported to result from accumulation and toxicity of PQ in lung tissue and to occur at mean lethal dose levels (LD_{50}) ranging between 40 – 200 mg/kg bw and 3 – 60 mg/kg bw, respectively (Dinis-Oliveira et al. 2008; Roberts 2013; Watts 2011).

In the past many (fatal) cases have been reported associated with accidental and particular intentional ingestion of PQ. The case studies reported provide limited information on exposure and time of admission to the hospital after ingestion. One study reported on the ingested PQ dose in grams and several other studies report the dose in terms of the percentage of PQ in the ingested formula (Houze et al. 1990; Proudfoot et al. 1979; Sawada et al. 1988). Once admitted in the hospital blood samples were taken and measured regularly until patients died or in some cases survived. Proudfoot et al. (1979) collected these data of 71 cases and generated a time-dependent blood concentration survival curve for the first 24 hours following ingestion where all cases with blood levels reported below this curve would survive the exposure to PQ. This survival curve has

been extended to days after ingestion by Scherrmann et al. (1987) using a hyperbolic equation. Defining a dose response curve for PQ acute toxicity in human using a PBK model based New Approach Methodology (NAM) would support the evaluation of the hazards and risks of PQ exposure based on external as well as internal dose levels.

Thus, the aim of the present study was to use the developed PBK model and to evaluate how this PBK model based reverse dosimetry for quantitative *in vitro* to *in vivo* extrapolation of *in vitro* toxicity data, would perform and how such a NAM could support the hazard and risk assessment of PQ. To this end, upon evaluation of the developed PBK model by comparison of predictions made to available *in vivo* kinetic data for PQ in rats and human, the PBK model was used for reverse dosimetry to predict the *in vivo* acute toxicity of PQ from *in vitro* data on acute toxicity in cells from rat lung epithelial cell lines (RLE-6TN and L2) and the human lung epithelial cell line (A549). Comparison of the predicted dose response curves to available toxicity data was performed to further evaluate the PBK model and at the same time provide insight into the role of active renal excretion in the kinetics of PQ and derive a point of departure (PoD) for evaluation of the acute toxicity of PQ.

4.2   Materials and Methods

Chemicals
Paraquat (PQ) dichloride hydrate, ammonium formate, bovine serum albumin (BSA) and formic acid were purchased from Sigma-Aldrich (Zwijndrecht, the Netherlands). Hydrochloride acid (HCl) was purchased from Merck (Darmstadt, Germany). Doxepin hydrochloride was purchased from Carbosynth (Berkshire, UK). Dimethyl sulfoxide (DMSO) used for dissolving doxepin was purchased from Merck (Darmstadt, Germany). Acetonitrile and methanol were purchased from Biosolve (Valkenswaard, the Netherlands). Ultrapure water was used from a system of Arium Pro VF Sartonius (Rotterdam, the Netherlands).

Cell culture
Lung cell line
The rat lung epithelial cell line (RLE-6TN) (ATCC® CRL-2300™, Wesel, Germany) was cultured in Ham's F12 medium supplemented with 10 µg/mL bovine pituitary extract, 2 mM L-glutamine, 1% penicillin/streptomycin, 30 µg/mL gentamicin (all from Thermo Fischer Scientific Bleiswijk, the Netherlands), 5 µg/mL insulin (Sigma-Aldrich, Zwijndrecht, the Netherlands), 1.25 µg/mL transferrin, 10% foetal bovine serum (FBS) (both from Capricorn, Leusden, the Netherlands), 2.5 ng/mL recombinant rat insulin-like growth factor (BioTechnology, Abingdon, U.K.), 2.5 ng/mL epidermal growth

factor (Lonza, Breda, the Netherlands) at 37°C with 5% (v/v) CO_2 and 95% (v/v) humidity. Cells used in this study were between 2 – 11 cell passages. In this study all concentrations and doses of PQ relate to its dichloride salt form.

Kidney cell line

The human renal proximal tubule epithelial cell (RPTEC) line SA7K (Sigma-Aldrich, Zwijndrecht, the Netherlands) was cultured in MEMα (Sigma-Aldrich, Zwijndrecht, the Netherlands) supplemented with RPTEC Complete Supplement (Sigma-Aldrich, Zwijndrecht, the Netherlands), 2.5 mM L-glutamine, 30 μg/mL gentamicin and 0.015 μg/mL amphotericin B (all from Thermo Fischer Scientific Bleiswijk, the Netherlands) at 37°C with 5% (v/v) CO_2 and 95% (v/v) humidity. For uptake studies cells were seeded in 6-well plates at a density of $5 \times 10^5 – 7.5 \times 10^5$ cells/well and grown for 2 days prior to use with a medium change after one day. Cells used in this study were between 7 – 17 cell passages.

Cytotoxicity of PQ

Experimental

RLE-6TN cells were seeded in 96-well plates at a density of 1×10^4 cells/well and after a 24 hour incubation for cell attachment the cells were exposed to PQ (final concentrations 5, 10, 25, 50, 75, 100, 125, 150, 175 and 200 μM) (added from 200 times concentrated stock solutions in ultrapure water) for 24 hours. Then 5 μL water soluble tetrazolium-1 (WST-1) was added to each well and the cells were incubated for an hour at 37°C. Finally, the absorbance was measured at two wavelengths (440 nm; 620 nm) using a microplate reader (SpectraMax® iD3). Each concentration was tested in sextuplet with a biological replicate of four times. The data were calculated as percentage of the solvent control.

Literature

Additional *in vitro* cytotoxicity data of PQ were collected from the literature. Three more studies reported on the PQ cytotoxicity in RLE-6TN cells (Wang et al. 2016; Wang et al. 2018; Zhu et al. 2016). One study reported on PQ cytotoxicity in another rat lung cell line L2 (Chen et al. 2012). All reported studies exposed the cells for 24 hours. Furthermore, PQ cytotoxicity data collected in the human cell line A549 were reported in four studies where three studies exposed the cells for 24 hours and two studies for 48 hours (Kanno et al. 2019; Kim et al. 2011; Wang et al. 2016; Zhu et al. 2016).

OCT2 uptake of PQ
Experimental work
SA7K cells were pre-incubated in pre-warmed (37°C) uptake buffer (136 mM NaCl, 5.3 mM KCl, 1.1 mM KH_2PO_4, 0.8 mM $MgSO_4·7H_2O$, 1.8 mM $CaCl_2·2H_2O$, 11 mM D-glucose, 10 mM HEPES, pH 7.4) within the presence or absence of the OCT2 inhibitor doxepin (Chan et al. 1998; Hacker et al. 2015; Li et al. 2017c; Samai et al. 2008) (final concentration 100 µM added from a 200 times concentrated stock solution in DMSO) for 10 minutes at 37°C. After 10 minutes, PQ (final concentration 10 µM added from a 200 times concentrated stock solution in methanol:HCl 0.1 M (1:1)) was added and the cells were incubated for 2, 5, 10, 15, 30 and 60 minutes. Each experimental condition was measured in a technical triplicate and a biological duplicate. After incubation, medium was removed and cells were washed twice with ice-cold PBS containing 0.2% (w/v) BSA and once with ice-cold PBS alone (to eliminate unspecific binding). Cells were lysed with methanol:HCl 0.1 M (1:1) in a freeze-thaw cycle. Protein was measured using the Pierce BCA protein assay kit (Thermo Fischer Scientific Bleiswijk, the Netherlands). PQ present in the cell lysate was quantified using LC-MS/MS. It is also important and crucial to note that at all times polypropylene/polystyrene materials were used for PQ, because of its ability to adsorb to glass (Muhamad et al. 2011).

Literature
A literature search was done in PubMed using search terms: paraquat, OCT2 AND/OR, Vmax AND/OR, Km AND/OR kinetics to collect all the available *in vitro* kinetic data on OCT2 transport of PQ reporting the Km and Vmax. This provided two reported data sets on the OCT2 specific transport of PQ in human embryonic kidney (HEK) 293 cells overexpressing the OCT2 transporters in one study (Chen et al. 2007).

Liquid chromatography mass spectrometry (LC–MS/MS)
For quantification of PQ the protocol described by Pizzutti et al. (2016) was used. In brief, PQ was quantified on an LC-MS/MS system (Shimadzu, Kyoto, Japan), containing a Nexera XR LC-20AD SR UPLC system coupled to a triple quadrupole mass spectrometer LCMS-8040 with a Sielc Obelisc R column (100 x 2.1 mm, 5 µm particle size). The mobile phase consisted of (A) 20 mM ammonium formate with formic acid (pH 3.0) and (B) acetonitrile with 0.1 % (v/v) formic acid (gradient: 0.00 - 5.50 min 80-20% B, 5.50 - 8.50 min 20% B, 8.50 - 11.50 min 20-80% B, 11.50 - 14.00 min 80% B). The flow rate was 0.4 mL/min. The injection volume was 5 µL and the column oven was set at 40°C. Under these conditions the retention time of PQ was 7.0 min. The mass spectrometer was set in the positive electron spray mode. The MRM transitions used to determine and quantify PQ were 186.2 à 171.0, 186.2 à 77.0 and 186.2 à 155.0 (m/z for all masses).

Physiologically based kinetic (PBK) modelling

A physiologically based kinetic model for PQ was developed for rat and human. The models consisted of separate compartments for GI-tract, kidney, lung, liver, fat and blood (Figure 2). The rest of the organs/tissues were placed either under rapidly perfused tissue (brain, heart) or slowly perfused tissue (bone, skin, muscle). The parameters for tissue weight and tissue blood flow were collected from Brown et al. (1997a). The QIVIVE toolbox developed by Punt et al. (2020) was used to obtain tissue:blood partition coefficients based on Rodgers and Rowland (2006). Toolbox input of PQ: LogP = -4.22, molecular weight = 257.2 g/mol, ticked box for the presence of quaternary N atom(s) (see supplementary material A table S1 for overview of parameters). Only 5% of the orally administered PQ crosses the GI-tract into the blood (Houze et al. 1990). Transport of PQ into the alveolar tissue via the polyamine uptake system is incorporated in the model via the Michaelis-Menten parameter values Vmax (300 nmol/g tissue/h for both rat and human) and Km (70 and 40 µM for rat and human, respectively) derived from a study with lung slices (Dinis-Oliveira et al. 2008). The accumulation is simulated based on these active uptake parameters with inclusion of a low transport rate back into the lung blood (k_{er} = 0.003 hr^{-1}) (Lohitnavy et al. 2017). PQ is hardly metabolised in the body (Lock 2010), therefore no equations and kinetic parameters for hepatic clearance were included in the model. In the PBK model the clearance of PQ is completely depending on glomerular filtration and active transport via OCT2 in the kidney, which in the model is described as follows:

$$AKe = \left(GFR \times (CVK \cdot Fub)\right) + \left(\frac{Vmax_{OCT2} \times CVK}{(Km_{OCT2} + CVK)}\right) \tag{1}$$

where AKe is the amount of PQ excreted via the kidney over time (µmol/hr), GFR is the glomerular filtration rate of rat (L/hr), CVK the venous concentration of PQ in the kidney (µmol/L), $Vmax_{OCT2}$ and Km_{OCT2} the maximum rate (µmol/hr) and Michaelis-Menten constant (µmol/L) for the active transport of PQ by OCT2, and Fub the fraction unbound of PQ in blood, which was 0.7 for rat and 0.65 for human (Stevens et al. 2021). Berkeley Madonna software (UC, Berkeley, CA, USA version 10.2.8) was used to solve the equations with the Rosenbrock-stiff model.
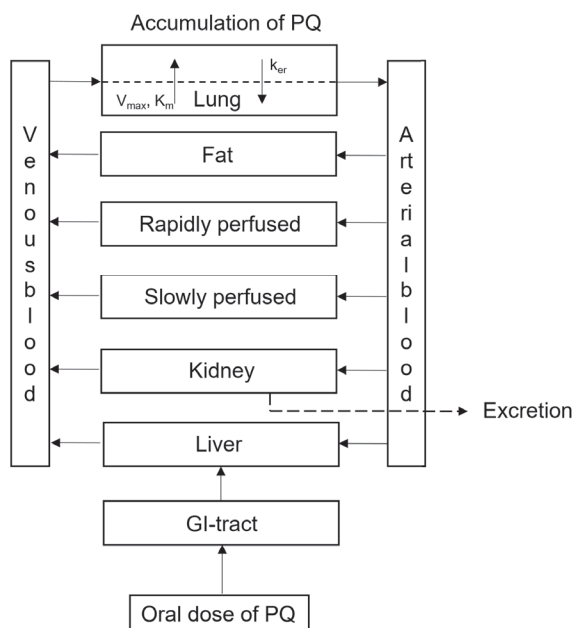
Figure 2.
Schematic overview of the conceptual PBK model for PQ including renal excretion and active uptake in lung tissue.

Scaling factor

Conversion of the *in vitro* obtained Vmax value for OCT2 uptake of PQ in SA7K cells expressed in pmol/min/mg protein into an *in vivo* Vmax expressed in μmol/hr/ kidneys is done with a scaling factor, which has been extensively elaborated on in our previous work (Noorlander et al. 2021b). Briefly, the scaling factor consisted of three parts. 1) Converting the activity in the cells *in vitro* expressed in pmol/min/mg cellular protein to the activity expressed in a unit that represents the activity in the two whole kidneys expressed in pmol/min/g kidneys. 2) Including only the part of the kidney – kidney cortex - where OCT2 is expressed. 3) Scaling to account for the fact that the expression and activity of OCT2 in the *in vitro* system differs from its expression and activity in the renal tubule cells in the kidney cortex, which includes: i) the differences in OCT2 expression levels, ii) potential differences in membrane potential between the relevant cells *in vitro* and *in vivo* and, iii) interspecies differences between human (SA7K/HEK293 cell line) and rat (the PBK model). Fitting the *in vitro* obtained Vmax in Berkeley Madonna to available *in vivo* data informed on the actual size of this third part of the scaling factor. The overall scaling factor was acquired by multiplying the three factors. For conversion of the *in vitro* Vmax for OCT2 mediated transport of PQ to the *in vivo* Vmax for OCT2 mediated transport the following formula was used:

$$In\ vivo\ \text{Vmax} = \left(\frac{In\ vitro\ \text{Vmax}}{1{,}000{,}000}\right) \times 60 \times \text{SF} \times (\text{Volume of kidneys}) \times 1000 \tag{2}$$

where the factor 1,000,000 is used to convert pmol to μmol, 60 to convert minutes to hours, 1000 to convert kg kidney weight to g kidney weight and SF is the scaling factor encompassing the three parts mentioned above expressed in mg protein/g kidney.

The full model code is presented in Appendix B of the supplementary material.

Evaluation of the PBK model and sensitivity analysis

The developed PBK model for PQ in rat was evaluated by comparing the predicted oral blood concentration time curve with available experimental data on the blood concentration time curve of PQ in rat at non-toxic levels (0.039 mg/kg bw) (Chui et al. 1988). To quantify the contribution of active renal excretion via OCT2 to the overall clearance of PQ, the PBK model-predicted blood concentration time curve was compared with the predicted blood concentration time curve obtained with only passive glomerular filtration. For human, the focus was on the blood concentration time curves of the patients who survived the PQ exposure (Proudfoot et al. 1979). However, most of the literature studies reporting blood-concentration time curves did not quantify the starting dose. Only Houze et al. (1990) reported on the dose of survivors which was between 0.5 and 0.8 gram. Translating these doses back to doses in mg/kg bw taking 70 kg as the average bodyweight, survivors took 7.1 to 11.4 mg/kg bw. Blood concentration time curves were predicted at these doses assuming the model was well validated for rat and therefore suitable for human (see supplementary material A figure S1).

To identify the model parameters with the highest influence on the model output (maximum blood concentration (C_{max})) a sensitivity analysis was performed. The sensitivity analysis was performed at the dose level used in the available rat study (0.039 mg/kg bw). Normalised sensitivity coefficients (SCs) were calculated for the model parameters based on the method reported in the literature (Evans and Andersen 2000) as follows:

$$SC = \frac{C' - C}{P' - P} \times \left(\frac{P}{C}\right) \tag{3}$$

were C is the initial value of the model output, C' is the modified value of the model output resulting from an increase in the parameter value. P is the initial parameter value and P' is the modified parameter value after a 5% increase in its value. (See supplementary material A figure S2)

Translation of the *in vitro* cytotoxicity data of PQ to in vivo dose response data

Determining fraction unbound in vitro

The obtained concentration-response data for the cytotoxicity of PQ in RLE-6TN, L2 and A549 cells were used to predict the dose levels that are required to reach the respective effect concentrations of PQ in blood, using PBK modelling-based reverse dosimetry. Important to realize is that only the free fraction of the compound will exert the effects, meaning that a correction is required for differences in protein binding in the *in vitro* and *in vivo* situation prior to applying reverse dosimetry. Therefore, the fraction unbound *in vitro* ($f_{ub\ in\ vitro}$) and the fraction unbound *in vivo* ($f_{ub\ in\ vivo}$) needed to be determined. Although it has been reported frequently that the $f_{ub\ in\ vivo}$ of PQ is 1.0 due to its two quaternary positively charged N-atoms, a thoroughly executed protein binding assay recently performed by the group of Campbell (Campbell et al. 2021; Stevens et al. 2021) reported the $f_{ub\ in\ vivo}$ of PQ to be 0.7 and 0.65 for rat and human, respectively. To determine the $f_{ub\ in\ vitro}$ a previously reported method by van Tongeren et al. (2021) was used where a linear relation between the fraction unbound and the protein content in a biological matrix was assumed based on the work of Gulden et al. (2002). This means that the fraction unbound in the absence of protein is 1.0. The protein content is reported to be 7% in rat plasma and 8% in human plasma (Martinez 2011; Mathew et al. 2022). However, the PBK model is run for whole blood, therefore the percentages need to be recalculated. Blood plasma is around 60% of whole blood (Dean 2005) so a dilution factor of 100/60 = 1.67 is used to calculate a whole blood protein content of 4.2 % for rat and 4.8% for human. The assay medium used in all the cytotoxicity assays contained 10% FCS and was considered to be a 10% protein content. Based on these considerations, the $f_{ub\ in\ vitro}$ for PQ was calculated by linear extrapolation to the 10% protein content using the f_{ub} of 1.0 in the absence of protein and the respective $f_{ub\ in\ vivo}$ value from Campbell et al. (2021) and Stevens et al. (2021) of 0.7 and 0.65 for a 4.2% protein content in rat *in vivo* blood and an 4.8% protein content in human *in vivo* blood, respectively, and found to amount to 0.29 for rat and 0.27 for human.

PBK modelling-based reverse dosimetry

Pneumotoxicity was assumed to depend on the maximum unbound concentration (C_{max}) of PQ reached in the blood and is therefore the chosen dose metric in this study for reverse dosimetry (Rietjens et al. 2019). To apply reverse dosimetry, first the *in vitro* unbound concentration ($C_{ub,\ in\ vitro}$) was set equal to the unbound C_{max} in blood ($C_{ub,\ in\ vivo}$). To estimate the $C_{ub,\ in\ vitro}$ and the $C_{ub,\ in\ vivo}$ the following equations were used: $C_{ub,\ in\ vitro} = C_{in\ vitro} \times f_{ub,\ in\ vitro}$ and $C_{ub,\ in\ vivo} = C_{in\ vivo} \times f_{ub,\ in\ vivo}$, respectively, where $C_{in\ vitro}$ is the nominal concentration applied in the *in vitro* assay and $f_{ub,\ in\ vitro}$ is the fraction unbound of PQ in the *in vitro* assay medium as determined in the previously described section and where $C_{in\ vivo}$ is the nominal blood concentration in rat/human and $f_{ub,\ in\ vivo}$ is the

f_{ub} in rat/human. Then, assuming that for the prediction of *in vivo* toxicity, the $C_{ub, in vitro}$ is the same as $C_{ub, in vivo}$, the nominal blood concentration in rat and human used to calculate the corresponding dose level can be described by the following equation: $C_{in vivo} = (C_{in vitro} \times f_{ub, in vitro})/f_{ub, in vivo}$. The *in vitro* concentration-response curve can thus be translated into an *in vivo* dose-response curve by repeating these steps for all *in vitro* test concentrations applied.

The same steps were applied to *in vitro* concentration-response curves obtained for PQ in RLE-6TN cells, L2 cells and the human A549 cells in previously reported studies (Chen et al. 2012; Kanno et al. 2019; Kim et al. 2011; Wang et al. 2016; Zhu et al. 2016). The contribution of including active renal secretion via OCT2 to the PBK model was evaluated by translating the *in vitro* concentration-response curves with the PBK model with or without taking active transport in the kidney into account.

Point of departure for acute toxicity of PQ

For the obtained and literature found *in vitro* concentration response curves in the different cell lines EC_{50} and ED_{50} values were derived by interpolating the exponential or sigmoidal function. In this case 50% viability is considered to be reached at the EC_{50}/ED_{50}. Upon translation using PBK model based reverse dosimetry Benchmark dose (BMD) analysis was applied on the predicted *in vivo* dose response curves using the European Food Safety Authority (EFSA) online BMD software. The lower and upper bound BMD levels for 50% lethality ($BMDL_{50}$ and $BMDU_{50}$) were determined under the EFSA default settings for Akaike information criterion being 2 and a confidence interval of 95%. Only $BMDL_{50}$ and $BMDU_{50}$ values as a result of model averaging were taken. The obtained $BMDL_{50}$-$BMDU_{50}$ ranges were compared to respectively the *in vivo* reported LD_{50} values collected from the literature for both rat and human.

4.3   Results

Cytotoxicity of PQ

Exposure of the RLE-6TN cells to PQ resulted in a concentration dependent decrease in cell viability (Fig. 3a; black data) with an EC_{50} established at 128 µM. Comparing the results to existing literature data reveals that these results are well in line with reported EC_{50} values that range from 79 – 166 µM, (Fig. 3a; red data and blue data, respectively). The literature data reported by Wang et al. (2018) were not considered and not included in Fig. 3a as the cell viability did not reach and extend past the 50% cell viability. In comparison, cytotoxicity data of another rat lung cell line, the L2 cell line, (Fig. 3b) shows this latter cell line to be less sensitive to PQ with an EC_{50} of 319 µM.
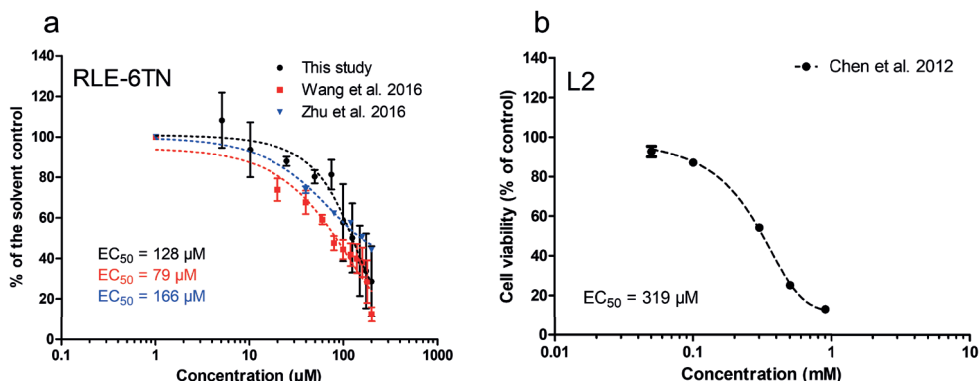
Figure 3.
Cell viability after exposure to increasing concentrations of PQ for 24 hours expressed as percentage of the solvent control for (a) RLE-6TN cells as determined in this study (EC$_{50}$ 128 µM; black). For comparison the figure also presents previously reported cytotoxicity data reported by Wang et al. (2016) (EC$_{50}$: 79 µM; red) and Zhu et al. (2016) (EC$_{50}$: 166 µM; blue) and (b) L2 cells as reported by Chen et al. (2012) (EC$_{50}$: 319 µM). Data points represent the mean ± SD; n = 3-4 for all data sets.

The literature reported *in vitro* data for the human lung cell line A594 resulted in an EC$_{50}$ range of 400 – 889 µM when exposed to PQ for 24 hours (Kim et al. 2011; Wang et al. 2016; Zhu et al. 2016) (Fig. 4a) and a 4- to 12-fold lower EC$_{50}$ range of 72-97 µM upon 48 hour PQ exposure (Kanno et al. 2019; Kim et al. 2011) (Fig. 4b).
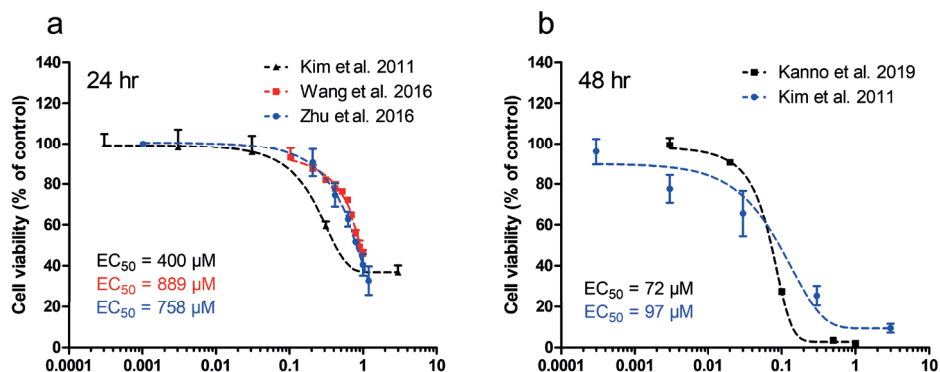
Figure 4.
Cell viability of A594 cells expressed as percentages of the solvent control after exposure to increasing concentrations of PQ for (a) 24 hours as reported by Kim et al. (2011) (EC$_{50}$: 400 µM; black), Wang et al. (2016) (EC$_{50}$: 889 µM; red) and Zhu et al. (2016) (EC$_{50}$: 758 µM; blue) and (b) 48 hours as reported by Kanno et al. (2019) (EC$_{50}$: 72 µM; black) and Kim et al. (2011) (EC$_{50}$: 97 µM; blue). Data points represent the mean ± SD; n = 3-6 for all data sets.

Uptake of PQ in the SA7K cells

Figure 5 presents the time dependent uptake of PQ in SA7K cells in the absence and in the presence of the OCT2 inhibitor doxepin. These data reveal that PQ is taken up by the SA7K cells (black solid line) with this uptake being inhibited in the presence of doxepin (grey solid line). The difference between the curves in the absence or presence of the inhibitor reveals that the OCT2 mediated uptake of PQ (black striped line) amounts on average to 42% of the total uptake. The data also reveal that uptake does not increase in time hampering quantification of the rate of uptake (in pmol/min/mg protein) from a linear part of the concentration-time curve.
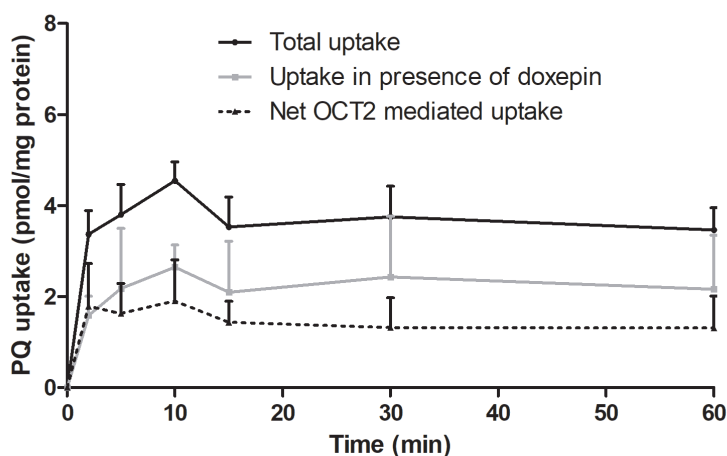
Figure 5.
Time dependent uptake of PQ (10 μM) in SA7K cells in the presence of 100 μM doxepin. The uptake remaining in the presence of the inhibitor (grey solid line) was subtracted from the total uptake (black solid line) to obtain the net OCT2 mediated uptake of PQ (black striped line). Each data point represents the mean ± SEM; n = 2

Kinetic data from literature

As the rate of PQ uptake in the SA7K cell line appeared too fast to determine the PQ concentration dependent rate of transport, Vmax and Km for PQ uptake via OCT2 were obtained from literature. Two data sets were reported by Chen et al. (2007) using the HEK293 cell line overexpressing the human OCT2 transporter (Km: 95 μM and 114 μM and Vmax: 198 pmol/min/mg protein and 174 pmol/min/mg protein). To further optimize the PBK model predictions with incorporation of *in vitro* OCT2 uptake of PQ the data of the HEK293 cells were used and averaged (Km: 104.5 μM and Vmax: 186 pmol/min/mg protein).

Evaluation of the model

The PBK model was evaluated based on comparison of predicted Cmax levels for PQ in rats to Cmax values from *in vivo* kinetic rat data reported by Chui et al. (1988) at an oral dose of 0.039 mg/kg bw (Fig. 6) using different subsequent steps. The first step is based on comparison of the experimental data to the PBK model based predictions including only passive excretion via glomerular filtration (GF) in the PBK model (dotted line). The predicted time-dependent concentration curve predicts a Cmax value for PQ that is 1.5 fold higher than the Cmax derived from the reported *in vivo* data (open circles) indicating excretion is somewhat underestimated. In a second step active excretion was added to the PBK model using the *in vitro* OCT2 data for PQ transport obtained in HEK293 cells (solid line). The Vmax value was scaled to the *in vivo* situation taking into account the reported mg protein/g kidney (300 mg protein/g kidney (Kumar et al. 2018)) and the fact that OCT2 is located in only the kidney cortex that makes up 70% of the kidney weight (300 x 70%; 210 mg protein/g kidney). Use of this scaling factor is further referred to as partially scaled. The predicted Cmax under these conditions is 1.3 fold higher than the reported *in vivo* data. Given the fact that the scaling factor used did not yet account for differences in expression level of OCT2 in the HEK293 cells and the *in vivo* tubular cells in a third step the optimised scaling factor was defined fitting the predictions to the *in vivo* data resulting in an extra scaling factor of 5.5 and an overall scaling factor of 1,155 mg protein/g kidney (300 mg protein/g kidney x 70% x 5.5). Use of this scaling factor is further referred to it as fully scaled. As reported by our previous work (Noorlander et al. 2021b), here too, the virtual amount of protein exceeds the kidney weight due to the lower expression level of OCT2 in the HEK293 cells as compared to kidney tissue and requires a virtually large amount of HEK293 protein to equal the amount OCT2/g kidney. The predicted time-dependent blood concentration curve of PQ with the fully scaled scaling factor (striped line) adequately describes the reported *in vivo* kinetic data especially within the first phase. A comparison of the amount of PQ excreted in time reflected by the slope of the glomerular filtration versus time curve (0.25 nmol/hr) and the slope of PQ excreted in time by only the scaled active transport (0.7 nmol/hr) showed that the contribution of excretion via active transport in time was 1.8 fold higher than that via GF. This results in 73% of the urinary PQ being excreted by active excretion at a dose of 0.039 mg/kg bw (Fig 7). The PBK model also reveals that the relative contribution of OCT2 decreases when the PQ dose increases (at 39 and 390 mg/kg bw active excretion is 67% and 34%, respectively) pointing at saturation of the OCT2 transport. A final comparison was made between the partial scaling and full scaling indicating that the OCT2 contribution in partial scaling was at most 33.5% and also decreased with increasing doses.

Based on the evaluation of the rat model it was assumed that the human PBK model that was developed by the same method and principles would also be adequate. This

assumption was supported by the observation that the predicted concentrations for the time dependent blood concentration in human at a non-toxic dose (0.036 mg/kg bw) were all well below Proudfoot's survival curve (see supplemental materials A Fig S1).
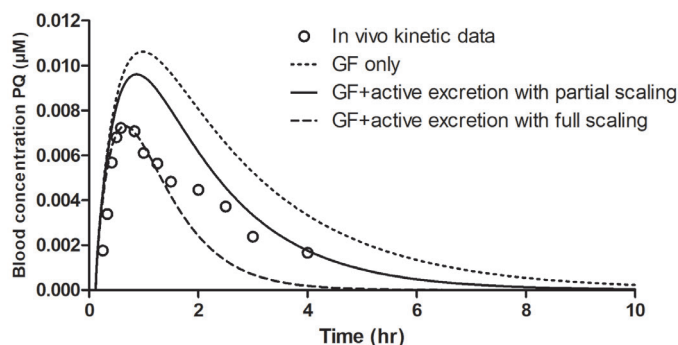
Figure 6.
Predicted blood concentration time curves in rats upon orally administered PQ at dosage 0.039 mg/kg with a bioavailability of 5% as reported by Chui et al. (1988) (open circles). The predictions were executed under the following conditions: 1) with glomerular filtration (GF only) (dotted line), 2) with GF and active excretion, the latter with partial scaling of the *in vitro* OCT2 transport data of PQ in HEK293 cells overexpressing OCT2 reported by Chen et al. (2007) based on the amount of protein/g kidney and fraction of kidney where OCT2 is located (300 mg/g kidney x 0.7) (solid line) and 3) with GF and active excretion, the latter with full scaling also correcting for a 5.5 fold difference in OCT2 expression in the HEK293 cells and kidney cells, resulting in a full scaling factor of 300 mg/g kidney x 0.7 x 5.5 = 1,155 mg protein/g kidney used when translating the *in vitro* Vmax to an *in vivo* Vmax.
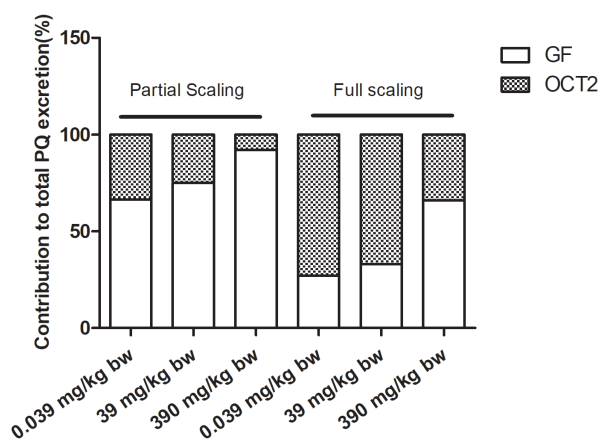
Figure 7.
Contribution (%) of glomerular filtration (GF) and OCT2 mediated excretion to the total amount of PQ excreted as predicted by the PBK model when using different scaling factors. Included are partial scaling of the Vmax (SF; 300* 0.7 = 210 mg protein/g kidney) and full scaling of the Vmax (SF; 300 x 0.7 x 5.5 = 1.155 mg protein/g kidney). The contributions were predicted at dose levels of 0.039 mg/kg bw, 39 mg/kg bw and 390 mg/kg bw.

Applying reverse based dosimetry

Using the developed PBK models for rat and human reverse based dosimetry was applied to translate the *in vitro* concentration-response data into *in vivo* dose-response curves (Fig.8). For rat, the three *in vitro* RLE-6TN data sets and the *in vitro* L2 data set were converted to *in vivo* data using the $f_{ub\ in\ vivo}$ (0.7) and the $f_{ub\ in\ vitro}$ (0.29), quantified as described in the materials and methods section, to correct for differences in protein binding in the *in vitro* and *in vivo* situation. The ED_{50} values for PQ derived from the *in vivo* dose response curves obtained range from 9.3 – 17.8 mg/kg bw for the data based on the RLE-6TN cytotoxicity studies, while the ED_{50} was predicted at 35.3 mg/kg bw based on the L2 cytotoxicity data (Fig.8a). For human, all five *in vitro* data sets obtained in A594 cells were translated to *in vivo* data using the $f_{ub\ in\ vivo}$ (0.65) and the $f_{ub\ in\ vitro}$ (0.27) to correct for differences in protein binding in the *in vitro* and *in vivo* situation (Fig. 8b). There are clear differences in the *in vitro* EC_{50} values and as a result also in the predicted ED_{50} values when based on 24 or 48h exposure duration. Using 24 hour exposure *in vitro* data the predicted ED_{50} values for PQ range from 38.8 – 85.9 mg/kg bw while based on the *in vitro* data obtained upon 48 hour exposure the ED_{50} values are 4 – 12 fold lower ranging from 7.0 – 9.2 mg/kg bw.
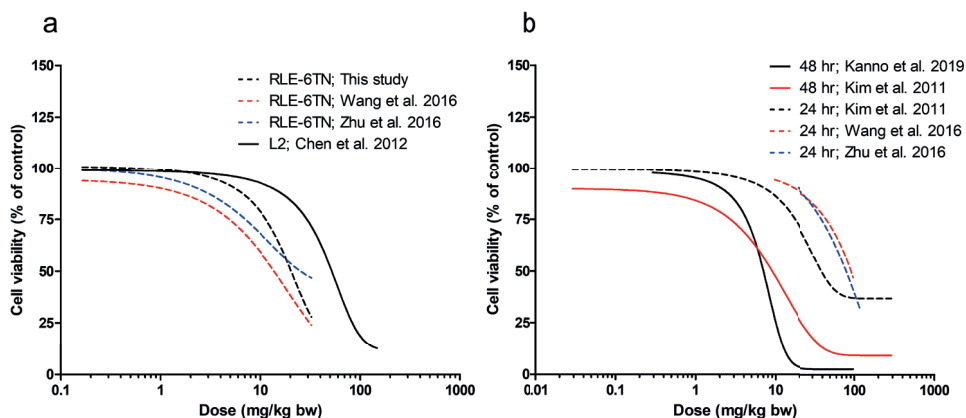
Figure 8.
Predicted dose-response curves for PQ obtained using (a) data from *in vitro* RLE-6TN and L2 cytotoxicity assays and the rat oral PBK model and (b) data from *in vitro* A594 cytotoxicity assays and the human PBK model. The *in vitro* data used to make the predictions were (a) derived from either the present study (black striped line; ED_{50}: 13.3 mg/kg bw) or from literature as reported by Wang et al. (2016) (red striped line; ED_{50}: 9.3 mg/kg bw) and Zhu et al. (2016) (blue striped line; ED_{50}: 17.8 mg/kg bw) and data from an *in vitro* L2 cytotoxicity assay reported by Chen et al. (2012) (black solid line; ED_{50}: 35.3 mg/kg bw) and (b) previously reported by Kanno et al. (2019) (black solid line; ED_{50}: 7.0 mg/kg bw), Kim et al. (2011) (48 hr: red solid line; ED_{50}: 9.22 mg/kg bw and 24 hr: black striped line; ED_{50}: 38.8 mg/kg bw) and Wang et al. (2016) (red striped line; ED_{50}: 85.9 mg/kg bw) Zhu et al. (2016) (blue striped line; ED_{50}: 80.2 mg/kg bw). Data points represent the mean ± SD; n = 3-6.

Predicted point of departure for safety assessment

Based on the predicted acute *in vivo* toxicity data sets BMDL$_{50}$ BMDU$_{50}$ values were generated to allow a comparison to available *in vivo* toxicity data. There were data available on LD$_{50}$ values especially in rat while some studies reported a human value (Bailey and White 1965; Clark et al. 1966; Duerden 1994; Kimbrough and Gaines 1970; Mehani 1972; Murray and Gibson 1974; Sharp et al. 1972; Shirasu 1977). As shown in figure 9 the predicted BMDL$_{50}$ to BMDU$_{50}$ ranges based on the rat *in vitro* cytotoxicity data are conservative compared to the reported *in vivo* LD$_{50}$ data with the prediction by Chen et al. (2012) using the L2 cell line being 4.1-fold lower and closest to the average *in vivo* LD$_{50}$ values, the latter varying up to 8-fold between the different *in vivo* studies.
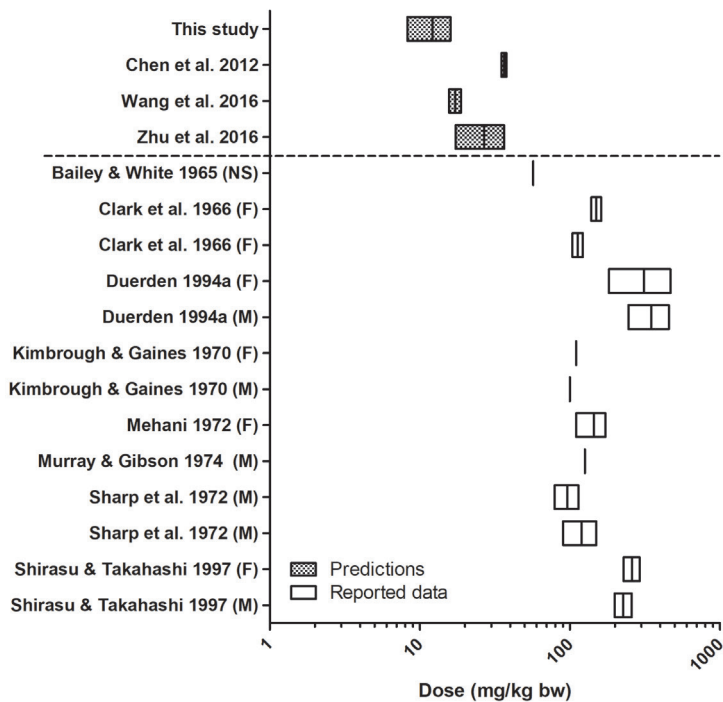
Figure 9.
Comparison of predicted BMDL$_{50}$ to BMDU$_{50}$ values for PQ in rat obtained by PBK model based QIVIVE of *in vitro* cytotoxicity data obtained in RLE-6TN and L2 cells (data obtained in this study and reported by Wang et al. (2016), Zhu et al. (2016) and Chen et al. (2012)) depicted by the chequered bars and literature reported *in vivo* rat LD$_{50}$ values (open bars). F; female, M; male, NS; not specified.

The human A594 cytotoxicity assays in combination with the human PBK model resulted in predictions for the BMDL$_{50}$ BMDU$_{50}$ range in human that were in line with the limited reported LD$_{50}$ values for human (figure 10). The predictions overall vary

between 3.8 and 101 mg/kg bw while the available human *in vivo* data vary between 3 and 60 mg/kg bw pointing at the suitability of the A594 cell line to predict PQ toxicity.
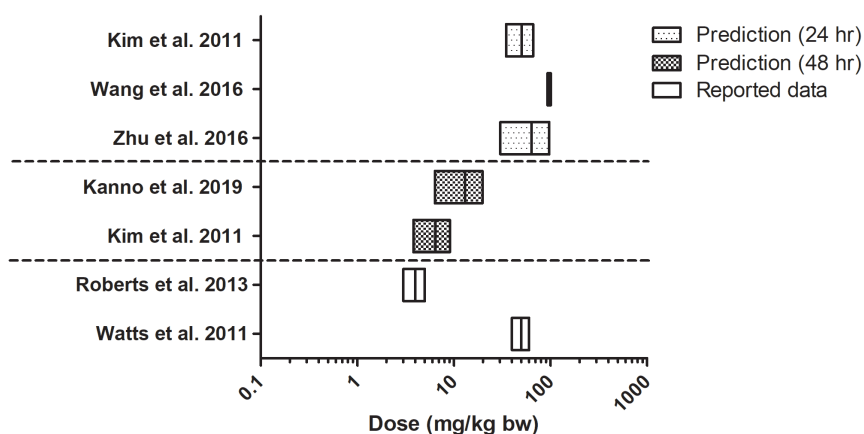
Figure 10.
Comparison of predicted $BMDL_{50}$ to $BMDU_{50}$ values for PQ in human obtained by PBK model based QIVIVE of *in vitro* cytotoxicity data obtained in A594 cells (data reported by Kanno et al. (2019), Kim et al. (2011), Wang et al. (2016) and Zhu et al. (2016)) depicted by the dotted bars (exposure 24 hours) and the chequered bars (exposure 48 hr) and the literature reported *in vivo* human LD_{50} values for acute exposure (open bars).

4.4 Discussion

The present study aimed at evaluating a new approach methodology (NAM) for predicting the acute toxicity of PQ. The NAM consisted of using PBK models that included *in vitro* kinetic data for active renal excretion via the OCT2 transporter and *in vitro* cytotoxicity curves obtained in rat and human alveolar cell lines that were translated to *in vivo* dose response curves by applying PBK model based reverse dosimetry. From the predicted *in vivo* dose-response curves $BMDL_{50}$ to $BMDU_{50}$ ranges were derived and compared to the *in vivo* reported LD_{50} values in rat and human.

A secondary aim of the study was to provide a further proof of principle for using the *in vitro* cell line SA7K to obtain PBK parameters for transporter kinetics for OCT2 mediated renal excretion using PQ as the model compound. Although in the SA7K cells there was net cellular uptake via OCT2, an apparent equilibrium was reached already within a minute, hampering use of the cell line to generate a linear uptake of PQ in time. As a result, Vmax or Km could not be determined from concentration-

dependent uptake studies. Whether this fast equilibrium is due to efficient cellular excretion balancing the OCT2 mediated uptake, possibly via MATE, remains open for further investigation. Thus the OCT2 mediated transport was included in the PBK model based on kinetic data reported in literature and obtained in a HEK293 OCT2 transfected model.

The contribution of OCT2 transport to the total renal clearance of PQ as predicted by the PQ kinetic data appeared to amount to 73% of the total renal excretion achieved via glomerular filtration and active OCT2 mediated excretion at low dose levels where OCT2 transport was not saturated. The OCT2 contribution to PQ excretion was predicted to decrease upon higher dose levels when saturation occurs. The derived percentage was only slightly lower than what was observed for the contribution of OCT2 transport in our previous reported work on MQ, where active OCT2 mediated excretion amounted to 85% of the total excretion (Noorlander et al. 2021b).

The Vmax of OCT2 mediated PQ transport in HEK293 cells overexpressing OCT2 was scaled from the *in vitro* to the *in vivo* situation in a way similar to what was done previously for the OCT2 mediated Vmax for transport of MQ in SA7K cells (Noorlander et al. 2021b). A three step scaling factor was derived including 1) the amount of protein per gram kidney, 2) a correction for the location of the OCT2 transporter in the kidney in only the kidney cortex (70% of whole kidney) and 3) the differences between the *in vitro* cell system and the *in vivo* situation including: i) the difference in expression of the OCT2 transporter in the HEK293 cells overexpressing human OCT2 as compared to the *in vivo* expression in rat renal cells (Hayer-Zillgen et al. 2002; Koepsell et al. 2003), ii) the species differences in transporters involved in the *in vitro* model and the *in vivo* situation being OCT2 in human and OCT1, OCT2 and OCT3 in rat kidney (Chu et al. 2013a; Slitt et al. 2002), iii) the difference in the negative membrane potential between *in vitro* and *in vivo* known to affect transporter efficiency (Kumar et al. 2018). The factor of 5.5 defined as extra scaling factor by comparison of predictions based on the transfected human HEK293 cell line and rat *in vivo data* accounts for all these three factors.

Another way to scale from HEK293 cells with overexpression of a transporter of interest to the *in vivo* situation is to look at previously reported work where the relative expression factor (REF) and the relative activity factor (RAF) were defined to use *in vitro* transporter kinetic data to model *in vivo* biliary excretion (Chan et al. 2019; Izumi et al. 2018; Jamei et al. 2014; Kunze et al. 2014; Poirier et al. 2009). More recently, these REF and RAF values have been successfully applied in renal excretion via OAT (Kumar et al. 2020; Mathialagan et al. 2017). Defining a REF is based on quantifying the OCT2 transporter protein levels in the HEK293 cells (or SA7K cells) and in rat/human kidney

cells with proteomics. The difference can be used to define a scaling factor. In addition, considering that it would be even more accurate to base the comparison on activity rather than on protein expression levels, the RAF is defined by using a probe substrate for the transporter of interest in both the *in vitro* and *in vivo* situation. However, up until now for OCT2 no probe substrate has been defined (Burt et al. 2016). As a result reported RAF values for OCT2 transport result from fitting predictions to experimental data, just as done for the scaling factor in the present study.

The PBK model predictions for the lethal dose ($BMDL_{50}$-$BMDU_{50}$ range) for rats was conservative and revealed humans to be more sensitive to PQ than rat, which was also shown by the reported LD_{50} values. Especially for human the predicted $BMDL_{50}$-$BMDU_{50}$ for acute toxicity of PQ matched the available LD_{50} values. For rat the predictions were on the conservative side, which may in part be due to the relevance of the *in vitro* cell model for the *in vivo* endpoint. The *in vivo* toxicity of PQ is described by an adverse outcome pathway where the molecular initiating event starts in the lungs, therefore an alveolar *in vitro* model (RLE-6TN and L2) was used to measure cytotoxicity. Although the acute toxicity of PQ starts in the lung where in the first few hours it manifests as acute pulmonary oedema and early lung damage through redox cycling the main cause of death, however, is respiratory failure by pulmonary fibrosis and can occur up until 7-14 days after PQ ingestion (Roberts 2013). Therefore, a lung fibrotic *in vitro* model could have been a better alternative in mimicking the *in vivo* endpoint. Fibrotic *in vitro* models come with high complexity due to the interplay between many factors that cause fibrosis (Kiener et al. 2021; Martinez et al. 2017; Wolters et al. 2014). It is therefore that 3D models such as precision cut lung slices and lung on a chip are preferred over 2D models which are too static forcing fibroblasts to polarize and are also incapable of replicating the complex gradient nature of soluble cues *in vivo* and the different cell-cell and cell-matrix interactions experienced by cells within the normal lung (Kiener et al. 2021; Sundarakrishnan et al. 2018; Vazquez-Armendariz et al. 2022). It might be interesting for future research to investigate whether a 3D lung fibrotic model for rat would result in predictions less sensitive compared to the predictions based on cytotoxicity corroborating the reported LD_{50} data.

In this study, the developed PBK model for PQ was capable of predicting the time-dependent blood concentration of PQ upon oral administration at a non-toxic dose. Previously published PBK models on PQ had similar success but were more extensively parameterized (Campbell et al. 2021; Stevens et al. 2021) or were even less parameterized (Lohitnavy et al. 2017) and in all cases did not take active renal excretion into account fitting a model with only glomerular filtration to the reported *in vivo* data. The present model was also able to make adequate predictions for the *in vivo* acute toxicity of PQ especially in humans. Thus, proof of principle was provided for the developed NAM

showing how to include *in vitro* obtained active excretion in PBK modelling and how to apply the model for QIVIVE translation to predict the acute *in vivo* toxicity in both rat and human, using PQ as the model compound.

Declaration of Competing Interest
The authors report no declaration of interest.

Supplementary materials A

Table S1.
Physiological and anatomical parameter values and partition coefficients used for the PBK models

Parameters	Rat[a]	Human[a]
Body weight (kg)	0.25	70
Fraction of tissue volumes		
Fat	0.070	0.214
Liver	0.034	0.026
Kidney	0.007	0.004
Lung	0.005	0.008
Arterial blood	0.0246	0.0263
Venous blood	0.0494	0.0527
Kidney	0.007	0.004
Rapidly perfused tissue	0.086	0.089
Slowly perfused tissue	0.724	0.58
Cardiac output[b]	15	15
Fraction of blood flow to tissue		
Fat	0.070	0.052
Liver	0.174	0.227
Kidney	0.141	0.175
Lung	1	1
Rapidly perfused tissue	0.072	0.23
Slowly perfused tissue	0.543	0.316
Partition coefficients[c]		
$LogP_{ow}$	-4.5	
Fat/blood partition coefficient	0.14	0.14
Liver/blood partition coefficient	0.66	0.66
Kidney/blood partition coefficient	0.69	0.69
Lung/blood partition coefficient	0.58	0.58
Rapid perfused tissue/blood partition coefficient	0.66	0.66
Slowly perfused tissue/blood partition coefficient	0.42	0.42

a Brown et al. (1997a)
b $L/hr \times kg \times bw^{0.74}$
c Punt et al. (2020)
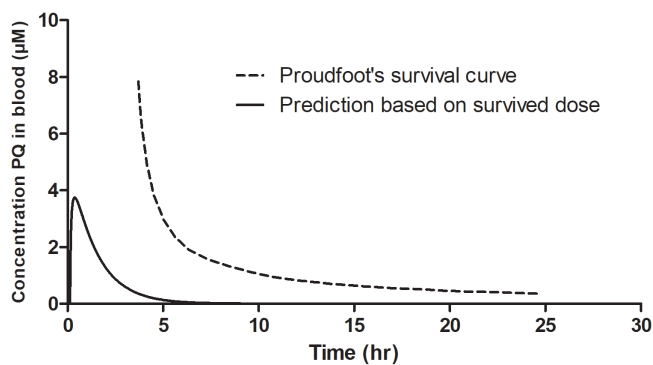
Figure S1.
Predicted blood concentration time curve of orally administered PQ in human (solid line). The dose was based on the highest reported ingestion leading to survival 11.4 mg/kg bw (Houze et al. 1990). The striped line represents Proudfoot's survival curve based on many reported cases on orally ingested PQ (Proudfoot et al. 1979).
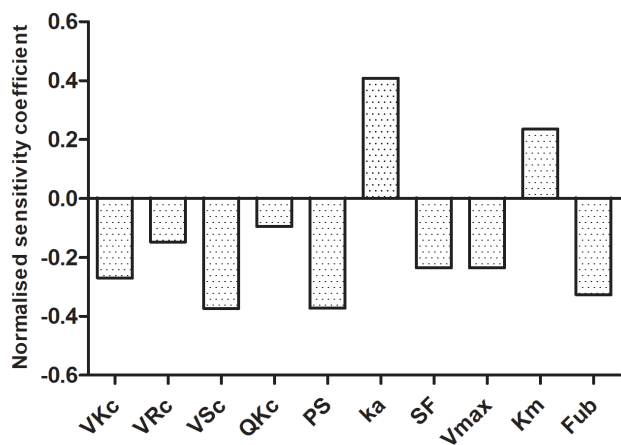
Figure S2.
Normalized sensitivity coefficients of PBK model parameters for the predicted C_{max} of PQ in blood after an oral administration of 39 μg/kg bw. Only model parameters with normalized sensitivity coefficients with an absolute value higher than 0.1 are shown. VKc = volume of the kidneys, VRc = volume of the rapidly perfused tissues, VSc = volume of the slowly perfused tissues, QKc = fraction of blood flow to the kidneys, PS = partition coefficient of slowly perfused tissue, ka = absorption rate constant, SF = scaling factor, Vmax = maximum rate of PQ transport via OCT2, Km = Michaelis-Menten constant of PQ transport via OCT2, Fub = fraction unbound.

Supplementary materials B

PBK-model for rat

```
; Date: September, 2020
; Purpose: PBK Model of paraquat (PQ), built with in vitro and in silico derived parameter values
; Species: Rat
; Compiled by: Annelies Noorlander
; Organisation: Wageningen University


;======================================================================
;Physiological parameters
;======================================================================
; tissue volumes, arterial and venous blood based on Crowell, et al. 2011 33% arterial, 67% venous.
;reference: Brown et al. Table 21 (1997)


BW = 0.250 (Kohane et al.)    ; body weight rat (variable, dependent on study)
VFc = 0.07                    ; fraction of fat tissue
VLc = 0.034                   ; fraction of liver tissue
VKc = 0.007                   ; fraction of kidney tissue
VLuc = 0.005                  ; fraction of lung
VRc = 0.086                   ; fraction of richly perfused tissue
VSc = 0.724                   ; fraction of slowly perfused tissue
VABc = 0.0246                 ; fraction of arterial blood
VVBc = 0.0494                 ; fraction of venous blood



VF = VFc*BW                {L or Kg} ; volume of fat tissue (calculated)
VL = VLc*BW                {L or Kg} ; volume of liver tissue (calculated)
VK = VKc*BW                {L or Kg} ; volume of kidney tissue (calculated)
VLu = VLuc*BW   {L or Kg} ; volume of lung tissue (calculated)
VR = VRc*BW                {L or Kg} ; volume of  richly perfused tissue (calculated)
VS = VSc*BW                {L or Kg} ; volume of  slowly perfused tissue (calculated)
VAB = VABc*BW   {L or Kg} ; volume of arterial blood (calculated)
VVB = VVBc*BW   {L or Kg} ; volume of  venous blood (calculated)


;------------------------------------------------------------------------------------------------------------
;blood flow rates    reference: Brown et al. Table 25 (1997)

QC = 15*BW^0.74 {L/hr}                        ; cardiac output reference: Brown et al. p.453 (1997)
QFc = 0.07                                    ; fraction of blood flow to fat
QLc = 0.174                                   ; fraction of blood flow to liver
QKc = 0.141                                   ; fraction of blood flow to kidney

QLuc = 1                                      ; fraction of blood flow to lung
QRc = 0.072                                   ; fraction of blood flow to richly perfused tissue
QSc = 0.543                                   ; fraction of blood flow to slowly perfused tissue

QF = QFc*QC              {L/hr}               ; blood flow to fat tissue (calculated)
QL = QLc*QC              {L/hr}               ; blood flow to liver tissue (calculated)
QK = QKc*QC              {L/hr}               ; blood flow to kidney tissue (calculated)
```

```
QLu = QLuc*QC          {L/hr}              ; blood flow to lung tissue (calculated)
QS = QSc*QC            {L/hr}              ; blood flow to  slowly perfused tissue (calculated)
QR = QRc*QC            {L/hr}              ; blood flow to richly perfused tissue (calculated)


;================================================================
;Physicochemical parameters
;================================================================


;partition coefficients --> logP PQ: -4.5 (https://www.ilo.org/dyn/ics257.25c/showcard.display?p_
version=2&p_card_id=0005)
;using the qivive tool from A. Punt; input --> PQ is inert due to quaternary ammonium atom (considered
neutral), logP -4.5, MW; partition data based on Rodgers and Rowland (2006)

;Tissue partition coefficients in plasma
PF = 0.14                    ; fat/blood partition coefficient
PL = 0.66                    ; liver/blood partition coefficient
PK = 0.69                    ; kidney/blood partition coefficient
PLu = 0.58                   ; lung/blood partition coefficient
PR = 0.66                    ; richly perfused tissue/blood partition coefficient
PS = 0.42                    ; slowly perfused tissue/blood partition coefficient



;================================================================
;Kinetic parameters
;================================================================


;Transport from needle to blood
kn  =  1000000       ; injection {/hr}

;Uptake rate from stomach
ka = 2.3              ; absorption {/hr}
;----------------------------------------------------------------------------------------------------------------
;Excretion from kidney

;Active uptake is described in first order kinetics where Vmax and Km become one constant number.
VmaxOCT2c = 198             ;{pmol/min/mg}

VmaxOCT2 = (VmaxOCT2c/1000000)*60*SF*VK*1000     ;{umol/hr}
;300 mg prot./g kidney (Kumar et al. 2018)
;only 70% of whole kidney is cortex --> in cortex tubule cells thus OCT-2s are present (Kumar et al. 2018)
; 300 * 0.7 = 210 mg prot./g kidney

KmOCT2 = 95                 ; {uM} transport constant of PQ via OCT2
SF = 210                    ; mg/g protein


;----------------------------------------------------------------------------------------------------------------
;Accumulation in lung of PQ
VmaxPQLuc = 300             ;{nmol/g tissue/hr}

VmaxPQLu = (VmaxPQLuc/1000)*VLu*1000 ; {umol/hr}
```

KmPQLu = 70   ; {uM} transport constant of PQ into the alveolar cells

ker = 0.003   ; lung elimination rate {/hr}
;==
;Run settings
;==

;Molecular weight PQ
MW = 257.2
 ;--

;ORAL dose
ODOSEmg = 0.039*0.05 {mg/kg bw}   ; ODOSEmg = given Oral dose in mg/kg bw

ODOSEumol2 = ODOSEmg*1E-3/MW*1E6 {umol/kg bw}   ; ODOSEumol2 = given Oral dose recalculated to umol/kg bw

ODOSEumol=ODOSEumol2*BW;   ; ODOSEumol = umol given Orally

;IV dose
IVDOSEmg = 0.039 {mg/kg bw}   ; IVDOSEmg = given IV dose in mg/kg bw

IVDOSEumol2 = IVDOSEmg*1E-3/MW*1E6 {umol/kg bw}   ; IVDOSEumol2 = given IV dose recalculated to umol/kg bw

IVDOSEumol=IVDOSEumol2*BW;   ; IVDOSEumol = umol given IV

;time
Starttime = 0.1217   ; in hr
Stoptime = 24   ; in hr

;Lagtime for oral uptake = 0.1217 hr   ;Chui et al. 1988 Lt = 7.3 min
;==
;Model calculations
;==
;Intravenous dosing
;needle compartment
;ANe = amount in needle, umol
;ANe' = Change in amount of PQ in time in the needle, umol/hr

ANe' = -kn*ANe
Init ANe = IVDOSEumol
;--
;Oral dosing
;Stomach compartment
;ASt = amount in stomach, umol
;ASt' = Change in amount of PQ in time in the stomach, umol/hr

ASt' = -ka*ASt
Init ASt = ODOSEumol
;--
;liver compartment

111

;AL = Amount PQ in liver tissue, umol
;AL' = Change in amount of PQ in time in liver (umol/hr)

AL' = ka*ASt + QL*(CAB - CVL)
Init AL = 0
CL = AL/VL
CVL = CL/PL
;--
;kidney compartment

;AK = Amount of PQ in kidney (umol)

;AK' = Change in amount of PQ in time in kidney (umol/hr)

AK' = QK*(CAB-CVK)-GF'-AKe'
        Init AK = 0
        CK = AK/VK
        CVK = CK/PK

;GFR = glomerular filtration rate {L/hr} ; Reference: Walton et al., 2004)
; GFR rat = 5.2 {mL/min/kg bw}
                GFR = 0.0052 * BW * 60 {L/hr}

;GF = glomerular filtration of paraquat (umol/hr)
        GF' = GFR*(CVK*Fub)
        Init GF = 0

;Fub = fraction unbound of PQ
        Fub = 0.7

;AKe = amount paraquat actively excreted from the kidney (umol)
;AKe' = amount paraquat actively excreted from the kidney in time (umol/hr)
AKe' = VmaxOCT2*(CVK*Fub)/(KmOCT2 + (CVK*Fub))
        Init AKe = 0
;--
;lung compartment

;ALu = Amount PQ in lung tissue (umol)
;ALu' = Change in amount of PQ in time in lung (umol/hr)
    ALu' = QLu*(CVB-CVLu)-AALu' + ALue'
    Init ALu = 0
    CLu = ALu/VLu
    CVLu = CLu/PLu
;--
;lung deep tissue compartment (alveolar tissue)
;Accumulation of PQ into the alveolar tissues

;AALu = Amount PQ accumulating in alveolar cells in lung (umol)
;AALu' = Amount PQ accumulating in alveolar cells in lung in time (umol/hr)
AALu' = VmaxPQLu *(CVLu*Fub)/ (KmPQLu + (CVLu*Fub))
        Init AALu = 0

;PQ eliminated back into the blood from alveolar tissue.
;ALue = Amount PQ eliminated back into the blood (umol)
;ALue' = Amount PQ eliminated back into the blood in time (umol/hr)
ALue' = ker* AALu
            Init ALue= AALu
;---
;fat compartment

;AF = Amount PQ in fat tissue (umol)
     AF' = QF*(CAB-CVF)
     Init AF = 0
     CF = AF/VF
     CVF = CF/PF
;---
;tissue compartment richly perfused tissue

;AR = Amount PQ in richly perfused tissue (umol)
     AR' = QR*(CAB-CVR)
     Init AR = 0
     CR = AR/VR
     CVR = CR/PR
;---
;tissue compartment slowly perfused tissue

;AS = Amount PQ in slowly perfused tissue (umol)
     AS' = QS*(CAB-CVS)
     Init AS = 0
     CS = AS/VS
     CVS = CS/PS
;---
; blood compartment
; Venous blood
;AVB = Amount PQ in venous blood (umol)
;AVB' = Change in amount of PQ in time in venous blood (umol/hr)
    AVB' = (kn*ANe + ((QF*CVF) + (QL*CVL) + (QK*CVK) + (QS*CVS) + (QR*CVR)) - (QLu*CVB))
    Init AVB = 0
    CVB = AVB/VVB
    AUCVB' = CVB
    init AUCVB = 0

; Arterial blood
;AAB = Amount PQ in arterial blood (umol)
;AAB' = Change in amount of PQ in time in arterial blood (umol/hr)
    AAB'= (QLu*(CVLu-CAB))
    Init AAB = 0
    CAB = AAB/VAB
    AUCAB' = CAB
    init AUCAB = 0
;===
;Mass balance calculations
;===

Total = IVDOSEumol + ODOSEumol
Calculated = ANe + ASt + AL + AK + GF + AKe + ALu + AALu - ALue+ AF + AS + AR + AAB + AVB

ERROR=((Total-Calculated)/Total+1E-30)*100
MASSBBAL=Total-Calculated + 1

PBK-model for human

; Date: September, 2020
; Purpose: PBK Model of paraquat (PQ), built with *in vitro* and *in silico* derived parameter values
; Species: Human
; Compiled by: Annelies Noorlander
; Organisation: Wageningen University

;===
;Physiological parameters
;===
; tissue volumes, arterial and venous blood based on Crowell, et al. 2011 33% arterial, 67% venous.
;reference: Brown et al. Table 21 (1997)

BW = 70 (Kohane et al.)   ; body weight human (variable, dependent on study)
VFc = 0.214   ; fraction of fat tissue
VLc = 0.026   ; fraction of liver tissue
VKc = 0.004   ; fraction of kidney tissue
VLuc = 0.008   ; fraction of lung
VRc = 0.089   ; fraction of richly perfused tissue
VSc = 0.580   ; fraction of slowly perfused tissue
VABc = 0.0263   ; fraction of arterial blood
VVBc = 0.0527   ; fraction of venous blood

VF = VFc*BW   {L or Kg} ; volume of fat tissue (calculated)
VL = VLc*BW   {L or Kg} ; volume of liver tissue (calculated)
VK = VKc*BW   {L or Kg} ; volume of kidney tissue (calculated)
VLu = VLuc*BW   {L or Kg} ; volume of lung tissue (calculated)
VR = VRc*BW   {L or Kg} ; volume of richly perfused tissue (calculated)
VS = VSc*BW   {L or Kg} ; volume of slowly perfused tissue (calculated)
VAB = VABc*BW   {L or Kg} ; volume of arterial blood (calculated)
VVB = VVBc*BW   {L or Kg} ; volume of venous blood (calculated)

;--
;blood flow rates   reference: Brown et al. Table 27 (1997)

QC = 15*BW^0.74 {L/hr}   ; cardiac output   reference: Brown et al. p.453 (1997)
QFc = 0.052   ; fraction of blood flow to fat
QLc = 0.227   ; fraction of blood flow to liver
QKc = 0.175   ; fraction of blood flow to kidney
QLuc = 1   ; fraction of blood flow to lung
QRc = 0.23   ; fraction of blood flow to richly perfused tissue
QSc = 0.316   ; fraction of blood flow to slowly perfused tissue

QF = QFc*QC   {L/hr}   ; blood flow to fat tissue (calculated)
QL = QLc*QC   {L/hr}   ; blood flow to liver tissue (calculated)
QK = QKc*QC   {L/hr}   ; blood flow to kidney tissue (calculated)
QLu = QLuc*QC   {L/hr}   ; blood flow to lung tissue (calculated)
QS = QSc*QC   {L/hr}   ; blood flow to slowly perfused tissue (calculated)

QR = QRc*QC   {L/hr}   ; blood flow to richly perfused tissue (calculated)

```
;==================================================================
;Physicochemical parameters
;==================================================================
```

;partition coefficients --> logP PQ: -4.5 (https://www.ilo.org/dyn/ics257.25c/showcard.display?p_version=2&p_card_id=0005)
;using the qivive tool from A. Punt; input --> PQ is inert due to quaternary ammonium atom (considered neutral), logP -4.5, MW; partition data based on Rodgers and Rowland (2006)

;Tissue partition coefficients in plasma
PF = 0.14   ; fat/blood partition coefficient
PL = 0.66   ; liver/blood partition coefficient
PK = 0.69   ; kidney/blood partition coefficient
PLu = 0.58   ; lung/blood partition coefficient
PR = 0.66   ; richly perfused tissue/blood partition coefficient
PS = 0.42   ; slowly perfused tissue/blood partition coefficient

```
;==================================================================
;Kinetic parameters
;==================================================================
```

;Uptake rate from stomach
ka = 2.3   ; absorption {/hr}
;---
;Excretion from kidney

;Active uptake is described in first order kinetics where Vmax and Km become one constant number.
VmaxOCT2c = 198   ;{pmol/min/mg}

VmaxOCT2 = (VmaxOCT2c/1000000)*60*SF*VK*1000   ;{umol/hr}
;300 mg prot./g kidney (Kumar et al. 2018)
;only 70% of whole kidney is cortex --> in cortex tubule cells thus OCT-2s are present (Kumar et al. 2018)
; 300 * 0.7 = 210 mg prot./g kidney

KmOCT2 = 95   ; {uM} transport constant of PQ via OCT2
SF = 210   ; mg/g protein

;---
;Accumulation in lung of PQ
VmaxPQLuc = 300   ;{nmol/g tissue/hr}

VmaxPQLu = (VmaxPQLuc/1000)*VLu*1000 ; {umol/hr}

KmPQLu = 70   ; {uM} transport constant of PQ into the alveolar cells

ker = 0.003   ; lung elimination rate {/hr}

```
;=================================================================
;Run settings
;=================================================================

;Molecular weight PQ
MW = 257.2
 ;----------------------------------------------------------------------------------------------------

;ORAL dose
ODOSEmg = 60*0.1 {mg/kg bw}                          ; ODOSEmg = given Oral dose in
                                                       mg/kg bw

ODOSEumol2 = ODOSEmg*1E-3/MW*1E6 {umol/kg bw}        ; ODOSEumol2 = given Oral
                                                       dose recalculated to umol/kg bw

ODOSEumol=ODOSEumol2*BW;                             ; ODOSEumol = umol given
Orally

;time
Starttime = 0.1217          ; in hr
Stoptime = 24          ; in hr

;Lagtime for oral uptake = 0.1217 hr              ;Chui et al. 1988 Lt = 7.3 min
;=================================================================
;Model calculations
;=================================================================
;Oral dosing
;Stomach compartment
;ASt  = amount in stomach, umol
;ASt' = Change in amount of PQ in time in the stomach,  umol/hr

ASt'  = -ka*ASt
Init ASt = ODOSEumol
;----------------------------------------------------------------------------------------------------
;liver compartment

;AL = Amount PQ in liver tissue, umol
;AL' = Change in amount of PQ in time in liver (umol/hr)

AL' = ka*ASt + QL*(CAB - CVL)
Init AL = 0
CL = AL/VL
CVL = CL/PL
;----------------------------------------------------------------------------------------------------
;kidney compartment

;AK = Amount of PQ in kidney (umol)

;AK' = Change in amount of PQ in time in kidney (umol/hr)

AK' = QK*(CAB-CVK)-GF'-AKe'
         Init AK = 0
         CK = AK/VK
```

CVK = CK/PK

;GFR = glomerular filtration rate {L/hr}   ; Reference: Walton et al., 2004)
; GFR rat = 5.2 {mL/min/kg bw}
$$GFR = 0.0052 * BW * 60 \ \{L/hr\}$$

;GF = glomerular filtration of paraquat (umol/hr)
GF' = GFR*(CVK*Fub)
Init GF = 0

;Fub = fraction unbound of PQ
Fub = 0.65

;AKe = amount paraquat actively excreted from the kidney (umol)
;AKe' = amount paraquat actively excreted from the kidney in time (umol/hr)
AKe' = VmaxOCT2*(CVK*Fub)/(KmOCT2 + (CVK*Fub))
Init AKe = 0
;---
;lung compartment

;ALu = Amount PQ in lung tissue (umol)
;ALu' = Change in amount of PQ in time in lung (umol/hr)
ALu' = QLu*(CVB-CVLu)-AALu' + ALue'
Init ALu = 0
CLu = ALu/VLu
CVLu = CLu/PLu
;---
;lung deep tissue compartment (alveolar tissue)
;Accumulation of PQ into the alveolar tissues

;AALu = Amount PQ accumulating in alveolar cells in lung (umol)
;AALu' = Amount PQ accumulating in alveolar cells in lung in time (umol/hr)
AALu' = VmaxPQLu *(CVLu*Fub)/ (KmPQLu + (CVLu*Fub))
Init AALu = 0

;PQ eliminated back into the blood from alveolar tissue.
;ALue = Amount PQ eliminated back into the blood (umol)
;ALue' = Amount PQ eliminated back into the blood in time (umol/hr)
ALue' = ker* AALu
Init ALue= AALu
;---
;fat compartment

;AF = Amount PQ in fat tissue (umol)
AF' = QF*(CAB-CVF)
Init AF = 0
CF = AF/VF
CVF = CF/PF
;---
;tissue compartment richly perfused tissue

```
;AR = Amount PQ in richly perfused tissue (umol)
    AR' = QR*(CAB-CVR)
    Init AR = 0
    CR = AR/VR
    CVR = CR/PR
;-----------------------------------------------------------------------------------------------------
;tissue compartment slowly perfused tissue

;AS = Amount PQ in slowly perfused tissue (umol)
    AS' = QS*(CAB-CVS)
    Init AS = 0
    CS = AS/VS
    CVS = CS/PS
;-----------------------------------------------------------------------------------------------------
; blood compartment
; Venous blood
;AVB = Amount PQ in venous blood (umol)
;AVB' = Change in amount of PQ in time in venous blood (umol/hr)
    AVB' = (QF*CVF) + (QL*CVL) + (QK*CVK) + (QS*CVS) + (QR*CVR) - (QLu*CVB)
    Init AVB = 0
    CVB = AVB/VVB
    AUCVB' = CVB
    init AUCVB = 0


; Arterial blood
;AAB = Amount PQ in arterial blood (umol)
;AAB' = Change in amount of PQ in time in arterial blood (umol/hr)
    AAB'= (QLu*(CVLu-CAB))
    Init AAB = 0
    CAB = AAB/VAB
    AUCAB' = CAB
    init AUCAB = 0




;====================================================================
;Mass balance calculations
;====================================================================

Total = ODOSEumol
Calculated = ASt + AL + AK + GF + AKe + ALu + AALu - ALue+ AF + AS + AR + AAB + AVB

ERROR=((Total-Calculated)/Total+1E-30)*100
MASSBBAL=Total-Calculated + 1
```
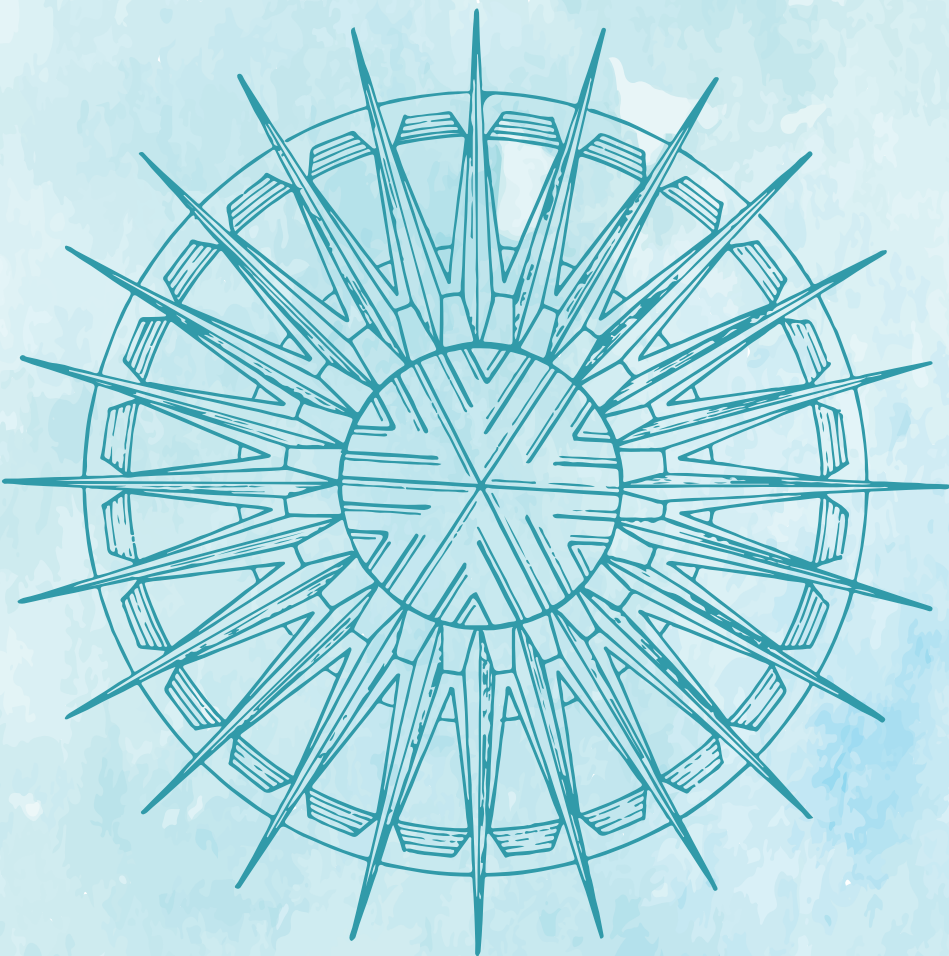
Chapter 5

Use of physiologically based kinetic modelling-facilitated reverse dosimetry to predict *in vivo* acute toxicity of tetrodotoxin in rodents

Annelies Noorlander, Mengying Zhang, Bennard van Ravenzwaay,
Ivonne M.C.M. Rietjens

Abstract

In the present study the ability of a new *in vitro* / *in silico* quantitative *in vitro – in vivo* extrapolation (QIVIVE) methodology was assessed to predict the *in vivo* neurotoxicity of tetrodotoxin (TTX) in rodents. *In vitro* concentration-response data of TTX obtained in a multielectrode array assay with primary rat neonatal cortical cells and in an effect study with mouse neuro-2a cells were quantitatively extrapolated into *in vivo* dose-response data, using newly developed physiologically based kinetic (PBK) models for TTX in rats and mice. Incorporating a kidney compartment accounting for active renal excretion in the PBK-models proved to be essential for its performance. To evaluate the predictions, QIVIVE derived dose-response data were compared to *in vivo* data on neurotoxicity in rats and mice upon oral and parenteral dosing. The results revealed that for both rats and mice the predicted dose-response data matched the data from available *in vivo* studies well. It is concluded that PBK modelling-based reserve dosimetry of *in vitro* TTX effect data can adequately predict the *in vivo* neurotoxicity of TTX in rodents, providing a novel proof-of-principle for this methodology.

Keywords; physiologically based kinetic modelling; reverse dosimetry; tetrodotoxin (TTX), neurotoxicity; new approach methodology.

List of abbreviations: ADME (absorption, distribution, metabolism, excretion), **ARfD** (acute reference dose), **BMD** (Benchmark dose), **BMDL$_{10}$** (lowest observed adverse effect level), **EFSA** (European Food Safety Authority), **HEK293** (human embryonic kidney cell line), **IM** (intramuscular), **IV** (intravenous), **LC-MS/MS** (Liquid chromatography mass spectrometry), **LD$_{50}$** (median lethal dose), **LOAEL** (lowest observed adverse effect level), **MATE** (multidrug and toxin extrusion transporter), **MEA** (multielectrode array assay), **MRM** (multiple reaction monitoring), **NAM** (new approach methodology), **NOAEL** (no observed adverse effect level), **OCT2** (Organic cation transporter 2), **PBK** (Physiologically based kinetic), **PoD** (Point of departure), **QIVIVE** (quantitative *in vitro – in vivo* extrapolation), **RPTEC** (renal proximal tubule epithelial cell), **TE** (transporter efficiency), **TTX** (tetrodotoxin)

5.1   Introduction

Tetrodotoxin (TTX) (fig. 1) is a naturally occurring neurotoxin that can be found in various marine gastropods and some fish species (Bane et al. 2014; Control and Prevention 1996). There are over 30 structural analogues of TTX (Huang et al. 2008). TTX has potent voltage gated sodium channel blocker activity (Sui et al. 2002), preventing depolarization and propagation of action potentials in nerve cells, resulting in the loss of sensation (Bane et al. 2014). The acute exposure to TTX leads to a wide range of acute adverse effects including skeletal muscle fasciculations, apathy, lethargy, ataxia, paralysis and even death (Bane et al. 2014).

The European Food Safety Authority (EFSA) established an acute reference dose (ARfD) for TTX of 0.25 µg/kg bw based on an acute toxicity study with a single intragastric dose in mice with a no observed adverse effect level (NOAEL) of 75 µg/kg bw choosing apathy as the critical effect observed at a lowest observed adverse effect level (LOAEL) of 125 µg/kg bw (Abal et al. 2017; EFSA et al. 2017). In this study, lethality was observed at 250 µg/kg bw with a steep dose-response curve from which a lowest observed adverse effect level ($BMDL_{10}$)of 112 µg/kg bw could be derived (EFSA et al. 2017). Because this $BMDL_{10}$ value for lethality was considered to be close to the NOAEL for apathy, the EFSA Panel argued that it cannot be excluded that effects can still occur at 75 µg/kg bw. Therefore, they established the ARfD based on the next lower test dose (25 µg/kg bw) using an uncertainty factor of 100 to derive the ARfD of 0.25 µg/kg bw. The EFSA opinion also provided an overview of the median lethal dose (LD_{50}) data from mouse studies upon different routes of exposure, indicating toxicity upon oral gavage or intragastric dosing, with LD_{50} values amounting to 232 µg/kg bw (Abal et al. 2017) and 532 µg/kg bw (Xu et al. 2003), to be substantially lower than the LD_{50} values reported upon intraperitoneal or subcutaneous dosing, for which LD_{50} values ranged from 9-12.5 µg/kg bw (Kao 1966; Kao and Fuhrman 1963; Marcil et al. 2006; Xu et al. 2003). In addition, the LD_{50} in rats upon intramuscular administration was reported to amount to 10 - 11.1 µg/kg bw (Hong et al. 2017; Marcil et al. 2006), while Finch et al. (2018) and Hong et al. (2018) reported LD_{50} values for rats upon oral dosing of 909 µg/kg bw and 571.43 µg/kg bw, respectively, that were not included in the EFSA overview.

The available TTX data for human are too limited to provide a point of departure (PoD) for risk assessment, with only a minimum lethal oral dose of 2 mg being mentioned in literature, which is equivalent to 40 µg/kg bw for a 50 kg Japanese subject (EFSA et al. 2017). Additionally, Kasteel and Westerink (2017) proposed an ARfD of 1.33 µg/kg bw for human based on a so-called universal mammalian LD_{50} of 400 µg/kg bw derived from reported oral LD_{50} values in mice (334-700 µg/kg bw). They applied a conservative factor of 10 to go from an LD_{50} value to a LOAEL value (40 µg/kg bw) and added another factor of 3 to obtain a NOAEL value (13.3 µg/kg bw). Finally, they took a factor

of 10 into account for intraspecies differences.

Given the available data sets on acute toxicity of TTX in rodents and the many analogues of TTX for which experimental toxicity data are lacking, it is of interest to study whether the acute toxicity of TTX can be adequately predicted by a new approach methodology (NAM) such as quantitative *in vitro in vivo* extrapolation (QIVIVE) using physiologically based kinetic (PBK) modelling with integrated *in vitro* and *in silico* data and applying reverse-based dosimetry. Thus, the present study aimed to evaluate the potential of using *in vitro* toxicity data obtained with primary rat neonatal cortical cells on a multielectrode array (MEA) assay or an effect study in mouse neuro-2a cells combined with PBK model based-reverse dosimetry to predict the *in vivo* acute neurotoxicity of TTX in rodents. As TTX is hardly metabolized, highly hydrophilic and has been identified as a substrate for organic cation transporters in the kidneys (Matsumoto et al. 2017), active renal transport can be expected to contribute substantially to the *in vivo* TTX kinetics and has to be accounted for in the PBK models to be developed to facilitate the QIVIVE.
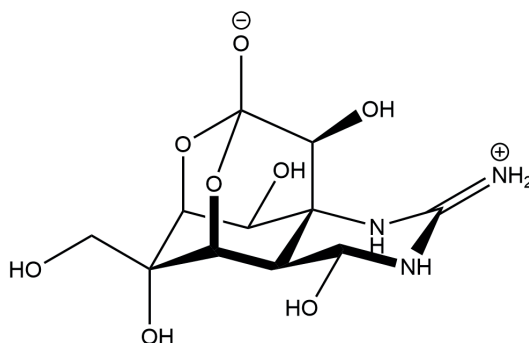
Figure 1.
Structural formula of tetrodotoxin.

5.2   Materials and Methods

Materials

Tetrodotoxin ≥ 98% (TTX, CAS 4368-28-9), was purchased from Sigma-Aldrich (Zwijndrecht, the Netherlands). Dimethyl sulfoxide (DMSO) was purchased from Acros Organics (Geel, Belgium) and phosphate-buffered saline (PBS) was purchased from Invitrogen (Breda, the Netherlands). Pooled hepatocytes from male Sprague-Dawley rats, cryopreserved hepatocyte recovery medium (CHRM, CM7000), and primary hepatocytes thawing and plating supplements (CM4000) were purchased from Thermo Fisher (Landsmeer, the Netherlands).

Methods

Clearance of TTX

It was assumed that the *in vivo* acute toxicity of TTX is induced by the parent compound as there is no evidence of potential metabolites exerting a similar effect. Therefore, only the overall hepatic clearance of TTX was included in the PBK model. Primary hepatocytes from male Sprague-Dawley rats were used to determine the hepatic clearance by the substrate depletion approach. To this end, pooled primary hepatocytes were thawed in a 37 water bath and transferred to 50 ml cryopreserved hepatocyte recovery medium (CHRM, CM7000). The cell suspension was centrifuged at 100×g for 15 min at room temperature, and the supernatant was removed. The collected hepatocytes were dissolved in 1 ml pre-warmed hepatocyte incubation medium, which contained 4% primary hepatocyte thawing and plating supplements (CM4000) in Williams' Medium E1 without phenol red. The density and viability of the hepatocytes were measured using the Cellometer (Auto T4, Nexcelom Bioscience). Hepatocytes with more than 90% viability were used for the incubation. The cells were diluted with incubation medium to reach a density of 1×10^6 cells/ml. TTX was dissolved in DMSO to obtain a stock solution of 600 µM. 20 µl Stock solution of TTX was added to 1980 µl medium to generate the exposure medium (final DMSO concentration 1% v/v). The exposure medium was pre-incubated for 5 min. The incubation was started by adding 100 µl primary hepatocytes into 100 µl pre-incubated exposure medium, giving a final concentration of 0.5×10^6 cells/ml and 3 µM TTX (a non-toxic concentration to hepatocytes as shown by the WST-1 assay (data not shown)) (final DMSO concentration 0.5% v/v). The incubation was done using a shaker (Titramax 1000, Heidolph, Germany) at 150 rpm in a 5% CO_2, 95% air-humidified incubator. The incubation time points were: 0, 1, 2, 3, 4, 5, 7, 8.5, 10, 15, 30, 45, 60 and 90 min. For each incubation time point a corresponding control was included, consisting of an incubation performed in the absence of primary hepatocytes. The incubation was terminated by adding 100 µl cold acetonitrile and the samples were put on ice for 30 min, then centrifuged at 3500 rpm (1200 g) for 15 min at 4 . Supernatants were collected and the concentration of TTX was quantified using LC-MS/MS analysis. All incubations were performed in triplicate in three independent studies. The ratio of the remaining parent compound concentration in the incubation sample ($C_{compound}$) and in the sample at time 0 as control ($C_{control}$) was calculated for each incubation time (taking the amount of TTX left in the corresponding control incubations into account) and the depletion curve of the parent compound ($\ln(C_{compound}/C_{control})$) against time was derived. The slope of the linear part of the depletion curve represents the elimination rate constant (k, in 1/min) of the parent compound. The *in vitro* clearance ($CL_{int, \ in \ vitro}$) of the parent compound was calculated using the following equation: $CL_{int, \ in \ vitro}$ (ml/min/10^6 cells) = k (1/min)/ V (10^6 cells/ml) (Obach 1999; Sjögren et al. 2009). V represents the number of hepatocytes per ml incubation mixture, (0.5×10^6 cells/ml). The *in vitro* CL_{int} of the parent compound was

scaled to a whole liver using the scaling factor of 135,000 (cell density liver expressed in 10^6 cells/kg) (Houston 1994b).

Analysis of TTX by LC–MS/MS

LC-MS/MS analysis was performed on a Shimadzu Nexera XR LC-20AD SR UPLC system coupled with a Shimadzu LCMS-8045 mass spectrometer (Shimadzu Benelux, 's Hertogenbosch, the Netherlands). The samples (1μl) were loaded onto a BEH C18 column (1.7 μm, 2.1×100 mm) at a flow rate of 0.3 ml/min. The column temperature was set to 40°C. The mobile phase consisted of ultrapure water with 0.1% (v/v) formic acid as mobile phase A and acetonitrile containing 0.1% (v/v) formic acid as mobile phase B. The initial condition of the eluents was 5% A, then changed to 50% A in 2 min and subsequently returned to the initial condition in the next 5 min, and was kept at these starting conditions for another 5 min. The total runtime was 12 min. A Shimadzu LCMS-8045 triple quadrupole with electrospray ionization (ESI) interface was used to perform the MS-MS analysis. The instrument was operated in the positive ion mode in the multiple reaction monitoring (MRM) mode with a spray voltage of 4.5 kV. TTX was monitored at the $[M+H]^+$ of precursor to product 320.1>302.19, 320.1>162.4 and 320.1>60.2 m/z. The Postrun Analysis function from the LabSolutions software (Shimadzu, Kyoto, Japan) was used to obtain the peak area of the total ion chromatogram (TIC).

Development of the PBK model for TTX

The generic PBK model developed in our previous study (Zhang et al. 2019) was used with minor modifications, defining a PBK model for TTX in both rat and mouse. To allow model evaluation based on the three available *in vivo* kinetic data sets, all with different administration routes, the PBK model was built for oral, intravenous (IV) and intramuscular (IM) administration (Hong et al. 2017; Hong et al. 2018). For the IM administration it was assumed that TTX was solely taken up in the blood via the muscle tissue at the injection site, thereby excluding the role of the subcutaneous and lymph routes. To distinguish between IM and IV administration the rate of absorption from the IM injection site was set to a much lower value (50 hr^{-1}) than that for an IV injection (1000,000 hr^{-1}). Given that the study by Hong et al. (2017) concluded that the predominant route of the elimination of TTX is by urinary excretion, a kidney compartment was included in the PBK models. The developed PBK model for TTX consisted of eight compartments, including the site of injection, GI-tract, blood, fat, liver, kidney, rapidly perfused tissue and slowly perfused tissue. The schematic representation of the PBK model is displayed in figure 2. A separate compartment for the brain was not included given the inability of TTX to pass the blood brain barrier (Melnikova et al. 2018). The values for physiological and anatomical parameters for rat were obtained from Brown et al. (1997b) and for mouse from Hall et al. (2012). The partition coefficients to describe the distribution of TTX over

the different tissues were estimated using the quantitative property-property relationship (QPPR) approach from Rodgers and Rowland (2006) facilitated by a QIVIVE toolbox (input: zwitterion, pKa1: 8.76, pKa2: 11 logP: -6.2 and molecular weight: 319.27 g/mol) (Punt et al. 2020). The assumption was made that the distribution of TTX in rat is the same as in mouse. The glomerular filtration (GF) was added to the model according to the equation: $GF = GFR \times (CVK \times fub_{in\ vivo})$, where GFR is the glomerular filtration rate, which is 5.2 ml/min/kg bw for rat and 14 ml/min/kg bw for mouse (Walton et al. 2004), CVK is the concentration of TTX in the kidney compartment and $fub_{in\ vivo}$ is the fraction of TTX unbound in the *in vivo* situation. As mentioned by Matsumoto et al. (2017), TTX seems to be a substrate for some active transporters in the proximal tubule cells in the kidney. Since it is unknown which transporter has the highest contribution it was decided to work with an estimated apparent overall Vmax and Km; one Vmax and one Km for all transporters involved. After running model predictions including only glomerular filtration as the excretion pathway, data for the apparent overall Vmax and Km were estimated based on manual input of Vmax and Km searching for the optimal transporter efficiency (TE = Vmax/Km in µl/min/mg protein) by fitting to the available *in vivo* kinetic data. Matsumoto et al. (2017) reported Papp values for the bidirectional transport of TTX over an LLC-PK1 kidney cell layer. Future use of such Papp values to define the *in vivo* kinetic parameters for urinary excretion of TTX in a PBK model requires definition of the scaling factor(s) needed to convert these *in vitro* Papp values to the kinetic constants for active transport of TTX in the kidney *in vivo*. This scaling could be achieved by scaling the model predictions to fit available *in vivo* data, as done in the present study for Vmax, as well as in other studies for other transport parameters, including parameters for renal excretion in PBK models, such as for the PBK model for perfluorooctanoic acid (PFOA) in rats (Worley and Fisher 2015) and the PBK model for mepiquat in rats (Noorlander et al. 2021b). The model equations were coded and numerically integrated in Berkeley Madonna 8.0.1 (UC Berkeley, CA, USA), using the Rosenbrock's algorithm for stiff systems (see supplementary materials A for the model codes).

5
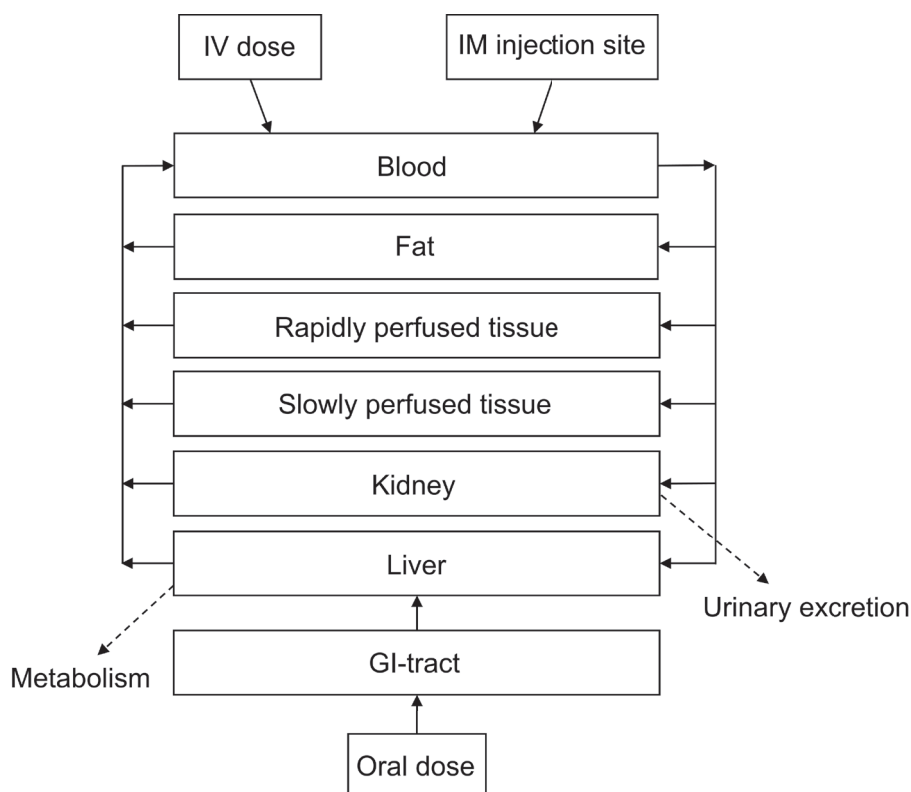
Figure 2.
Schematic representation of the rodent PBK model for TTX.

PBK model evaluation

For evaluation of the PBK model, *in vivo* kinetic data of the TTX blood concentration in time upon oral, IV or IM dosing were available for rats (Hong et al. 2017; Hong et al. 2018). It was assumed that evaluation of the model in rats would support its use for mice as well. It is important to note that the *in vivo* kinetic data were obtained in plasma, whereas the PBK model predicts the concentration in whole blood. Thus, an adjustment of the reported concentrations in plasma to concentrations in blood was made by multiplying the plasma data with the blood:plasma ratio (0.42; derived from Hong et al. (2017). For the IM administration kinetic data presented by Hong et al. (2017) for the dried plasma curve were used since these data were corrected for the formed tritiated water by the hydrogen-tritium exchange of 11-[^{3}H]TTX in the plasma possibly interfering with the results. To identify the most influential parameters of the PBK model on the model prediction of the maximum blood concentration (C_{max}) upon oral and IM administration, a sensitivity analysis was performed (see figure S1 of supplementary materials B). To this end, an initial input parameter value was increased by

5% and the sensitivity coefficients (SC) were calculated using the equation SC=(C'-C)/(P'-P)×(P/C), in which P and P' represent the initial and modified parameter value respectively, while C and C' are the initial and modified model output for C_{max} (Evans and Andersen 2000). Each parameter was analyzed individually by changing one parameter at a time keeping the other parameters at their original value, while the total blood flow fraction was kept as 1. The sensitivity analysis was performed for exposure to 6 µg/kg for the oral and IM routes, representing the dose level actually used in the available *in vivo* studies (Hong et al. 2017; Hong et al. 2018).

Translation of the in *vitro* neurotoxicity data for TTX to in vivo dose response data

For rat, two *in vitro* concentration-response data sets were available. Both studies performed the multielectrode array (MEA) assay using primary rat neonatal cortical cells for measuring neuronal activity upon exposure to TTX (Kasteel and Westerink 2017; Nicolas et al. 2014). For mouse, four *in vitro* concentration-response data sets were available, where in all studies mouse neuro-2a cells were used to detect the inhibition by TTX on cellular toxicity (Hamasaki et al. 1996; Kogure et al. 1988; Nicolas et al. 2015; Yamashoji and Isshiki 2001; Yeo et al. 1996). The inhibition is induced by first exposing the cells to veratridine (sodium channel opener) and ouabain (blocking of Na$^+$/K$^+$-ATPase) which may result in disturbance of the sodium ion homeostasis in the cells resulting in cell death (Kogure et al. 1988; Rossini and Hartung 2012). When the veratridine/ouabain-treated cells are exposed to TTX the sodium channels are blocked and sodium accumulation in the cells is prevented, counteracting the toxic effects of veratridine and ouabain thereby leading to cell survival (Kogure et al. 1988). Throughout the present study this assay is further referred to as the neuro-2a assay. The available concentration-response data were used to predict the dose levels that were required to reach the respective effect concentrations of TTX in blood, using PBK modelling-based reverse dosimetry. It is of importance to realize that only the free fraction of the compound will exert the effects, which implies that a correction for protein binding prior to applying reverse dosimetry should be considered. However, due to the physicochemical characteristics of TTX the fraction unbound *in vivo* is 1 (see toolbox Punt et al. (2020)) and therefore, given the excellent water solubility of TTX, it was assumed that in the *in vitro* MEA medium and neuro-2a medium containing 10% fetal bovine serum the fu$_{in\ vitro}$ of TTX was 1, too. Thus, the *in vitro* effect concentration (EC$_{in\ vitro}$) of TTX was set equal to an *in vivo* effect concentration (EC$_{in\ vivo}$), without a need for correction for potential differences in protein binding in the *in vitro* and *in vivo* situation. The C$_{max}$ was the chosen dose metric for reverse dosimetry of TTX as the mode of action of its toxicity, sodium channel blocking, shows to be a concentration-dependent endpoint with a threshold (Rietjens et al. 2019). So, the estimated EC$_{in\ vitro}$ was set equal to C$_{max}$ of TTX in the PBK model. By repeating these steps for all the *in*

vitro test concentrations, the *in vitro* concentration-response data were converted to define the corresponding *in vivo* dose-response data.

Comparing predicted dose–response curves to *in vivo* toxicity data

After evaluation of the model the predicted *in vivo* dose-response curves were compared to the available *in vivo* TTX toxicity data. For this comparison the most sensitive endpoint for toxicity was chosen for each route and species as described in the result section. To quantify the comparison bench mark dose (BMD) responses were generated using the EFSA online BMD software. The BMD_{10} and $BMDL_{10}$ were determined under the EFSA default settings for Akaike information criterion (AIC) being 2 and a confidence interval of 95%. Only BMD_{10} and $BMDL_{10}$ values as a result of model averaging were taken. Furthermore, a medium effective dose (and concentration) (ED_{50} and EC_{50}) was calculated in Excel using the TREND function as follows: 1) calculate from the dataset the halfway response: *lowest γ_{value} + (highest γ_{value} - lowest γ_{value}) /2* and 2) use the TREND function, which includes the 2 x-values with corresponding y-values in between where the halfway response lies to calculate its x-value, also the ED_{50} (or EC_{50}). EC_{50} values were used to compare the *in vitro* data sets.

Human model

In spite of the limited available human data on TTX kinetics, a human PBK-model was defined, assuming that the evaluation of the model in rat would support its use for humans. The physiological and physicochemical parameters for the human model were taken from the literature in a similar way as for rat (Brown et al. 1997a; Punt et al. 2020) and are presented in Table 1. The kinetic constants were taken from the rat model and adjusted to human using human scaling factors. For reverse dosimetry one *in vitro* data set was available (Kasteel and Westerink 2017) describing a concentration response curve for the effect of TTX on human-induced pluripotent stem cell (hIPSC)-derived iCell® neurons in co-culture with hIPSC-derived iCell® astrocytes in the MEA assay. Using our human PBK-model, this *in vitro* concentration-response curve was translated to an *in vivo* dose-response curve for oral exposure to TTX and a BMD_{10}, $BMDL_{10}$ and ED_{50} were derived that were compared to available (on mouse study based) human data on TTX toxicity.

5.3   Results

Substrate depletion of TTX

Figure 3 shows the depletion of TTX in incubations with rat hepatocytes. The *in vitro* hepatic clearance (CL_{int}) derived from these data amounted to $1.6 \times 10^{-7} \pm 0.01$ ml/min/10^6

cells converted to an *in vivo* CL_{int} of 1.1×10^{-5} L/hr for the rat, indicating that clearance of TTX via metabolism is limited. It was assumed that the mouse hepatic clearance would be similarly limited.
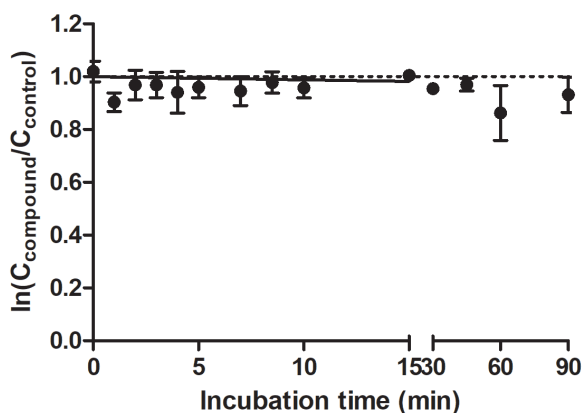
Figure 3.
Time-dependent substrate depletion of TTX in incubations with primary rat hepatocytes. Symbols represent the average $ln(C_{compound}/C_{control})$ at different incubation time points (mean ± SD of 3 independent experiments). Straight line represents the depletion curve and the dotted line represents zero depletion.

In vitro concentration-response data for TTX in rodent cells

The available *in vitro* concentration-response data for neurotoxicity of TTX in rat primary neonatal cortical cells in the MEA assay and for the neurotoxicity of TTX in the mouse neuro-2a assay are summarized in figure 4. Both the rat MEA data (Fig. 4a) and the mouse neuro-2a data (Fig. 4b) reported in different studies provide comparable results, except for the data of Nicolas et al. (2015) for the mouse neuro-2a assay, which indicate at a somewhat greater sensitivity. Nevertheless, these data together provide a suitable data set for QIVIVE and conversion into *in vivo* dose-response curves. Given the similarity of the concentration-response curves for the TTX induced neurotoxicity in the neuro-2a assay reported in the studies of Hamasaki et al. (1996), Yamashoji and Isshiki (2001) and Yeo et al. (1996) these three data sets were used for the mice predictions by reverse dosimetry. The graphs in figure 4 show that the rat primary neonatal cortical cells in the MEA assay (EC_{50} values 0.0035 μM and 0.0055 μM) (Figure 4a) seem to be only slightly more sensitive than the mouse neuro-2a cells in the neuro-2a assay (EC_{50} values of the 3 corresponding data sets amounting to 0.0082 μM).
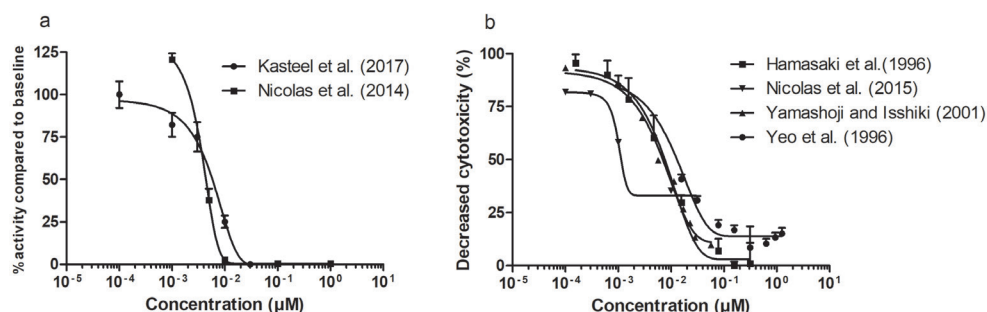
Figure 4.

In vitro concentration response curves for the effects of TTX on (a) primary rat neonatal cortical cells in the MEA assay (circles; Kasteel and Westerink (2017) EC_{50} = 0.0055 mM, squares; Nicolas et al. (2014) EC_{50} = 0.0035 mM) and (b) neurotoxicity in mouse neuro-2a cells (squares; Hamasaki et al. (1996) EC_{50} = 0.0075 mM, inverted triangles; Nicolas et al. (2015), triangles; Yamashoji and Isshiki (2001) EC_{50} = 0.0053 mM, and circles; Yeo et al. (1996) EC_{50} = 0.0121 mM). Data points represent mean (± SD/SEM, where available).

PBK model evaluation

The evaluation of the PBK model using different routes of administration and the parameter input presented in table 1 is shown in figure 5. Predictions were fitted to the *in vivo* data by estimating the rate of absorption for the oral route (ka: 0.18/hr) and IM route (kb: 50/hr) and optimizing the contribution of active renal excretion based on the transporter efficiency, which was 90 µl/min/mg protein (Vmax = 180 pmol/min/mg protein, Km = 2 µM). It appeared important to include this active excretion since it accounts for a substantial improvement in the predictions (compare figure 5 with renal excretion, to figure S2 in the supplementary materials B for data without taking renal excretion into account). For all administration routes, oral (fig. 5a) IM (fig. 5b) and IV (fig. 5c), the model was able to adequately predict the *in vivo* data. To enable subsequent PBK model-based reverse dosimetry for both the oral and the IM mode of administration a plot of the dose against Cmax was made, which was used to convert the *in vitro* concentrations from figure 4 to *in vivo* dose levels to generate the dose-response curves. As explained in the materials and methods section, the high water solubility of TTX eliminated the need for a correction for differences in protein binding with the fub *in vitro* and *in vivo* both being 1.
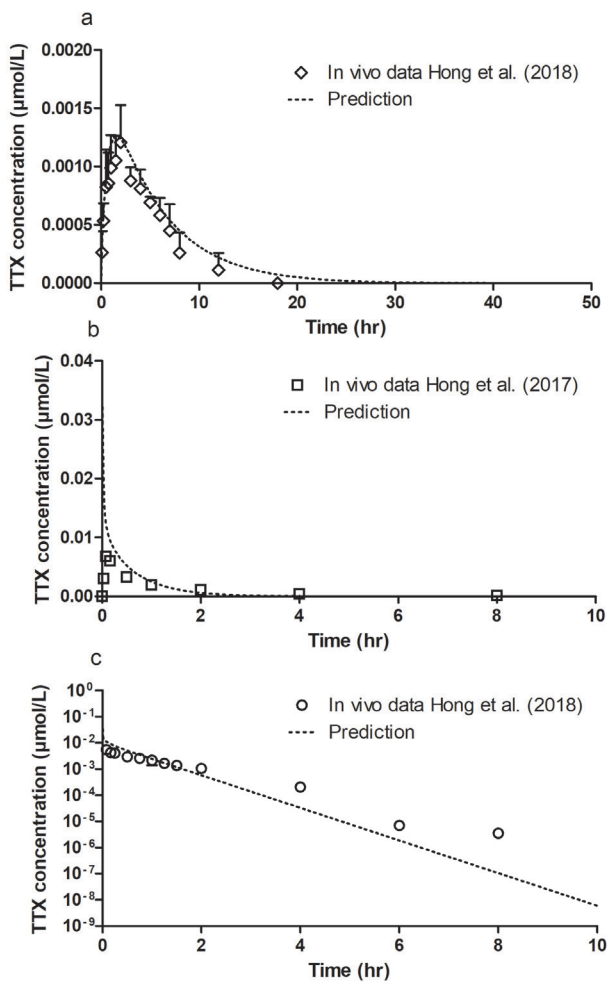
Figure 5.
Predicted concentration time curves of TTX in whole blood of rat (striped lines) dosed with TTX via (a) oral (diamonds), (b) IM (squares) and (c) IV (circles) administration. The literature data reported as plasma concentrations were adjusted to blood concentrations assuming a blood:plasma ratio of 0.42 (Hong et al. 2017). Dosage used: oral 100 µg/kg bw with 6.7% bioavailability, IM and IV 6 µg/kg bw. Data points represent mean (± SD/SEM, where available).

Table 1.
Physiological and anatomical parameter values and the partition coefficients used for the PBK models

Parameters	Rat[a]	Mouse[b]	Human[a]
Body weight (kg)	0.24	0.03	70
Fraction of tissue volumes			
Fat	0.070	0.070	0.214
Liver	0.034	0.055	0.026
Blood	0.074	0.067	0.079
Kidney	0.007	0.017	0.004
Rapidly perfused tissue	0.091	0.137	0.064
Slowly perfused tissue	0.724	0.654	0.613
Cardiac output	15[1]	15.4[2]	15[1]
Fraction of blood flow to tissue			
Fat	0.070	0.070	0.052
Liver	0.174	0.158	0.227
Kidney	0.141	0.114	0.175
Rapidly perfused tissue	0.093	0.516	0.195
Slowly perfused tissue	0.512	0.142	0.351
Partition coefficients[c]			
$LogP_{ow}$	-6.2[d]		
pKa1	8.76[e]		
pKa2	11[e]		
Fat/blood partition coefficient	0.46	0.46	0.46
Liver/blood partition coefficient	4.29	4.29	4.29
Kidney/blood partition coefficient	4.70	4.70	4.70
Rapid perfused tissue/blood partition coefficient	4.29	4.29	4.29
Slowly perfused tissue/blood partition coefficient	0.95	0.95	0.95

[a] Brown et al. (1997a)
[b] Hall et al. (2012)
[c] Punt et al. (2020)
[d] Hort et al. (2020)
[e] Camougis et al. (1967)
[1] L/hr×kg×bw$^{0.74}$
[2] L/hr×kg×bw$^{0.75}$

Literature reported *in vivo* dose–response data in rodents

Figure 6 summarizes the available *in vivo* dose-response data for TTX in rodents available in literature for evaluation of the QIVIVE predictions. It must be noted that although the reported *in vivo* data are used for evaluation of the QIVIVE predictions made in the current study using a NAM, this does not imply that the authors of the present study agree with the ethics of these animal studies as they involve pain and discomfort to the animals. Three data sets for rat (fig. 6a) originate from studies reporting on the pharmacological application of TTX as a morphine-like painkiller (Kohane et al. 2000; Kohane et al. 1998; Marcil et al. 2006). The dose response curves from these three studies reveal substantial differences in sensitivity depending on the endpoint used to quantify the effect. The data reported by Marcil et al. (2006) using the so-called Von Fray hair test to quantify the TTX induced reduction in mechanical allodynia (pain) showed effects at 16-fold lower dose levels (fig. 6a left y-axis) than the dose response curves defined based on TTX induced thermal nociceptive blocking (blocking of the peripheral sensory neurons; nociceptors) (fig. 6a right y-axis). The route of administration in all three studies was comparable consisting of subcutaneous/percutaneous injection. The data set reporting mechanical allodynia, apparently relating to the most sensitive endpoint, was selected for QIVIVE-based predictions. For mouse (fig. 6b), six data sets were identified in the available literature of which two related to parenteral administration and four to oral administration (Abal et al. 2017; Finch et al. 2018; Marcil et al. 2006). Here too, the data sets for the parenteral route differ markedly, as the endpoint 'time to death' in minutes requires higher doses to be affected than the more sensitive endpoint including a so-called writhing test where the number of contractions of the abdomen was measured after exposure to acetic acid following increasing concentrations of TTX (both shown on left y-axis of figure 6b). The latter study was selected for further QIVIVE-based predictions. The data sets for the oral route show a lower sensitivity to TTX compared to the parenteral route likely related to the low oral bioavailability of TTX of 6.7% reported by Hong et al. (2018). For the oral route, dose-response curves for the macroscopically observed neurological symptoms apathy, numbness, seizures and mortality were available (shown on right y-axis of figure 6b), where apathy was the most sensitive endpoint and therefore selected for the QIVIVE-based predictions.
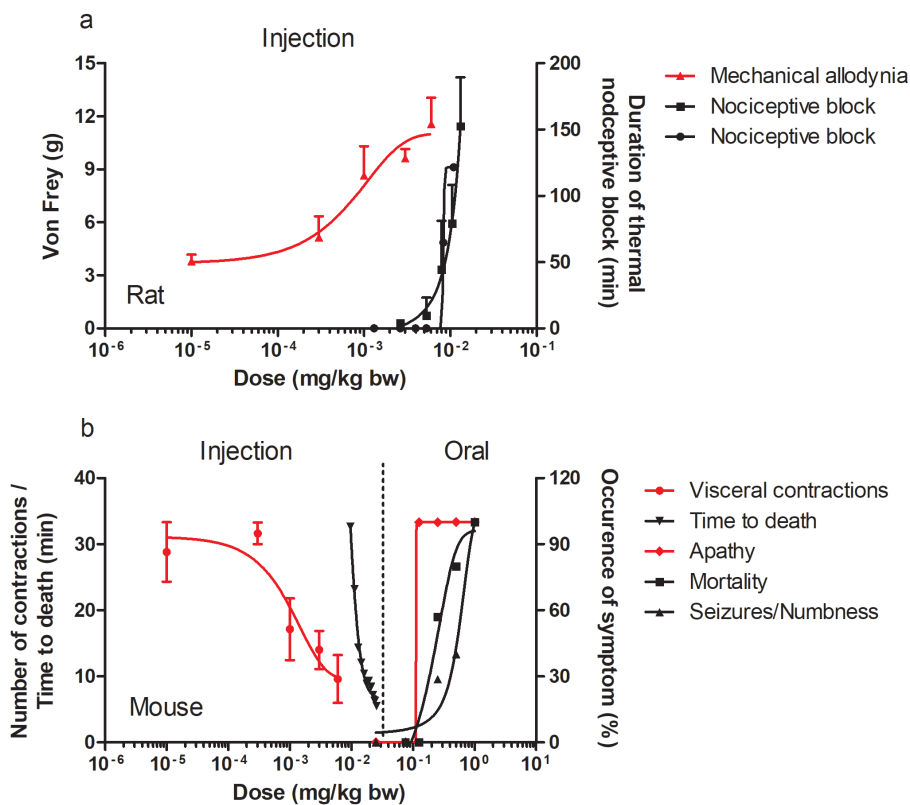
Figure 6.
Overview of *in vivo* dose response data for TTX in rodents found in literature including (a) *in vivo* data sets for rat after TTX injection: triangles; Von Frey (g) hair test ;(Marcil et al. 2006) (left y-axis), squares and circles; duration of the nociceptive block (min) (Kohane et al. (1998) (right y-axis), and Kohane et al. (2000), respectively) and (b) *in vivo* data sets for mouse: either upon injection: circles; writhing test (Marcil et al. 2006), inverted triangles; time to death (min) (Finch et al. 2018) (left y-axis) or after oral administration: diamonds; apathy (%) (Abal et al. 2017), squares; mortality (%) (Abal et al. 2017), triangles; numbness and seizures (%) (Abal et al. 2017) (right y-axis). The red data sets present the dose-response curves for the most sensitive endpoint that were chosen for evaluation of the QIVIVE predictions. Data points represent mean (± SD/SEM, where available).

QIVIVE to translate *in vitro* neurotoxicity data for TTX into in vivo dose response data

The *in vitro* concentration response curves were translated to *in vivo* dose response curves using the PBK models for reverse dosimetry and QIVIVE. This resulted in the predicted dose response curves presented in figure 7 on the left y-axis. This figure also presents, for comparison, the reported *in vivo* dose response curves for the most sensitive endpoint as taken from figure 6a on the right y-axis. The results thus obtained reveal an adequate

match between the predicted and actual experimentally obtained dose response curves, with the predicted ED_{50} values differing only 1-1.4-fold from the *in vivo* ED_{50} value (Table 2).
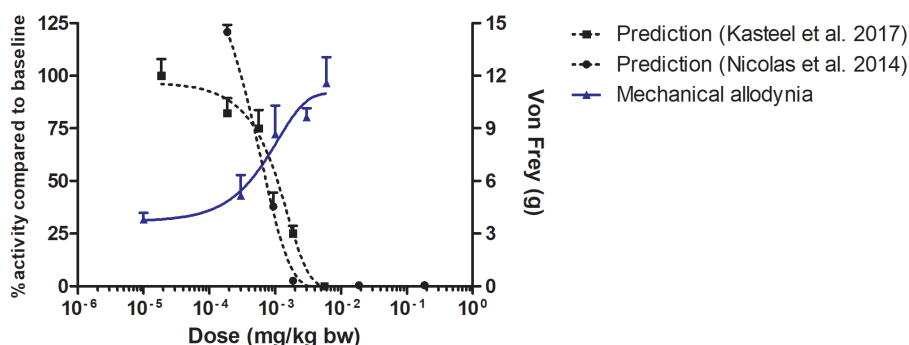
Figure 7.
Predicted *in vivo* dose-response curve for TTX in rat upon injection (IM model) on the left y-axis compared to the *in vivo* data reported by Marcil et al. (2006) in the Von Frey hair test (blue line and triangles) on the right y-axis. The predictions were based on the rat MEA assay data reported by Nicolas et al. (2014) (black circles) or Kasteel and Westerink (2017) (black squares). Data points represent mean (± SD/SEM, where available).

For mouse, both the IM model and the oral PBK model were used to translate the respective *in vitro* concentration-response data into *in vivo* dose-response data (fig. 8). For the parenteral route, the most sensitive endpoint was the number of visceral contractions for which the *in vivo* dose-response curve was provided by Marcil et al. (2006). Figure 8a presents a comparison of the *in vivo* experimental data (right y-axis) to the predicted dose-response curves (left y-axis) for TTX in mice. This comparison reveals that the predicted dose-response curves based on the *in vitro* data obtained in the neuro-2a assay are in line with the observed *in vivo* dose-response data as the predicted ED_{50} values varies 1.8-fold to a maximum of 3-fold from the *in vivo* ED_{50} value (Table 2). Apathy was the most sensitive endpoint for the oral route and therefore chosen for the comparison to the predicted dose-response curve upon oral administration of TTX (fig. 8b). Here too, the predicted dose-response curves (left y-axis) appear to be in accordance with the observed *in vivo* data (right y-axis) with the predicted ED_{50} values being at most up to 2.3-fold lower than the observed *in vivo* ED_{50} value (Table 3).
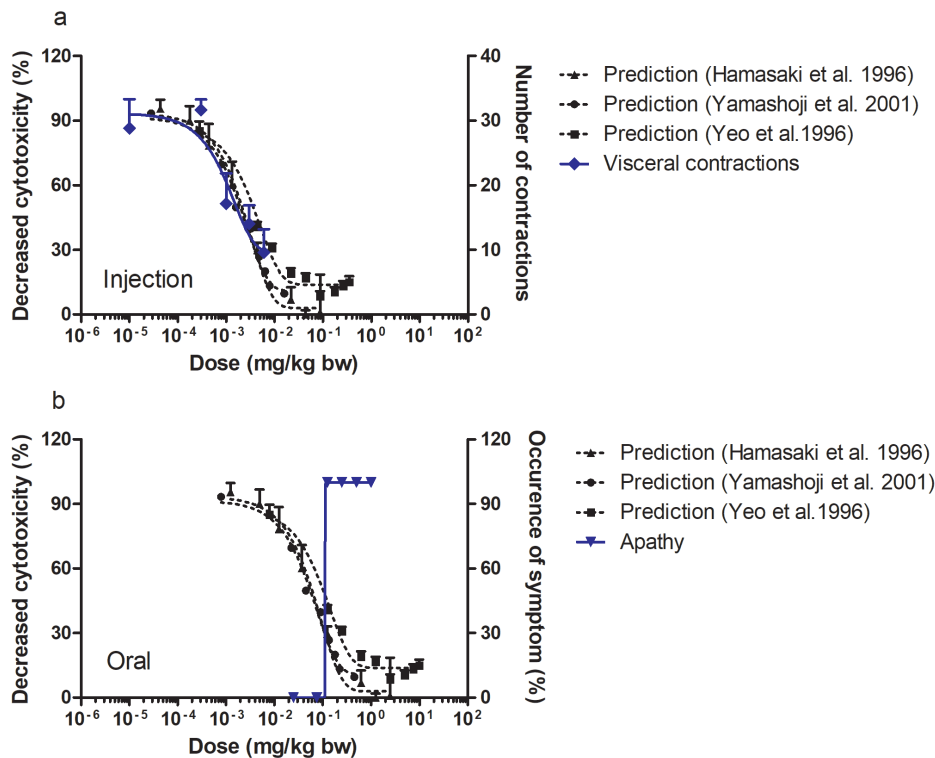
Figure 8.
Predicted *in vivo* dose-response curves for TTX in mice upon (a) injection (IM model) and (b) oral administration (oral model). In blue the *in vivo* endpoints visceral contractions (diamonds; Marcil et al. (2006)) (fig. 8a) and apathy (inverted triangles; Abal et al. (2017)) (fig 8b) displayed on right y-axes. The predictions were based on the mouse neuro-2a assay data reported by Hamasaki et al. (1996) (triangles); Yamashoji and Isshiki (2001) (circles) and Yeo et al. (1996) (squares) displayed on the left y-axes. Data points represent mean (± SD/SEM, where available).

Table 2.
Established ED_{50} values for the predicted *in vivo* dose-response data and *in vivo* data for rat and mouse via parenteral administration. The literature reported ED_{50} values used for comparison to the predicted ED_{50} values are printed in bold.

	ED_{50} (µg/kg bw)	Endpoint	Literature
Injection			
Rat			
Predicted	1	MEA Spike	Kasteel and Westerink (2017)
	0.7	MEA Spike	Nicolas et al. (2014)
In vivo	**0.7**	Von Frey	Marcil et al. (2006)
	10.4	Nociceptive block	Kohane et al. (1998)
Mice			
Predicted	2.1	Cytotoxicity inhibition	Hamasaki et al. (1996)
	1.5	Cytotoxicity inhibition	Yamashoji and Isshiki (2001)
	2.4	Cytotoxicity inhibition	Yeo et al. (1996)
In vivo	**0.84**	No. visceral contractions	Marcil et al. (2006)
	12	Time to death	Finch et al. (2018)

Table 3.
Established ED_{50} values for the predicted *in vivo* dose-response data and *in vivo* data for mouse via oral administration. The literature reported ED_{50} values used for comparison to the predicted ED_{50} values are printed in bold.

	ED_{50} (µg/kg bw)	Endpoint	Literature
Oral			
Mice			
Predicted	61	Cytotoxicity inhibition	Hamasaki et al. (1996)
	42	Cytotoxicity inhibition	Yamashoji and Isshiki (2001)
	69	Cytotoxicity inhibition	Yeo et al. (1996)
In vivo	**96**	Apathy	
	560	Seizures/Numbness	Abal et al. (2017)
	223	Mortality	

Predicting TTX neurotoxicity in human and estimating a tentative point of departure

Upon evaluation of the rat TTX model the model code was used to define a human oral PBK-model. For predicting TTX neurotoxicity in human by QIVIVE an *in vitro* data set reported by Kasteel and Westerink (2017) was used describing TTX toxicity towards human IPSC-derived iCell° neurons in co-culture with hIPSC-derived iCell° astrocytes exposed to TTX in the MEA (multielectrode array assay) (fig. 9a). The dose-response curve obtained of TTX in this MEA cell model was translated to an *in vivo* dose-response curve applying PBK model based reverse- dosimetry with the human PBK-model resulting in an *in vivo* dose response curve with an ED_{50} of 18 µg/kg bw (fig. 9b). Further BMD analysis on this predicted *in vivo* dose response curve resulted in a BMD_{10} of 4.3 µg/kg bw, and a $BMDL_{10}$ of 1.8 µg/kg bw (See supplementary materials B, Figure S3 and S4 and Table S1 for details). Taking the $BMDL_{10}$ as a point of departure for the risk assessment of TTX and using a factor 10 for interindividual variability would result in an Acute Reference Dose (ARfD) of 0.18 µg/kg bw. This tentative point of departure is only 1.4-fold different from the previously established ARfD by EFSA of 0.25 µg/kg bw based on an acute toxicity study in mice (Abal et al. 2017).
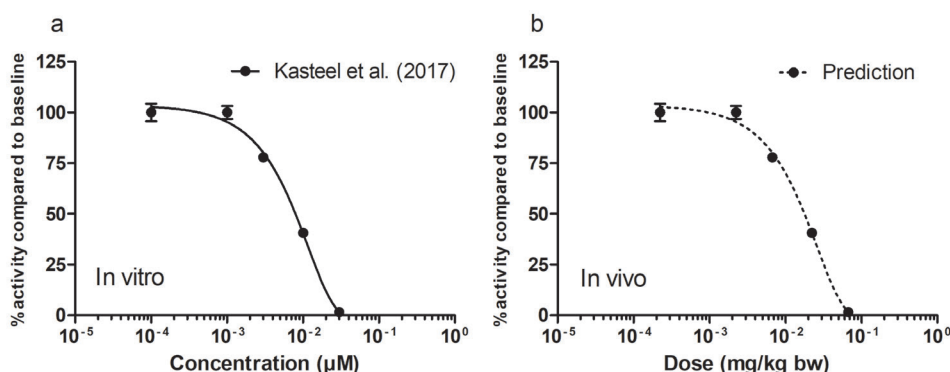
Figure 9.
In vitro concentration response curve of (a) TTX in human IPSC-derived iCell° neurons in co-culture with hIPSC-derived iCell° astrocytes in the MEA assay (Kasteel and Westerink 2017) and (b) the predicted *in vivo* dose-response curve acquired by PBK model facilitated reverse-dosimetry using a human oral model (b). Data points represent mean ± SEM.

5.4   Discussion

TTX is an acute neurotoxin, which upon systemic exposure affects both action potential generation and impulse conduction by extracellular blockade of the voltage gated sodium channels. The available acute reference dose (ARfD) of TTX (0.25 μg/kg bw), is derived from a study on mice in which TTX was dosed orally (via gavage) (EFSA et al. 2017). Given the available data sets on acute toxicity of TTX in rodents and the many analogues of TTX for which experimental toxicity data are lacking, it is of interest to study whether the acute toxicity of TTX can be adequately predicted by a new approach methodology (NAM) based on *in vitro* and *in silico* data.

PBK modelling based reverse dosimetry has proven to be a promising NAM to derive quantitative data, which can potentially be used in risk assessment to estimate *in vivo* toxicity in rodents and human (Chen et al. 2018; Li et al. 2017a; Louisse et al. 2014; Ning et al. 2019c; Shi et al. 2020; Strikwold et al. 2017a; Zhang et al. 2018b; Zhang et al. 2019). The present study aimed to assess the potential of using the PBK modelling-based reverse dosimetry approach as a NAM to predict the neurotoxicity of TTX in rodents, based on *in vitro* toxicity data obtained in the MEA assay using primary rat neonatal cortical cells or data obtained using the mouse neuro-2a assay.

Evaluation of the PBK model performance for TTX demonstrated its adequacy for predicting kinetic data for different routes of administration. In line with the results from Hong et al. (2017) who reported that less than 10% of TTX was metabolized, the results of the present study corroborated that hepatic metabolism does not contribute substantially to the systemic clearance of TTX (*in vitro* CL_{int}: $1.6×10^{-7}±0.01$ ml/min/10^6 cells; *in vivo* CL_{int}: $1.15×10^{-5}$ L/hr), while renal excretion plays a major role in TTX kinetics. Furthermore, the PBK modelling data of the present study revealed that up to 86% of TTX clearance in the kidney could be ascribed to active transport by the proximal tubule cells. This active transport of TTX was previously also demonstrated in the renal proximal tubule cell line LLC-PK1 (Matsumoto et al. 2017). In this *in vitro* study, TTX was shown to be primarily transported by the organic cation transporters and the organic cation/carnitine transporters. To a lesser extent organic anion transporters and multidrug resistance-associated proteins were involved, too. The PBK model evaluation of the present study provides insight in the efficiency of this active transport and revealed that it contributes considerably to TTX clearance. To substantiate the values used in this paper it would be of interest to perform *in vitro* transport studies with TTX for the organic cation transporters in stably transfected cell lines such as the human embryonic kidney cell line HEK293 and investigate to what extent such *in vitro* data can provide the kinetic data defined in the present study by fitting the PBK model to available *in vivo* data for TTX kinetics.

The results obtained revealed that the NAM used in this study could adequately predict the dose-response curves for the selected most sensitive endpoints reported in the available *in vivo* studies. This, in spite of the fact that the spike rates used as readout in the MEA assay (Nicolas et al. 2014) and the endpoint quantified in the MTT assay using the mouse neuroblastoma cell line, both used to generate the *in vitro* concentration-response curves, may detect TTX neurotoxicity based on different endpoints than the endpoints quantified in the *in vivo* neurotoxicity studies. This is possible because the underlying mode of action for all *in vivo* endpoints relates to the TTX mediated blocking of sodium channels. The reasons underlying the differential sensitivity of the various *in vivo* endpoints may relate to as yet unidentified differences in the toxicodynamics and/or toxicokinetics of TTX in the target tissue of interest underlying the respective adverse effects (mechanical allodynia, thermal nociceptive blocking, visceral contractions, apathy, seizures).

So the question arises as to what extent the endpoints quantified in the MEA assay or the neuro-2a assay match these *in vivo* endpoints. Although the mechanism of action underlying all the *in vitro* and *in vivo* endpoints studied for TTX is blocking of the voltage-gated sodium channels, thereby interfering with the production of action potentials, it is of interest to consider the different endpoints in some more detail. For the rat *in vivo* data, the sensory neurons stimulated in the Von Frey hair test and the thermal nociceptive blocking test are non-visceral (or somatic) sensory neurons that can respond to (noxious) events such as mechanical, (extreme) heat/cold or chemical stimuli (Dubin and Patapoutian 2010; Robinson and Gebhart 2008). In both experiments the hind paw of the rats was exposed to either mechanical stimuli by Von Frey filaments or heat stimuli by a hot plate (56°C) until paw withdrawal was observed. Apparently, enduring the pain of heat (uncomfortable sensation) requires higher doses of TTX than enduring the pinprick of a Von Frey filament until uncomfortable sensation, and the type of stimuli (mechanical, heat) and/or the underlying pathway determines how sodium channel blocking is perceived. Here, the Von Frey hair test seems to be the more sensitive endpoint than the thermal nociceptive blocking test. The underlying neuronal/neuromuscular processes to further explain this difference between the different *in vivo* endpoints lies beyond the scope of this study (Dubin and Patapoutian 2010).

In the MEA assay primary rat neonatal cortical neurons isolated from cortices form a network of inhibitory and excitatory cells with different subtypes and amongst them non-visceral neurons (Masland 2004; Nicolas et al. 2014; Schnitzler et al. 1999). In the MEA assay the neuronal cells are directly exposed to TTX and show a decrease in activity compared to baseline with increasing concentrations of TTX. The sodium channel block is therefore directly measurable, whereas this effect *in vivo* is only indirectly noticeable via neuromuscular communication with the central nervous system. Nevertheless, the MEA

assay provides a very sensitive endpoint, therefore the *in vivo* endpoint chosen for the comparison to data predicted based on the *in vitro* assay should be as sensitive as possible.

A similar evaluation for *in vitro* endpoints and *in vivo* endpoints can be performed for the mouse assays. The *in vivo* data on mice, generated in the writhing test, are based on innervation of the visceral sensory neurons by exposure to acetic acid, which via the acid-sensing ion channels lead to pain sensation expressed as abdomen contraction together with twisting and turning of the trunk and arching of the back (Holzer 2011; Marcil et al. 2006; Robinson and Gebhart 2008). These effects are decreased by increasing TTX concentrations blocking the sodium channels and preventing signal transduction. This endpoint appears much more sensitive than measuring the time of death that requires higher doses of TTX (Finch et al. 2018). Comparing the endpoint of the TTX effect in the *in vivo* writhing test -decrease of visceral contractions- to the TTX effect in the *in vitro* neuro-2a assay-cell survival- suggests that these endpoints are not exactly the same in spite of the similar underlying mechanism of action. However, in spite of this apparent difference, the use of the neuro-2a assay for QIVIVE did provide adequate *in vivo* predictions for the writhing test. Similarly, outcomes of the *in vitro* embryonic stem cells test (EST) for developmental toxicity, detecting the inhibition of the development of mouse embryonic ES-D3 stem cells to beating cardiomyocytes, appeared to provide a suitable *in vitro* endpoint to predict a wide range of *in vivo* endpoints for developmental toxicity including malformations, number of live pups and fetal body weight (Kamelia et al. 2017; Li et al. 2017b; Strikwold et al. 2013).

With respect to neurotoxicity, previous studies already concluded that for determining the toxicity of neurotoxins *in vitro* the two most promising assays are the MEA assay (using rat primary neonatal cortical cells) and the mouse neuro-2a assay (Bodero et al. 2018; Nicolas et al. 2015; Nicolas et al. 2014). The results of the present study reveal that these two assays are adequate to define concentration-dependent *in vitro* toxicity data for TTX for QIVIVE using PBK model based-reverse dosimetry. Moreover, using a human IPSC *in vitro* MEA assay showed to have potential to generate data for establishing a tentative point of departure ($BMDL_{10}$) for human TTX toxicity in line with the previously established ARfD by EFSA. To confirm this with more proof, more research should be conducted on the kinetics of TTX in human.

To recapitulate, in this study we have successfully built a PBK model for the marine biotoxin TTX in rodents (rat, mouse) where renal excretion via active transport seems to play a major role in its kinetics. The results presented provide support for the use of this NAM for predicting the acute neurotoxicity of TTX (and its analogues). Thereby, a cautious attempt has been made to predict TTX toxicity in human using only *in vitro* and *in silico* data applying reverse based dosimetry enabled by PBK-modelling and

5

shows to have potential.

Funding

Declaration of conflicting interests
The authors declared no potential conflicts of interest with respect to the research, authorship, and/or publication of this article.

Supplementary material A

Model code for PBK-model built in Berkeley Madonna for rat

```
;Date: November 2019
;Species: Rats
;Compound: Tetrodotoxin (TTX)
;Compiled by: Mengying Zhang and Annelies Noorlander
;Organization: Wageningen University
;====================================================================
;Physiological parameters
;====================================================================
;tissue volumes              >> reference: Brown et al.,1997 Table 21
BW = 0.240                    ; body weight rat (from in vivo kinetic study, Hong et al. 2017)
VFc = 0.070                   ; fraction of fat tissue
VLc = 0.034                   ; fraction of liver tissue
VKc = 0.007                   ; fraction of kidney tissue
VBc = 0.074                   ; fraction of blood
VRc = 0.091                   ; fraction of rapidly perfused tissue
VSc = 0.724                   ; fraction of slowly perfused tissue

VF = VFc*BW          ;(L or Kg)          ; volume of fat tissue (calculated)
VL = VLc*BW          ;(L or Kg)          ; volume of liver tissue (calculated)
VK = VKc*BW          ;(L or Kg)          ; volume of kidney tissue (calculated)
VB = VBc*BW          ;(L or Kg)          ; volume of blood (calculated)
VR = VRc*BW          ;(L or Kg)          ; volume of  richly perfused tissue (calculated)
VS = VSc*BW          ;(L or Kg)          ; volume of  slowly perfused tissue (calculated)

;-----------------------------------------------------------------------------------------------------
;blood flow rates      >> reference: Brown et al.,1997 Table 25
QC = 15*BW^0.74 ;cardiac output      (L/hr)                ;reference: Brown et al., 1997 p. 453
QFc = 0.070                   ; fraction of blood flow to fat
QLc = 0.174                   ; fraction of blood flow to liver
QKc = 0.141                   ; fraction of blood flow to kidney
QRc = 0.093                   ; fraction of blood flow to rapidly perfused tissue
QSc = 0.522                   ; fraction of blood flow to slowly perfused tissue

QF = QFc*QC          ;(L/hr)    ; blood flow to fat tissue (calculated)
QL = QLc*QC          ;(L/hr)    ; blood flow to liver tissue (calculated)
QK = QKc*QC          ;(L/hr)    ; blood flow to kidney tissue (calculated)
QR = QRc*QC          ;(L/hr)    ; blood flow to rapidly perfused tissue (calculated)
QS = QSc*QC          ;(L/hr)    ; blood flow to  slowly perfused tissue (calculated)

;====================================================================
;Partition Coefficients
;====================================================================
; Partition coefficients are derived from Rodgers and Rowland using the QIVIVE tool from A. Punt www.
qivivetools.wur.nl

PF = 0.46            ;fat/blood partition coefficient
```

```
PL = 4.29            ;liver/blood partition coefficient
PK = 4.70            ;kidney/blood partition coefficient
PR = 4.29            ;rapidly perfused tissue/blood partition coefficient
PS = 0.95            ;slowly perfused tissue/blood partition coefficient


;====================================================================
;Kinetic parameters
;====================================================================
kb = 50                      ; (/hr) rate from muscle to blood
ka = 0.18                    ; (/hr) uptake rate from stomach
kn = 1000000                 ; (/hr) rate needle to blood


;--------------------------------------------------------------------------------------------------
;Metabolism liver

;metabolism of TTX, scaled maximum rate of metabolism

CLint = CellDL*VL*(CLintHep*60*1E-3)      ;(L/hr)                    ;Hepatic clearance

CLintHep = 0.00000016                     ;(ml/min/million cells)    ;Hepatic    clearance
                                                                      derived        from
                                                                      hepatocytes

CellDL = 135*1000                         ;(million cells/kg liver)
```

;Hepatocyte number in rat = 1.35 *10E8 cells/g liver = 135 million cells/g liver = 135*1000 million cells/ kg liver
;reference: (Houston et al., 1994)

```
;--------------------------------------------------------------------------------------------------
;Excretion from kidney

;Active uptake of TTX is based on the OCT2 transporter
VmaxTTXc = 180              ;{pmol/min/mg protein}

VmaxTTX = (VmaxTTXc/1000000)*60*SF*VK*1000        ;{umol/hr}
;300 mg prot./g kidney (Kumar et al. 2018)
;only 70% of whole kidney is cortex --> in cortex tubule cells thus OCT-2s are present (Kumar et al. 2018)
; 300 * 0.7 = 210 mg prot./g kidney

Km = 2                     ; {uM} transport constant of TTX
SF = 210                   ; mg/g protein


;====================================================================
;Run settings
;====================================================================
;Molecular weight
MW = 319.27                                       ; Molecular weight TTX (PubChem)
```

;Intramuscular dose is 6 ug/kg bw = 0.006 mg/kg bw (Hong et al., 2017)

```
IMDOSEmg = 0.006                          ; (mg/kg bw)          ; IMDOSEmg = given IM dose in
mg/kg bw

IMDOSEumol2 = IMDOSEmg*1E-3/MW*1E6  ;(umol/ kg bw)

;IMDOSEumol2 = given intramuscular dose recalculated to umol/kg bw
IMDOSEumol = IMDOSEumol2*BW                ;IMDOSEumol = umol given IM


;Oral dose is 100 ug/kg bw = 0.1 mg/kg bw (Hong et al., 2018)
;Bioavailability via oral route = 6.7%

ODOSEmg = 0.1*0.067                        ; (mg/kg bw)          ; ODOSEmg = given oral dose in
                                                                   mg/kg bw

ODOSEumol2 = ODOSEmg*1E-3/MW*1E6       ;(umol/ kg bw)

;ODOSEumol2 = given oral dose recalculated to umol/kg bw
ODOSEumol=ODOSEumol2*BW                                          ; ODOSEumol = umol given oral


;Intravenous dose is 6 ug/kg bw = 0.006 mg/kg bw (Hong et al., 2018)

IVDOSEmg = 0.006                          ; (mg/kg bw)          ; IVDOSEmg = given IV dose in
mg/kg bw

IVDOSEumol2 = IVDOSEmg*1E-3/MW*1E6     ;(umol/ kg bw)

;IVDOSEumol2 = given intravenous dose recalculated to umol/kg bw
IVDOSEumol = IVDOSEumol2*BW                                      ;IVDOSEumol = umol given IV

;time
Starttime = 0                    ; in hr
Stoptime = 48                    ; in hr

DTMIN = 1e-6                     ; minimum integration time (DT)
DTMAX = 0.0015                   ; maximum integration time (DT)


;====================================================================
;Model calculations
;====================================================================
; model of TTX
;--------------------------------------------------------------------------------------------------------
;ANe = amount in needle, umol

ANe' = -kn*ANe                            ;(umol/hr)
Init ANe = IVDOSEumol


;--------------------------------------------------------------------------------------------------------
```

```
;stomach compartment
;Ast  = amount in stomach, umol

Ast' = -ka*Ast                                    ;(umol/hr)
Init ASt = ODOSEumol


;--------------------------------------------------------------------------------------------------------
;liver compartment

;AL = Amount TTX in liver tissue, umol
AL' = ka*ASt + QL*(CB - CVL) - AMint'             ;(umol/hr)
Init AL = 0
CL = AL/VL
CVL = CL/PL

;AMint = amount TTX metabolized
    AMint' = CLint*CVL                            ;(umol/hr)
    init AMint = 0


;--------------------------------------------------------------------------------------------------------
; kidney compartment

; AK =  Amount of TTX in kidney tissue, umol

AK' = QK*(CB-CVK) -GF'-AKe'                        ;(umol/hr)
        Init AK = 0
        CK = AK/VK
        CVK = CK/PK

;GFR = glomerular filtration rate {L/hr}   ; Walton, et al 2004
;GFR rat = 5.2                                     ; mL/min/kg bw
        GFR = 0.0052*BW*60                        ;L/hr

;GF = glomerular filtration of TTX (umol/hr)
        GF' = GFR*(CVK*Fub)
        Init GF = 0

;Fub = fraction unbound of TTX
        Fub = 1

;AKe = amount TTX actively excreted from the kidney (umol)
;AKe' = amount TTX actively excreted from the kidney in time (umol/hr)
AKe' = VmaxTTX*(CVK*Fub)/(Km + (CVK*Fub))
        Init AKe = 0


;--------------------------------------------------------------------------------------------------------
;fat compartment

;AF = Amount TTX in fat tissue (umol)
    AF' = QF*(CB-CVF)                   ;(umol/hr)
    Init AF = 0
```

```
    CF = AF/VF
    CVF = CF/PF
;-------------------------------------------------------------------------------------------------------------
;Intramuscular (IM) injection site compartment

;AInj = Amount TTX in IM injection site compartment (umol)
        AInj' =  -kb *AInj                    ;(umol/hr)
        Init AInj = IMDOSEumol


;-------------------------------------------------------------------------------------------------------------
;tissue compartment richly perfused tissue

;AR = Amount TTX in rapidly perfused tissue (umol)
    AR' = QR*(CB-CVR)                ;(umol/hr)
    Init AR = 0
    CR = AR/VR
    CVR = CR/PR
;-------------------------------------------------------------------------------------------------------------
;tissue compartment slowly perfused tissue

;AS = Amount TTX in slowly perfused tissue (umol)
    AS' = QS*(CB-CVS)                              ;(umol/hr)
    Init AS = 0
    CS = AS/VS
    CVS = CS/PS
;-------------------------------------------------------------------------------------------------------------
; blood compartment

;AB = Amount TTX in blood (umol)
    AB' = (QF*CVF +  QL*CVL  + QK*CVK + QS*CVS + QR*CVR + kb*AInj + kn*ANe - QC*CB)
;(umol/hr)
    Init AB = 0
    CB = AB/VB
;===================================================================
;Mass balance calculations
;===================================================================
Total = IMDOSEumol + ODOSEumol + IVDOSEumol
Calculated =  ANe + ASt + AL + AMint + AF + AK + AKe + GF + AInj + AS + AR  + AB

ERROR=((Total-Calculated)/Total+1E-30)*100
MASSBBAL=Total-Calculated + 1
```

5

Model code for PBK-model built in Berkeley Madonna for mouse


```
;Date: March 2021
;Species: Mouse
;Compound: Tetrodotoxin (TTX)
;Compiled by: Mengying Zhang and Annelies Noorlander
;Organization: Wageningen University
;====================================
;Physiological parameters
;================================================================
;tissue volumes              >> reference: Hall et al., 2012 Table 2
BW = 0.03              ; body weight mouse (kg)
VFc = 0.07             ; fraction of fat tissue
VLc = 0.055            ; fraction of liver tissue
VKc = 0.017            ; fraction of kidney tissue
VBc = 0.067            ; fraction of blood
VRc = 0.137            ; fraction of rapidly perfused tissue
VSc = 0.654            ; fraction of slowly perfused tissue

VF = VFc*BW            ;(L or Kg)           ; volume of fat tissue (calculated)
VL = VLc*BW            ;(L or Kg)           ; volume of liver tissue (calculated)
VK = VKc*BW            ;(L or Kg)           ; volume of kidney tissue (calculated)
VB = VBc*BW            ;(L or Kg)           ; volume of blood (calculated)
VR = VRc*BW            ;(L or Kg)           ; volume of  richly perfused tissue (calculated)
VS = VSc*BW            ;(L or Kg)           ; volume of  slowly perfused tissue (calculated)


;----------------------------------------------------------------------------------------------------------
;blood flow rates             >> reference: Hall et al., 2012 Table 4
;Cardiag output (QC) is based on the formula for mice found in Brown et al., 1997: 0.257*BW^0.75 {L/min}

QC = 15.4*BW^0.75          ;(L/hr)     ; cardiac output
QFc = 0.070            ; fraction of blood flow to fat
QLc = 0.158            ; fraction of blood flow to liver
QKc = 0.114            ; fraction of blood flow to kidney
QRc = 0.516            ; fraction of blood flow to rapidly perfused tissue
QSc = 0.142            ; fraction of blood flow to slowly perfused tissue

QF = QFc*QC            ;(L/hr)     ; blood flow to fat tissue (calculated)
QL = QLc*QC            ;(L/hr)     ; blood flow to liver tissue (calculated)
QK = QKc*QC            ;(L/hr)     ; blood flow to kidney tissue (calculated)
QR = QRc*QC            ;(L/hr)     ; blood flow to rapidly perfused tissue (calculated)
QS = QSc*QC            ;(L/hr)     ; blood flow to  slowly perfused tissue (calculated)


;================================================================
;Partition Coefficients
;================================================================
; Partition coefficients are derived from Rodgers and Rowland using the QIVIVE tool from A. Punt www.
qivivetools.wur.nl
```

PF = 0.46   ;fat/blood partition coefficient
PL = 4.29   ;liver/blood partition coefficient
PK = 4.70   ;kidney/blood partition coefficient
PR = 4.29   ;rapidly perfused tissue/blood partition coefficient
PS = 0.95   ;slowly perfused tissue/blood partition coefficient

```
;====================================================================
;Kinetic parameters
;====================================================================
kb = 50                      ; (/hr) intramuscular uptake rate constant
ka = 0.18            ; (/hr) uptake rate from stomach
kn = 1000000                 ; (/hr) uptake rate from needle
```

;--
;Metabolism liver

;metabolism of TTX, scaled maximum rate of metabolism

CLint = CellDL*VL*(CLintHep*60*1E-6)   ;(L/hr)   ;Hepatic clearance

CLintHep = 0.00016   ;(ul/min/million cells)   ;Hepatic clearance derived from hepatocytes

CellDL = 135*1000   ;(million cells/kg liver)

;Hepatocyte number in rat = 1.35 *10E8 cells/g liver = 135 million cells/g liver = 135*1000 million cells/ kg liver
;reference: (Sohlenius-Sternbeck., 2006)

;--
;Excretion from kidney

;Active uptake of TTX is based on the OCT2 transporter
VmaxTTXc = 180   ;{pmol/min/mg protein}

VmaxTTX = (VmaxTTXc/1000000)*60*SF*VK*1000   ;{umol/hr}
;300 mg prot./g kidney (Kumar et al. 2018)
;only 70% of whole kidney is cortex --> in cortex tubule cells thus OCT-2s are present (Kumar et al. 2018)
; 300 * 0.7 = 210 mg prot./g kidney

Km = 2   ; {uM} transport constant of TTX
SF = 210   ; mg/g protein

```
;====================================================================
;Run settings
;====================================================================
;Molecular weight
MW = 319.27                      ; Molecular weight TTX (PubChem)
```

;Intramuscular dose is 6 ug/kg bw = 0.006 mg/kg bw (Hong et al., 2017)

IMDOSEmg = 0.006   ; (mg/kg bw)   ; IMDOSEmg = given IM dose in mg/kg bw

IMDOSEumol2 = IMDOSEmg*1E-3/MW*1E6 ;(umol/ kg bw)

;IMDOSEumol2 = given intramuscular dose recalculated to umol/kg bw
IMDOSEumol = IMDOSEumol2*BW   ;IMDOSEumol = umol given IM

;Oral dose is 100 ug/kg bw = 0.1 mg/kg bw (Hong et al., 2018)
;Bioavailability via oral route = 6.7%

ODOSEmg = 0.1*0.067   ; (mg/kg bw)   ; ODOSEmg = given oral dose in mg/kg bw

ODOSEumol2 = ODOSEmg*1E-3/MW*1E6   ;(umol/ kg bw)

;ODOSEumol2 = given oral dose recalculated to umol/kg bw
ODOSEumol=ODOSEumol2*BW   ; ODOSEumol = umol given oral

;Intravenous dose is 6 ug/kg bw = 0.006 mg/kg bw (Hong et al., 2018)

IVDOSEmg = 0.006   ; (mg/kg bw)   ; IVDOSEmg = given IV dose in mg/kg bw

IVDOSEumol2 = IVDOSEmg*1E-3/MW*1E6 ;(umol/ kg bw)

;IVDOSEumol2 = given intravenous dose recalculated to umol/kg bw
IVDOSEumol = IVDOSEumol2*BW   ;IVDOSEumol = umol given IV

;===
;Model calculations
;===
; model of TTX
;--
;ANe = amount in needle, umol

ANe' = -kn*ANe   ;(umol/hr)
Init ANe = IVDOSEumol

;--
;stomach compartment
;Ast = amount in stomach, umol

Ast' = -ka*Ast   ;(umol/hr)
Init ASt = ODOSEumol

```
;----------------------------------------------------------------------------------------------------------
;liver compartment

;AL = Amount TTX in liver tissue, umol
AL' =  ka*ASt + QL*(CB - CVL)-AMint' ;(umol/hr)
Init AL = 0
CL = AL/VL
CVL = CL/PL

;AMint = amount TTX metabolized
     AMint' = CLint*CVL                     ;(umol/hr)
     init AMint = 0


;----------------------------------------------------------------------------------------------------------
; kidney compartment

; AK =  Amount of TTX in kidney tissue, umol

AK' = QK*(CB-CVK)-GF'-AKe'              ;(umol/hr)
          Init AK = 0
          CK = AK/VK
          CVK = CK/PK

;GFR = glomerular filtration of TTX rate (L/hr)            ; reference (Walton et al. 2004)
;GFR in mouse is 14 mL/min/kg BW

GFR = 0.014*BW*60            ;{L/hr}

;GF = glomerular filtration of TTX (umol/hr)
          GF'= GFR*(CVK*fub)
          Init GF = 0
; fub = fraction unbound of TTX                                      ; obtained from QSAR/RED exp
          Fub = 1

;AKe = amount TTX actively excreted from the kidney (umol)
;AKe' = amount TTX actively excreted from the kidney in time (umol/hr)
AKe' = VmaxTTX*(CVK*Fub)/(Km + (CVK*Fub))
          Init AKe = 0
;----------------------------------------------------------------------------------------------------------
;fat compartment

;AF = Amount TTX in fat tissue (umol)
     AF' = QF*(CB-CVF)       ;(umol/hr)
     Init AF = 0
     CF = AF/VF
     CVF = CF/PF
;----------------------------------------------------------------------------------------------------------
;Intramuscular (IM) injection site compartment

;AInj = Amount TTX in IM injection site compartment (umol)
          AInj' =  -kb *AInj                     ;(umol/hr)
```

```
        Init AInj = IMDOSEumol

;---------------------------------------------------------------------------------------------------------------
;tissue compartment richly perfused tissue

;AR = Amount TTX in rapidly perfused tissue (umol)
    AR' = QR*(CB-CVR)              ;(umol/hr)
    Init AR = 0
    CR = AR/VR
    CVR = CR/PR
;---------------------------------------------------------------------------------------------------------------
;tissue compartment slowly perfused tissue

;AS = Amount TTX in slowly perfused tissue (umol)
    AS' = QS*(CB-CVS)             ;(umol/hr)
    Init AS = 0
    CS = AS/VS
    CVS = CS/PS
;---------------------------------------------------------------------------------------------------------------
; blood compartment

;AB = Amount TTX in blood (umol)
    AB' = (QF*CVF +  QL*CVL  + QK*CVK + QS*CVS + QR*CVR + kb*AInj +kn*ANe - QC*CB)
;(umol/hr)
    Init AB = 0
    CB = AB/VB
    AUC' = CB                ;umol*hr/L
    Init AUC = 0


;=====================================================================
;Mass balance calculations
;=====================================================================
Total = IMDOSEumol + ODOSEumol + IVDOSEumol
Calculated =  ANe + ASt + AL + AMint + AF + AK + AKe + GF + AInj + AS + AR  + AB

ERROR=((Total-Calculated)/Total+1E-30)*100
MASSBBAL=Total-Calculated + 1
Model code for PBK-model built in Berkeley Madonna for human
```

Model code for PBK-model built in Berkeley Madonna for human

```
;Date: December 2021
;Species: Human
;Compound: Tetrodotoxin (TTX)
;Compiled by: Annelies Noorlander
;Organization: Wageningen University
;====================================
;Physiological parameters
;=================================================================
;tissue volumes               >> reference: Brown et al., 1997 (Table 21)

BW = 70                    ; body weight human (kg)
VFc = 0.214                ; fraction of fat tissue
VLc = 0.026                ; fraction of liver tissue
VKc = 0.004                ; fraction of kidney tissue
VBc = 0.079                ; fraction of blood
VRc = 0.064                ; fraction of rapidly perfused tissue
VSc = 0.613                ; fraction of slowly perfused tissue

VF = VFc*BW        ;(L or Kg)              ; volume of fat tissue (calculated)
VL = VLc*BW        ;(L or Kg)              ; volume of liver tissue (calculated)
VK = VKc*BW        ;(L or Kg)              ; volume of kidney tissue (calculated)
VB = VBc*BW        ;(L or Kg)              ; volume of blood (calculated)
VR = VRc*BW        ;(L or Kg)              ; volume of   richly   perfused   tissue
                                             (calculated)
VS = VSc*BW        ;(L or Kg)              ; volume of   slowly   perfused   tissue
                                             (calculated)

;--------------------------------------------------------------------------------------------------------------
;blood flow rates      >> reference: Brown et al.,1997 Table 27
;Cardiac output (QC) for human is found in Brown et al., 1997 page 453

QC = 15*BW^0.74 ;(L/hr)    ; cardiac output
QFc = 0.052                ; fraction of blood flow to fat
QLc = 0.227                ; fraction of blood flow to liver
QKc = 0.175                ; fraction of blood flow to kidney
QRc = 0.195                ; fraction of blood flow to rapidly perfused tissue
QSc = 0.351                ; fraction of blood flow to slowly perfused tissue

QF = QFc*QC        ;(L/hr)   ; blood flow to fat tissue (calculated)
QL = QLc*QC        ;(L/hr)   ; blood flow to liver tissue (calculated)
QK = QKc*QC        ;(L/hr)   ; blood flow to kidney tissue (calculated)
QR = QRc*QC        ;(L/hr)   ; blood flow to rapidly perfused tissue (calculated)
QS = QSc*QC        ;(L/hr)   ; blood flow to  slowly perfused tissue (calculated)

;--------------------------------------------------------------------------------------------------------------

;=================================================================
;Partition Coefficients
```

```
;====================================================================
; Partition coefficients are derived from Rodgers and Rowland using the QIVIVE tool from A. Punt www.
qivivetools.wur.nl


PF = 0.46              ;fat/blood partition coefficient
PL = 4.29              ;liver/blood partition coefficient
PK = 4.70              ;kidney/blood partition coefficient
PR = 4.29              ;rapidly perfused tissue/blood partition coefficient
PS = 0.95              ;slowly perfused tissue/blood partition coefficient


;====================================================================
;Kinetic parameters
;====================================================================


ka = 0.18              ; (/hr) uptake rate from stomach
;--------------------------------------------------------------------------------------------------------------
;Metabolism liver

;metabolism of TTX, scaled maximum rate of metabolism

CLint = CellDL*VL*(CLintHep*60*1E-6)          ;(L/hr)    ;Hepatic clearance

CLintHep = 0.00016                            ;(ul/min/million cells)    ;Hepatic    clearance
                                                                         derived      from
                                                                         hepatocytes

CellDL = 139*1000                             ;(million cells/kg liver)

;Hepatocyte number in human = 1.39 *10E8 cells/g liver = 139 million cells/g liver = 139*1000 million
cells/ kg liver
;reference: (Sohlenius-Sternbeck., 2006)


;--------------------------------------------------------------------------------------------------------------
;Excretion from kidney

;Active uptake of TTX is based on the OCT2 transporter
VmaxTTXc = 180              ;{pmol/min/mg protein}

VmaxTTX = (VmaxTTXc/1000000)*60*SF*VK*1000          ;{umol/hr}
;300 mg prot./g kidney (Kumar et al. 2018)
;only 70% of whole kidney is cortex --> in cortex tubule cells thus OCT-2s are present (Kumar et al. 2018)
; 300 * 0.7 = 210 mg prot./g kidney

Km = 2              ; {uM} transport constant of TTX
SF = 210            ; mg/g protein


;====================================================================
;Run settings
;====================================================================
;Molecular weight
MW = 319.27                            ; Molecular weight TTX (PubChem)
```

```
;Oral dose is 100 ug/kg bw = 0.1 mg/kg bw (Hong et al. 2018)
;Bioavailability via oral route = 6.7%

ODOSEmg = 0.1*0.067                 ; (mg/kg bw)         ; ODOSEmg = given oral dose in mg/kg bw

ODOSEumol2 = ODOSEmg*1E-3/MW*1E6       ;(umol/ kg bw)

;ODOSEumol2 = given oral dose recalculated to umol/kg bw
ODOSEumol=ODOSEumol2*BW                 ; ODOSEumol = umol given oral


;====================================================================
;Model calculations
;====================================================================
; model of TTX
;---------------------------------------------------------------------------------------------------------------
;stomach compartment
;Ast  = amount in stomach, umol

Ast' = -ka*Ast                  ;(umol/hr)
Init ASt = ODOSEumol


;----------------------------------------------------------------------------------------------------------
;liver compartment

;AL = Amount TTX in liver tissue, umol
AL' =  ka*ASt + QL*(CB - CVL)-AMint' ;(umol/hr)
Init AL = 0
CL = AL/VL
CVL = CL/PL

;AMint = amount TTX metabolized
    AMint' = CLint*CVL                ;(umol/hr)
    init AMint = 0


;----------------------------------------------------------------------------------------------------------
; kidney compartment

; AK =  Amount of TTX in kidney tissue, umol

AK' = QK*(CB-CVK)-GF'-AKe'          ;(umol/hr)
        Init AK = 0
        CK = AK/VK
        CVK = CK/PK

;GFR = glomerular filtration of TTX rate (L/hr)                ; reference (Walton et al. 2004)
;GFR in human is 1.8 mL/min/kg BW

GFR = 0.0018*BW*60         ;{L/hr}

; GF = glomerular filtration of TTX (umol/hr)
        GF'= GFR*(CVK*fub)
```

```
        Init GF = 0
; fub = fraction unbound of TTX                                  ; obtained from QSAR/RED exp
        Fub = 1


;AKe = amount TTX actively excreted from the kidney (umol)
;AKe' = amount TTX actively excreted from the kidney in time (umol/hr)
AKe' = VmaxTTX*(CVK*Fub)/(Km + (CVK*Fub))
        Init AKe = 0
;----------------------------------------------------------------------------------------------------------------
;fat compartment

;AF = Amount TTX in fat tissue (umol)
    AF' = QF*(CB-CVF)                    ;(umol/hr)
    Init AF = 0
    CF = AF/VF
    CVF = CF/PF


;----------------------------------------------------------------------------------------------------------------
;tissue compartment richly perfused tissue

;AR = Amount TTX in rapidly perfused tissue (umol)
    AR' = QR*(CB-CVR)                    ;(umol/hr)
    Init AR = 0
    CR = AR/VR
    CVR = CR/PR
;----------------------------------------------------------------------------------------------------------------
;tissue compartment slowly perfused tissue

;AS = Amount TTX in slowly perfused tissue (umol)
    AS' = QS*(CB-CVS)                    ;(umol/hr)
    Init AS = 0
    CS = AS/VS
    CVS = CS/PS
;----------------------------------------------------------------------------------------------------------------
; blood compartment

;AB = Amount TTX in blood (umol)
    AB' = (QF*CVF +  QL*CVL  + QK*CVK + QS*CVS + QR*CVR +kn*ANe - QC*CB) ;(umol/hr)
    Init AB = 0
    CB = AB/VB
    AUC' = CB                     ;umol*hr/L
    Init AUC = 0


;====================================================================
;Mass balance calculations
;====================================================================
Total = IMDOSEumol + ODOSEumol + IVDOSEumol
Calculated =  ANe + ASt + AL + AMint + AF + AK + AKe + GF + AS + AR  + AB

ERROR=((Total-Calculated)/Total+1E-30)*100
MASSBBAL=Total-Calculated + 1
```

5

Supplementary material B
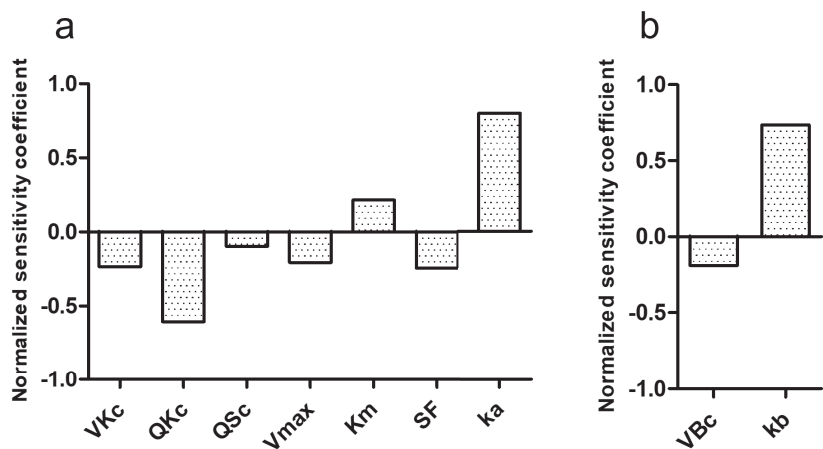
Figure S1.

Normalized sensitivity coefficients of PBK model parameters in rats for the predicted Cmax of TTX in blood after (a) oral administration of 6 μg/kg bw and (b) intramuscular administration of 6 μg/kg bw. Model parameters with normalized sensitivity coefficients with an absolute value higher than 0.1 are shown. VKc = volume of the kidneys, QKc = fraction of blood flow to the kidneys, QSc = fraction of blood flow to the slowly perfused tissues, PS = partition coefficient of slowly perfused tissue, Vmax = maximum rate of TTX transport via OCT2, Km = Michaelis-Menten constant of TTX transport via OCT2, SF = scaling factor, ka = absorption rate constant, VBc = volume of the blood, kb = rate of uptake after intramuscular injection
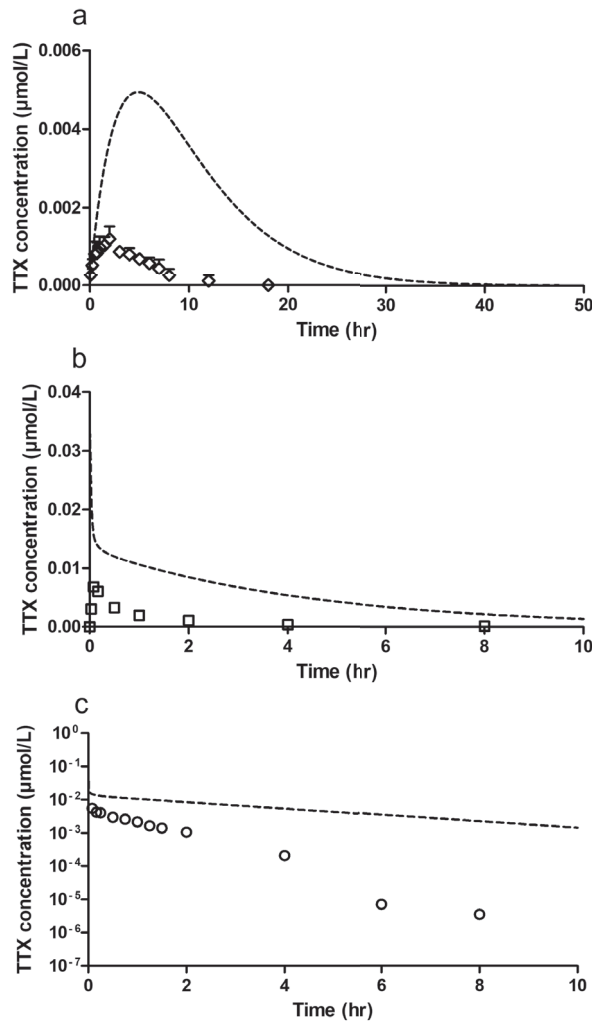
Figure S2.
Predicted concentration time curves of TTX in whole blood of rat (striped lines) dosed TTX via (a) oral (diamonds), (b) IM (squares) and (c) IV (circles) administration based on passive glomerular filtration. The literature data reported as plasma concentrations were adjusted to blood concentrations assuming a blood:plasma ratio of 0.42 (Hong et al. 2017). Dosage used: oral 100 µg/kg bw with 6.7% bioavailability, IM and IV 6 µg/kg bw with 100% bioavailability. Data points represent mean (± SD/SEM, where available).

Fitted models

Table S1.
Results BMD modelling of predicted human dose-response data, applying model averaging

Model	converged	loglik	npar	AIC
full model	yes	16.75	5	-23.5
null model	yes	-5.21	2	14.42
Expon. m3-	yes	15.43	4	-22.86
Expon. m5-	yes	16.74	5	-23.48
Hill m3-	yes	15.44	4	-22.88
Hill m5-	yes	16.72	5	-23.44
Inv.Expon. m3-	yes	16.03	4	-24.06
Inv.Expon. m5-	yes	16.49	5	-22.98
LN m3-	yes	15.77	4	-23.54
LN m5-	yes	16.53	5	-23.06
Weights for model averaging				
EXP	HILL	INVEXP	LOGN	
0.23	0.23	0.31	0.24	
Final BMD values				
Endpoint	Subgroup	BMDL	BMDU	
Response	all	0.00178	0.0062	
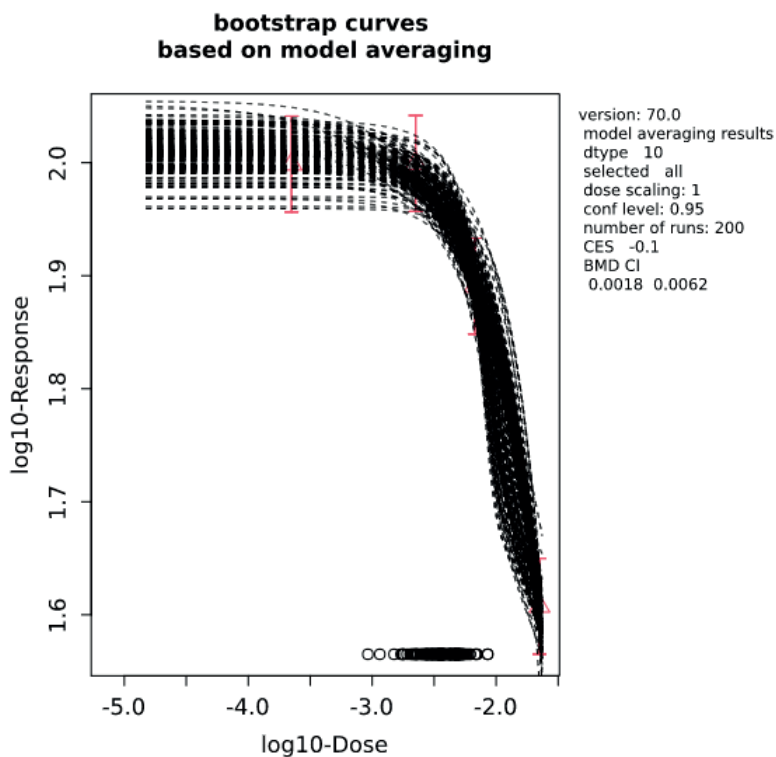
Figure S3.
Bootstrap curves based on model averaging for the predicted human TTX dose-response data.
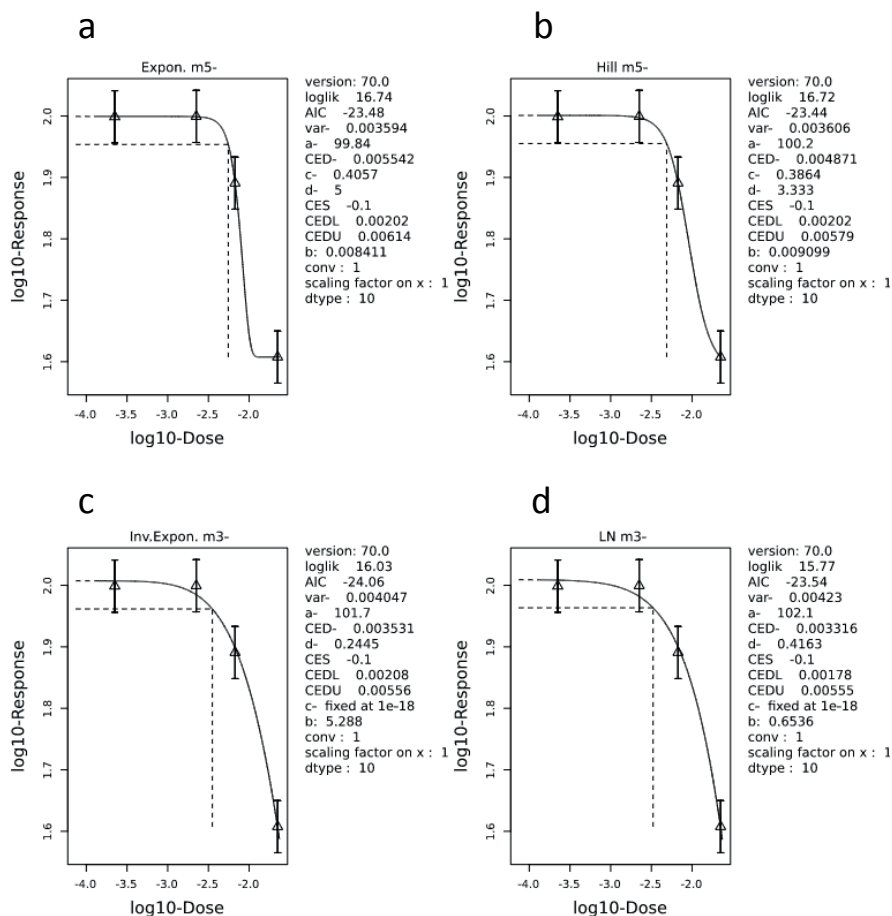
Figure S4.
BMD modelling results of individual models for the predicted human TTX dose-response data. a) Exponential model 5, b) Hill model 5, c) Inverted exponential model 3, d) Log normal model 3

Chapter 6

General discussion

Chapter 6

6.1   Overview of the main findings

Developing new approach methodologies (NAMs) is inextricably linked to many challenges. One that is receiving less attention, but equally important is the translation of *in vitro* concentrations to *in vivo* internal concentrations and/or external dose levels and the prediction of human relevant kinetics and toxicity. The use of physiologically based kinetic (PBK) models is an essential tool to achieve these goals and explore the potentials of predicting human toxicity and safety via non-animal based methodologies. Several proofs of principle of using PBK models as a tool to predict different types of toxicity for both experimental animals and human have been delivered in the last decade (Abdullah et al. 2016; Louisse et al. 2014; Ning et al. 2019b; Shi et al. 2020; Strikwold et al. 2017b; Wang et al. 2021). The PBK models were including mostly (*in vitro*) kinetic input parameter values for only the absorption, distribution and metabolism of the studied compounds in order to predict the time-dependent blood concentration. The fourth component to kinetics -excretion- has not yet been explored extensively in PBK modelling. Especially for compounds for which their kinetics is depending on active transport in the kidneys or liver, resulting in excretion through urine and bile, excretion this aspect needs to be considered in the PBK model. The limited use of PBK modelling for compounds that require modelling of active excretion is likely due to many challenges, for example the type of *in vitro* assays to be used to define excretion parameters and the scaling factors needed to translate *in vitro* obtained kinetic data to the *in vivo* situation.

This thesis provides proofs of principle on tackling the challenges regarding incorporation of active excretion into PBK modelling. It does so by incorporating *in vitro* active transporter data for either urinary or biliary excretion in the respective PBK models. Scaling factors for converting the kinetic data from the *in vitro* model to the *in vivo* situation were obtained by fitting predictions made to literature available *in vivo* data and evaluated by estimations based on assumptions about the differences between the respective *in vitro* cell system and the organ of interest. The developed PBK models were in accordance with the corresponding *in vivo* kinetic data, and their application for quantitative *in vitro in vivo* extrapolation (QIVIVE) resulted in adequate predictions of the acute toxicity of the selected model compounds for both rodents and human.

Chapter 2 provided a PBK model for the prediction of rat biliary excretion of intravenously administered estradiol-17β glucuronide ($E_2$17βG). For this study, freshly isolated primary hepatocytes were the *in vitro* model used to define the parameters needed for incorporating the transport of $E_2$17βG via the organic anion transporting polypeptides (Oatps) into the PBK model. A major challenge was the definition of the scaling factor for the *in vitro* to *in vivo* conversion of the PBK model parameter

for this transport, Vmax. The *in vitro* values for the Vmax and Km for transport of E$_2$17βG were found in the literature in four different studies based on three experiments with primary hepatocytes in suspension and one experiment with plated primary hepatocytes. For each *in vitro* data set for the Vmax and Km of the transporter, the PBK model predictions were fitted to three *in vivo* data sets on the time-dependent blood concentration of E$_2$17βG and three *in vivo* data sets on the cumulative biliary excretion of E$_2$17βG by optimising the scaling factor. This resulted in 24 individual predictions and fitted scaling factors. Averaging the 24 fitted scaling factors resulted in a scaling factor of 129 mg protein/g liver. This factor appeared to match well within the scaling factor that can be derived theoretically by using the hepatocellularity number, the protein concentration in a hepatocyte suspension and the weight of the liver amounting to 115 to 132 mg protein/g liver. With this scaling factor the PBK model predicted the *in vivo* data for blood and cumulative biliary E$_2$17βG levels with on average of less than 1.8-fold deviation. The study provided a proof of principle on how biliary excretion can be included in a PBK model using primary hepatocytes to define the kinetic parameters that describe the biliary excretion.

In **Chapter 3** active renal excretion via the organic cation transporter 2 (OCT2) was incorporated in a rat PBK model using the *in vitro* human renal proximal tubular epithelial cell line (RPTEC) SA7K and mepiquat (MQ) chloride as the model compound. The SA7K cell line is a physiologically relevant cell line with maintained expression of functionally active transporters. The Vmax and Km of OCT2 transport of MQ were determined by quantifying the time-dependent and concentration-dependent uptake of MQ in SA7K cells using doxepin as OCT2 inhibitor and amounted to 10.5 pmol/min/mg protein and 20.6 µM, respectively. PBK model predictions incorporated these values in the PBK model with scaling of the *in vitro* Vmax to an *in vivo* Vmax using a scaling factor consisting of 3 components: 1) the scaling for the amount of protein per gram kidney (300 mg protein/g kidney), 2) the scaling for the location of the OCT2 transporter in the kidney, which is the kidney cortex making up 70% of the kidney, and 3) a factor to correct for potential differences in OCT2 activity in the SA7K cells and the *in vivo* kidney cortex and for species differences (human cell line, rat PBK model). Application of the first two components of the scaling factor, referred to as partial scaling, led to PBK model predictions that deviated 6.7–8.4-fold from the reported *in vivo* data on the blood concentration of MQ in rat. The inclusion of the third component of the scaling factor resulted in an overall scaling that provided adequate predictions for the *in vivo* blood concentrations of MQ in rat (2.3–3.2-fold difference). As compared to the previous chapter (**Chapter 2**), defining a scaling factor for active renal excretion appeared to come with more complexity than what was required for biliary excretion by liver hepatocytes scaled to whole liver. The results, however, indicate that the use of SA7K cells to define PBK model parameters for active renal OCT2 mediated excretion

combined with adequate scaling, enables incorporation of renal excretion via the OCT2 transporter in PBK modelling to correctly predict *in vivo* kinetics of MQ in rat.

In further studies on renal excretion, **Chapter 4** describes a PBK model for paraquat (PQ) dichloride, another OCT2 substrate. The first goal of this study was to obtain the kinetic parameters Vmax and Km for *in vitro* OCT2 transport of PQ using the SA7K cells as was shown adequate for defining OCT2 mediated transporter kinetics for MQ (**Chapter 3**). However, it appeared that for PQ the transport into the SA7K cells was hampered by rapid establishment of an equilibrium between uptake and excretion resulting in a steady state that hampers kinetic experiments on uptake alone. Thus, the values for transport were taken from the literature where they were determined in the human embryonic kidney cell line (HEK293) overexpressing OCT2. Appropriate scaling factors were applied to translate the *in vitro* Vmax to an *in vivo* Vmax in a way comparable to what was done in **Chapter 3**. The model thus obtained resulted in an adequate prediction of PQ kinetics. As a second goal, the developed PBK model was applied for PBK modelling based reverse dosimetry for QIVIVE converting *in vitro* concentration response curves for PQ toxicity to predicted dose response curves for acute *in vivo* toxicity of PQ in both rats and human. The target organ for PQ toxicity is the lung, and thus the *in vitro* toxicity data used were from cytotoxicity studies performed in alveolar cell lines. For rat, cytotoxicity data were defined in the RLE-6TN and L2 cell lines. For humans, cytotoxicity data were obtained from the A549 cell line. With the developed PBK model the *in vitro* cytotoxicity concentration-response curves were translated to predicted *in vivo* toxicity dose-response curves whereafter Benchmark dose (BMD) analysis was applied to derive the $BMDL_{50}$-$BMDU_{50}$ ranges from the predicted dose response curves, which were compared to the *in vivo* reported mean lethal dose (LD_{50}) values for rat and human. It became clear from the reported LD_{50} values that humans are more sensitive to PQ toxicity than rats. The translated *in vitro* toxicity data range from the rat cell lines was underpredicting the *in vivo* LD_{50} range by 6.9 – 12.4 -fold difference, with the highest translated $BMDU_{50}$ being the closest to the lowest reported LD_{50} by 1.5-fold. Whereas for human QIVIVE of the A594 cell line data, adequately predicted the acute toxicity by 1.3 – 1.7-fold. In this study, using PQ as the model compound, a proof of principle was provided showing how to include *in vitro* obtained active excretion in PBK modelling and how to apply the PBK model obtained for QIVIVE to predict acute *in vivo* toxicity.

In the last chapter, **Chapter 5**, another proof of principle for PBK model based QIVIVE for a compound with a role for active transport in its kinetics was provided. The method was applied to predict the *in vivo* neurotoxicity of tetrodotoxin (TTX) in rodents. The clearance of TTX was shown not to depend on metabolism since substrate depletion in incubations of TTX with rat liver hepatocytes appeared to be negligible. Clearance of

6

TTX was dependent on excretion in the kidneys. Incorporating a kidney compartment accounting for active renal excretion in the PBK models improved the accuracy and was shown to be essential for their performance. The incorporation this time was not based on *in vitro* input such as in the previous chapters (**Chapter 2, 3 and 4**), but was based on fitting of the transporter efficiency (Vmax/Km), to adequately match available kinetic data. The PBK model was evaluated for three administration routes: oral, intravenous and intramuscular and for both rats and mice. Once validated the PBK models were used to translate *in vitro* concentration–response data of TTX obtained in a multielectrode array assay with primary rat neonatal cortical cells and in an effect study with mouse neuro-2a cells, into *in vivo* dose–response data for rats and mice respectively. To evaluate the predictions, QIVIVE-derived dose–response data were compared with *in vivo* data on neurotoxicity in rats and mice upon oral and parenteral dosing. The results revealed that for both rats and mice the predicted dose–response data matched the data from available *in vivo* studies well. Upon this validation also a human PBK model for TTX was defined assuming that the model was well-evaluated based on the rat and mice model outcomes. The human PBK model was used for QIVVE of the human *in vitro* concentration-response curve obtained in a multielectrode array assay using human-induced pluripotent stem cell (hIPSC)-derived iCell neurons in coculture with hIPSC-derived iCell astrocytes to a predicted human *in vivo* dose response curve for TTX toxicity. BMD analysis was applied on the curve and revealed a $BMDL_{10}$ of 1.8 µg/kg bw that was converted with an uncertainty factor of 10 for interindividual differences to a health-based guidance value (HBGV) of 0.18 µg/kg bw, a value that was only 1.4-fold different from the ARfD previously established by EFSA of 0.25 µg/kg bw based on an acute toxicity study in mice providing a tentative HBGV for TTX human risk assessment. It is concluded that PBK modelling-based reserve dosimetry of *in vitro* TTX effect data can adequately predict the *in vivo* neurotoxicity of TTX in rodents and even human, providing a novel proof-of-principle for this methodology.

General discussion

6.2 In vitro kinetic models

In this thesis the focus was on implementing active transport into PBK models to be used in NAMs. The key element when implementing active transport is to base it, preferably, on kinetic data obtained in *in vitro* model systems although results obtained in the present thesis revealed that at the current state-of-the-art *in vivo* kinetic data are still required for defining adequate scaling factors and/or evaluating the model performance.

6.2.1 Liver

For biliary excretion (**Chapter 2**), the *in vitro* kinetic model used in the present thesis consisted of freshly isolated primary hepatocytes either cultivated in suspension or in monolayer (Brock and Vore 1984; Brouwer et al. 1987; Ishizuka et al. 1998; Kouzuki et al. 1999). This model is well established and widely used to obtain especially metabolism data but is also frequently applied to obtain transport data (Louisse et al. 2020; Yoshikado et al. 2021). Advantages of using this primary hepatocyte model is that it is close to the real liver, and still contains all the elements of a hepatocyte including the expression and functioning of the transporters. Disadvantages of using this model is the non-high throughput character, the differences from batch to batch, the hepatocytes' activity in suspension that expires after 4 to 6 hours, and that in suspension only uptake can be measured, not efflux. Other *in vitro* systems that have been applied to obtain data for transporter kinetics are sandwich-cultured hepatocytes, HepaRG cells, HepG2 cells (Kotani et al. 2012; Le Vee et al. 2006; Le Vee et al. 2013; Swift et al. 2010) and simple cell lines, such as the Chinese hamster ovaries (CHO) cell line, the human embryonic kidney cell line (HEK-293) and the Alexander hepatoma cell line with overexpression of a transporter of interest (Han et al. 2019; Herraez et al. 2017). The *in vitro* model to be used to define kinetic transport data, that is to be implemented into PBK models, should be as concise as possible in terms of translation from the *in vitro* to the *in vivo* situation. This will be discussed in more detail in a later section.

6.2.2 Kidney

In the present thesis, the *in vitro* kinetic transport data for the renal active transport were obtained from a cell model that was physiologically as relevant and as close to the *in vivo* renal cells as possible (figure 1). There were three cell lines considered, which were all of human origin, including; 1) the immortalized RPTEC/TERT1 cell line (Secker et al. 2018; Secker et al. 2019), 2) the conditionally immortalized proximal tubule epithelial cell line (ciPTEC) (Wilmer et al. 2010) and 3) a pseudo-immortalized kidney cell line (SA7K-clone) developed by the group of Li et al. (2017c). The latter was the model of choice for the studies in **Chapter 3 and 4**. As shown from the reported work (**Chapter 3**) the SA7K cell line appeared capable of generating transport data for the OCT2-

mediated transport of the model compound MQ. The use of an inhibitor was essential in generating the data for the transporter of interest, since the OCT2-mediated transport rate was derived from the difference between uptake into the cells in the absence minus uptake in the presence of the OCT2 inhibitor. In **Chapter 4** the use of the same cell model and approach to define the time-dependent OCT2 uptake, to establish the required Vmax and Km for another substrate for the OCT2 transporter, PQ, appeared hampered by a rapid equilibrium that hampered kinetic uptake experiments during time frames and at concentrations of PQ that were experimentally feasible. In the SA7K cells uptake of both compounds was inhibited by doxepin a known inhibitor of the OCT2 transporter (Belzer et al. 2013; Hacker et al. 2015). Use of another known inhibitor of the OCT2 transporter, cimetidine (Boof et al. 2020; Sprowl et al. 2013) gave similar results.
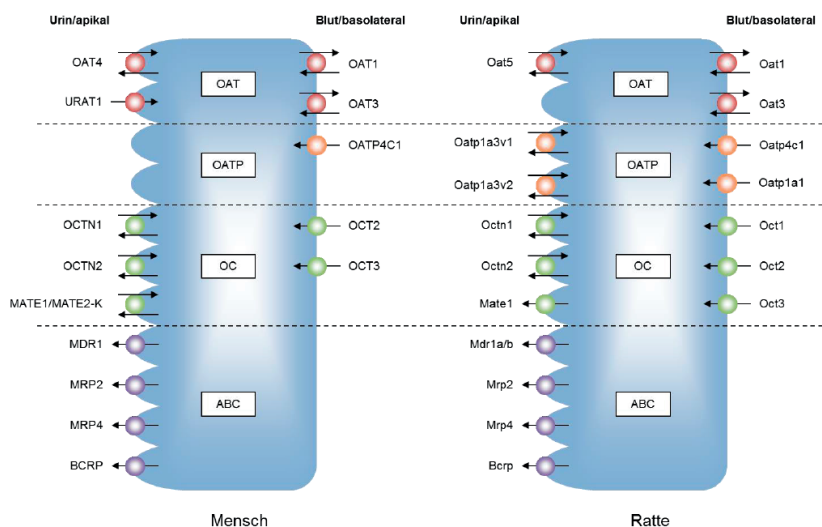
Figure 1.
Renal proximal tubule epithelial cells of human and rat with their uptake and efflux transporters. (Adapted from Lechner (2014))

Similar to liver, also for the kidney use of primary cells could be considered as a suitable *in vitro* models to define kinetic transport parameters, such as for example primary renal proximal tubule epithelial cells that can be harvested and used for transporter studies. These cells are, however, difficult to isolate from the kidneys (Lechner et al. 2021; Taub 1997; Vessey 200). This is reflected in the pricing of the commercially available primary RPTEC cells compared to primary hepatocytes, which are about 2 – 3-fold more expensive per 10^6 cells (ATCC 2022; Lonza 2022). In theory, similar experiments for the primary RPTEC in suspension can be performed as for the primary

hepatocytes in suspension, with focus on uptake transporters such as OCT2 (and/or OCT1 and OCT3 in case of rat) or OATP4C1 (Taghikhani et al. 2019). A more recent study by Sanchez-Romero reported on a relatively simple and cost-effective method to isolate and cultivate large numbers of primary RPTEC from human nephrectomies with high enrichment of RPTEC phenotypic characteristics (Sanchez-Romero et al. 2020). They stress that this cell model could be a powerful tool for future *in vitro* studies in renal physiology, pathology, pharmacology, toxicology and regenerative nephrology. Even though the investigation of appropriate and relevant *in vitro* kidney cell models is in upward motion, it remains challenging on how to apply them for *in vitro in vivo* extrapolation in PBK models due to issues connected to scaling (**section 6.3**).

In **Chapter 3** the transport kinetics for MQ were based on parameters for OCT2 mediated uptake into the SAK7 cells. This approach assumes that this uptake is the rate limiting step in the urinary excretion and thus assumes that transporters for allocation of the compound from the inside of the SA7K cells to the pro-urine may not be rate limiting. In addition to using data for cellular uptake, one could also consider to actually define the kinetics for transport across an SA7K cell layer. The uptake studies in SA7K cells in this thesis (**Chapter 3** and **Chapter 4**) have been performed in normal well plates, which is a known and often used method to perform uptake studies (Boonnop 2017; George et al. 2021; Li et al. 2017c; More et al. 2010). To study transport SA7K cells could have been cultured in so-called transwells. The SA7K cells can form good monolayers and therefore might be a good candidate to use in a transwell formation. From reported data it appears that the cell line is even used for growing 3D proximal tubules (Vormann et al. 2018). If such a transwell transport method would be used, first the SA7K monolayer should be checked for barrier integrity with well-developed tight junctions by measuring the transepithelial electrical resistance (TEER). Moreover, polarisation should be characterized. If adequate polarization is established, transport studies can be performed using substrates and inhibitors to identify transporters involved. The downside of using a transwell system for a physiologically relevant cell line is that it becomes more challenging to characterize the contribution of the individual transporters. Characterization of only uptake will not be sufficient as transport will reflect the combined effect of uptake and efflux taken together. It is however possible to extract kinetic parameter values referring to the overall transport as an overall Vmax and Km of transcellular transport of the relevant compound (Li et al. 2017d). It is therefore not uncommon to study directional transport with transfected or even double transfected cell lines using transwells (Lee et al. 2017; Muller et al. 2013; Yin et al. 2016).

Preferred kidney kinetic model

A favoured and preferred method for obtaining kinetic parameter values Vmax and Km for uptake or efflux of a compound is the use of a simple cell system with overexpression of a transporter of interest or membrane vesicles derived from such transfected cells preferably in combination with radioactively labelled compounds (Hacker et al. 2015; Izumi et al. 2013). Such methods allow for clean uptake studies (and efflux studies with inside out membrane vesicles containing the efflux transporter of interest) and there is no need for using inhibitors, just simply a comparison to uptake in the same cell system without the transporter of interest in overexpression. Especially, in the case of PQ (**Chapter 4**) use of a transfected cell line would most likely have been more successful in enabling definition of kinetics. This approach would equally well be interesting for describing the elimination of TTX (**Chapter 5**) as the contribution of active renal transport to its clearance is substantiated by its lack of clearance through the liver and the finding of Matsumoto et al. (2017) of its role as a substrate for different transporters in the kidney.

6.3 Scaling

Another factor that turned out to be of great importance when including biliary or renal excretion via active transporters in PBK models was the scaling of the data obtained in the selected *in vitro* model to the *in vivo* situation. In this thesis two different approaches for scaling have been used. The first approach is a theoretical approach based on scientific considerations of the differences between the *in vitro* model and the *in vivo* situation and relevant data to quantify these differences. A second approach is to fit the predictions to the *in vivo* reported kinetic data thereby defining the most adequate scaling factor.

6.3.1 Scaling to the liver

For incorporation of *in vitro* obtained kinetic data into a PBK model, scaling factors are needed for the *in vitro* to *in vivo* translation. Scaling factors for conversion of *in vitro* data obtained in liver microsomal or S9 incubations to the liver have been well established and enable conversion of the *in vitro* Vmax expressed in pmol/min/mg protein for an enzymatic reaction to an *in vivo* Vmax expressed in µmol/hr for the whole liver, thereby scaling from microsomes/S9 to a whole liver (Pelkonen and Turpeinen 2007). Scaling factors have also been defined for data obtained *in vitro* with subcellular fractions of other metabolizing tissues such as the intestine, kidneys and lungs (Abdullah et al. 2016; Wang et al. 2021). However, results of the present thesis revealed that scaling factors for conversion of kinetic data for active transport obtained in *in vitro* model systems to the *in vivo* situation appear less well defined and often also less straight forward. Such scaling factors will differ with the different *in vitro* systems applied. For

instance, the scaling factor that appeared suitable to translate the *in vitro* Vmax for the Oatp transport of E$_2$17βG in liver (**Chapter 2**) could be defined in a way similar to the definition of the scaling factor for translation of data using the amount of protein/gram tissue calculated from the hepatocellularity number, the protein concentration in the hepatocytes and the weight of the liver. So, using the fitting approach in this chapter resulted in a similar scaling factor thereby corroborating its value. In future research, generating proofs of principle for other Oatp transported model compounds would further validate the respective scaling factor for *in vitro* data obtained using primary hepatocytes. Since the only component scaled is the amount of protein per gram liver, it can even be further validated for substrates of other hepatic uptake transporters such as OCT1, and organic anion transporter (OAT) 1 and 3 (the expression of transporters in hepatocyte is close to equal to the expression of the transporters in the liver). To facilitate this further validation of the scaling factors by generating more proofs of principle, model compounds to be studied should preferably have multiple data sets on *in vitro* kinetic transport data using primary hepatocytes and multiple *in vivo* kinetic data sets such as data on the blood concentration in time and data on excretion. In the present thesis a first proof of principle for defining biliary excretion based on scaling of data obtained *in vitro* using hepatocytes has been established for rat (**Chapter 2**). It seems of interest for future studies to perform similar studies and define a similar scaling factor for human. Using the data of human primary hepatocytes transporting typical OATP substrates such as rosuvastatin, fluvastatin, valsartan and irbesartan and available clinical data would suffice to apply the approach and obtain a scaling factor (Chan et al. 2019; Chapy et al. 2015; Jamei et al. 2014; Poirier et al. 2009). Overall, it is concluded that for the liver, primary hepatocytes are the preferred model for generating the PBK model parameters for biliary excretion, also because scaling the data to the *in vivo* situation appears relatively straight forward.

6.3.2 Scaling to the kidney

For the kidney it is quite a different story. Especially, due to the fact that the actual levels of transporters of interest in the different renal models may vary substantially (as outlined in the previous section) scaling of the *in vitro* kinetic data obtained in these *in vitro* models to the *in vivo* kidney becomes challenging. Fitting the PBK model parameters to available *in vivo* data appeared to be of help to derive the respective scaling factors. For instance, fitting PBK model based predicted data for OCT2 transport of the model compounds excreted via active renal transport used in this thesis (MQ, PQ or TTX) to available *in vivo* data revealed that the translation of the *in vitro* Vmax to the *in vivo* Vmax required a scaling factor, based on the amount of protein per gram tissue, the location of the transporter in the kidney and an extra factor encompassing all differences between the *in vitro* system and the *in vivo* situation.

The challenge of defining an adequate scaling factor became evident in the studies described in **Chapter 3 and 4** of this thesis when using the RPTEC cell line SA7K and the HEK293 cell line with OCT2 overexpression. For scaling of the OCT2 transport of MQ (**Chapter 3**) a simple scaling for protein content per gram kidney (reported to be 300 mg protein/g kidney (Kumar et al. 2018)) and location of OCT2) in only 70% of the overall kidney tissue (resulting in: 300 x 0.7 = 210 mg protein/g kidney), was not sufficient to translate the *in vitro* Vmax from SA7K cells to an *in vivo* Vmax in kidney as the predicted maximum blood concentration (Cmax) under these conditions differed 6-fold from the reported *in vivo* data. To solve the discrepancy, an additional component had to be taken into account when defining the scaling factor. The scaling factor should encompass everything that is different between the *in vitro* system used and the *in vivo* system described by the PBK model, which for MQ also included:

i)   The species differences (human cell line, rat PBK model) as human RPTEC cells only have OCT2, while in rat kidney cells *in vivo* also OCT1 and OCT3 are present (figure 1) (Chu et al. 2013a; Lechner et al. 2021; Slitt et al. 2002), which have a broad overlap with OCT2 substrates (Nies et al. 2011; Volk 2013) and the amino acid identity between rat and human OCT2 is for 90% similar (Hayer-Zillgen et al. 2002; Koepsell et al. 2003), and there is a difference in quantitative abundance of OCT2 in rat (253.5 pmol/gram kidney) and in human (164.2 pmol/gram kidney) (Basit et al. 2019).

ii)   The difference in OCT2 expression *in vitro* and *in vivo*.

iii)   The difference in membrane potential *in vitro* and *in vivo* given that membrane potential has been described to influence transporter activity (Kumar et al. 2018), and iv) the possibility that MQ can also be transported by non-specific membrane channels due to its small size which may be different in the *in vitro* model and the *in vivo* situation (Koepsell et al. 2003).

Given that actual data on all these characteristics and their differences between the *in vitro* model and the *in vivo* situation are unknown defining the scaling factor had to depend on fitting the PBK model predictions to the available *in vivo* data. This resulted in an additional factor of 100 and led to a scaling factor (21,000 mg protein/g kidney) that exceeded by far the actual amount of protein that can theoretically be present per gram tissue. Consequently, here a virtual amount of protein per gram tissue was defined to be used for scaling the *in vitro* Vmax from SA7K cells to an *in vivo* Vmax in rat RPTEC cells. In this factor of 100 especially the difference in abundance/expression of OCT2 in the *in vitro* system, which was very low, compared to the *in vivo* situation, is included. Elaborating on this, the developers of the SA7K cell line compared the relative abundance of OCT2 in their newly defined SA7K cell line to that in the human kidney (HK2) cell line and to early passage primary human donor cells (RPTEC) (Li et al.

2017c). Compared to the HK2 the relative abundance of OCT2 in SA7K was 5 times higher, whereas compared to the primary RPTEC cells it was 4 times lower. It is therefore not surprising that scaling was necessary given that the expression of OCT2 makes up around a quarter (24%) of all expressed transporters in the RPTEC and transporter expression is prone to change when cells are dedifferentiated when developed for culture purposes (Basit et al. 2019; Lechner et al. 2021). For rat this number is around 20% for OCT1 and OCT2 together. All in all, the different scientific based considerations have been adequately taken into account.

It would be of use to further validate this scaling factor and investigate whether the scaling factor defined in **Chapter 3** for scaling the *in vitro* data obtained for MQ in SA7K cells would also be valid for another OCT2 substrate studied in the SA7K cell line. To this end, in **Chapter 4** PQ was chosen as the model compound. However, for PQ the SA7K cells appeared not to provide an adequate *in vitro* model to quantify OCT2 mediated transport kinetics mainly because cellular uptake via OCT2 transport appeared to rapidly equal cellular excretion resulting in stable time-dependent cellular concentrations of PQ from which uptake kinetics could not be derived. With the use of literature reported HEK-293 cell data for OCT2 transport of PQ a scaling factor could be defined with a similar approach as described in **Chapter 3**. Here too, scaling for protein and transporter location (300 mg protein/g kidney x 70% = 210 mg protein/g kidney) was not enough to adequately predict the Cmax of the reported *in vivo* kinetic data with the PBK model. So, again the scaling factor was fitted to encompass all the differences between the *in vitro* HEK293 cells and the *in vivo* rat RPTEC. In this case, the difference between the predicted Cmax for PQ to the reported Cmax was much smaller than for MQ so the final scaling factor was substantially lower (1,155 mg protein/g kidney) than that defined in **Chapter 3** for SA7K cells and MQ (21,000 mg protein/g kidney). This may in part also due to the probability that the OCT2 expressed in HEK293 is different (probably higher) than that in the SA7K cells. Therefore, it can be speculated that if MQ was measured in HEK293 cells, the scaling factor obtained in **Chapter 3** would have been different.

If primary RPTEC cells could be used as a suitable cell model for transport experiments scaling would have been more straight forward as it would be expected to be similar to the method shown suitable for scaling data from primary hepatocytes to liver (**Chapter 2**). The scaling factor expressed in mg protein/g kidney could again be based on fitting the PBK model predictions obtained using the RPTEC *in vitro* transporter kinetic data to available *in vivo* data. The scaling factor expressed in mg protein/g kidney thus obtained would likely be within a more realistic range as no correction would be required for the expression difference between the *in vitro* and *in vivo* situation since it can be assumed that primary RPTEC have a comparable level of transporter expression as the RPTEC

in vivo. As compared to the scaling factor for hepatocytes to liver it would be however more challenging to verify the scaling factor obtained with a theoretical calculated scaling factor. This because as opposed to liver where hepatocellulartiy numbers (10^6 hepatocytes/gram liver) have been reported multiple times, for kidney so-called RPTEC-cellularity numbers (10^6 RPTEC cells/gram kidney) have not been reported.

6.3.3 Transfected cell lines, relative expression factors and relative activity factors

In the present thesis, scaling *in vitro* kinetic transport data to the *in vivo* situation was successfully applied for both a non-transfected model (**Chapter 3**) and a transfected model (**Chapter 4**). The latter model has already been used for defining *in vitro* data that were extrapolated to *in vivo*, especially for compounds following biliary excretion (Chan et al. 2019; Izumi et al. 2018; Jamei et al. 2014; Kunze et al. 2014; Poirier et al. 2009). Utilizing *in vitro* transport kinetic data from transfected cell lines, either relative expression factors (REF) or a relative activity factors (RAF) are used to scale to the *in vivo* situation. The definition of a REF is based on quantifying the transporter of interest in the *in vitro* system (HEK293, CHO) and in the cells of the relevant tissue (liver/kidney) and species (human/rat) with proteomics. The difference can be used as a scaling factor. Where the capability of the REF has been useful for IVIVE, it has not yet been applied extensively in PBK modelling. One group in particular has reported on its use, which is the group of James Chan from the National University of Singapore incorporating REF in models that describe biliary excretion (Chan et al. 2019) and renal excretion (unpublished data, Society of Toxicology annual meeting 2022 (Thakur and Chan 2022)). For biliary excretion, Chan et al. (2019) defined a new REF by multiplying the REF for *in vitro* OATP1B1 uptake of the compounds rosuvastatin, fluvastatin and pitavastatin in HEK293 cells in isolated human hepatocytes (scaling factor 1) by the REF for the isolated human hepatocytes to a human liver (scaling factor 2). With this new REF the PBK model (Simcyp®) predictions for Cmax stayed withing two-fold from the observed Cmax for single intravenous, single oral and multiple oral dosing. However, no predictions were made for the cumulative biliary excretion of the three statins. In another study (unpublished data, Society of Toxicology annual meeting 2022 (Thakur and Chan 2022)), the model compound used for studies on renal excretion was the herbicide 2,4-dinitrophenoxyacetic acid (2,4-D), found to be a strong substrate for OAT1. Concentration dependent uptake studies were performed with 2,4-D in HEK293 cells overexpressing OAT1 obtaining Vmax and Km values. The level of OAT1 in HEK293 cells and in human kidney RPTEC was quantified to enable definition of the scaling factor required to perform *in vitro* to *in vivo* extrapolation. The scaling factor that resulted was implemented in a human PBK model using Simcyp® to subsequently predict the time-dependent plasma concentration and cumulative renal excretion of 2,4-D. As 2,4-D is partly prone to metabolism, hepatic clearance data were

also included in the model. Implementing kinetic parameters for both hepatic clearance and active renal clearance with the adequate scaling factor in the model resulted in PBK model predictions closely recapitulating the reported clinical data (Thakur and Chan 2022).

In case of using a RAF, a probe substrate for the transporter of interest is used in both the *in vitro* and *in vivo* situation. The RAF is determined by dividing the *in vivo* transport activity by the *in vitro* transport activity. Probe substrates for which RAF values for kidney and liver transporters are reported to date include tenofovir (OAT1), acyclovir and ganciclovir (OAT2), benzylpenicillin and oseltamivir acid (OAT3), estrone sulphate (OATP1B1) and cholecystokinin octapeptide (OATP1B3) (Izumi et al. 2018; Maeda 2015; Mathialagan et al. 2017). While the RAF value has been used successfully in extrapolating from *in vitro* to *in vivo*, Izumi et al. (2018) reported solely on the extrapolation from OATP1B1/B3 overexpressed HEK293 cells to human hepatocytes in suspension, whereas Mathialagan et al. (2017) reported on incorporating the RAF into a two-compartment mechanistic model extrapolating *in vitro* renal secretion to the *in vivo* situation in human resulting in a model that was further extended for prediction of drug interactions. A proof of principle for use of RAF values in whole body PBK modelling remains to be established. Regarding the OCT2 transporter, no probe substrate has been defined yet (Burt et al. 2016). As a result, so far reported RAF values for OCT2 transport result from fitting predictions to experimental data.

6.3.4 Scaling in future research

The question that remains is how to define scaling factors for new chemicals tested in the available *in vitro* transport models when *in vivo* kinetic data for fitting are not available? Based on the results of the present thesis and the discussion above on *in vitro* kinetic models and scaling the best way forward seems to be the use of transfected cell lines with an overexpression of the relevant transporter(s). This will result in a definition of the kinetic parameters for uptake of the new chemical by the transporter(s) of interest without a need for inhibitors, and without confounding contributions of other transporters. On the other hand, knowledge on confounding contributions by other transporter could also be necessary. It could therefore be argued to use primary RPTEC cells and establish the kinetics of the overall uptake of a new chemical reporting on an overall apparent Vmax and an overall apparent Km. The scaling factor would then be obtained by quantifying the level of the transporter of interest in both the *in vitro* model and the *in vivo* situation by proteomics or western blotting obtaining a REF value (Basit et al. 2019; Bay et al. 2022; Lundquist et al. 2014; Prasad and Unadkat 2014). As described in **section 6.3.3** use of a RAF value could also be considered, although not for all transporters verified probe substrates are available. The availability of well-established and characterized commercially available transfected cell lines with well-defined levels of overexpression of transporters

of interest compared to the *in vivo* situation would facilitate the further development of including active transport processes in PBK models. Thereby, information on quantified levels of transporters in transport-abundant tissues (kidney, liver, intestine, blood-brain-barrier, placenta) from different species should become available such as the data reported by Basit et al. (2019) (Table 1). To work towards implementation of new approach methodologies and generating these data when considering ADME characteristics the mindset of ADME research and especially the field of transporter research needs to change. The likelihood of this change happening anywhere in the coming ten to twenty years is low also due to the fact that for around 70% of the chemicals excretion is not the rate-limiting step in their kinetics. If change would happen, it potentially moves faster when pharma gets more and more convinced of using NAMs instead of animals to obtain the ADME of a drug candidate as drug transporters play a large role in pharma due to potential drug-drug interactions (Keogh 2012).

Table 1.
Quantitative data on the abundance of the different kidney transporters across species adapted from Basit et al. (2019).

Transporters	Protein abundance (pmol/gram kidney)				
	Mouse	Rat	Dog	Monkey	Human
SLC22A6 /OAT1	156.2 ± 92.06	308.8 ± 79.24	75.4 ± 43.07	242.5 ± 62.69	107.7 ± 56.83
SLC22A7 /OAT2	120.3 ± 39.3	BLQ	NC	27.3 ± 10.2	19.8 ± 8.36
SLC22A8 /OAT3	NC	NC	NC	124.7 ± 32.57	78.5 ± 37.38
SLC22A11 /OAT4	NC	NC	NC	17.5 ± 6.28	10.6 ± 5.64
SLCO4C1 /OATP4C1*	NC	NC	NC	0.7 ± 0.28	0.3 ± 0.03
SLC22A1 /OCT1*	18 ± 3.96	38.3 ± 6.45	NC	BLQ	BLQ
SLC22A2 /OCT2	429.1 ± 134.67	253.5 ± 70.92	NC	464.8 ± 147.18	164.2 ± 53.27
SLC22A3 /OCT3*	NC	NC	BLQ	BLQ	0.03 ± 0.01
SLC22A4 /OCTN1	NC	NC	NC	19 ± 10.55	27.2 ± 13.44
SLC22A5 /OCTN2	41.4 ± 9.29	96.6 ± 22.51	16 ± 5.84	45 ± 14.35	13.1 ± 5.8
ABCB1 /MDR1	15.5 ± 5.99	39.3 ± 11.76	32.1 ± 9.34	52 ± 9.44	42.3 ± 16.16
SLC47A1 /MATE1	NC	NC	NC	161.2 ± 56.23	105.6 ± 47.52
ABCG2 /BCRP*	3.1 ± 0.88	1.3 ± 0.4	NC	NC	NC
ABCC1 /MRP1*	50 ± 9.68	58.3 ± 11.41	42.2 ± 10.95	54.7 ± 15.7	20.1 ± 4.54
ABCC2 /MRP2	NC	NC	NC	56 ± 13.99	30.1 ± 16.52
ABCC3 /MRP3*	29.4 ± 18.42	108.7 ± 12.66	NC	27.7 ± 9.01	20.1 ± 1.78
ABCC4 /MRP4	8.6 ± 3.94	37.5 ± 7.51	NC	71.3 ± 18.73	19.5 ± 20.58
SLC5A2 /SGLT2	391.7 ± 89.62	395.1 ± 67.87	356.7 ± 84.85	182 ± 49.56	76.4 ± 41.25
ATP1A1 /Na+K+ATPase*	114.9 ± 17.87	119 ± 14.63	70.7 ± 15.19	51.7 ± 10.91	20.1 ± 1.17

*data are presented in relative protein abundance (arbitrary unit)/gram kidney. NC = not conserved peptide, BLQ = Below limit of quantitation

6.4   PBK models

The PBK models used in the thesis work were all defined as generic as possible so that compound specific kinetics were described in detail only for the compartments that are essential for either the kinetics or dynamics of the compounds of interest. These PBK models contained the following set of parameters: weight and blood flow for the included tissues, the blood:tissue partition coefficients, the fraction unbound in blood, kinetic parameters for metabolism (if substantial) and renal and biliary transport. For all model compounds studied in the present thesis compound specific kinetic parameters were derived from *in vitro* cell models describing PBK models with different active excretion processes in the different chapters. The models developed in the present thesis included a PBK model with a liver compartment with biliary excretion (**Chapter 2**), one with a kidney compartment with glomerular filtration and active transport (**Chapter 3 and 4**) and one including both liver metabolism and kidney excretion (**Chapter 5**). This thesis described for the first time PBK models for the model compounds MQ and TTX. For E$_2$17βG, a PBK model has been defined previously by Sun et al. (2006) from a more pharmaceutical perspective fitting parameters to *in vivo* data. For PQ (**Chapter 4**) multiple studies have reported on PBK models. For instance, PQ PBK models have been developed by Lohitnavy et al. (2017) for rat, by Campbell et al. (2021) for rat, mouse and dog and by Stevens et al. (2021) for non-human primates enabling extrapolation to humans. A comparison of all these studies reveals that PQ PBK model kinetic parameters are hard to define. Campbell et al. (2021) performed an in-depth study on the kinetics of PQ showing that the blood compartment plays a big role in its distribution as the blood:plasma ratio is changing over time, as does the fraction unbound in blood and plasma which was thoroughly investigated as well. Moreover, not touched upon at all by any of the reported PQ models, another study indicated that the muscles serve as a reservoir for PQ too (Dinis-Oliveira et al. 2008). The main difference between the model of Lohitnavy et al. (2017) and the other two models is the inclusion of the lung. Lohitnavy et al. (2017) built an oral PBK model and included the lung where PQ is taken up from the blood via the polyamine uptake system in the alveolar cells showing saturating kinetics. The dosage used in this modelling study and the accompanying *in vivo* study was higher than for the other two models resulting in the need of including the lung. Although the authors were able to predict PQ levels in the lungs well for the first four hours, there was an underprediction at 24 hours. This is due to the *in vivo* accumulation of PQ in the lung over time which is not included in the PBK model, and the subsequent renal failure resulting in reduced PQ clearance. These long term effects complicate modelling of PQ kinetics upon prolonged exposure and/ or dosing at high toxic levels. This is also the reason why in Campbell et al. (2021), in Stevens et al. (2021) and also in the study reported in **Chapter 4** of this thesis the dosage used to make predictions and evaluate the model performance was at a non-toxic level.

6.4.1 Applicability domain for PBK models including active excretion

The present thesis resulted in proofs of principle on incorporating *in vitro* active hepatic or active renal excretion into PBK models for the prediction of the blood concentrations and cumulative biliary excretion of chemicals for which active excretion contributes to their clearance. Even if the group of chemicals relying on active excretion for their clearance is not large, this is an important step forward in the field of PBK modelling. Chemicals chosen to generate the proofs of principle have to rely on active transport in either liver or kidney for their clearance and are thus preferably not or minimally (< 10%) cleared via metabolic conversion (as can be shown in appropriate *in vitro* test systems such as incubations with liver microsomes and S9 or primary hepatocytes). Characteristics of chemicals that can be expected to comply with these requirements are chemicals that have ionizable groups, are above a certain molecular weight, and/or chemicals that are small, hydrophilic, and have charged groups such as quaternary ammonium compounds. For new chemicals it will help to estimate a potential role for active excretion in their clearance that there are tools such as quantitative structure-activity relationships (QSARs) to identify the potential of a chemical to be a substrate for a transporter (Dave and Morris 2015; Hazai et al. 2013; Sharifi and Ghafourian 2014; Wang et al. 2005).

6.5   Protein binding

In the development of PBK models protein binding in blood (and plasma) is an important factor to be taken into account for adequate *in vitro* to *in vivo* extrapolation. This is due to the fact that only the free fraction of a compound in blood is able to undergo kinetic processes such as metabolic clearance or transporter clearance (Schmidt et al. 2010). Moreover, on a dynamic level only the free fraction of a compound is able to exert an adverse effect in the target tissues. Most of the hepatic clearance and uptake studies and all transporter studies performed in the present thesis have used serum-free buffer in the *in vitro* system. Thereby assuming that when no protein is present, the fraction unbound in the incubation ($f_{u,inc}$) equals 1 and a maximum concentration of compound is available for binding to transporters or for intrinsic clearance (CL_{int}). However, in *in vitro* systems nonspecific binding may occur as a consequence of binding of the compound to the incubation plate ($f_{b,plate}$), to proteins and lipids of microsomes or cells ($f_{b,mic/cell}$) or to proteins in the assay medium ($f_{b,prot}$) (if it contains any). As a result the $f_{u,inc}$ no longer equals 1 and the Km values that are obtained from the literature and/or from the performed transporter studies in this thesis are likely to be an overestimation as they are based on total substrate concentration rather than free substrate concentration (Obach 1996). It would have been more precise to have measured the unspecific binding of the compounds of the present thesis by measuring $f_{b,plate}$ and $f_{b,mic/cell}$. With

these results, the $f_{u,inc}$ would in reality be likely lower than 1. Moreover, these binding studies were also not executed for the literature derived *in vitro* kinetic data. However, in the transport studies with the RPTEC cells unspecifc binding to the cells was avoided by washing the cells with PBS containing 0.2 % BSA at the end of the incubation. For newly to test compounds and incubation conditions the $f_{u,inc}$ for the different ways of unspecific might be considered, ($f_{b,\ plate}$, $f_{b,\ mic/cell}$, $f_{b,\ prot}$) and can either be determined *in vitro* or *in silico* for example by using rapid equilibrium dialysis for protein and/or system binding (Waters et al. 2008), by using QSARs (Austin et al. 2002; Austin et al. 2005)and/or by determining the binding to the incubation plate/Eppendorf tubes. For hepatocytes, such *in vitro* methods are already described in the literature (Di et al. 2012; Hallifax and Houston 2006; Kilford et al. 2008). However, for the binding to RPTEC this is not the case. To determine the $f_{b,\ mic/cell}$ for RPTEC, the transporters present need to be inactivated to avoid loss of substrate that is subject to uptake into the RPTEC. An approach on how to inactivate transporters could be by performing the experiment in the presence of a cocktail of inhibitors blocking the uptake transporters.

6.5.1 Hepatic transport and protein binding

Although the free fraction theory is widely accepted, there is some evidence of hepatic uptake directly facilitated by the albumin-compound complex, suggesting compounds can be taken up in their protein bound form as well (Baker and Bradley 1966; Forker and Luxon 1981; Forker and Luxon 1983; Tsao et al. 1988; Weisiger and Ma 1987). A review by Bowman and Benet (2018) has elaborated on the different processes underlying the protein or albumin facilitated uptake and clearance of compounds but only one of them will be explained here further. It involves the transporter induced protein binding shift (TIPBS) where the presence of protein can decrease the Km of a highly protein bound compound for its transport leading to uptake in the hepatocytes. For the *in vitro* to *in vivo* extrapolation of hepatic uptake via transporters it is known that especially for the highly bound compounds the IVIVE is the poorest. It has been shown by Bowman et al. (2019) in a study where substrates for OATP uptake were included of which two lower protein bound (pravastatin and rosuvastatin) and two highly protein bound (atorvastatin and pitavastatin) drugs that the presence of protein decreased the Km of the highly protein bound drugs (Table 2). Uptake studies were performed in serum-free buffer and in 100% plasma. As is shown in table 2 for the lower protein bound drugs the medium (buffer or plasma) did not affect the Km or the Cl,int (Vmax/Km). However, for the highly protein bound drugs the Km decreased substantially in the presence of 100% plasma. The authors explained that the underlying theory for this occurrence is that in the case of the highly protein bound drugs the affinity for transporter might be higher than for the albumin thereby it is able to potentially strip off the drug from protein whereas for the lower bound protein drugs there is already free drug available and there for stripping off the drug directly is less preferred.

Table 2.
Measured Km and Vmax in rat hepatocytes of four statins either in buffer (no proteins) or 100% plasma. (Adapted from Bowman et al. (2019)).

Compound	Incubation	Km	Vmax	Clint
		μM	$pmol/min/10^6\ cells$	$\mu L/min/10^6\ cells$
Pravastatin	Buffer	16.5 ± 4.43	208 ± 14.3	12.6 ± 3.50
	Plasma	9.66 ± 3.27	97.9 ± 8.84	10.1 ± 3.55
	Fold difference	1.71	2.12	1.25
Rosuvastatin	Buffer	4.00 ± 0.962	323 ± 20.2	80.8 ± 20.1
	Plasma	0.995 ± 0.148	339 ± 15.6	341 ± 53.0
	Fold difference	4.02	0.953	4.22
Atorvastatin	Buffer	3.61 ± 1.96	1650 ± 203	458 ± 254
	Plasma	0.115 ± 0.116	272 ± 65.5	2370 ± 2450
	Fold difference	31.4	6.07	5.16
Pitavastatin	Buffer	8.71 ± 2.12	600 ± 47.0	68.9 ± 17.6
	Plasma	0.0812 ± 0.0157	39.9 ± 2.45	491 ± 99.7
	Fold difference	107	15.0	7.13

In the case of **chapter 2** with model compound $E_2 17\beta G$ for the Oatp transporter the phenomenon as described above has not been taken into account. Although it would be interesting to do so as the protein binding of $E_2 17\beta G$ is high ($\approx$ 80% (Sun et al. 2006)) thereby the Km of the different reported rat hepatocyte studies used in **chapter 2** might have been overestimated due to the absence of protein in the incubation systems.

6.5.2 Renal transport and protein binding

Taking into account the reported findings of Bowman et al. (2019), the effects of protein binding can be considered also to be relevant for the transporters in the RPTEC. One older study has reported on the protein facilitated uptake in isolated rabbit segment 2 proximal tubules where organic anions (p-aminohippurate and methotrexate) and an organic cation (N^1-methylnicotinamide (NMN)) were investigated for their ability to use proteins as a facilitator for cellular uptake (Besseghir et al. 1989). The experiment was executed in isolated rabbit segment 2 proximal tubules with increasing concentrations (0 – 5 g/dl) of bovine serum albumin (BSA) resulting in an increased secretion (uptake + efflux) of the organic anions p-aminohippurate and methotrexate in the presence of BSA until 1 g/dl. The presence of BSA, however, did not influence the secretion of the organic cation NMN which can be explained by the fact that NMN does not bind (well) to BSA. NMN has, just like MQ and PQ a quaternary N atom in its structure (quaternary

ammonium cation), hampering protein binding. This observation is substantiated by the findings of Neef and Meijer (1984) who reported protein binding of 14 quaternary ammonium cation compounds measured by equilibrium dialysis. The number of carbon atoms showed to be of importance in the binding of quaternary ammonium cations to protein where structures up to 13 carbon atoms showed no protein binding. For the organic cations of the present thesis that are quaternary ammonium compounds and especially MQ this corroborates the high fraction unbound values of MQ (7 C-atoms) and PQ (12 C-atoms), where of course PQ is the exception pointing at the thorough investigation for its protein binding by Campbell et al. (2021) (**section 6.4**).

When protein binding does occur one could also consider the importance of protein facilitated uptake. However, based on the findings by Besseghir et al. (1989) and Neef and Meijer (1984) it is concluded that it is unlikely that protein facilitated uptake or secretion of organic cations will occur. On the other hand for organic anions it may be relevant to take the protein binding and the possible protein facilitated uptake into account when performing uptake studies using for example OATs or OATPs in RPTEC.

6.5.3 Fraction unbound in PBK modelling

The fraction unbound in PBK modelling is a subject of ongoing debate as the question remains: what is the actual concentration available for uptake or metabolism? In many cases use of the venous concentration of the target tissue in the Michaelis-Menten equation, which is the concentration corrected for the blood:tissue partition coefficient, is sufficient to take protein and tissue binding into account and describe the concentration available for metabolism or transport in the PBK model. This is for example applied in **chapter 2**. Alternatively one could additionally correct the venous concentration for protein binding. This approach may be required for compounds that are highly bound to protein, although this may equally well lead to an overcorrection of protein and tissue binding of the concentration in the blood/plasma for protein resulting in underprediction of the unbound concentrations and overprediction of the corresponding dose levels by the PBK model.

6.6   Quantitative *in vitro in vivo* extrapolation (QIVIVE)

An ultimate reason to develop PBK models is their use in NAMs as they are capable of predicting the dose of a chemical that gives rise to the Cmax or AUC thus enabling the translation of the *in vitro* data into an *in vivo* dose response curve and/or predicting the *in vivo* relevance of toxic *in vitro* concentrations. The metric to use for this so-called PBK model based reverse dosimetry can be a matter for debate (Rietjens et al. 2019). For compounds for which toxicity is caused by a thresholded mode of action, including

the toxic endpoints of the model compounds used in the present thesis, Cmax is the parameter of choice. Thus the PBK model based QIVIVE performed in **Chapter 4 and 5** of this thesis was based on Cmax for translation.

6.6.1 QIVIVE requirements

The key to successful QIVIVE depends on three requirements. First, a PBK model should be developed and its performance evaluated by comparison of predictions made to available kinetic data. Evaluation may also include a sensitivity analysis to elucidate parameters that are most influential for the model based predicted outcome of interest. Second, the *in vitro* toxicity model of choice used to define the *in vitro* concentration response data should meet certain requirements. One of these requirements is that the *in vitro* model should adequately reflect the target tissue, mode of action and endpoint of the *in vivo* toxicity to be predicted. Lastly, after QIVIVE comparison of the predicted *in vivo* dose response curve and/or of the point of departure (PoD) derived from the predicted *in vivo* dose response curve to the dose response curve and/or PoD derived from already available *in vivo* toxicity data should be made. Evaluation of the PBK model for PQ and TTX has shown the PBK model to be successful in predicting the reported Cmax where in the case of TTX it was successful for three administration routes (oral, intravenous and intramuscular). Choosing the right *in vitro* model meant for PQ the lungs as being the target tissue and this was reflected in the chosen *in vitro* model, which were alveolar cells in a cytotoxicity assay (**Chapter 4**). A difference in sensitivity was shown within the two rat alveolar cell lines with the RLE-6TN cells being more sensitive (EC_{50}: 79-166 μM) than the L2 cells (EC_{50}: 319 μM). A different sensitivity upon prolonged exposure duration was shown in the human alveolar cell line A549 for data sets obtained upon 24 hour exposure (EC_{50}: 400-889 μM) and a 48 hour exposure (EC_{50}: 72-97 μM). These differences in sensitivity will have an effect on the final predicted *in vivo* dose response curve and PoD derived from it after QIVIVE-based translation. In such cases all predicted values may be used for the subsequent comparison to available *in vivo* data, with the latter often also showing inter-study variations. For TTX where the target tissue is the central nervous system, a MEA assay with cortical neurons (for rat and human) or a cytotoxicity assay with the neuronal cell line neuro-2a (for mouse) were the chosen *in vitro* models (**Chapter 5**). For all the *in vitro* models the sensitivity towards TTX was in similar range (rat; EC_{50}: 3.5-5.5 nM, mice; EC_{50}: 5.3-12.1 nM. human; EC_{50}: 10 nM), pointing at the potency of TTX to block voltage gated sodium channels (VGSCs) regardless of the species.

6.6.2 Comparing predictions with reported PoD

The final step in QIVIVE is the comparison of the predicted *in vivo* toxicity to the reported *in vivo* toxicity with subsequent comparison to the available PoDs. For PQ the acute toxicity and for TTX the acute neurotoxicity were predicted using PBK model based reverse dosimetry

of available *in vitro* toxicity data. Predicted PoDs thus obtained were compared to available PoDs in literature. Reported PoDs for PQ (**Chapter 4**) were mainly LD_{50} values, provided in a large number of studies. However, none of these studies reported full LD_{50} dose-response curves, which made it difficult to define for example a predicted $BMDL_{10}$ for mortality for the comparisons. Moreover, there is a lack of other, more sensitive endpoints pointing at early onset of acute PQ toxicity. It was however possible to predict $BMDL_{50}$ values where it turned out that in particular in rat the predicted $BMDL_{50}$-$BMDU_{50}$ range was in line or underpredicted the reported LD_{50} values, with the latter potentially being due to the fact that *in vitro* cytotoxicity is not encompassing fully the *in vivo* endpoint, pulmonary fibrosis, of PQ toxicity (Roberts 2013). In case of human PQ toxicity, humans are known to be more sensitive to PQ toxicity (LD_{50}: 3-60 mg/kg bw) than rat (LD_{50}: 40-200 mg/kg bw). Together with the two different exposure times used to generate the *in vitro* data it was interesting to observe how well the predictions (LD_{50}: 3.8-101 mg/kg bw) matched the reported LD_{50} values. In the case of TTX (**Chapter 5**), EFSA established certain PoDs to derive HBGVs based on mouse studies (EFSA et al. 2017). In these studies, different endpoints for acute TTX toxicity were monitored and reported PoDs for apathy were considered to represent the most sensitive endpoint resulting in a LOAEL of 125 µg/kg bw, and a NOAEL of 75 µg/kg bw, the latter with an uncertainty factor of 100 resulting in an acute reference dose (ARfD) of 0.25 µg/kg bw. Also a $BMDL_{10}$ of 112 µg/kg bw for mortality was derived. With the human *in vitro* cytotoxicity data and the PBK model it was possible to predict a $BMDL_{10}$ that, with the default uncertainty factor of 10 for human interindividual differences, resulted in a HBGV of 0.18 µg/kg bw that matched the reported ARfD of 0.25 µg/kg bw, indicating the potential of using non-animal based methods for future risk assessment purposes.

6.6.3 *In vitro* and *in vivo* endpoints TTX

It is also of interest to note that for TTX the *in vitro* and *in vivo* endpoints considered were not identical in spite of the fact that the underlying mode of action was for all endpoints the blockage of the voltage gated sodium channels. *In vitro*, the endpoints were either a decrease in spikes compared to baseline activity in the neonatal cortical cells (MEA rat/human) or cell survival in the neuro-2a cells (mice) in the presence of veratridine and ouabain. For the mouse oral toxicity it was possible to use the most sensitive endpoint (apathy) for comparison of the predicted oral *in vivo* toxicity based on the mouse *in vitro* cytotoxicity data (**section 6.6.2**). For the parental route for both rat and mice, the most sensitive endpoints were chosen from the available *in vivo* toxicity data sets for the comparison. For rat, the most sensitive endpoint resulted from the *in vivo* toxicity test of measuring mechanical allodynia where Von Frey filaments were pushed against the paws of the rat until paw withdrawal was observed (with increasing concentration of TTX larger (heavier) filaments could be used before withdrawal occurred). For mouse, the most sensitive endpoint was a writhing test where visceral contractions upon exposure to acetic acid were measured. With increasing concentrations of TTX the number of

visceral contractions was decreasing. These endpoints imply for rat a parameter related to non-visceral sensory neurons and for mice to visceral sensory neurons. In spite of the fact that these different *in vivo* endpoints (apathy, mechanical allodynia, writhing test) do not seem to fully match the *in vitro* endpoints, it was possible to predict the acute *in vivo* toxicity of TTX in the different species, following different administration routes, likely because all are based on the same underlying mode of action.

6.7   Perspective on the field and future directions

Good kinetic predictability by PBK modelling is currently possible for around 70% of the compounds (Ahmad et al. 2020; Punt et al. 2022a; Punt et al. 2022b). For the other 30% of chemicals PBK models are not sufficiently able to correctly predict the kinetics, pointing towards the limitations of PBK model use and the apparent lack of including all relevant factors. When still 30% of the chemicals are mostly overpredicted (10x or more) trust in such models, for regulatory applications will be limited, particularly for new and data poor chemicals. One key factor explaining the lack of accuracy of PBK model predictions for at least part of the 30% of chemicals relates to the lack of including processes of active excretion via bile or urine. The present thesis focussed on investigating how to include this active excretion via bile and urine in PBK models using *in vitro* model systems to define the respective kinetic parameters. This might increase the applicability domain of PBK modelling and the % of chemicals for which adequate PBK models can be defined. In light of transitioning from *in vivo* risk assessment towards *in vitro* risk assessment it is essential to achieve this goal based on use of *in vitro* kinetic data. The present thesis has clarified that the inclusion of active excretion for compounds that are not metabolised is needed and that without it predictions are deviating from what has been reported *in vivo*. The results also elucidated that at the present state-of-the-art scaling of the *in vitro* data to the *in vivo* situation often still needs *in vivo* data to enable fitting of the predictions and the scaling factor to be used to the *in vivo* situation to define the adequate scaling. Future work in this field should be directed at defining *in vitro* model systems and accompanying methods to define the respective scaling factors, as well as on increasing the proofs of principle evaluating *in vitro* models and corresponding scaling factors for one compound also for related compounds. In the present thesis this was done for PQ, but results obtained revealed that the *in vitro* model and scaling factor shown valid for MQ, did not work for the related OCT2 substrate PQ. The results, however, also indicated that future work may better be directed at defining suitable transfected cell lines and their accompanying REF or RAF values for scaling to the *in vivo* situation. In addition, it is important that *in silico* techniques such as QSARs are developed further so that based on the molecular structure and the subsequently extracted physico-chemical data processes and even

PBK model parameters for absorption, distribution, metabolism and excretion can be predicted. For blood:tissue partition coefficients and absorption constants this appears to be already feasible, while future work should focus on predicting / QSARs for kinetic constants for metabolism and transport. Such methods should also enable prediction of compounds that are resistant to metabolic clearance, since for such compounds active excretion may play a prominent part in their clearance and kinetics. Alternatively *in vitro* techniques might prove of use to define this metabolic resistance as was shown in the present thesis for TTX shown to be stable in incubations with rat hepatocytes. These future efforts should also enable making predictions based on the physico-chemical data, on whether chemicals are likely to be excreted passively and/or actively, via the bile or the urine and even which transporter is involved. While it is important to continue developing NAMs it will require a substantial amount of time and money to define and build these *in vitro* and *in silico* models.

6.8   Conclusion

The present thesis demonstrated proofs of principle for taking into account active excretion via liver and kidney in PBK modelling and showed that it is possible to incorporate this active excretion using *in vitro* transporter kinetic data provided that adequate scaling factors are used to translate the Vmax *in vitro* to a Vmax *in vivo*. The SA7K cell line showed to have some potential as an *in vitro* model for obtaining *in vitro* kinetics for OCT2 mediated transport. The approaches for defining the scaling factors can either be based on theoretical considerations where the differences between the *in vitro* model and the *in vivo* situation are quantified or can be derived by fitting of the predictions to the *in vivo* reported kinetic data. It was also concluded that transfected cell lines would provide the preferred *in vitro* model to define kinetic parameters, given that there is no confounding by other transporters and that a scaling factor can be defined more easily by quantifying them with proteomics/western blotting in both the cell line and the *in vivo* tissue of interest to establish adequate scaling factors to be used for *in vitro* to *in vivo* translation. Moreover, it was shown that the PBK models obtained enabled the adequate prediction of PoDs and HBGVs by PBK modelling based QIVIVE of available *in vitro* toxicity data thereby building more confidence into using this tool as a NAM aiming at replacement, reduction and refinement (3Rs) of animal experimentation.

References

References

References

(EU) EU (2007) Judgment of the Court of First Instance in Case T-229/04 Kingdom of Sweden

(TPI) TPI (2020) Terugblik op TPI. In. https://www.rijksoverheid.nl/onderwerpen/dierproeven/alternatieven-voor-dierproeven#:~:text=Subsidie%20onderzoek%20alternatieven%20voor%20dierproeven&text=Voor%20het%20derde%20programma%2C%20dat,naar%20proefdiervrije%20innnovatie%20(TPI). Accessed April 8, 2022

Abal P, Louzao MC, Antelo A, et al. (2017) Acute Oral Toxicity of Tetrodotoxin in Mice: Determination of Lethal Dose 50 (LD50) and No Observed Adverse Effect Level (NOAEL). Toxins (Basel) 9(3) doi:10.3390/toxins9030075

Abdullah R, Alhusainy W, Woutersen J, Rietjens IM, Punt A (2016) Predicting points of departure for risk assessment based on *in vitro* cytotoxicity data and physiologically based kinetic (PBK) modeling: The case of kidney toxicity induced by aristolochic acid I. Food Chem Toxicol 92:104-16 doi:10.1016/j.fct.2016.03.017

Agency UEP (1997) Reregistration Eligibility Decision(RED) Mepiquat Chloride. Washington, D.C. 20460, p 1-136

Ahmad A, Pepin X, Aarons L, et al. (2020) IMI - Oral biopharmaceutics tools project - Evaluation of bottom-up PBPK prediction success part 4: Prediction accuracy and software comparisons with improved data and modelling strategies. Eur J Pharm Biopharm 156:50-63 doi:10.1016/j.ejpb.2020.08.006

Allen SG, M.; Boylan, A.M.; Highland, K.B.; Germinario, A.; McCauley, M.; Malone, M. (2019) Paraquat Poisoning: Survival after Oral Ingestion. J Fam Med Dis Prev 5(107) doi:10.23937/2469-5793/1510107

ATCC (2022) Primary Renal Proximal Tubule Epithelial Cells; Normal, Human (RPTEC). In. https://www.atcc.org/products/pcs-400-010#:~:text=400%2D010%E2%84%A2-,Primary%20Renal%20Proximal%20Tubule%20Epithelial%20Cells%3B%20Normal%2C%20Human%20(RPTEC,Epithelial%20Cell%20Growth%20Kit%20components. Accessed 29th of May 2022

Austin RP, Barton P, Cockroft SL, Wenlock MC, Riley RJ (2002) The influence of nonspecific microsomal binding on apparent intrinsic clearance, and its prediction from physicochemical properties. Drug Metab Dispos 30(12):1497-503 doi:10.1124/dmd.30.12.1497

Austin RP, Barton P, Mohmed S, Riley RJ (2005) The binding of drugs to hepatocytes and its relationship to physicochemical properties. Drug Metab Dispos 33(3):419-25 doi:10.1124/dmd.104.002436

Bailey GW, White JL (1965) Herbicides: a compilation of their physical, chemical, and biological properties. Residue Rev 10:97-122 doi:10.1007/978-1-4615-8398-1_5

Bajaj P, Chowdhury SK, Yucha R, Kelly EJ, Xiao G (2018) Emerging Kidney Models to Investigate Metabolism, Transport, and Toxicity of Drugs and Xenobiotics. Drug Metab Dispos 46(11):1692-1702 doi:10.1124/dmd.118.082958

Baker KJ, Bradley SE (1966) Binding of sulfobromophthalein (BSP) sodium by plasma albumin. Its role in hepatic BSP extraction. J Clin Invest 45(2):281-7 doi:10.1172/JCI105341

Bane V, Lehane M, Dikshit M, O'Riordan A, Furey A (2014) Tetrodotoxin: Chemistry, toxicity, source, distribution and detection. Toxins 6(2):693-755

References

Basit A, Radi Z, Vaidya VS, Karasu M, Prasad B (2019) Kidney Cortical Transporter Expression across Species Using Quantitative Proteomics. Drug Metab Dispos 47(8):802-808 doi:10.1124/dmd.119.086579

Bay C, Bajraktari-Sylejmani G, Haefeli WE, Burhenne J, Weiss J, Sauter M (2022) Functional Characterization of the Solute Carrier LAT-1 (SLC7A5/SLC2A3) in Human Brain Capillary Endothelial Cells with Rapid UPLC-MS/MS Quantification of Intracellular Isotopically Labelled L-Leucine. Int J Mol Sci 23(7) doi:10.3390/ijms23073637

Bayliss MK, Bell JA, Jenner WN, Park GR, Wilson K (1999) Utility of hepatocytes to model species differences in the metabolism of loxtidine and to predict pharmacokinetic parameters in rat, dog and man. Xenobiotica 29(3):253-68 doi:10.1080/004982599238650

Belzer M, Morales M, Jagadish B, Mash EA, Wright SH (2013) Substrate-dependent ligand inhibition of the human organic cation transporter OCT2. J Pharmacol Exp Ther 346(2):300-10 doi:10.1124/jpet.113.203257

Berezhkovskiy LM (2004) Volume of distribution at steady state for a linear pharmacokinetic system with peripheral elimination. J Pharm Sci 93(6):1628-40 doi:10.1002/jps.20073

Bertram JF, Douglas-Denton RN, Diouf B, Hughson MD, Hoy WE (2011) Human nephron number: implications for health and disease. Pediatr Nephrol 26(9):1529-33 doi:10.1007/s00467-011-1843-8

Besseghir K, Mosig D, Roch-Ramel F (1989) Transport of methotrexate by the *in vitro* isolated rabbit proximal tubule. J Pharmacol Exp Ther 250(2):688-95

Bessems J, Coecke S, Gouliarmou V, Whelan M, Worth A (2015) EURL ECVAM strategy for achieving 3Rs impact in the assessment of toxicokinetics and systemic toxicity. Publications Office of the European Union

Bodero M, Bovee TFH, Wang S, et al. (2018) Screening for the presence of lipophilic marine biotoxins in shellfish samples using the neuro-2a bioassay. Food Addit Contam Part A Chem Anal Control Expo Risk Assess 35(2):351-365 doi:10.1080/19440049.2017.1368720

Boof ML, Halabi A, Ufer M, Dingemanse J (2020) Impact of the organic cation transporter 2 inhibitor cimetidine on the single-dose pharmacokinetics of the glucosylceramide synthase inhibitor lucerastat in healthy subjects. Eur J Clin Pharmacol 76(3):431-437 doi:10.1007/s00228-019-02808-9

Boonnop RS, S. (2017) Interaction of Compounds Isolated from Boesenbergia rotunda with Human Renal Organic Anion and Cation Transporters. J Physiol Biomed Sci 30(2):5

Bowman CM, Benet LZ (2018) An examination of protein binding and protein-facilitated uptake relating to *in vitro-in vivo* extrapolation. Eur J Pharm Sci 123:502-514 doi:10.1016/j.ejps.2018.08.008

Bowman CM, Okochi H, Benet LZ (2019) The Presence of a Transporter-Induced Protein Binding Shift: A New Explanation for Protein-Facilitated Uptake and Improvement for *In vitro-In vivo* Extrapolation. Drug Metab Dispos 47(4):358-363 doi:10.1124/dmd.118.085779

Bradford MM (1976) A rapid and sensitive method for the quantitation of microgram quantities of protein utilizing the principle of protein-dye binding. Anal Biochem 72:248-54 doi:10.1006/abio.1976.9999

Brock WJ, Vore M (1984) Characterization of uptake of steroid glucuronides into isolated male and female

rat hepatocytes. J Pharmacol Exp Ther 229(1):175-81

Brouwer KL, Durham S, Vore M (1987) Multiple carriers for uptake of [3H]estradiol-17 beta(beta-D-glucuronide) in isolated rat hepatocytes. Mol Pharmacol 32(4):519-23

Brown RP, Delp MD, Lindstedt SL, Rhomberg LR, Beliles RP (1997a) Physiological parameter values for physiologically based pharmacokinetic models. Toxicol Ind Health 13(4):407-84 doi:10.1177/074823379701300401

Brown RP, Delp MD, Lindstedt SL, Rhomberg LR, Beliles RP (1997b) Physiological Parameter Values for Physiologically Based Pharmacokinetic Models. Toxicology and Industrial Health 13(4):407-484 doi:10.1177/074823379701300401

Burckhardt G (2012) Drug transport by Organic Anion Transporters (OATs). Pharmacol Ther 136(1):106-30 doi:10.1016/j.pharmthera.2012.07.010

Burlingham BT, Widlanski TS (2003) An Intuitive Look at the Relationship of Ki and IC50: A More General Use for the Dixon Plot. J Chem Educ 80(2):5 doi:https://doi.org/10.1021/ed080p214

Burt HJ, Neuhoff S, Almond L, et al. (2016) Metformin and cimetidine: Physiologically based pharmacokinetic modelling to investigate transporter mediated drug-drug interactions. Eur J Pharm Sci 88:70-82 doi:10.1016/j.ejps.2016.03.020

Camougis G, Takman BH, Tasse JR (1967) Potency difference between the zwitterion form and the cation forms of tetrodotoxin. Science 156(3782):1625-7 doi:10.1126/science.156.3782.1625

Campbell JL, Jr., Travis KZ, Clewell HJ, 3rd, et al. (2021) Integration of paraquat pharmacokinetic data across species using PBPK modelling. Toxicol Appl Pharmacol 417:115462 doi:10.1016/j.taap.2021.115462

Cantrill CH, J. B. (2017) Understanding the Interplay Between Uptake and Efflux Transporters Within *In vitro* Systems in Defining Hepatocellular Drug Concentrations. Journal of Pharmaceutical Sciences 106(9):11 doi:https://doi.org/10.1016/j.xphs.2017.04.056

Cattori V, van Montfoort JE, Stieger B, et al. (2001) Localization of organic anion transporting polypeptide 4 (Oatp4) in rat liver and comparison of its substrate specificity with Oatp1, Oatp2 and Oatp3. Pflugers Arch 443(2):188-95 doi:10.1007/s004240100697

Chan BS, Lazzaro VA, Seale JP, Duggin GG (1998) The renal excretory mechanisms and the role of organic cations in modulating the renal handling of paraquat. Pharmacol Ther 79(3):193-203 doi:10.1016/s0163-7258(98)00015-1

Chan BS, Seale JP, Duggin GG (1997) The mechanism of excretion of paraquat in rats. Toxicol Lett 90(1):1-9 doi:10.1016/s0378-4274(96)03820-9

Chan JCY, Tan SPF, Upton Z, Chan ECY (2019) Bottom-up physiologically-based biokinetic modelling as an alternative to animal testing. ALTEX 36(4):597-612 doi:10.14573/altex.1812051

Chapy H, Klieber S, Brun P, Gerbal-Chaloin S, Boulenc X, Nicolas O (2015) PBPK modeling of irbesartan: incorporation of hepatic uptake. Biopharm Drug Dispos 36(8):491-506 doi:10.1002/bdd.1961

Chen L, Ning J, Louisse J, Wesseling S, Rietjens IM (2018) Use of physiologically based kinetic modelling-facilitated reverse dosimetry to convert *in vitro* cytotoxicity data to predicted *in vivo* liver toxicity of lasiocarpine and riddelliine in rat. Food and Chemical Toxicology 116:216-226

Chen Y, Teranishi K, Li S, et al. (2009) Genetic variants in multidrug and toxic compound extrusion-1,

References

hMATE1, alter transport function. Pharmacogenomics J 9(2):127-36 doi:10.1038/tpj.2008.19

Chen Y, Zhang S, Sorani M, Giacomini KM (2007) Transport of paraquat by human organic cation transporters and multidrug and toxic compound extrusion family. J Pharmacol Exp Ther 322(2):695-700 doi:10.1124/jpet.107.123554

Chen YW, Yang YT, Hung DZ, Su CC, Chen KL (2012) Paraquat induces lung alveolar epithelial cell apoptosis via Nrf-2-regulated mitochondrial dysfunction and ER stress. Arch Toxicol 86(10):1547-58 doi:10.1007/s00204-012-0873-8

Choi GW, Lee YB, Cho HY (2019) Interpretation of Non-Clinical Data for Prediction of Human Pharmacokinetic Parameters: *In vitro-In vivo* Extrapolation and Allometric Scaling. Pharmaceutics 11(4) doi:10.3390/pharmaceutics11040168

Chu X, Bleasby K, Evers R (2013a) Species differences in drug transporters and implications for translating preclinical findings to humans. Expert Opin Drug Metab Toxicol 9(3):237-52 doi:10.1517/1742 5255.2013.741589

Chu X, Korzekwa K, Elsby R, et al. (2013b) Intracellular drug concentrations and transporters: measurement, modeling, and implications for the liver. Clin Pharmacol Ther 94(1):126-41 doi:10.1038/clpt.2013.78

Chui YC, Poon G, Law F (1988) Toxicokinetics and bioavailability of paraquat in rats following different routes of administration. Toxicol Ind Health 4(2):203-19 doi:10.1177/074823378800400205

Clark DG, McElligott TF, Hurst EW (1966) The toxicity of paraquat. Br J Ind Med 23(2):126-32 doi:10.1136/oem.23.2.126

Colas C, Ung PM, Schlessinger A (2016) SLC Transporters: Structure, Function, and Drug Discovery. Medchemcomm 7(6):1069-1081 doi:10.1039/C6MD00005C

Control CfD, Prevention (1996) Tetrodotoxin poisoning associated with eating puffer fish transported from Japan--California, 1996. MMWR Morbidity and mortality weekly report 45(19):389

Council NR (2011) Animal Research in a Global Environment: Meeting the Challenges: Proceedings of the November 2008 International Workshop. The National Academies Collection: Reports funded by National Institutes of Health, Washington (DC)

Cronholm T, Eriksson H, Gustafsson JA (1971) Excretion of endogenous steroids and metabolites of (4-14C) pregnenolone in bile of female rats. Eur J Biochem 19(3):424-32 doi:10.1111/j.1432-1033.1971. tb01332.x

Dave RA, Morris ME (2015) Quantitative structure-pharmacokinetic relationships for the prediction of renal clearance in humans. Drug Metab Dispos 43(1):73-81 doi:10.1124/dmd.114.059857

Dean L (2005) Chapter 1, Blood an the cells it contains. In: Blood groups and red cell antigens. National Center for Biotechnology Information (US). https://www.ncbi.nlm.nih.gov/books/NBK2263/ Accessed 23rd of May 2022

DeJongh J, Verhaar HJ, Hermens JL (1997) A quantitative property-property relationship (QPPR) approach to estimate *in vitro* tissue-blood partition coefficients of organic chemicals in rats and humans. Arch Toxicol 72(1):17-25

Di L, Keefer C, Scott DO, et al. (2012) Mechanistic insights from comparing intrinsic clearance values between human liver microsomes and hepatocytes to guide drug design. Eur J Med Chem 57:441-

8 doi:10.1016/j.ejmech.2012.06.043

Dinis-Oliveira RJ, Duarte JA, Sanchez-Navarro A, Remiao F, Bastos ML, Carvalho F (2008) Paraquat poisonings: mechanisms of lung toxicity, clinical features, and treatment. Crit Rev Toxicol 38(1):13-71 doi:10.1080/10408440701669959

Dresser MJ, Leabman MK, Giacomini KM (2001) Transporters involved in the elimination of drugs in the kidney: organic anion transporters and organic cation transporters. J Pharm Sci 90(4):397-421 doi:10.1002/1520-6017(200104)90:4<397::aid-jps1000>3.0.co;2-d

Dubin AE, Patapoutian A (2010) Nociceptors: the sensors of the pain pathway. J Clin Invest 120(11):3760-72 doi:10.1172/JCI42843

Duerden L (1994) Paraquat Dichloride Technical Concentrate: Acute Oral Toxicity to the Rat. . Zeneca Central Toxicology Laboratory, U.K.

Eckhardt U, Schroeder A, Stieger B, et al. (1999) Polyspecific substrate uptake by the hepatic organic anion transporter Oatp1 in stably transfected CHO cells. Am J Physiol 276(4):G1037-42 doi:10.1152/ajpgi.1999.276.4.G1037

EFSA, Knutsen HK, Alexander J, et al. (2017) Risks for public health related to the presence of tetrodotoxin (TTX) and TTX analogues in marine bivalves and gastropods. EFSA Journal 15(4):e04752

EPA U (2019) Paraquat Dichloride: Draft Human Health Risk Assessment in Support of Registration Review. p 103

Evans MV, Andersen ME (2000) Sensitivity analysis of a physiological model for 2,3,7,8-tetrachlorodibenzo-p-dioxin (TCDD): assessing the impact of specific model parameters on sequestration in liver and fat in the rat. Toxicol Sci 54(1):71-80 doi:10.1093/toxsci/54.1.71

Fabian E, Gomes C, Birk B, et al. (2019) *In vitro*-to-*in vivo* extrapolation (IVIVE) by PBTK modeling for animal-free risk assessment approaches of potential endocrine-disrupting compounds. Arch Toxicol 93(2):401-416 doi:10.1007/s00204-018-2372-z

Fagerholm U (2007) Prediction of human pharmacokinetics - renal metabolic and excretion clearance. J Pharm Pharmacol 59(11):1463-71 doi:10.1211/jpp.59.11.0002

Felmlee MA, Dave RA, Morris ME (2013) Mechanistic models describing active renal reabsorption and secretion: a simulation-based study. AAPS J 15(1):278-87 doi:10.1208/s12248-012-9437-3

Felmlee MA, Wang Q, Cui D, Roiko SA, Morris ME (2010) Mechanistic toxicokinetic model for gamma-hydroxybutyric acid: inhibition of active renal reabsorption as a potential therapeutic strategy. AAPS J 12(3):407-16 doi:10.1208/s12248-010-9197-x

Finch SC, Boundy MJ, Harwood DT (2018) The Acute Toxicity of Tetrodotoxin and Tetrodotoxin(-)Saxitoxin Mixtures to Mice by Various Routes of Administration. Toxins (Basel) 10(11) doi:10.3390/toxins10110423

Flecknell P (2002) Replacement, reduction and refinement. ALTEX 19(2):73-8

Flockerzi V (2008) Non-selective Cation Channels. In: Offermanns S, Rosenthal W (eds) Encyclopedia of Molecular Pharmacology. Springer Berlin Heidelberg, Berlin, Heidelberg, p 870-871

Forker EL, Luxon BA (1981) Albumin helps mediate removal of taurocholate by rat liver. J Clin Invest 67(5):1517-22 doi:10.1172/jci110182

Forker EL, Luxon BA (1983) Albumin-mediated transport of rose bengal by perfused rat liver. Kinetics of

the reaction at the cell surface. J Clin Invest 72(5):1764-71 doi:10.1172/JCI111136

Ge S, Tu Y, Hu M (2016) Challenges and Opportunities with Predicting *in vivo* Phase II Metabolism via Glucuronidation from *in vitro* Data. Curr Pharmacol Rep 2(6):326-338 doi:10.1007/s40495-016-0076-8

George B, Wen X, Jaimes EA, Joy MS, Aleksunes LM (2021) *In vitro* Inhibition of Renal OCT2 and MATE1 Secretion by Antiemetic Drugs. Int J Mol Sci 22(12) doi:10.3390/ijms22126439

George B, You D, Joy MS, Aleksunes LM (2017) Xenobiotic transporters and kidney injury. Adv Drug Deliv Rev 116:73-91 doi:10.1016/j.addr.2017.01.005

Gotoh Y, Kato Y, Stieger B, Meier PJ, Sugiyama Y (2002) Gender difference in the Oatp1-mediated tubular reabsorption of estradiol 17beta-D-glucuronide in rats. Am J Physiol Endocrinol Metab 282(6):E1245-54 doi:10.1152/ajpendo.00363.2001

Greim HS, R. (2018) Toxicology and risk assessment: a comprehensive introduction, second edn

Guguen-Guillouzo C, Guillouzo A (2010) General review on *in vitro* hepatocyte models and their applications. Methods Mol Biol 640:1-40 doi:10.1007/978-1-60761-688-7_1

Gulden M, Morchel S, Tahan S, Seibert H (2002) Impact of protein binding on the availability and cytotoxic potency of organochlorine pesticides and chlorophenols *in vitro*. Toxicology 175(1-3):201-13 doi:10.1016/s0300-483x(02)00085-9

Hacker K, Maas R, Kornhuber J, Fromm MF, Zolk O (2015) Substrate-Dependent Inhibition of the Human Organic Cation Transporter OCT2: A Comparison of Metformin with Experimental Substrates. PLoS One 10(9):e0136451 doi:10.1371/journal.pone.0136451

Hagenbuch B, Meier PJ (2003) The superfamily of organic anion transporting polypeptides. Biochim Biophys Acta 1609(1):1-18 doi:10.1016/s0005-2736(02)00633-8

Hall C, Lueshen E, Mosat A, Linninger AA (2012) Interspecies scaling in pharmacokinetics: a novel whole-body physiologically based modeling framework to discover drug biodistribution mechanisms *in vivo*. J Pharm Sci 101(3):1221-41 doi:10.1002/jps.22811

Hallifax D, Houston JB (2006) Binding of drugs to hepatic microsomes: comment and assessment of current prediction methodology with recommendation for improvement. Drug Metab Dispos 34(4):724-6; author reply 727 doi:10.1124/dmd.105.007658

Hamasaki K, Kogure K, Ohwada K (1996) A biological method for the quantitative measurement of tetrodotoxin (TTX): tissue culture bioassay in combination with a water-soluble tetrazolium salt. Toxicon 34(4):490-5 doi:10.1016/0041-0101(95)00151-4

Han LW, Gao C, Zhang Y, Wang J, Mao Q (2019) Transport of Bupropion and its Metabolites by the Model CHO and HEK293 Cell Lines. Drug Metab Lett 13(1):25-36 doi:10.2174/1872312813666181129101507

Harris AJ, Shaddock JG, Delongchamp R, Dragan Y, Casciano DA (2004) Comparison of Basal gene expression in cultured primary rat hepatocytes and freshly isolated rat hepatocytes. Toxicol Mech Methods 14(5):257-70 doi:10.1080/15376520490434629

Hayer-Zillgen M, Bruss M, Bonisch H (2002) Expression and pharmacological profile of the human organic cation transporters hOCT1, hOCT2 and hOCT3. Br J Pharmacol 136(6):829-36 doi:10.1038/sj.bjp.0704785

Hazai E, Hazai I, Ragueneau-Majlessi I, Chung SP, Bikadi Z, Mao Q (2013) Predicting substrates of

the human breast cancer resistance protein using a support vector machine method. BMC Bioinformatics 14:130 doi:10.1186/1471-2105-14-130

Herraez E, Sanchez-Vicente L, Macias RIR, Briz O, Marin JJG (2017) Usefulness of the MRP2 promoter to overcome the chemoresistance of gastrointestinal and liver tumors by enhancing the expression of the drug transporter OATP1B1. Oncotarget 8(21):34617-34629 doi:10.18632/oncotarget.16119

Hirano M, Maeda K, Shitara Y, Sugiyama Y (2004) Contribution of OATP2 (OATP1B1) and OATP8 (OATP1B3) to the hepatic uptake of pitavastatin in humans. J Pharmacol Exp Ther 311(1):139-46 doi:10.1124/jpet.104.068056

Hjelle JJ, Klaassen CD (1984) Glucuronidation and biliary excretion of acetaminophen in rats. J Pharmacol Exp Ther 228(2):407-13

Holzer P (2011) Acid sensing by visceral afferent neurones. Acta Physiol (Oxf) 201(1):63-75 doi:10.1111/j.1748-1716.2010.02143.x

Hong B, Chen H, Han J, et al. (2017) A study of 11-[3H]-tetrodotoxin absorption, distribution, metabolism and excretion (ADME) in adult sprague-dawley rats. Marine drugs 15(6):159

Hong B, Sun J, Zheng H, et al. (2018) Effect of Tetrodotoxin Pellets in a Rat Model of Postherpetic Neuralgia. Mar Drugs 16(6) doi:10.3390/md16060195

Hort V, Arnich N, Guerin T, Lavison-Bompard G, Nicolas M (2020) First Detection of Tetrodotoxin in Bivalves and Gastropods from the French Mainland Coasts. Toxins (Basel) 12(9) doi:10.3390/toxins12090599

Houston JB (1994a) Relevance of *in vitro* kinetic parameters to *in vivo* metabolism of xenobiotics. Toxicol *In vitro* 8(4):507-12 doi:10.1016/0887-2333(94)90002-7

Houston JB (1994b) Utility of *in vitro* drug metabolism data in predicting *in vivo* metabolic clearance. Biochemical pharmacology 47(9):1469-1479

Houze P, Baud FJ, Mouy R, Bismuth C, Bourdon R, Scherrmann JM (1990) Toxicokinetics of paraquat in humans. Hum Exp Toxicol 9(1):5-12 doi:10.1177/096032719000900103

Huang H-N, Lin J, Lin H-L (2008) Identification and quantification of tetrodotoxin in the marine gastropod Nassarius by LC–MS. Toxicon 51(5):774-779

Huang W, Isoherranen N (2018) Development of a Dynamic Physiologically Based Mechanistic Kidney Model to Predict Renal Clearance. CPT Pharmacometrics Syst Pharmacol 7(9):593-602 doi:10.1002/psp4.12321

Ishizuka H, Konno K, Naganuma H, et al. (1998) Transport of temocaprilat into rat hepatocytes: role of organic anion transporting polypeptide. J Pharmacol Exp Ther 287(1):37-42

Izumi S, Nozaki Y, Komori T, et al. (2013) Substrate-dependent inhibition of organic anion transporting polypeptide 1B1: comparative analysis with prototypical probe substrates estradiol-17beta-glucuronide, estrone-3-sulfate, and sulfobromophthalein. Drug Metab Dispos 41(10):1859-66 doi:10.1124/dmd.113.052290

Izumi S, Nozaki Y, Kusuhara H, et al. (2018) Relative Activity Factor (RAF)-Based Scaling of Uptake Clearance Mediated by Organic Anion Transporting Polypeptide (OATP) 1B1 and OATP1B3 in Human Hepatocytes. Mol Pharm 15(6):2277-2288 doi:10.1021/acs.molpharmaceut.8b00138

Jamei M, Bajot F, Neuhoff S, et al. (2014) A mechanistic framework for *in vitro-in vivo* extrapolation

of liver membrane transporters: prediction of drug-drug interaction between rosuvastatin and cyclosporine. Clin Pharmacokinet 53(1):73-87 doi:10.1007/s40262-013-0097-y

Jenkinson SE, Chung GW, van Loon E, Bakar NS, Dalzell AM, Brown CD (2012) The limitations of renal epithelial cell line HK-2 as a model of drug transporter expression and function in the proximal tubule. Pflugers Arch 464(6):601-11 doi:10.1007/s00424-012-1163-2

Jetter A, Kullak-Ublick GA (2020) Drugs and hepatic transporters: A review. Pharmacol Res 154:104234 doi:10.1016/j.phrs.2019.04.018

Jones HM, Barton HA, Lai Y, et al. (2012) Mechanistic pharmacokinetic modeling for the prediction of transporter-mediated disposition in humans from sandwich culture human hepatocyte data. Drug Metab Dispos 40(5):1007-17 doi:10.1124/dmd.111.042994

Jusko WJ, Levy G (1970) Pharmacokinetic evidence for saturable renal tubular reabsorption of riboflavin. J Pharm Sci 59(6):765-72 doi:10.1002/jps.2600590608

Kamelia L, Louisse J, de Haan L, Rietjens I, Boogaard PJ (2017) Prenatal developmental toxicity testing of petroleum substances: Application of the mouse embryonic stem cell test (EST) to compare *in vitro* potencies with potencies observed *in vivo*. Toxicol *In vitro* 44:303-312 doi:10.1016/j.tiv.2017.07.018

Kanai N, Lu R, Bao Y, Wolkoff AW, Vore M, Schuster VL (1996) Estradiol 17 beta-D-glucuronide is a high-affinity substrate for oatp organic anion transporter. Am J Physiol 270(2 Pt 2):F326-31 doi:10.1152/ajprenal.1996.270.2.F326

Kanno S, Hirano S, Mukai T, et al. (2019) Cellular uptake of paraquat determines subsequent toxicity including mitochondrial damage in lung epithelial cells. Leg Med (Tokyo) 37:7-14 doi:10.1016/j.legalmed.2018.11.008

Kao CY (1966) Tetrodotoxin, saxitoxin and their significance in the study of excitation phenomena. Pharmacol Rev 18(2):997-1049

Kao CY, Fuhrman FA (1963) Pharmacological studies on tarichatoxin, a potent neurotoxin. J Pharmacol Exp Ther 140:31-40

Kasteel EE, Westerink RH (2017) Comparison of the acute inhibitory effects of Tetrodotoxin (TTX) in rat and human neuronal networks for risk assessment purposes. Toxicol Lett 270:12-16 doi:10.1016/j.toxlet.2017.02.014

Kasteel EEJ, Lautz LS, Culot M, Kramer NI, Zwartsen A (2021) Application of *in vitro* data in physiologically-based kinetic models for quantitative *in vitro-in vivo* extrapolation: A case-study for baclofen. Toxicol *In vitro* 76:105223 doi:10.1016/j.tiv.2021.105223

Keogh JP (2012) Membrane transporters in drug development. Adv Pharmacol 63:1-42 doi:10.1016/B978-0-12-398339-8.00001-X

Kiener M, Roldan N, Machahua C, et al. (2021) Human-Based Advanced *in vitro* Approaches to Investigate Lung Fibrosis and Pulmonary Effects of COVID-19. Front Med (Lausanne) 8:644678 doi:10.3389/fmed.2021.644678

Kilford PJ, Gertz M, Houston JB, Galetin A (2008) Hepatocellular binding of drugs: correction for unbound fraction in hepatocyte incubations using microsomal binding or drug lipophilicity data. Drug Metab Dispos 36(7):1194-7 doi:10.1124/dmd.108.020834

Kim H, Lee SW, Baek KM, Park JS, Min JH (2011) Continuous hypoxia attenuates paraquat-induced cytotoxicity in the human A549 lung carcinoma cell line. Exp Mol Med 43(9):494-500 doi:10.3858/emm.2011.43.9.056

Kimbrough RD, Gaines TB (1970) Toxicity of paraquat to rats and its effect on rat lungs. Toxicol Appl Pharmacol 17(3):679-90 doi:10.1016/0041-008x(70)90042-6

Koepsell H (2013) The SLC22 family with transporters of organic cations, anions and zwitterions. Mol Aspects Med 34(2-3):413-35 doi:10.1016/j.mam.2012.10.010

Koepsell H, Schmitt BM, Gorboulev V (2003) Organic cation transporters. Rev Physiol Biochem Pharmacol 150:36-90 doi:10.1007/s10254-003-0017-x

Kogure K, Tamplin ML, Simidu U, Colwell RR (1988) A tissue culture assay for tetrodotoxin, saxitoxin and related toxins. Toxicon 26(2):191-7 doi:10.1016/0041-0101(88)90171-7

Kohane DS, Lu NT, Gökgöl-Kline AC, et al. (2000) The local anesthetic properties and toxicity of saxitonin homologues for rat sciatic nerve block *in vivo*.

Kohane DS, Yieh J, Lu NT, Langer R, Strichartz GR, Berde CB (1998) A re-examination of tetrodotoxin for prolonged duration local anesthesia. Anesthesiology 89(1):119-31 doi:10.1097/00000542-199807000-00019

Komiya I (1986) Urine flow dependence of renal clearance and interrelation of renal reabsorption and physicochemical properties of drugs. Drug Metab Dispos 14(2):239-45

Kotani N, Maeda K, Debori Y, et al. (2012) Expression and transport function of drug uptake transporters in differentiated HepaRG cells. Mol Pharm 9(12):3434-41 doi:10.1021/mp300171p

Kouzuki H, Suzuki H, Ito K, Ohashi R, Sugiyama Y (1999) Contribution of organic anion transporting polypeptide to uptake of its possible substrates into rat hepatocytes. J Pharmacol Exp Ther 288(2):627-34

Krewski D, Acosta D, Jr., Andersen M, et al. (2010) Toxicity testing in the 21st century: a vision and a strategy. J Toxicol Environ Health B Crit Rev 13(2-4):51-138 doi:10.1080/10937404.2010.483176

Kumar AR, Prasad B, Bhatt DK, Mathialagan S, Varma MVS, Unadkat JD (2020) *In vivo*-to-*In vitro* Extrapolation of Transporter-Mediated Renal Clearance: Relative Expression Factor Versus Relative Activity Factor Approach. Drug Metab Dispos 49(6):470-478 doi:10.1124/dmd.121.000367

Kumar V, Yin J, Billington S, et al. (2018) The Importance of Incorporating OCT2 Plasma Membrane Expression and Membrane Potential in IVIVE of Metformin Renal Secretory Clearance. Drug Metab Dispos 46(10):1441-1445 doi:10.1124/dmd.118.082313

Kunze A, Huwyler J, Camenisch G, Poller B (2014) Prediction of organic anion-transporting polypeptide 1B1- and 1B3-mediated hepatic uptake of statins based on transporter protein expression and activity data. Drug Metab Dispos 42(9):1514-21 doi:10.1124/dmd.114.058412

Le Vee M, Jigorel E, Glaise D, Gripon P, Guguen-Guillouzo C, Fardel O (2006) Functional expression of sinusoidal and canalicular hepatic drug transporters in the differentiated human hepatoma HepaRG cell line. Eur J Pharm Sci 28(1-2):109-17 doi:10.1016/j.ejps.2006.01.004

Le Vee M, Noel G, Jouan E, Stieger B, Fardel O (2013) Polarized expression of drug transporters in differentiated human hepatoma HepaRG cells. Toxicol *In vitro* 27(6):1979-86 doi:10.1016/j.

References

tiv.2013.07.003

Lechner C, Monning U, Reichel A, Fricker G (2021) Potential and Limits of Kidney Cells for Evaluation of Renal Excretion. Pharmaceuticals (Basel) 14(9) doi:10.3390/ph14090908

Lechner CA (2014) Nierenzellen als In-vitro-Modell zur Evaluierung der renalen Sekretion von Arzneistoffkandidaten Universität Heidelberg

Lee HH, Leake BF, Kim RB, Ho RH (2017) Contribution of Organic Anion-Transporting Polypeptides 1A/1B to Doxorubicin Uptake and Clearance. Mol Pharmacol 91(1):14-24 doi:10.1124/mol.116.105544

Li H, Zhang M, Vervoort J, Rietjens IM, van Ravenzwaay B, Louisse J (2017a) Use of physiologically based kinetic modeling-facilitated reverse dosimetry of *in vitro* toxicity data for prediction of *in vivo* developmental toxicity of tebuconazole in rats. Toxicology Letters 266:85-93

Li H, Zhang M, Vervoort J, Rietjens IM, van Ravenzwaay B, Louisse J (2017b) Use of physiologically based kinetic modeling-facilitated reverse dosimetry of *in vitro* toxicity data for prediction of *in vivo* developmental toxicity of tebuconazole in rats. Toxicol Lett 266:85-93 doi:10.1016/j.toxlet.2016.11.017

Li S, Zhao J, Huang R, et al. (2017c) Development and Application of Human Renal Proximal Tubule Epithelial Cells for Assessment of Compound Toxicity. Curr Chem Genom Transl Med 11:19-30 doi:10.2174/2213988501711010019

Li X, Mu P, Wen J, Deng Y (2017d) Carrier-Mediated and Energy-Dependent Uptake and Efflux of Deoxynivalenol in Mammalian Cells. Sci Rep 7(1):5889 doi:10.1038/s41598-017-06199-8

Lock EAW, M. F. (2010) Paraquat. In: Krieger R (ed) Hayes' Handbook of Pesticide Toxicology. Elsevier Inc.

Lohitnavy M, Chitsakhon A, Jomprasert K, Lohitnavy O, Reisfeld B (2017) Development of a physiologically based pharmacokinetic model of paraquat. Annu Int Conf IEEE Eng Med Biol Soc 2017:2732-2735 doi:10.1109/EMBC.2017.8037422

Lonza (2022) RPTEC – Human Renal Proximal Tubule Epithelial Cells. In. https://bioscience.lonza.com/lonza_bs/NL/en/Primary-and-Stem-Cells/p/000000000000185055/RPTEC-%E2%80%93-Human-Renal-Proximal-Tubule-Epithelial-Cells Accessed 29th of May 2022

Lote CJ (2012) Essential Anatomy of the Kidney., 5 edn. Springer, New York

Louisse J, Alewijn M, Peijnenburg A, et al. (2020) Towards harmonization of test methods for *in vitro* hepatic clearance studies. Toxicol *In vitro* 63:104722 doi:10.1016/j.tiv.2019.104722

Louisse J, Beekmann K, Rietjens IM (2017) Use of Physiologically Based Kinetic Modeling-Based Reverse Dosimetry to Predict *in vivo* Toxicity from *in vitro* Data. Chem Res Toxicol 30(1):114-125 doi:10.1021/acs.chemrestox.6b00302

Louisse J, Bosgra S, Blaauboer B, Rietjens ICM, Verwei M (2014) Prediction of *in vivo* developmental toxicity of all-trans-retinoic acid based on *in vitro* toxicity data and *in silico* physiologically based kinetic modeling. Archives of Toxicology:1-14 doi:10.1007/s00204-014-1289-4

Louisse J, Bosgra S, Blaauboer BJ, Rietjens IM, Verwei M (2015) Prediction of *in vivo* developmental toxicity of all-trans-retinoic acid based on *in vitro* toxicity data and *in silico* physiologically based kinetic modeling. Arch Toxicol 89(7):1135-48 doi:10.1007/s00204-014-1289-4

Louisse J, de Jong E, van de Sandt JJ, et al. (2010) The use of *in vitro* toxicity data and physiologically based kinetic modeling to predict dose-response curves for *in vivo* developmental toxicity of glycol ethers in rat and man. Toxicol Sci 118(2):470-84 doi:10.1093/toxsci/kfq270

Lowry OH, Rosebrough NJ, Farr AL, Randall RJ (1951) Protein measurement with the Folin phenol reagent. J Biol Chem 193(1):265-75

Lozano E, Herraez E, Briz O, et al. (2013) Role of the plasma membrane transporter of organic cations OCT1 and its genetic variants in modern liver pharmacology. Biomed Res Int 2013:692071 doi:10.1155/2013/692071

Lu JX, J. (2019) Chapter 101 - Poisoning: Kinetics to Therapeutics, Third Edition edn. Elsevier

Lundquist P, Englund G, Skogastierna C, et al. (2014) Functional ATP-binding cassette drug efflux transporters in isolated human and rat hepatocytes significantly affect assessment of drug disposition. Drug Metab Dispos 42(3):448-58 doi:10.1124/dmd.113.054528

Maeda K (2015) Organic anion transporting polypeptide (OATP)1B1 and OATP1B3 as important regulators of the pharmacokinetics of substrate drugs. Biol Pharm Bull 38(2):155-68 doi:10.1248/bpb.b14-00767

Marada VV, Florl S, Kuhne A, Muller J, Burckhardt G, Hagos Y (2015) Interaction of human organic anion transporter 2 (OAT2) and sodium taurocholate cotransporting polypeptide (NTCP) with antineoplastic drugs. Pharmacol Res 91:78-87 doi:10.1016/j.phrs.2014.11.002

Marcil J, Walczak JS, Guindon J, Ngoc AH, Lu S, Beaulieu P (2006) Antinociceptive effects of tetrodotoxin (TTX) in rodents. Br J Anaesth 96(6):761-8 doi:10.1093/bja/ael096

Martinez FJ, Collard HR, Pardo A, et al. (2017) Idiopathic pulmonary fibrosis. Nat Rev Dis Primers 3:17074 doi:10.1038/nrdp.2017.74

Martinez MN (2011) Factors influencing the use and interpretation of animal models in the development of parenteral drug delivery systems. AAPS J 13(4):632-49 doi:10.1208/s12248-011-9303-8

Masland RH (2004) Neuronal cell types. Curr Biol 14(13):R497-500 doi:10.1016/j.cub.2004.06.035

Mathew J, Sankar P, Varacallo M (2022) Physiology, Blood Plasma StatPearls. Treasure Island (FL)

Mathialagan S, Piotrowski MA, Tess DA, Feng B, Litchfield J, Varma MV (2017) Quantitative Prediction of Human Renal Clearance and Drug-Drug Interactions of Organic Anion Transporter Substrates Using *In vitro* Transport Data: A Relative Activity Factor Approach. Drug Metab Dispos 45(4):409-417 doi:10.1124/dmd.116.074294

Matsumoto T, Ishizaki Y, Mochizuki K, et al. (2017) Urinary Excretion of Tetrodotoxin Modeled in a Porcine Renal Proximal Tubule Epithelial Cell Line, LLC-PK(1). Mar Drugs 15(7) doi:10.3390/md15070225

Mehani S (1972) The toxic effect of paraquat in rabbits and rats. Ain Shams med J 23:3

Melnikova DI, Khotimchenko YS, Magarlamov TY (2018) Addressing the Issue of Tetrodotoxin Targeting. Mar Drugs 16(10) doi:10.3390/md16100352

More SS, Li S, Yee SW, et al. (2010) Organic cation transporters modulate the uptake and cytotoxicity of picoplatin, a third-generation platinum analogue. Mol Cancer Ther 9(4):1058-69 doi:10.1158/1535-7163.MCT-09-1084

Morikawa A, Goto Y, Suzuki H, Hirohashi T, Sugiyama Y (2000) Biliary excretion of 17beta-estradiol

17beta-D-glucuronide is predominantly mediated by cMOAT/MRP2. Pharm Res 17(5):546-52

Morrissey KM, Stocker SL, Wittwer MB, Xu L, Giacomini KM (2013) Renal transporters in drug development. Annu Rev Pharmacol Toxicol 53:503-29 doi:10.1146/annurev-pharmtox-011112-140317

Motohashi H, Inui K (2013) Organic cation transporter OCTs (SLC22) and MATEs (SLC47) in the human kidney. AAPS J 15(2):581-8 doi:10.1208/s12248-013-9465-7

Moxon TE, Li H, Lee MY, et al. (2020) Application of physiologically based kinetic (PBK) modelling in the next generation risk assessment of dermally applied consumer products. Toxicol *In vitro* 63:104746 doi:10.1016/j.tiv.2019.104746

Muhamad H, Ismail BS, Sameni M, Mat N (2011) Adsorption study of 14C-paraquat in two Malaysian agricultural soils. Environ Monit Assess 176(1-4):43-50 doi:10.1007/s10661-010-1565-6

Muller F, Konig J, Hoier E, Mandery K, Fromm MF (2013) Role of organic cation transporter OCT2 and multidrug and toxin extrusion proteins MATE1 and MATE2-K for transport and drug interactions of the antiviral lamivudine. Biochem Pharmacol 86(6):808-15 doi:10.1016/j.bcp.2013.07.008

Murray RE, Gibson JE (1974) Paraquat disposition in rats, guinea pigs and monkeys. Toxicol Appl Pharmacol 27(2):283-91 doi:10.1016/0041-008x(74)90199-9

Nakagawa H, Hirata T, Terada T, et al. (2008) Roles of organic anion transporters in the renal excretion of perfluorooctanoic acid. Basic Clin Pharmacol Toxicol 103(1):1-8 doi:10.1111/j.1742-7843.2007.00155.x

Neef C, Meijer DK (1984) Structure-pharmacokinetics relationship of quaternary ammonium compounds. Correlation of physicochemical and pharmacokinetic parameters. Naunyn Schmiedebergs Arch Pharmacol 328(2):111-8 doi:10.1007/BF00512059

Nicolas J, Hendriksen PJ, de Haan LH, Koning R, Rietjens IM, Bovee TF (2015) *In vitro* detection of cardiotoxins or neurotoxins affecting ion channels or pumps using beating cardiomyocytes as alternative for animal testing. Toxicol *In vitro* 29(2):281-8 doi:10.1016/j.tiv.2014.11.010

Nicolas J, Hendriksen PJ, van Kleef RG, et al. (2014) Detection of marine neurotoxins in food safety testing using a multielectrode array. Molecular nutrition & food research 58(12):2369-2378

Nies AT, Koepsell H, Damme K, Schwab M (2011) Organic cation transporters (OCTs, MATEs), *in vitro* and *in vivo* evidence for the importance in drug therapy. Handb Exp Pharmacol(201):105-67 doi:10.1007/978-3-642-14541-4_3

Nieskens TT, Peters JG, Schreurs MJ, et al. (2016) A Human Renal Proximal Tubule Cell Line with Stable Organic Anion Transporter 1 and 3 Expression Predictive for Antiviral-Induced Toxicity. AAPS J 18(2):465-75 doi:10.1208/s12248-016-9871-8

Ning J, Chen L, Rietjens I (2019a) Role of toxicokinetics and alternative testing strategies in pyrrolizidine alkaloid toxicity and risk assessment; state-of-the-art and future perspectives. Food Chem Toxicol 131:110572 doi:10.1016/j.fct.2019.110572

Ning J, Chen L, Strikwold M, Louisse J, Wesseling S, Rietjens I (2019b) Use of an *in vitro-in silico* testing strategy to predict inter-species and inter-ethnic human differences in liver toxicity of the pyrrolizidine alkaloids lasiocarpine and riddelliine. Arch Toxicol 93(3):801-818 doi:10.1007/s00204-019-02397-7

Ning J, Chen L, Strikwold M, Louisse J, Wesseling S, Rietjens IM (2019c) Use of an *in vitro–in silico*

testing strategy to predict inter-species and inter-ethnic human differences in liver toxicity of the pyrrolizidine alkaloids lasiocarpine and riddelliine. Archives of toxicology:1-18

Noorlander A, Fabian E, van Ravenzwaay B, Rietjens I (2021a) Novel testing strategy for prediction of rat biliary excretion of intravenously administered estradiol-17beta glucuronide. Arch Toxicol 95(1):91-102 doi:10.1007/s00204-020-02908-x

Noorlander A, Wesseling S, Rietjens I, van Ravenzwaay B (2021b) Incorporating renal excretion via the OCT2 transporter in physiologically based kinetic modelling to predict *in vivo* kinetics of mepiquat in rat. Toxicol Lett 343:34-43 doi:10.1016/j.toxlet.2021.02.013

Noorlander A, Zhang M, van Ravenzwaay B, Rietjens I (2022) Use of Physiologically Based Kinetic Modeling-Facilitated Reverse Dosimetry to Predict *In vivo* Acute Toxicity of Tetrodotoxin in Rodents. Toxicol Sci 187(1):127-138 doi:10.1093/toxsci/kfac022

Obach RS (1996) The importance of nonspecific binding in *in vitro* matrices, its impact on enzyme kinetic studies of drug metabolism reactions, and implications for *in vitro-in vivo* correlations. Drug Metab Dispos 24(10):1047-9

Obach RS (1999) Prediction of human clearance of twenty-nine drugs from hepatic microsomal intrinsic clearance data: an examination of *in vitro* half-life approach and nonspecific binding to microsomes. Drug Metabolism and Disposition 27(11):1350-1359

Paine SW, Menochet K, Denton R, McGinnity DF, Riley RJ (2011) Prediction of human renal clearance from preclinical species for a diverse set of drugs that exhibit both active secretion and net reabsorption. Drug Metab Dispos 39(6):1008-13 doi:10.1124/dmd.110.037267

Patel M, Taskar KS, Zamek-Gliszczynski MJ (2016) Importance of Hepatic Transporters in Clinical Disposition of Drugs and Their Metabolites. J Clin Pharmacol 56 Suppl 7:S23-39 doi:10.1002/jcph.671

Pelkonen O, Turpeinen M (2007) *In vitro-in vivo* extrapolation of hepatic clearance: biological tools, scaling factors, model assumptions and correct concentrations. Xenobiotica 37(10-11):1066-89 doi:10.1080/00498250701620726

Pizzutti IR, Vela GM, de Kok A, et al. (2016) Determination of paraquat and diquat: LC-MS method optimization and validation. Food Chem 209:248-55 doi:10.1016/j.foodchem.2016.04.069

Poirier A, Cascais AC, Funk C, Lave T (2009) Prediction of pharmacokinetic profile of valsartan in human based on *in vitro* uptake transport data. J Pharmacokinet Pharmacodyn 36(6):585-611 doi:10.1007/s10928-009-9139-3

Poulin P, Theil FP (2000) A priori prediction of tissue:plasma partition coefficients of drugs to facilitate the use of physiologically-based pharmacokinetic models in drug discovery. J Pharm Sci 89(1):16-35 doi:10.1002/(SICI)1520-6017(200001)89:1<16::AID-JPS3>3.0.CO;2-E

Prasad B, Unadkat JD (2014) Optimized approaches for quantification of drug transporters in tissues and cells by MRM proteomics. AAPS J 16(4):634-48 doi:10.1208/s12248-014-9602-y

Probst RJ, Lim JM, Bird DN, Pole GL, Sato AK, Claybaugh JR (2006) Gender differences in the blood volume of conscious Sprague-Dawley rats. J Am Assoc Lab Anim Sci 45(2):49-52

Proudfoot AT, Stewart MS, Levitt T, Widdop B (1979) Paraquat poisoning: significance of plasma-paraquat concentrations. Lancet 2(8138):330-2 doi:10.1016/s0140-6736(79)90345-3

Punt A, Aartse A, Bovee TFH, et al. (2019) Quantitative *in vitro*-to-*in vivo* extrapolation (QIVIVE) of

estrogenic and anti-androgenic potencies of BPA and BADGE analogues. Arch Toxicol 93(7):1941-1953 doi:10.1007/s00204-019-02479-6

Punt A, Freidig AP, Delatour T, et al. (2008) A physiologically based biokinetic (PBBK) model for estragole bioactivation and detoxification in rat. Toxicol Appl Pharmacol 231(2):248-59 doi:10.1016/j.taap.2008.04.011

Punt A, Louisse J, Beekmann K, et al. (2022a) Predictive performance of next generation human physiologically based kinetic (PBK) models based on *in vitro* and *in silico* input data. ALTEX 39(2):221-234 doi:10.14573/altex.2108301

Punt A, Louisse J, Pinckaers N, Fabian E, van Ravenzwaay B (2022b) Predictive Performance of Next Generation Physiologically Based Kinetic (PBK) Model Predictions in Rats Based on *In vitro* and *In silico* Input Data. Toxicol Sci 186(1):18-28 doi:10.1093/toxsci/kfab150

Punt A, Pinckaers N, Peijnenburg A, Louisse J (2020) Development of a Web-Based Toolbox to Support Quantitative In-Vitro-to-In-Vivo Extrapolations (QIVIVE) within Nonanimal Testing Strategies. Chem Res Toxicol doi:10.1021/acs.chemrestox.0c00307

Richard AM, Judson RS, Houck KA, et al. (2016) ToxCast Chemical Landscape: Paving the Road to 21st Century Toxicology. Chem Res Toxicol 29(8):1225-51 doi:10.1021/acs.chemrestox.6b00135

Richert L, Liguori MJ, Abadie C, et al. (2006) Gene expression in human hepatocytes in suspension after isolation is similar to the liver of origin, is not affected by hepatocyte cold storage and cryopreservation, but is strongly changed after hepatocyte plating. Drug Metab Dispos 34(5):870-9 doi:10.1124/dmd.105.007708

Rietjens I, Ning J, Chen L, Wesseling S, Strikwold M, Louisse J (2019) Selecting the dose metric in reverse dosimetry based QIVIVE : Reply to 'Comment on 'Use of an *in vitro-in silico* testing strategy to predict inter-species and inter-ethnic human differences in liver toxicity of the pyrrolizidine alkaloids lasiocarpine and riddelliine' by Ning et al., Arch Toxicol doi: https://doi.org/10.1007/s00204-019-02397-7', Arch Toxicol doi: https://doi.org/10.1007/s0020 4-019-02421-w. Arch Toxicol 93(5):1467-1469 doi:10.1007/s00204-019-02438-1

Rietjens IM, Louisse J, Punt A (2011) Tutorial on physiologically based kinetic modeling in molecular nutrition and food research. Mol Nutr Food Res 55(6):941-56 doi:10.1002/mnfr.201000655

Roberts JRRR, J. (2013) Recognition and Management of Pesticide Poisonings, 6th edn. Environmental protection agency, United states of America

Robinson DR, Gebhart GF (2008) Inside information: the unique features of visceral sensation. Mol Interv 8(5):242-53 doi:10.1124/mi.8.5.9

Rodgers T, Rowland M (2006) Physiologically based pharmacokinetic modelling 2: predicting the tissue distribution of acids, very weak bases, neutrals and zwitterions. J Pharm Sci 95(6):1238-57 doi:10.1002/jps.20502

Rollins DE, Klaassen CD (1979) Biliary excretion of drugs in man. Clin Pharmacokinet 4(5):368-79 doi:10.2165/00003088-197904050-00003

Rossini GP, Hartung T (2012) Towards tailored assays for cell-based approaches to toxicity testing. ALTEX 29(4):359-72 doi:10.14573/altex.2012.4.359

Russel FG, Wouterse AC, van Ginneken CA (1987) Physiologically based pharmacokinetic model for the

renal clearance of salicyluric acid and the interaction with phenolsulfonphthalein in the dog. Drug Metab Dispos 15(5):695-701

Sahi J, Grepper S, Smith C (2010) Hepatocytes as a tool in drug metabolism, transport and safety evaluations in drug discovery. Curr Drug Discov Technol 7(3):188-98 doi:10.2174/157016310793180576

Samai M, Hague T, Naughton DP, Gard PR, Chatterjee PK (2008) Reduction of paraquat-induced renal cytotoxicity by manganese and copper complexes of EGTA and EHPG. Free Radic Biol Med 44(4):711-21 doi:10.1016/j.freeradbiomed.2007.11.001

Sanchez-Romero N, Martinez-Gimeno L, Caetano-Pinto P, et al. (2020) A simple method for the isolation and detailed characterization of primary human proximal tubule cells for renal replacement therapy. Int J Artif Organs 43(1):45-57 doi:10.1177/0391398819866458

Sawada Y, Yamamoto I, Hirokane T, Nagai Y, Satoh Y, Ueyama M (1988) Severity index of paraquat poisoning. Lancet 1(8598):1333 doi:10.1016/s0140-6736(88)92143-5

Scherrmann JM, Houze P, Bismuth C, Bourdon R (1987) Prognostic value of plasma and urine paraquat concentration. Hum Toxicol 6(1):91-3 doi:10.1177/096032718700600116

Schmidt S, Gonzalez D, Derendorf H (2010) Significance of protein binding in pharmacokinetics and pharmacodynamics. J Pharm Sci 99(3):1107-22 doi:10.1002/jps.21916

Schnitzler A, Volkmann J, Enck P, Frieling T, Witte OW, Freund HJ (1999) Different cortical organization of visceral and somatic sensation in humans. Eur J Neurosci 11(1):305-15 doi:10.1046/j.1460-9568.1999.00429.x

Secker PF, Luks L, Schlichenmaier N, Dietrich DR (2018) RPTEC/TERT1 cells form highly differentiated tubules when cultured in a 3D matrix. ALTEX 35(2):223-234 doi:10.14573/altex.1710181

Secker PF, Schlichenmaier N, Beilmann M, Deschl U, Dietrich DR (2019) Functional transepithelial transport measurements to detect nephrotoxicity *in vitro* using the RPTEC/TERT1 cell line. Arch Toxicol 93(7):1965-1978 doi:10.1007/s00204-019-02469-8

Sharifi M, Ghafourian T (2014) Estimation of biliary excretion of foreign compounds using properties of molecular structure. AAPS J 16(1):65-78 doi:10.1208/s12248-013-9541-z

Sharp CW, Ottolenghi A, Posner HS (1972) Correlation of paraquat toxicity with tissue concentrations and weight loss of the rat. Toxicol Appl Pharmacol 22(2):241-51 doi:10.1016/0041-008x(72)90174-3

Sherrmann JM (2008) Chapter 26 - Drug Transport Mechanisms and their Impact on the Disposition and Effects of Drugs. In: Camille Georges Wermuth DA, Pierre Raboisson, Didier Rognan (ed) The Practice of Medicinal Chemistry. 4th edn. Academic Press

Shi M, Bouwmeester H, Rietjens I, Strikwold M (2020) Integrating *in vitro* data and physiologically based kinetic modeling-facilitated reverse dosimetry to predict human cardiotoxicity of methadone. Arch Toxicol 94(8):2809-2827 doi:10.1007/s00204-020-02766-7

Shirasu YT, K. (1977) Study report: acute toxicity of AT-5 in rat and mouse. Institute of Environmental Toxicology, Unpublished

Sjögren E, Lennernäs H, Andersson TB, Gråsjö J, Bredberg U (2009) The multiple depletion curves method provides accurate estimates of intrinsic clearance (CLint), maximum velocity of the metabolic reaction (Vmax), and Michaelis constant (Km): accuracy and robustness evaluated through experimental data and Monte Carlo simulations. Drug Metabolism and Disposition 37(1):47-58

References

Slikker W, Jr., Vore M, Bailey JR, Meyers M, Montgomery C (1983) Hepatotoxic effects of estradiol-17 beta-D-glucuronide in the rat and monkey. J Pharmacol Exp Ther 225(1):138-43

Slitt AL, Cherrington NJ, Hartley DP, Leazer TM, Klaassen CD (2002) Tissue distribution and renal developmental changes in rat organic cation transporter mRNA levels. Drug Metab Dispos 30(2):212-9 doi:10.1124/dmd.30.2.212

Sohlenius-Sternbeck AK (2006) Determination of the hepatocellularity number for human, dog, rabbit, rat and mouse livers from protein concentration measurements. Toxicol *In vitro* 20(8):1582-6 doi:10.1016/j.tiv.2006.06.003

Sprowl JA, van Doorn L, Hu S, et al. (2013) Conjunctive therapy of cisplatin with the OCT2 inhibitor cimetidine: influence on antitumor efficacy and systemic clearance. Clin Pharmacol Ther 94(5):585-92 doi:10.1038/clpt.2013.145

Stevens AJ, Campbell JL, Jr., Travis KZ, et al. (2021) Paraquat pharmacokinetics in primates and extrapolation to humans. Toxicol Appl Pharmacol 417:115463 doi:10.1016/j.taap.2021.115463

Strikwold M, Spenkelink B, de Haan LH, Woutersen RA, Punt A, Rietjens IM (2017a) Integrating *in vitro* data and physiologically based kinetic (PBK) modelling to assess the *in vivo* potential developmental toxicity of a series of phenols. Archives of toxicology 91(5):2119-2133

Strikwold M, Spenkelink B, de Haan LHJ, Woutersen RA, Punt A, Rietjens I (2017b) Integrating *in vitro* data and physiologically based kinetic (PBK) modelling to assess the *in vivo* potential developmental toxicity of a series of phenols. Arch Toxicol 91(5):2119-2133 doi:10.1007/s00204-016-1881-x

Strikwold M, Spenkelink B, Woutersen RA, Rietjens IM, Punt A (2013) Combining *in vitro* embryotoxicity data with physiologically based kinetic (PBK) modelling to define *in vivo* dose-response curves for developmental toxicity of phenol in rat and human. Arch Toxicol 87(9):1709-23 doi:10.1007/s00204-013-1107-4

Sui L, Chen K, Hwang P, Hwang D (2002) Identification of tetrodotoxin in marine gastropods implicated in food poisoning. Journal of natural toxins 11(3):213-220

Sun H, Liu L, Pang KS (2006) Increased estrogen sulfation of estradiol 17beta-D-glucuronide in metastatic tumor rat livers. J Pharmacol Exp Ther 319(2):818-31 doi:10.1124/jpet.106.108860

Sundarakrishnan A, Chen Y, Black LD, Aldridge BB, Kaplan DL (2018) Engineered cell and tissue models of pulmonary fibrosis. Adv Drug Deliv Rev 129:78-94 doi:10.1016/j.addr.2017.12.013

Swift B, Pfeifer ND, Brouwer KL (2010) Sandwich-cultured hepatocytes: an *in vitro* model to evaluate hepatobiliary transporter-based drug interactions and hepatotoxicity. Drug Metab Rev 42(3):446-71 doi:10.3109/03602530903491881

Taghikhani E, Maas R, Fromm MF, Konig J (2019) The renal transport protein OATP4C1 mediates uptake of the uremic toxin asymmetric dimethylarginine (ADMA) and efflux of cardioprotective L-homoarginine. PLoS One 14(3):e0213747 doi:10.1371/journal.pone.0213747

Takikawa H, Yamazaki R, Sano N, Yamanaka M (1996) Biliary excretion of estradiol-17 beta-glucuronide in the rat. Hepatology 23(3):607-13 doi:10.1053/jhep.1996.v23.pm0008617443

Taub M (1997) Primary kidney cells. Methods Mol Biol 75:153-61 doi:10.1385/0-89603-441-0:153

Thakur A, Chan JC (2022) Physiologically Based Toxicokinetic Modeling of 2,4-dichlorophenoxyacetic Acid. Paper presented at the Society of Toxicology annual meeting, San Diego, CA, USA,

Tsao SC, Sugiyama Y, Sawada Y, Iga T, Hanano M (1988) Kinetic analysis of albumin-mediated uptake of warfarin by perfused rat liver. J Pharmacokinet Biopharm 16(2):165-81 doi:10.1007/BF01062259

Tung SAH, Y.; Hafeez, A.; Ali, S.; Liu, A.; Chattha, M.S.; Ahmad, S.; Yang, G. (2020) Morpho-physiological Effects and Molecular Mode of Action of Mepiquat Chloride Application in Cotton: A Review. J Soil Sci Plant Nutr 20:15 doi:https://doi.org/10.1007/s42729-020-00276-0

van de Steeg E, Greupink R, Schreurs M, et al. (2013) Drug-drug interactions between rosuvastatin and oral antidiabetic drugs occurring at the level of OATP1B1. Drug Metab Dispos 41(3):592-601 doi:10.1124/dmd.112.049023

van Staden CJ, Morgan RE, Ramachandran B, Chen Y, Lee PH, Hamadeh HK (2012) Membrane vesicle ABC transporter assays for drug safety assessment. Curr Protoc Toxicol Chapter 23:Unit 23 5 doi:10.1002/0471140856.tx2305s54

van Tongeren TCA, Moxon TE, Dent MP, Li H, Carmichael PL, Rietjens I (2021) Next generation risk assessment of human exposure to anti-androgens using newly defined comparator compound values. Toxicol *In vitro* 73:105132 doi:10.1016/j.tiv.2021.105132

Varma MV, Chang G, Lai Y, et al. (2012) Physicochemical property space of hepatobiliary transport and computational models for predicting rat biliary excretion. Drug Metab Dispos 40(8):1527-37 doi:10.1124/dmd.112.044628

Vazquez-Armendariz AI, Barroso MM, El Agha E, Herold S (2022) 3D *In vitro* Models: Novel Insights into Idiopathic Pulmonary Fibrosis Pathophysiology and Drug Screening. Cells 11(9) doi:10.3390/cells11091526

Vessey DAQ, W.; Chen, X.; Pollock, C. A.; Johnson, D. W. (200) Isolation and Primary Culture of Human Proximal Tubule Cells. In: Becker G. HT (ed) Kidney Research Methods in Molecular Biology (Methods and Protocols). vol 466. Humana Press

Vogel C, Marcotte EM (2012) Insights into the regulation of protein abundance from proteomic and transcriptomic analyses. Nat Rev Genet 13(4):227-32 doi:10.1038/nrg3185

Volk C (2013) OCTs, OATs, and OCTNs: structure and function of the polyspecific organic ion transporters of the SLC22 family. WIREs Membr Transp Signal 3(1):14 doi:https://doi.org/10.1002/wmts.100

Vormann MK, Gijzen L, Hutter S, et al. (2018) Nephrotoxicity and Kidney Transport Assessment on 3D Perfused Proximal Tubules. AAPS J 20(5):90 doi:10.1208/s12248-018-0248-z

Walton K, Dorne JL, Renwick AG (2004) Species-specific uncertainty factors for compounds eliminated principally by renal excretion in humans. Food Chem Toxicol 42(2):261-74 doi:10.1016/j.fct.2003.09.001

Wang D, Rietdijk MH, Kamelia L, Boogaard PJ, Rietjens I (2021) Predicting the *in vivo* developmental toxicity of benzo[a]pyrene (BaP) in rats by an *in vitro-in silico* approach. Arch Toxicol 95(10):3323-3340 doi:10.1007/s00204-021-03128-7

Wang J, Zhu Y, Tan J, Meng X, Xie H, Wang R (2016) Lysyl oxidase promotes epithelial-to-mesenchymal transition during paraquat-induced pulmonary fibrosis. Mol Biosyst 12(2):499-507 doi:10.1039/c5mb00698h

Wang Q, Darling IM, Morris ME (2006) Transport of gamma-hydroxybutyrate in rat kidney membrane vesicles: Role of monocarboxylate transporters. J Pharmacol Exp Ther 318(2):751-61 doi:10.1124/

References

jpet.106.105965

Wang X, Wang Q, Morris ME (2008) Pharmacokinetic interaction between the flavonoid luteolin and gamma-hydroxybutyrate in rats: potential involvement of monocarboxylate transporters. AAPS J 10(1):47-55 doi:10.1208/s12248-007-9001-8

Wang YH, Li Y, Yang SL, Yang L (2005) Classification of substrates and inhibitors of P-glycoprotein using unsupervised machine learning approach. J Chem Inf Model 45(3):750-7 doi:10.1021/ci050041k

Wang Z, Gu D, Sheng L, Cai J (2018) Protective Effect of Anthocyanin on Paraquat-Induced Apoptosis and Epithelial-Mesenchymal Transition in Alveolar Type II Cells. Med Sci Monit 24:7980-7987 doi:10.12659/MSM.910730

Watanabe T, Kusuhara H, Maeda K, et al. (2010) Investigation of the rate-determining process in the hepatic elimination of HMG-CoA reductase inhibitors in rats and humans. Drug Metab Dispos 38(2):215-22 doi:10.1124/dmd.109.030254

Watanabe T, Kusuhara H, Maeda K, Shitara Y, Sugiyama Y (2009) Physiologically based pharmacokinetic modeling to predict transporter-mediated clearance and distribution of pravastatin in humans. J Pharmacol Exp Ther 328(2):652-62 doi:10.1124/jpet.108.146647

Waters NJ, Jones R, Williams G, Sohal B (2008) Validation of a rapid equilibrium dialysis approach for the measurement of plasma protein binding. J Pharm Sci 97(10):4586-95 doi:10.1002/jps.21317

Watts M (2011) Paraquat. Pesticide Action Network Asia and the Pacific, p 44

Weaver YM, Ehresman DJ, Butenhoff JL, Hagenbuch B (2010) Roles of rat renal organic anion transporters in transporting perfluorinated carboxylates with different chain lengths. Toxicol Sci 113(2):305-14 doi:10.1093/toxsci/kfp275

Weisiger RA, Ma WL (1987) Uptake of oleate from albumin solutions by rat liver. Failure to detect catalysis of the dissociation of oleate from albumin by an albumin receptor. J Clin Invest 79(4):1070-7 doi:10.1172/JCI112920

Wilkens S (2015) Structure and mechanism of ABC transporters. F1000Prime Rep 7:14 doi:10.12703/P7-14

Wilmer MJ, Saleem MA, Masereeuw R, et al. (2010) Novel conditionally immortalized human proximal tubule cell line expressing functional influx and efflux transporters. Cell Tissue Res 339(2):449-57 doi:10.1007/s00441-009-0882-y

Wolters PJ, Collard HR, Jones KD (2014) Pathogenesis of idiopathic pulmonary fibrosis. Annu Rev Pathol 9:157-79 doi:10.1146/annurev-pathol-012513-104706

Worley RR, Fisher J (2015) Application of physiologically-based pharmacokinetic modeling to explore the role of kidney transporters in renal reabsorption of perfluorooctanoic acid in the rat. Toxicol Appl Pharmacol 289(3):428-41 doi:10.1016/j.taap.2015.10.017

Wright SH (2019) Molecular and cellular physiology of organic cation transporter 2. Am J Physiol Renal Physiol 317(6):F1669-F1679 doi:10.1152/ajprenal.00422.2019

Xu Q, Huang K, Gao L, Zhang H, Rong K (2003) [Toxicity of tetrodotoxin towards mice and rabbits]. Wei Sheng Yan Jiu 32(4):371-4

Yabe Y, Galetin A, Houston JB (2011) Kinetic characterization of rat hepatic uptake of 16 actively transported drugs. Drug Metab Dispos 39(10):1808-14 doi:10.1124/dmd.111.040477

Yamashiro W, Maeda K, Hirouchi M, Adachi Y, Hu Z, Sugiyama Y (2006) Involvement of transporters

in the hepatic uptake and biliary excretion of valsartan, a selective antagonist of the angiotensin II AT1-receptor, in humans. Drug Metab Dispos 34(7):1247-54 doi:10.1124/dmd.105.008938

Yamashoji S, Isshiki K (2001) Rapid detection of cytotoxicity of food additives and contaminants by a novel cytotoxicity test, menadione-catalyzed H(2)O (2) production assay. Cytotechnology 37(3):171-8 doi:10.1023/A:1020580818979

Yang X, Gandhi YA, Duignan DB, Morris ME (2009) Prediction of biliary excretion in rats and humans using molecular weight and quantitative structure-pharmacokinetic relationships. AAPS J 11(3):511-25 doi:10.1208/s12248-009-9124-1

Yeo DS, Ding JL, Ho B (1996) Neuroblastoma cell culture assay shows that Carcinoscorpius rotundicauda haemolymph neutralizes tetrodotoxin. Toxicon 34(9):1054-7 doi:10.1016/0041-0101(96)00062-1

Yin J, Duan H, Wang J (2016) Impact of Substrate-Dependent Inhibition on Renal Organic Cation Transporters hOCT2 and hMATE1/2-K-Mediated Drug Transport and Intracellular Accumulation. J Pharmacol Exp Ther 359(3):401-410 doi:10.1124/jpet.116.236158

Yin J, Wang J (2016) Renal drug transporters and their significance in drug-drug interactions. Acta Pharm Sin B 6(5):363-373 doi:10.1016/j.apsb.2016.07.013

Yoshikado T, Lee W, Toshimoto K, et al. (2021) Evaluation of Hepatic Uptake of OATP1B Substrates by Short Term-Cultured Plated Human Hepatocytes: Comparison With Isolated Suspended Hepatocytes. J Pharm Sci 110(1):376-387 doi:10.1016/j.xphs.2020.10.041

Zeidel ML, Hoenig MP, Palevsky PM (2014) A new CJASN series: Renal physiology for the clinician. Clin J Am Soc Nephrol 9(7):1271 doi:10.2215/CJN.10191012

Zeilinger K, Freyer N, Damm G, Seehofer D, Knospel F (2016) Cell sources for in vitro human liver cell culture models. Exp Biol Med (Maywood) 241(15):1684-98 doi:10.1177/1535370216657448

Zhang M, van Ravenzwaay B, Fabian E, Rietjens I, Louisse J (2018a) Towards a generic physiologically based kinetic model to predict in vivo uterotrophic responses in rats by reverse dosimetry of in vitro estrogenicity data. Arch Toxicol 92(3):1075-1088 doi:10.1007/s00204-017-2140-5

Zhang M, van Ravenzwaay B, Fabian E, Rietjens IM, Louisse J (2018b) Towards a generic physiologically based kinetic model to predict in vivo uterotrophic responses in rats by reverse dosimetry of in vitro estrogenicity data. Archives of toxicology 92(3):1075-1088

Zhang M, van Ravenzwaay B, Rietjens I (2019) Development of a generic physiologically based kinetic model to predict in vivo uterotrophic responses induced by estrogenic chemicals in rats based on in vitro bioassays. Toxicol Sci doi:10.1093/toxsci/kfz216

Zhu Y, Tan J, Xie H, Wang J, Meng X, Wang R (2016) HIF-1alpha regulates EMT via the Snail and beta-catenin pathways in paraquat poisoning-induced early pulmonary fibrosis. J Cell Mol Med 20(4):688-97 doi:10.1111/jcmm.12769

Zolk O, Solbach TF, Konig J, Fromm MF (2009) Structural determinants of inhibitor interaction with the human organic cation transporter OCT2 (SLC22A2). Naunyn Schmiedebergs Arch Pharmacol 379(4):337-48 doi:10.1007/s00210-008-0369-5

ZonMw (2020) programmatekst Meer Kennis met Minder Dieren 2021-2024. In. https://www.zonmw.nl/fileadmin/zonmw/documenten/Fundamenteel/MKMD/MKMD_Programmatekst_2021-2024.pdf Accessed April 8, 2022

Summary
Samenvatting

Summary

For a number of compounds the absorption, distribution, metabolism and excretion (ADME) characteristics are substantially influenced by active transport in for example the liver, kidneys, intestine, placenta or the blood-brain-barrier. Incorporating this active transport into physiologically based kinetic (PBK) models based on *in vitro* data is challenging due to a lack of adequate *in vitro* models to quantify the kinetics of the active transporters involved and the scaling factors needed to translate *in vitro* obtained data to the *in vivo* situation. In the present thesis, it was investigated how to incorporate active biliary and active renal excretion into PBK models using kinetic parameters defined in *in vitro* model systems seemingly suitable for quantification of transporter kinetics. To do this, model compounds preferably cleared from the systemic circulation via active transport in either the liver or the kidney were used. The kinetic parameters Vmax and Km for the active transport were obtained from *in vitro* models and collected experimentally or taken from the literature. The major challenge of incorporating the *in vitro* obtained kinetic data into the PBK models was the translation of the *in vitro* Vmax to an *in vivo* Vmax as this requires adequate scaling. The methods of scaling provided in this work were either theoretical and based on scientific considerations of the differences between the *in vitro* model and the *in vivo* situation or based on fitting the predictions to available literature reported *in vivo* kinetic data. The PBK models thus obtained provided proofs of principle for incorporating active excretion into PBK models. Model evaluation was further extended by using the PBK models obtained for quantitative *in vitro in vivo* extrapolation (QIVIVE) via PBK model based reverse dosimetry to predict toxicity and related points of departure (PoDs) enabling establishment of health based guidance values (HBGV). In this way the results of the thesis showed proofs of principle for a new approach methodology (NAM) in the risk and safety assessment of chemicals.

Chapter 1 introduces the background information on NAMs and the aim of the present thesis which is: to incorporate excretion via active transport through either urine or bile in generic PBK models based on *in vitro* data. Furthermore, excretion in liver and kidney and the involved active transporters are introduced, PBK modelling is explained as well as the application of PBK model based reverse dosimetry for QIVIVE translating *in vitro* concentration response curves to *in vivo* dose response curves for toxicity. In addition, an overview is provided on the available *in vitro* models for biliary and renal excretion. Also already published PBK models that included biliary or renal excretion are summarized. Lastly, the model compounds of the thesis are introduced.

In **Chapter 2** a proof of principle is shown for how to incorporate active biliary excretion into a PBK model using estradiol-17β-glucuronide (E$_2$17βG) as the model compound. The kinetic parameters for description of the transport of E$_2$17βG via the organic anion

transporting polypeptides (Oatps) in a PBK model for rat were obtained from literature studies. In these studies, freshly isolated primary rat hepatocytes were the *in vitro* model used to define the kinetic parameters Vmax and Km needed for incorporating the transport of E$_2$17βG via the Oatps in the PBK model. For all four *in vitro* transporter kinetic data sets (Vmax, Km), the scaling factor in the PBK model predictions was fitted. To this end, PBK model predictions for both the time-dependent blood concentration and the cumulative biliary excretion were fitted to respectively three *in vivo* data sets on the time-dependent blood concentration of E$_2$17βG and three *in vivo* data sets on the cumulative biliary excretion of E$_2$17βG. This resulted in 24 individual predictions and fitted scaling factors. Averaging the 24 fitted scaling factors resulted in a scaling factor of 129 mg protein/g liver. This scaling factor was in line with the theoretically derived scaling factor of 115 to 132 mg protein/g liver. With this newly defined scaling factor predictions were repeated and it was shown that with the obtained scaling factor the predictions were performed adequately (within 2-fold difference with reported *in vivo* data).

Chapter 3 establishes a first proof of principle on how to incorporate active renal excretion of the model compound mepiquat (MQ) chloride via the organic cation transporter 2 (OCT2) in a rat PBK model. To this end, the human renal proximal tubule epithelium cell (RPTEC) line (SA7K) was used to obtain the *in vitro* kinetic parameters Vmax and Km by executing time-dependent and concentration-dependent uptake of MQ in the absence and presence of the OCT2 inhibitor doxepin. This resulted in a Vmax of 10.5 pmol/min/mg protein and a Km of 20.6 µM. PBK model predictions incorporated these values in the PBK model with scaling of the *in vitro* Vmax to an *in vivo* Vmax using a scaling factor consisting of 3 components: 1) the scaling for the amount of protein per gram kidney (300 mg protein/g kidney), 2) the scaling for the location of the OCT2 transporter in the kidney, which is the kidney cortex making up 70% of the kidney, and 3) a factor to correct for potential differences in OCT2 activity in the SA7K cells and the *in vivo* kidney cortex, given the differences in expression levels, the effect of differences in membrane potential on this activity, and the species differences (human cell line, rat PBK model). Application of the first two components of the scaling factor, referred to as partial scaling, led to PBK model predictions of the maximum blood concentration (Cmax) of MQ that deviated 6.7–8.4-fold from the reported *in vivo* data on the Cmax. The inclusion of the third component of the scaling factor resulted in an overall scaling that provided adequate predictions for the *in vivo* blood concentrations of MQ in rat (2.3–3.2-fold difference) and showed proof of principle for incorporating active renal excretion into PBK modelling.

In **Chapter 4** the use of the SA7K cells and incorporation of OCT2 transport into PBK modelling is investigated to a further extent with the model compound and OCT2

substrate paraquat (PQ) dichloride. It was shown that the SA7K cells were not suitable to obtain the kinetic parameters Vmax and Km of the OCT2 mediated PQ transport, so instead kinetic data obtained using the human embryonic kidney cell line (HEK293) with OCT2 overexpression reported in literature were used. A scaling factor was derived in a similar way as was done in **Chapter 3** to translate the *in vitro* Vmax to an *in vivo* Vmax. The model thus obtained for rat resulted in an adequate prediction of PQ kinetics. For human a PBK model was defined based on the evaluated model for rat. Additionally, the rat and human PBK models were used to predict the acute toxicity of PQ in rat and human by applying PBK model based reverse based dosimetry. The target tissue of PQ acute toxicity is the lung. For this reason, *in vitro* concentration-response curves were obtained for cytotoxicity in rat alveolar type II cells (RLE-6TN) exposed to increasing concentrations of PQ. Reported *in vitro* toxicity data were also collected from the literature providing concentration response curves for the RLE-6TN cell line and the rat alveolar cell line L2. Additionally, human *in vitro* cytotoxicity data for the alveolar cell line A549 were collected from the literature. With the developed PBK model the *in vitro* cytotoxicity concentration-response curves were translated to predicted *in vivo* dose-response curves for PQ toxicity whereafter Benchmark dose (BMD) analysis was applied to derive the $BMDL_{50}$-$BMDU_{50}$ ranges from the predicted dose response curves, which were compared to the *in vivo* reported mean lethal dose (LD_{50}) values for rat and human. The translated *in vitro* toxicity data range from the rat cell lines was underpredicting the *in vivo* LD_{50} range by 6.9 – 12.4 -fold difference, with the highest translated $BMDU_{50}$ being the closest to the lowest reported LD_{50} by 1.5-fold. For human the QIVIVE of the A594 cell line data, adequately predicted the acute toxicity by 1.3 – 1.7-fold. In this study, using PQ as the model compound, a proof of principle was provided showing how to include *in vitro* obtained active excretion in PBK modelling and how to apply the PBK model obtained for QIVIVE to predict acute *in vivo* toxicity.

In **Chapter 5**, a proof of principle is provided for predicting acute neurotoxicity of the model compound tetrodotoxin (TTX) in rodents and human using PBK modelling. The clearance of TTX was shown not to depend on metabolism since substrate depletion in incubations of TTX with rat liver hepatocytes appeared negligible. Clearance of TTX was however dependent on excretion in the kidneys. Incorporating a kidney compartment accounting for active renal excretion in the PBK models improved the accuracy and was shown to be essential for their performance. The incorporation was based on fitting of the transporter efficiency (Vmax/Km) to adequately match available *in vivo* kinetic data. The PBK model was evaluated for three administration routes: oral, intravenous and intramuscular and for both rats and mice. Once validated the PBK models were used to translate *in vitro* concentration–response data of TTX obtained in a multielectrode array (MEA) assay with primary rat neonatal cortical cells and in

an effect study with mouse neuro-2a cells, into *in vivo* dose–response data for rats and mice respectively. To evaluate the predictions, QIVIVE-derived dose–response data were compared with *in vivo* data on neurotoxicity in rats and mice upon oral and parenteral dosing. The results revealed that for both rats and mice the predicted dose–response data matched the data from available *in vivo* studies well even though the endpoint *in vitro* differed from the endpoints *in vivo*. Upon this validation also a human PBK model for TTX was defined assuming that the model was well-evaluated based on the rat and mice model outcomes. The human PBK model was used for QIVVE of the human *in vitro* concentration-response curve obtained in a MEA assay using human-induced pluripotent stem cell (hIPSC)-derived iCell neurons in coculture with hIPSC-derived iCell astrocytes to generate a predicted human *in vivo* dose response curve for TTX toxicity. BMD analysis was applied on the curve and revealed a $BMDL_{10}$ of 1.8 µg/kg bw that was converted with an uncertainty factor of 10 for interindividual differences to a HBGV of 0.18 µg/kg bw, a value that was only 1.4-fold different from the ARfD previously established by EFSA of 0.25 µg/kg bw based on an acute toxicity study in mice providing a tentative HBGV for TTX human risk assessment. It is concluded that PBK modelling-based reverse dosimetry of *in vitro* TTX effect data can adequately predict the *in vivo* neurotoxicity of TTX in rodents and even human, providing a novel proof of principle for this NAM.

Chapter 6 gives an overview of the main findings in this thesis work and provides a general discussion on points that were beyond the scope of the individual chapters. The chapter reveals more insights in the use of *in vitro* models for incorporating transporter kinetics in PBK models and the pros and cons of using the SA7K cell line as a model to quantify transport kinetics *in vitro*. Moreover, it is discussed what would be the preferred *in vitro* model for obtaining kinetic parameters and an in-depth discussion of the scaling factor was provided. It is concluded that use of a transfected cell line with overexpression of the transporter of interest would provide the preferred model to define PBK model parameters for active transport processes involved in excretion. This allows for the definition of a scaling factor based on quantification of the abundance of the protein or its activity for transport of a model compound in the *in vitro* system and the *in vivo* tissue. Furthermore, a discussion is provided on the use of generic PBK-models, how the work of the present thesis contributes to the 3Rs, the importance of taking active excretion into account, the type of chemicals for which this will be essential, and the future potentials of *in silico* work.

Taken together, the results of the present thesis provide proofs of principle for taking into account active excretion via liver and kidney in PBK modelling and show that it is possible to incorporate this active excretion using *in vitro* transporter kinetic data provided that adequate scaling factors are used to translate the Vmax *in vitro* to a Vmax

in vivo. Moreover, it is shown that the PBK models obtained enabled the adequate prediction of PoDs and HBGVs by PBK modelling based QIVIVE of available *in vitro* toxicity data thereby building more confidence into using this tool as a NAM aiming at replacement, reduction and refinement (3Rs) of animal experimentation.

Samenvatting

Voor een aantal chemische stoffen wordt de absorptie, distributie, metabolisme en excretie (ADME) aanzienlijk beïnvloed door actief transport in bijvoorbeeld de lever, nieren, darmen, placenta of de bloed-hersenbarrière. Het opnemen van dit actief transport in fysiologisch gebaseerde kinetische (PBK) modellen op basis van *in vitro* data is een uitdaging vanwege een gebrek aan adequate *in vitro* modellen. Deze *in vitro* modellen genereren kinetisch data van de betrokken actieve transporters, en vervolgens spelen schalingsfactoren de hoofdrol bij het vertalen van de *in vitro* verkregen data naar de *in vivo* situatie. In dit proefschrift is onderzocht hoe actieve excretie via gal of urine in PBK-modellen kan worden opgenomen met behulp van kinetische parameters die zijn gedefinieerd in *in vitro* modelsystemen die mogelijk geschikt zijn voor kwantificering van transporterkinetiek. Om dit te doen, werden modelstoffen gebruikt die bij voorkeur via actief transport in de lever of de nier uit de systemische circulatie worden geklaard. De kinetische parameters Vmax en Km voor het actieve transport zijn verkregen uit *in vitro* modellen en experimenteel verzameld of overgenomen uit de literatuur. De grootste uitdaging bij het opnemen van de *in vitro* verkregen kinetische data in de PBK-modellen was de vertaling van de *in vitro* Vmax naar een *in vivo* Vmax, aangezien hiervoor adequate schalingsfactoren vereist zijn. De schalingsmethoden in dit werk waren ofwel theoretisch en gebaseerd op wetenschappelijke overwegingen van de verschillen tussen het *in vitro* model en de *in vivo* situatie of gebaseerd op het afstemmen van de voorspellingen op beschikbare *in vivo* kinetische data gerapporteerd in de literatuur. De aldus verkregen schalingsfactoren en PBK-modellen leverden principebewijzen voor het opnemen van actieve excretie in PBK-modellen. De modelevaluatie werd verder uitgebreid door de verkregen PBK-modellen te gebruiken voor kwantitatieve *in vitro in vivo* extrapolatie (quantitative *in vitro in vivo* extrapolation) (QIVIVE) via zogeheten PBK model based reverse dosimetry. Zo kon toxiciteit en gerelateerde uitgangspunten (points of departure) (PoD's) voorspeld worden, die gebruikt kunnen worden voor het vaststellen van veilige blootstellingsgrenzen voor de mens, zogeheten health based guidance values (HBGV). De resultaten van het proefschrift leveren een principebewijs voor een nieuwe benaderingsmethodologie (new approach methodology) (NAM) in de risico- en veiligheidsbeoordeling van chemicaliën.

Hoofdstuk 1 introduceert de achtergrondinformatie over NAMs en het doel van dit proefschrift, namelijk: het opnemen van excretie via actief transport via urine of gal in generieke PBK-modellen op basis van *in vitro* data. Verder worden excretie in de lever en nieren en de betrokken actieve transporters geïntroduceerd, wordt PBK-modellering uitgelegd, evenals de toepassing van PBK model based reverse dosimetry voor QIVIVE die *in vitro* concentratie-responscurves vertaalt naar *in vivo* dosis-responscurves voor toxiciteit. Daarnaast wordt een overzicht gegeven van de beschikbare *in vitro* modellen

voor actieve excretie in de lever en de nieren. Ook reeds gepubliceerde PBK-modellen met excretie via gal en urine worden samengevat. Ten slotte worden de modelstoffen van het proefschrift geïntroduceerd.

In Hoofdstuk 2 wordt een principebewijs getoond voor het opnemen van actieve excretie via de gal in een PBK-model voor oestradiol-17β-glucuronide (E$_2$17βG) als de modelstof. De kinetische parameters voor de beschrijving van het transport van E$_2$17βG via de organische anion-transporterende polypeptiden (Oatps) in een PBK-model voor ratten werden verkregen uit literatuurstudies. In deze studies waren vers geïsoleerde primaire hepatocyten van ratten het *in vitro*-model dat werd gebruikt om de kinetische parameters Vmax en Km te definiëren die nodig zijn voor het opnemen van het transport van E$_2$17βG via de Oatps in het PBK-model. Voor alle vier de *in vitro* transporter kinetische datasets (Vmax, Km), werd de schalingsfactor in de PBK-modelvoorspellingen bepaald door na te gaan met welke schalingsfactor de beschikbare *in vivo* data het beste werden voorspeld. Hiertoe werden PBK-modelvoorspellingen voor zowel de tijdsafhankelijke bloedconcentratie als de cumulatieve galexcretie gefit aan respectievelijk drie *in vivo* datasets over de tijdsafhankelijke bloedconcentratie van E$_2$17βG en drie *in vivo* datasets over de cumulatieve galexcretie van E$_2$17βG. Dit resulteerde in 24 individuele voorspellingen en gefitte schalingsfactoren. Het middelen van de 24 gefitte schaalfactoren resulteerde in een schalingsfactor van 129 mg eiwit/g lever. Deze schalingsfactor kwam overeen met de theoretisch afgeleide schalingsfactor van 115 tot 132 mg eiwit/g lever. Met deze nieuw gedefinieerde schalingsfactor werden voorspellingen herhaald en werd aangetoond dat met de verkregen schalingsfactor de voorspellingen adequaat werden uitgevoerd (resulterend in een minder dan een 2-voudig verschil met gerapporteerde *in vivo* data).

Hoofdstuk 3 levert een eerste principebewijs voor hoe actieve renale excretie van de modelstof mepiquat (MQ) chloride via de organische kation-transporter 2 (OCT2) in een PBK-model voor ratten kan worden opgenomen. Hiertoe werd de humane renale proximale tubulus-epitheelcellijn (RPTEC) SA7K gebruikt om de *in vitro* kinetische parameters Vmax en Km te verkrijgen door tijdsafhankelijke en concentratieafhankelijke opnamestudies van MQ uit te voeren in de aanwezigheid en afwezigheid van de OCT2 remmer doxepine. Dit resulteerde in een Vmax van 10,5 pmol/min/mg eiwit en een Km van 20,6 μM. Deze waarden werden opgenomen in het PBK-model voor modelvoorspellingen met het schalen van de *in vitro* Vmax naar een *in vivo* Vmax met behulp van een schalingsfactor bestaande uit 3 componenten: 1) schalen voor de hoeveelheid eiwit per gram nier (300 mg eiwit/g nier), 2) schalen voor de locatie van de OCT2-transporter in de nier, de niercortex die 70% van de nier vormt, en 3) een factor om te corrigeren voor verschillen in OCT2-activiteit in de SA7K-cellen en de *in vivo* niercortex, gezien de verschillen in expressieniveaus, het effect van verschillen in

activiteit van de membraanpotentiaal, en de soortverschillen (humane cellijn, rat PBK-model). Toepassing van de eerste twee componenten van de schalingsfactor, de partiële schalingsfactor genoemd, leidde tot voorspellingen door het PBK-model van de maximale bloedconcentraties (Cmax) van MQ die 6,7-8,4 keer afweken van de gerapporteerde *in vivo* data over de Cmax. De opname van de derde component van de schalingsfactor resulteerde in een algehele schalingsfactor die adequate voorspellingen opleverde voor de *in vivo* bloedconcentraties van MQ bij ratten (2,3-3,2-voudig verschil) en een bewijs van principe toonde voor het opnemen van actieve renale excretie in PBK-modellering .

In Hoofdstuk 4 wordt het gebruik van de SA7K-cellen en de opname van OCT2-transport in PBK-modellering verder onderzocht met de modelstof en OCT2-substraat paraquat (PQ) dichloride. Er werd aangetoond dat de SA7K-cellen niet geschikt waren om de kinetische parameters Vmax en Km van het OCT2-gemedieerde PQ-transport te verkrijgen. Daarom werden in plaats daarvan kinetische data gebruikt gerapporteerd in de literatuur die werden verkregen met behulp van de humane embryonale niercellijn (HEK293) met een overexpressie van OCT2. Een schalingsfactor werd afgeleid op eenzelfde manier als werd gedaan in **Hoofdstuk 3** om de *in vitro* Vmax te vertalen naar een *in vivo* Vmax. Het verkregen model voor rat resulteerde in een adequate voorspelling van de PQ-kinetiek. Het humane PBK-model werd gedefinieerd op basis van het geëvalueerde model voor ratten. Bovendien werden beide PBK-modellen gebruikt om de acute toxiciteit van PQ bij ratten en mensen te voorspellen door het toepassing van PBK model based reverse dosimetry. Het gevoeligste orgaan voor de acute toxiciteit van PQ is de long. Om deze reden werden *in vitro* concentratie-responscurven verkregen voor cytotoxiciteit in alveolaire type II-cellen van ratten (RLE-6TN) die waren blootgesteld aan toenemende concentraties van PQ. Ook werden gerapporteerde *in vitro* toxiciteitsdata verzameld uit de literatuur die concentratieresponscurves verschaften voor de RLE-6TN-cellijn en de alveolaire cellijn L2 van ratten. Daarnaast werden ook humane *in vitro* cytotoxiciteitsdata voor de alveolaire cellijn A549 verzameld uit de literatuur. Met het ontwikkelde PBK-model werden de *in vitro* cytotoxiciteitsconcentratie-responscurven vertaald naar voorspelde *in vivo* dosis-responscurven voor PQ-toxiciteit, waarna de zogenoemde benchmark dose (BMD) analyse werd toegepast om de $BMDL_{50}$-$BMDU_{50}$-range af te leiden uit de voorspelde dosis-responscurven. Deze werden vergeleken met de *in vivo* gerapporteerde waarden voor de gemiddelde letale dosis (LD_{50}) voor ratten en mensen. De range van de vertaalde *in vitro* toxiciteitsdata van de rattencellijnen was een onder voorspelling van de *in vivo* LD_{50}-range met een verschil van 6,9 – 12,4 keer, waarbij de hoogst vertaalde $BMDU_{50}$ het dichtst bij de laagst gerapporteerde LD_{50} lag met een factor 1,5 verschil. Voor de mens voorspelde de QIVIVE van de A594-cellijndata adequaat de acute toxiciteit met een factor 1,3 – 1,7. Deze studie laat zien dat met gebruik van de modelstof PQ een principebewijs werd geleverd dat aantoont hoe *in vitro* verkregen actieve excretie kan worden opgenomen in PBK-modellering en

hoe het PBK-model dat is verkregen voor QIVIVE kan worden toegepast om acute *in vivo* toxiciteit te voorspellen.

In Hoofdstuk 5 wordt een principebewijs geleverd voor het voorspellen van acute neurotoxiciteit van de modelstof tetrodotoxine (TTX) bij knaagdieren en mensen met behulp van PBK-modellering. De klaring van TTX bleek niet af te hangen van levermetabolisme, aangezien substraatdepletie van TTX in de incubaties met rat hepatocyten verwaarloosbaar was. De klaring van TTX is afhankelijk van uitscheiding via de nieren. Het opnemen van een niercompartiment dat verantwoordelijk is voor actieve renale excretie in de PBK-modellen verbeterde de nauwkeurigheid van de PBK modellen en bleek essentieel te zijn voor goede voorspellingen. De kinetische parameters voor het actieve transport in de nieren werden vastgesteld via het aanpassen van de transporter efficiëntie (Vmax/Km) om de beschikbare *in vivo* kinetische data adequaat te matchen. Het PBK-model werd geëvalueerd voor drie toedieningsroutes: oraal, intraveneus en intramusculair voor zowel ratten als muizen. Na validatie werden de PBK-modellen gebruikt om *in vitro* concentratie-responsdata van TTX, verkregen in een multi-electrode array (MEA)-assay met primaire neonatale corticale cellen van ratten en in een effectstudie met neuro-2a-cellen van muizen, te vertalen naar *in vivo* dosis-respons data voor respectievelijk ratten en muizen. Om de voorspellingen te evalueren, werden van QIVIVE afgeleide dosis-responsdata vergeleken met *in vivo* data over neurotoxiciteit van TTX bij ratten en muizen na orale en parenterale dosering. De resultaten lieten zien dat voor zowel ratten als muizen de voorspelde dosis-responsdata goed overeenkwamen met de data uit beschikbare *in vivo* onderzoeken, hoewel het eindpunt *in vitro* verschilde van de eindpunten *in vivo*. Na deze validatie werd ook een humaan PBK-model voor TTX gedefinieerd, ervan uitgaande dat het model goed was geëvalueerd op basis van de uitkomsten van het rat- en muismodel. Het humane PBK-model werd gebruikt voor QIVVE van de humane *in vitro* concentratie-responscurve verkregen in een MEA-assay met behulp van humane geïnduceerde pluripotente stamcel (hIPSC)-afgeleide iCell-neuronen in co-cultuur met hIPSC-afgeleide iCell-astrocyten om een voorspelde humane *in vivo* dosis-responscurve voor TTX-toxiciteit te verkrijgen. BMD-analyse werd toegepast op de curve en resulteerde in een $BMDL_{10}$ van 1,8 µg/kg bw die, met een onzekerheidsfactor van 10 voor interindividuele verschillen, resulteerde in een HBGV van 0,18 µg/kg bw, een waarde die slechts 1,4 keer verschilde van de door de EFSA eerder vastgestelde ARfD van 0,25 µg/kg bw op basis van een acute toxiciteitsstudie bij muizen. Dit leverde een voorlopige HBGV op voor TTX-risicobeoordeling bij de mens. Geconcludeerd wordt dat PBK modelling based reverse dosimetry van *in vitro* TTX-effectdata de *in vivo* neurotoxiciteit van TTX bij knaagdieren en zelfs mensen adequaat kan voorspellen, wat een nieuw principebewijs levert voor deze NAM.

Hoofdstuk 6 geeft een overzicht van de belangrijkste bevindingen in dit proefschrift en geeft een algemene discussie over punten die buiten het bestek van de afzonderlijke hoofdstukken vielen. Dit hoofdstuk onthult meer inzichten in het gebruik van *in vitro* modellen voor het opnemen van transportkinetiek in PBK-modellen en de voor- en nadelen van het gebruik van de SA7K-cellijn als een model om transportkinetiek *in vitro* te kwantificeren. Bovendien wordt besproken wat het voorkeursmodel *in vitro* zou zijn voor het verkrijgen van kinetische parameters voor actief transport en er werd een diepgaande bespreking van de schalingfactoren gegeven. Er wordt geconcludeerd dat het gebruik van een getransfecteerde cellijn met overexpressie van een gewenste transporter het voorkeursmodel is om PBK-modelparameters te definiëren voor actieve transportprocessen die betrokken zijn bij uitscheiding. Dit maakt de definitie mogelijk van een schalingsfactor op basis van kwantificering van de aanwezigheid van het eiwit of zijn activiteit voor transport van een modelstof in het *in vitro* systeem en het *in vivo* weefsel. Verder wordt een discussie gegeven over het gebruik van generieke PBK-modellen, hoe het werk van dit proefschrift bijdraagt aan de 3V's (vervanging, vermindering en verfijning) van dierproeven, het belang om rekening te houden met actieve excretie, het type stoffen waarvoor dit essentieel zal zijn, en de toekomstige mogelijkheden van *in silico* werk.

Samengevat bieden de resultaten van dit proefschrift nieuwe bewijzen voor het belang van het opnemen van actieve excretie via lever en nier in PBK-modellering en laten ze zien dat het mogelijk is om deze actieve excretie op te nemen met behulp van *in vitro* transporterkinetiek data, op voorwaarde dat adequate schalingsfactoren worden gebruikt om de Vmax *in vitro* te vertalen naar een Vmax *in vivo*. Bovendien is aangetoond dat de verkregen PBK-modellen de adequate voorspelling van PoD's en HBGV's mogelijk maken via op PBK-modellering gebaseerde QIVIVE van beschikbare *in vitro* toxiciteitsdata, waardoor meer vertrouwen wordt gewekt in het gebruik van dit hulpmiddel als een NAM gericht op vervanging, vermindering en verfijning (3V's) van dierproeven.

Acknowledgements

Acknowledgements

ins and outs on how to work efficiently on the labs and for the mental support that any PhD needs. And of course for the talks, laughs and sharing. A special thanks to Sebas for always making me laugh, his interest to listen to my stories and his funniness and humor! To all current and former PhDs and Postdocs at TOX (which are many great people): Aafke, Aïsh, Ashraf, Akanksha, Alexandra, Aziza, Benthe, Biyao, Chen, Christina, Danlei, Diana, Diego, Edith, Felicia, Georgia, Ghaliya, Hugo, Isaac, Ixchel, Jia, Jiaqi, Jing Jin, Jing Fang, Jingxuan, Katharina, Katja, Korphimol, Liang, Lu, Maartje, Marta, Matteo, Mebrah, Mengying, Menno, Merel, Miaoying, Nacho, Nina, Orsi, Phim, Qianrui, Qiuhui, Shensheng, Shivani, Shuo, Suparmi, Tessa, Thijs, Véronique, Weijia, Wisse, Xiyu, Yasser, Yiming.

To my offices
Number one: Anna and Tien, thank you for all the nice and supportive words when I was not yet starting my PhD. Anna thank you for your friendship and all the times we went to the GoalTrainers park and even organized the Wageningen PhD symposium together. Thank you for believing in me when I couldn't.

Number two: Mengying, Artem, Chen, Maartje, and later Frances, Orsi and Yasser. Without you this journey wouldn't have been the same. Mengying, thank you for your guidance along the PBK journey, for your friendship and support and for always having my back. Artem, thank you for your sometimes pessimistic view on (PhD) life and for toning down my enthusiasm to realism. You really are one of a kind and it was a pleasure getting to know you. Chen, we had so many talks and so much laughter on everything and I will never forget your enthusiasm and your compliments on my looks. I got ego got boosted by you! Maartje, we have talked, laughed and cried away so many of our precious PhD hours. It was so nice to have you in the office. You are an amazing and kind person and I had such fun with you, thank you for your friendship! Frances and Orsi, thank you so much for the nice chats and sharing on our highs and lows of the PhD and life. Yasser, mister big boss, thank you for how you encouraged me during my last months. You have always been so nice and down for a talk and laugh. Thank you for all the sweets and coffee you shared with us! I enjoyed our office Sinterklaas celebrations and dinners very much!

Number three: Marta, Danlei and Benthe. I am very grateful to have had you by my side for the last few months of hard work. Having experienced people like you supporting me helped me to keep on believing in myself and to keep working until the finish. And I made it!!!

To the WPC PhD symposium committee, I had a lot of fun organizing the PhD symposium with you in 2019. Right before the corona pandemic. It was hard work but it paid off

really well!

To Tessa, Véronique and Katja, thanks for the fabulous week we had in San Diego this year! It really was the highlight of the year for me and I am glad we got to experience this together US-style, in a loft, paying too much on tips for food and tequila, haha. Eating tacos, digesting science and dancing!

To my wonderful paranymphs Katja & Laura. Katja, I am so glad that I had you at the department as the only Dutch girl of the group (from the beginning). We clicked so well and really took on this job together. I had so much fun with you on the PhD trip to Japan, organizing the lab-trip and in San Diego for our international conference. We have grown into real friends and I know I can always count on you for your support and fun. Now we can continue as colleagues at WFSR! Laura, I feel that you and I met for a reason. The support that you gave me on a personal level will always warm my heart. I could always knock on your door when my personal life was in stormy weather (which has been often...). Thank you for your love, attention and never ending support. Your kind heart and your funny imaginations on any topic of conversation made me smile so often.

To my colleagues at WFSR, thank you so much for the interest and support that you showed in the last steps of my PhD journey. It was a rough time for me dividing my attention onto two jobs for a least a year, but I couldn't be happier to have a place at WFSR. A special thanks to Ans and Jochem with whom I could brainstorm on the content of the PhD as well as beyond it. This helped me a lot! I am very much looking forward now to spend my undivided attention on working with all of you.

Voor mijn lieve vrienden: Mathilde, als ik jou niet had, dan weet ik het ook niet meer. Dank je wel voor je onuitputtelijk support, luisterend oor en alle leuke dingen die we samen doen (Camino, Salamanca, en in de toekomst..?). Het was een zware weg en ik had dit niet zonder jou gekund! Eline, Tijmen en Max, dank jullie wel voor de gesprekken, het weglachen van toch wel pijnlijke zaken en jullie bijzondere kijk op dingen die soms voor mij heel moeilijk lijken. Judith dank je wel dat je er altijd voor me bent. Mijn oudste vriendin (25/26 jaar alweer). Je vrolijkheid en humor doen mij altijd goed. Wat ben ik blij dat ik jou in mijn leven heb! Kim, ik voel me blij en dankbaar om een vriendin als jou te hebben. Je zegt altijd waar het op staat en biedt me een luisterend oor en steun. Wanneer ik in Emmen langs waai voelt dat altijd als een minivakantie. Dank je wel daarvoor, mommy-to-be! Maaike, we hebben een aantal jaar in hetzelfde parket gezeten en ik vond dat heel fijn – gedeelde smart is halve smart. Soms lopen de dingen anders in het leven, maar over 1 ding ben ik zeker, ik kan altijd op jou rekenen! Dank je wel voor het toejuichen, het luisteren en alle gesprekken die we hebben gehad. Ik

ben echt onwijs trots op jou! Evelien, ik ontmoette je toen ik net begon aan m'n PhD en heb aan jou de beste mede salsa-lover die ik me kan bedenken. Zo blij dat ik jou in mijn leven heb! Dank je wel voor je support in de afgelopen jaren door te luisteren, maar ook gewoon om alles eruit te dansen op feestjes. Dit gaan we snel weer oppakken! Janneke, jij wandelde mijn hart binnen via het cel laboratorium van de 4^e verdieping Helix. Onze koffietjes/lunches/biertjes zorgden altijd voor een lach op mijn gezicht. Brainstormen over het academische leven, stellingen en de PhD zijn onze favoriete topics en natuurlijk gedichten schrijven... Bedankt voor al je steun door deze turbulente tijden. Ik ben heel blij dat ik jou heb leren kennen! Voor de buurvrouw, Sandra, dank je wel dat je er voor me was – en er nog steeds bent! Voor de intense en interessante gesprekken, je steun en dat je me pusht om een betere versie van mezelf te zijn. Aan Rav, wat ben ik jou dankbaar voor je fantastische tekenwerk voor op m'n boek en wat is het mooi geworden! Hoe bijzonder is het dat we elkaar weer hebben ontmoet! Zo fijn hoe we de tijd kunnen weg kletsen met kaas en wijn en heel hard kunnen lachen, heerlijk! Bedankt! Anne Marijke en Silvie, sjonge wat ben ik blij dat op de valreep de voorkant er toch nog zo mooi uit is komen te zien! Dank jullie wel daarvoor! Heel veel dank ook voor iedereen die mij op afstand heeft gesteund! Jean Michel, Stephanie, Timo, Jerre, Rick, Niels. Het leven veranderd na de studie en elkaar regelmatig zien/spreken is niet meer zo vanzelfsprekend, maar ik heb me altijd erg gesteund gevoeld door jullie! To Jan, thank you for being there for me. Every phone call I appreciated you listening to my stories about work, life or any other topic. Thank you for your support, humor and thoughtfulness. We will meet soon!

Aan Arco, dank je wel dat je met regelmaat contact met me zocht om te vragen hoe het is. Bedankt voor je steun door deze pittige tijd. Het was fijn om met jou en ook met Marlies te kunnen bomen over de PhD en natuurlijk over het leven. Aan Mark, Joelle en Lodewijk, wat vind ik het fijn dat ik er een tweede familie bij heb waar ik mag aan komen waaien voor een lekkere maaltijd, gezelligheid en leer hoe ik saxofoon speel. Wanneer alles erop zit kom ik graag terug voor lessen en gezellig tafelen!

En als laatste voor mijn lieve familie: mam, zonder jou was dit natuurlijk nooit gelukt. Ik ben zo onwijs dankbaar met jou als mijn moeder. Je oneindige steun, liefde en vooral al die bakjes met eten in de laatste maanden van afronding hebben gemaakt dat ik dit voor elkaar heb gekregen! Albert, Loyce en Céline dank jullie dat jullie er altijd voor me zijn. Lief en leed hebben we gedeeld en ik zal altijd weten dat ik voor 100% op jullie kan rekenen! Lieve aanhang van het gezin, Rob, Lyda + Sammie&Guus, Floran en sinds een paar maanden Jazz, jullie ook heel erg bedankt voor de support! Ik kan me geen leukere aanhang wensen! Lieve oma, dank je wel dat je er altijd voor me bent geweest, je steun en je liefde en mooie gezegdes van heel heel vroeger. Gezellig samen eten en kletsen tot half 12 's avonds. Nu alles erop zit, kom ik weer vaker op bezoek! Ook mijn opa

(overleden april 2019) ben ik heel dankbaar! Aan de rest van mijn familie, Sigrid, Albert, David & Lisa, Cecile, Eric, Daphne & Nigel, heel erg bedankt voor het toejuichen, aanmoedigen en steunen van deze prestatie. Jullie zijn geweldig! Aan mijn tantes uit Groningen, Karen en Pauline, fijn dat er weer contact is en dat jullie me komen steunen tijdens de verdediging!

About the author

Curriculum Vitae

Anne Elisabeth (Annelies) Noorlander was born on October 9, 1991 in Ede, the Netherlands. She completed her Bachelor Pharmaceutical Sciences at the University of Groningen in 2014, with an Education Minor allowing her to teach chemistry in secondary education. She continued in Groningen with her Master program Medical Pharmaceutical Sciences where she conducted her thesis at the department of Molecular Pharmacology. For her second thesis she spent nine months at the department of Physiology and Pharmacology, University of Salamanca, Spain and subsequently obtained her MSc degree in 2016. In 2017, Annelies started working at the division of Toxicology, Wageningen University, as a research assistant and went to do an internship at the Department of Experimental Toxicology and Ecology, BASF SE, in Ludwigshafen, Germany, prior to her PhD involving the two parties. In 2018, she commenced her PhD in Wageningen under supervision of prof. dr. ir. Bennard van Ravenzwaay (BASF SE) and prof. dr. ir. Ivonne M.C.M. Rietjens (division of Toxicology, Wageningen University). During her PhD, she followed the postgraduate education program in Toxicology, which will enable her to register as a European toxicologist (ERT) in the near future. Annelies is currently working as a researcher in team Toxicology at Wageningen Food Safety Research.

List of publications

This thesis

Noorlander, A., Fabian, E., Ravenzwaay, B., Rietjens, I.M.C.M. (2020). Novel testing strategy for prediction of rat biliary excretion of intravenously administered estradiol-17β glucuronide. *Archives of Toxicology*. 95, 91 – 102. DOI https://doi.org/10.1007/s00204-020-02908-x

Noorlander, A., Wesseling, S., Rietjens, I.M.C.M., Ravenzwaay, B. (2021). Incorporating renal excretion via the OCT2 transporter in physiologically based kinetic modelling to predict in vivo kinetics of mepiquat in rat. *Toxicology Letters*. 343, 34 – 43. DOI https://doi.org/10.1016/j.toxlet.2021.02.013

Noorlander, A., Zhang, M., Ravenzwaay, B., Rietjens, I.M.C.M. (2022). Use of Physiologically Based Kinetic Modeling-Facilitated Reverse Dosimetry to Predict In Vivo Acute Toxicity of Tetrodotoxin in Rodents. *Toxicological Sciences*. 187 (1), 127 -138. DOI https://doi.org/10.1093/toxsci/kfac022

Noorlander, A., Wesseling, S., Ravenzwaay, B., Rietjens, I.M.C.M. Predicting acute paraquat toxicity using physiologically based kinetic modelling incorporating *in vitro* active renal excretion via the OCT2 transporter. Submitted to Toxicology Letters.

Other publications

Chen, J., **Noorlander, A.**, Wesseling, S., de Haan, L., Bouwmeester, H., Kramer, N.I., Rietjens, I.M.C.M. Integrating in vitro data and physiologically based kinetic modelling facilitated reverse dosimetry to predict acute neurotoxicity of saxitoxin in rats, mice and human. To be submitted.

Liu, C., van Mil, J., **Noorlander, A.**, Rietjens, I.M.C.M. Use of Physiologically Based Kinetic Modeling-Based Reverse Dosimetry to Predict In Vivo Nrf2 Activation by EGCG and Its Colonic Metabolites in Humans. Accepted for publication in the Journal of Agricultural and Food Chemistry.

Overview of completed training activities

Discipline specific course
Environmental Toxicology, WUR (Wageningen, 2018)
General Toxicology, WUR (Wageningen, 2018)
Reproductive Toxicology, PET (Utrecht, 2018)
Regulatory Toxicology, PET (Bilthoven, 2018)
Cell Toxicology, PET (Leiden, 2019)
Medical and Forensic Toxicology, PET (Utrecht, 2019)
Animal Sciences, PET (Utrecht, 2019)
Organ Toxicology, PET (Nijmegen, 2020)
Pathobiology, PET (Online, 2020)

General courses
Reviewing a scientific paper, Wageningen Graduate School (WGS) (Wageningen, 2018)
VLAG PhD week, VLAG (Baarlo, 2018)
Brain training, WGS (Wageningen, 2018)
Teaching and supervising thesis students, WGS (Wageningen, 2018)
Risk assessment, PET (Wageningen, 2019)
Critical thinking and argumentation, WGS (Wageningen 2020)
Applied statistics, VLAG (Online, 2020)
Posters & Pitching, WGS (Online, 2021)

Optional courses and other activities
Preparation of research proposal, Wageningen
Group meetings and scientific discussions/presentations, TOX
PhD study tour to Japan (Japan, 2018)
Organization of the Wageningen PhD Councils' PhD symposium (Wageningen, 2019)

Conferences and meetings
45th Annual meeting of the Dutch Society of Toxicology (poster presentation), NVT (Ede, 2019)
60th Annual meeting Society of Toxicology, SOT (Online, 2021)
3rd SCI-RSC Symposium on Transporters in Drug Discovery and Development, RSC (Online, 2021)
61st Annual meeting Society of Toxicology (poster presentation), SOT (San Diego, CA, USA, 2022)

Approved by Graduate School VLAG